SAND76-8246
Unlimited Release

Mass Transport in Dead-End Tubes With Selectively Permeating Walls

D. R. Chenoweth

Prepared by Sandia Laboratories, Albuquerque, New Mexico 87115 and Livermore, California 94550 for the United States Energy Research and Development Administration under Contract AT (29-1)-789

Printed October 1976

Sandia Laboratories

F 2900 Q(7-73)

When printing a copy of any digitized SAND Report, you are required to update the markings to current standards.

Issued by Sandia Laboratories, operated for the United States Energy Research and Development Administration by Sandia Corporation.

NOTICE

This report was prepared as an account of work sponsored by the United States Government. Neither the United States nor the United States Energy Research and Development Administration, nor any of their employees, nor any of their contractors, subcontractors, or their employees, makes any warranty, express or implied, or assumes any legal liability or responsibility for the accuracy, completeness or usefulness of any information, apparatus, product or process disclosed, or represents that its use would not infringe privately owned rights.

SAND76-8246
Unlimited Release
Printed October 1976

MASS TRANSPORT IN DEAD-END TUBES WITH SELECTIVELY PERMEATING WALLS

D. R. Chenoweth, 8111

August 1976

ABSTRACT

The transport of gaseous species in dead-end tubes having selectively permeating walls is investigated. The limits of validity for the modeling assumptions used are established and are given in terms of a series of inequalities involving the key parameters. Detailed analytical results are generated via exact limiting solutions as well as numerical integration of the governing equations for both positive and negative global velocity cases. Tube materials having specie separation ratios varying from unity to very large or very small values are included in the study. The resulting effective separation ratio for a tube may be either greater or less than that for the tube material in slab form. The possibility of using secondary control species to favorably alter the flow characteristics of primary species is demonstrated. Some experimental data is given which verifies the large effects which the presence of a low permeating specie in the tube bore can have on the flow of another specie which readily permeates the tube walls. It is shown, in the near perfect filter limit, that the analytical model properly describes the effects obtained in both the balanced pressure and the convection dominated limits.

SUMMARY

The transport of gaseous species in dead-end tubes having selectively permeating walls is investigated. The assumptions of continuum, quasi-steady, fully developed, laminar bore flow of perfect gases which behave like an axially diffused plug flow through an approximately straight tube with nearly uniform bore temperature and pressure are used; the supply and receiving reservoirs are assumed to be well mixed so that uniform reservoir temperature and concentrations exist. The limits of validity for these assumptions are established and are given in terms of a series of inequalities involving the key parameters.

Detailed results are generated via exact physically limiting solutions as well as numerical integration of the governing equations for cases involving up to five species. Both positive and negative global velocity cases are examined and are used to show that better results can sometimes be obtained if the tube is immersed in the opposite reservoir. Tube materials having specie separation ratios varying from unity (non-selective) to very large or very small values (near perfect filters) are included in the study. It is shown that the flow of a given specie can be either enhanced or dehanced, and even reversed in direction, relative to the corresponding perfect mixing value due to the presence of other species. This leads to the definition of an effective separation ratio for specie flow from the tube which may be greater or less than that of the tube material in slab form which is approached in the perfect mixing limit. It is also shown that in certain

cases an individual specie can exhibit wall and bore stagnation points at different locations where the flow direction changes for that specie. From the consideration of such phenomena it is demonstrated, as a possible mode of operation, that secondary control species having very large or very small permeation rates can be used to favorably alter the flow characteristics of primary species.

Finally, some experimental data is given to verify the large effect which the presence of a low permeating specie in the tube bore can have on the flow of another specie which readily permeates the tube walls. It is shown, in the near perfect filter limit, that the mathematical model given here properly describes the effects obtained in both the balanced pressure and the convection dominated experimental limits.

The information contained in this document eliminates the need to operate such dead-end tubes with selectively permeating walls near the perfect mixing limit to avoid unknown effects; this is true because these effects are now predictable and well enough understood so that they can even be exploited to produce favorable effects in some cases.

ACKNOWLEDGEMENT

The author wishes to acknowledge R. Page for conducting the experiments described in this report, G. Miller for supplying the computer programming support, and S. Huston for typing the manuscript.

CONTENTS

	Page
INTRODUCTION	11
NOMENCLATURE	13
ANALYSIS	19
I. Governing Equations	19
(i) Fluid Mechanical Assumptions	21
(ii) Conservation of Mass	26
(iii) Diffusion Coefficient (Gas Phase)	27
(iv) Permeation Rate (Wall Diffusion)	28
(v) Boundary Conditions and Combined Auxiliary Equations	30
(vi) Non-Dimensional Governing Equations	31
II. Results	33
(i) Limiting Solutions	34
I = 1 (Single Specie)	34
I = 2 (Binary Mixture)	35
I ≥ 3 (Ternary Mixture or Greater Number of Species)	58
(ii) Numerical Results (Arbitrary C_{i0}, $C_{i\infty}$, β_{ij}, δ_{ij})	64
I = 2 (Binary Mixture)	66
I ≥ 3 (Ternary Mixture or Greater Number of Species)	110
(iii) Special Modes of Operation	124
Reservoir Switch	124
Addition of Control Species	126
Substitution for Secondary Species	126
III. Experimental Data	128
(i) Perfect Filter Limit	128
CONCLUSIONS	137
REFERENCES	139
APPENDIX	141

INTRODUCTION

Many materials (Jost, 1960) including metals (Al, Cu, Ag, Fe, Mo, Ni, Pd, Pt), ionic crystals (the alkali halides, quartz, rock salt, fluorite), glasses (SiO_2, Pyrex), organic polymers (rubber, various butadienes, paraffine, cellophane, cellulose compounds, neoprene, polystyrene, polyvinyl chloride), and zeolites or silicate compounds (analcite, chabazite, heulandite, natrolite, scolecite) are selective in varying degrees to the permeation of some of the common gases (Ar, Ne, He, O_2, N_2, H_2, CO, CO_2, NH_3, CH_4). Since most of these materials can be used to construct pipes, tubes and capillaries of various kinds which are often used to transport or store mixtures of common gases, the interaction between the selective permeation of the tube walls and the bore transport processes can be important in some cases. The author is not aware of any published investigations of this type of problem.

The analogous problem for porous tube flow has been extensively studied in some flow regimes, for example see Libby, et al. (1969), or Huang and Yu (1973). It must be made clear that such studies are very different from the problem briefly described above. Porous walled tubes exhibit flow and gas phase diffusion through open pore space. Such processes consist of global (viscous or non-viscous convective) flow, which is generally non-selective and may include mutual diffusion (intermolecular collisions are dominant) and/or Knudsen diffusion (wall collisions are dominant), which are only weakly selective in that they depend on the

square root of the molecular weight ratios of the various gas species. Also these processes have weak dependence on temperature. The term "selectively permeating walls" is used here to describe diffusion in the solid material via gas migration through the atomic lattice structure of the material. A much higher degree of selectivity can be observed for that mechanism, and also a strong dependence on temperature is usually present.

Another related problem area which has received considerable attention involves the transport of gas mixtures having varying spacial compositions in non-permeable pipes. A large body of literature on this subject is published under headings like "laminar dispersion in capillaries" and similar terminology; some of the key papers on this problem are Taylor (1953-4), Aris (1956), Bournia (1961), Evans (1965), Gill, et al. (1965-8), Dayan and Levenspiel (1968) and Nunge, et al. (1972). This work is found to be very helpful in formulating the analytical model given in this document.

Some previous work on flow in selectively permeating tubes has been done here at SLL; the work included both analysis and experimental verification of cases where the net flow was out of the tube's open end; only the near perfect filter limit was examined, so that two species were present and only one of those readily permeated the tube walls with the other being essentially trapped in the vent volume and tube bore. This previous work is included in this document as well as an analysis of cases where the net flow is into the tube's open end along with real filter cases involving two or more permeating species. No additional experimental data beyond the near perfect filter limit is given. The limits of validity for the fluid mechanical modeling assumptions are established, and the related analysis is given in detail in the Appendix.

NOMENCLATURE

a	thermal diffusivity
A_i	eq. (89)
A_s	effective surface area, eq. (A20)
A_v	Avogadro's number 0.61×10^{24}
a,b,c	eq. (66)
B_i	eq. (90)
c_{oi}	sound speed, eq. (A23)
C_i	$= P_i/P$, mole fraction ($P_i/P = \nu_i/\nu$)
C_{i0}	$= P_{i0}/P_0 = C_i$ $(X = 0)$
C_{i1}	$= C_i$ $(X = 1)$
$C_{i\infty}$	$= P_{i\infty}/P_0$, pseudo-mole fraction
d	coil diameter
D	tube inside diameter
D_i	wall material diffusion coefficient for gas species i
D_o	pre-exponential parameter for D_i
$\mathcal{D}_{ij}$	gas phase mutual diffusion coefficient
$\mathcal{D}_r$	reference $\mathcal{D}_{ij}$ at P_r and T_r
E_d	diffusion exponential parameter
E_s	solubility exponential parameter
f, F	eq. (71)
h	tube wall thickness

I number of gas species

J eq. (A63)

k thermal conductivity

K eq. (76), also eq. (A62)

$\overline{K}$ axial dispersion coefficient

Kn Knudsen number, λ/D

$K_i = S_i D_i$, permeability coefficient

L tube length

L_e entrance length, eq. (A9)

$\dot{m}$ mass flow rate

M Mach number

M_i eq. (14)

$M_{i0} = M_i(x=0)$

N temperature exponent, eq. (4)

N_{Pe} eq. (A27), Péclét number (diffusion)

P_i local partial pressure for species i

P_{i0} receiver partial pressure species i

$P_{i\infty}$ driver partial pressure species i

$P = \sum_{i=1}^{I} P_i$, mixture static pressure

$P_0 = \sum_{i=1}^{I} P_{i0}$, receiver mixture pressure

P_r reference pressure, eq. (4)

$\dot{q}$ heating rate per unit volume

r_i eq. (1)

$r_{ie} = r_i\ (t \to \infty)$, eq. (5)

R 82.06 cm^3 atm/mole °K

R_c 1.987 cal/mole °K

Re		Reynolds number
Re_w		wall Reynolds number
S		eq. (A36)
Sc	=	$\nu/\mathcal{D}_{ij}$, Schmidt number
S_i		solubility coefficient for gas species i
S_0		pre-exponential parameter for S_i
t		time
t_d		eq. (A18)
t_w		eq. (A19)
$t_{2\bar{u}}$		eq. (A24)
$t_{\mathcal{D}_{ij}}$		eq. (A31)
$t_{\bar{u}}$		eq. (A37)
$t_{\bar{K}}$		eq. (A38)
t_{CA}		eq. (A61)
t_{CR}		eq. (A22)
t_{VA}		eq. (A23)
t_{VR}		eq. (A21)
t_{FV}		eq. (A20)
t_{x_d}		eq. (A91)
t_{x_v}		eq. (A92)
T		temperature (static)
T_0		stagnation temperature
T_r		reference temperature, eq. (4)
u_i		velocity species i
u	=	$\sum_{i=1}^{I} C_i u_i$, molar averaged velocity
V_o		receiver volume

V_∞		driver volume
V'		eq. (A83)
V'_b		eq. (A83)
W_i		molecular weight species i
W		integration constant, eq. (48)
x		axial distance along tube bore
X	=	x/L
X_d		eq. (A91)
X_v		eq. (A92)
y	=	$\ln (1 - C_1)$
Y		eq. (74)
Z		eq. (75)
Z		compressibility factor, eq. (A4)
α		eq. (A18), α^{-1} = decay constant
α		eq. (77)
α'		$\alpha L^2/2\mathcal{D}_{ij}$
β_{ij}		eq. (20)
γ		ratio of specific heats
δ		$\bar{u}(t/\bar{K})^{1/2}$, eq. (A49)
δ_{ij}		eq. (19)
η		eq. (A50)
θ_{ij}		eq. (18)
λ		eq. (A2), mean free path (molecular)
μ		viscosity coefficient
ν_i		eq. (3), molar density species i

$\nu = \sum_{i=1}^{I} \nu_i$, total molar density; also $\nu = \mu/\rho$, kinematic viscosity

ρ mass density

τ_D eq. (A26)

τ_0 eq. (A57)

$\phi = \Phi_{ij}$ $(\delta_{ij} = 1)$

Φ eq. (A53)

Φ_{ij} eq. (17)

ω_{ie} eq. (6)

Ω_i eq. (91), separation ratio

$\Omega_{eff\ i}$ eq. (97), effective separation ratio

ANALYSIS

The analysis below consists of two main areas of investigation; the first area is primarily concerned with the physical description of the problem and its mathematical formulation. The governing equations are derived with a minimum of analysis due to the fact that each of the many fluid mechanical assumptions used is examined in great detail in the Appendix, although an important wall diffusion assumption is discussed below. The second area consists of results in the form of exact limiting solutions as well as more general cases obtained from the numerical solution of the governing equations. The solutions are increased in complexity via an increase in the number of gaseous species involved and special emphasis is given to the various modes of operation identified by means of unique physical or mathematical characteristics.

I. Governing Equations

Physically the problem investigated here consists of two volumes of gas which may be different mixtures of two or more chemical species at different pressure levels. The gases can pass from one volume to the other by means of a dead-end tube immersed in one volume with the open end connected to the other volume. The gases pass through the tube walls by selective permeation via diffusion, not by global flow processes through open pores. This situation is shown schematically in Figure 1 where one volume V_∞ is often

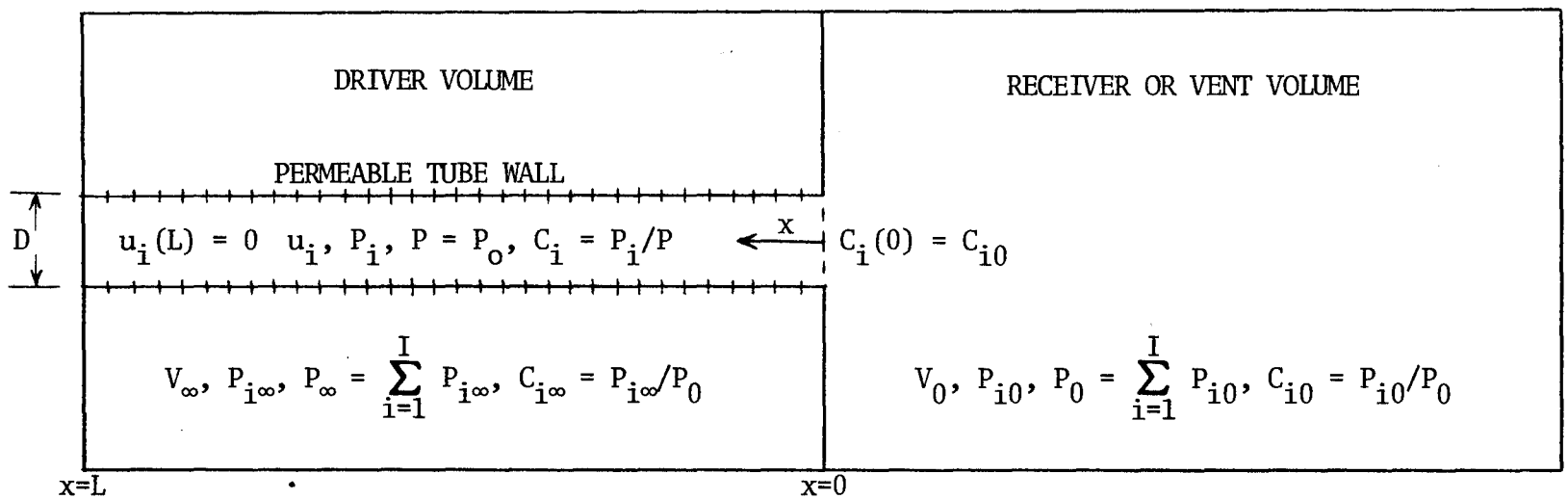

Figure 1. System Schematic Diagram

referred to as the driver and the other volume V_o is often referred to as the receiver or vent volume even though the flow direction is not specified or restricted here other than with respect to the different mathematical forms of solutions sometimes required. It must be emphasized that the volume sizes V_o and V_∞ are not directly relevant to the problem in the sense of transient mass inventory accounting; that is, the volumes do not enter into the model explicitly due to the assumptions of quasi-steady bore flow and uniform reservoirs. However, the volume symbols V_∞ and V_o as well as their names "driver" and "receiver" or "vent," respectively, are used extensively in the discussion as a means of identifying the gas mixture in contact with the exterior of the tube as opposed to the region surrounding the root or open end of the tube bore. The volume sizes are also required in the Appendix in order to establish that the quasi-steady bore flow and uniform reservoir assumptions are approximately valid.

(i) Fluid Mechanical Assumptions

The fluid mechanical assumptions which have been made in order to investigate the problem shown schematically in Figure 1 are listed in Table I with the independent dimensionless parameters (a total of eighteen) shown immediately after the assumption which first requires them. The restrictions (inequalities) found to be necessary via the detailed analysis given in the Appendix for each assumption to be valid are also given in Table I; first the dimensionless parameter restriction is given, then the equivalent restriction on the tube length, diameter, total mass flow rate, or other key dimensioned parameter for the problem is given. The parameter definitions and the units required in order to properly use the inequalities

TABLE I. Fluid Mechanical Assumptions and Related Parameter Restrictions

Continuum Flow [Kn]

$$Kn = \lambda/D < 10^{-2}/3 << 1 \tag{A1}$$

$$D\ P > 10^{-5}\ T \tag{A3}$$

Perfect Gases [Z]

$$0.94 \leq Z \leq 1.06 \tag{A5}$$

$$P < 100\ \text{atm} \tag{A6}$$

Fully Developed Laminar Bore Flow [Re, L/D]

(i) Laminar Flow

$$Re = \rho\bar{u}D/\mu = 4\ \dot{m}/\pi D\mu < 2000 \tag{A7}$$

$$\dot{m} < 500\ \pi D\mu \tag{A8}$$

(ii) Fully Developed Flow

$$L/D > 0.35\ Re \tag{A10}$$

$$\dot{m} < 0.7\ \ \pi D\mu\ (L/D) \tag{A11}$$

Uniform Bore Temperature and Pressure [M, γ]

(i) Uniform Bore Temperature

$$M < 0.3, \qquad 1 < \gamma \leq 5/3 \tag{A12}$$

$$\dot{m} < 37.5\ \pi\gamma^{1/2}\ D^2\ P(W/RT)^{1/2} \tag{A13}$$

(ii) Uniform Bore Pressue

$$\Delta P/P = (\dot{m}/W)(128\ \mu LRT/\pi D^4 P^2) < 1.28 \times 10^{-2} << 1 \tag{A15}$$

$$\dot{m} < 10^{-4}\ \pi D^4 P^2 W/\mu LRT \tag{A16}$$

Quasi-Steady, Axially-Diffused Plug Flow [N_{Pe}, h/D, V_o/V_∞, V', D_i', α', S_i']

(i) Axially Diffused Plug Flow

$$N_{Pe} < 1 \tag{A66}$$

$$\dot{m} < \pi D\mu/4Sc \tag{A67}$$

(ii) Quasi-Steady Bore Flow

$$t_{bore}/t_{system} < 0.2 \qquad \text{(A68) - (A80)}$$

$$D < 3 \times 10^4\ P^{-1/2} \tag{A81}$$

$$D < 0.9\ h\ (\mathcal{D}_{ij}/D_i)^{1/2} \tag{A82}$$

$$V' = (\pi D^2 L/4V_o) < 0.4 \left(1 + \frac{D}{h}\right)^{-1} \left(1 + \frac{V_o}{V_\infty}\right)^{-1} / D_i' S_i' = V_b' \tag{A83}$$

$$L < 2 \times 10^{11} \ (\gamma T/W)^{1/2} \tag{A84}$$

$$L < 1.5 \times 10^{4} \ F^{-1/2} \ P^{-1/2} \tag{A85}$$

$$L < 1.8 \times 10^{2} \ h^{2} \ (\gamma/TW)^{1/2} \ D_o^{-1} \exp \ (E_d/RT) \tag{A86}$$

$$L < (5F)^{-1/2} \ h \ (\mathcal{D}_{ij}/D_i)^{1/2} \tag{A87}$$

$$V' < V_b' \ (c_o D/\mathcal{D}_{ij})/40 \ (L/D) \tag{A88}$$

$$V' < V_b'/4(L/D)^2 \ F \tag{A89}$$

<u>Uniform Reservoirs</u> $[L/X_v, \ X_d/X_v, \ t_{stc}/t_{rc}, \ \Delta T_{max}/T]$

(i) Concentration

$$t_{X_d}/t_{FV} = 0.12 \ LV_\infty^{2/3}/V_o(V_b')_d < 10^{-2} << 1 \tag{A93}$$

$$t_{X_v}/t_{FV} = 0.32 \ L/V_o^{1/3}(V_b')_v < 10^{-2} << 1 \tag{A94}$$

$$L < 0.083 \ (V_b')_d \ V_o/V_\infty^{2/3} \tag{A95}$$

$$L < 0.031 \ (V_b')_v \ V_o^{1/3} \tag{A96}$$

(ii) Temperature

$$t_{stc}/t_{rc} = t(\text{sys. temp. change})/t(\text{res. conduction}) > 5 \tag{A100}$$

$$t(\text{sys. temp. change}) > 5 \ r_{res}^2/6a \tag{A101}$$

$$\Delta T_{max}/T < 10^{-1} \tag{A103}$$

$$r_{res}^2 < 0.6 \ kT/\dot{q} \tag{A104}$$

Straight Tube [d/D]

(i) Flow Rate

$$d/D > 10^{-2}\ Re^{2} \tag{A107}$$

(ii) Dispersion

$$d/D > 2.66\ Re^{1/8}\ (1 + 10^{-3}\ Re^{2}) \tag{A108}$$

Dead End Permeable Tube

$$Re_w/Re < 10^{-2}/4 << 1 \tag{A112}$$

$$|Re_w| < 10^{-1}/\pi << 1 \tag{A113}$$

$$L > 10^{2}\ D \tag{A114}$$

$$\dot{m} < 10^{-1}\ \mu L \tag{A115}$$

(A115) replaces (A11)

to determine if a given problem can be investigated via the model derived here are found in the Appendix near the corresponding equation number shown to the right of the inequalities in Table I. In general these restrictions are independent although (A115) does replace (A11), and when Sc is near unity as it usually is for most gaseous flows, then (A67) replaces (A8).

(ii) Conservation of Mass

The assumptions listed in Table I and analyzed in the Appendix in detail have eliminated the momentum and energy equations; also the time dependence is introduced only in a quasi-steady manner via the boundary conditions; therefore the problem has been reduced to one of conservation of mass for each specie i via the steady, one-dimensional equations

$$d(u_i C_i)/dx = r_i, \; i = 1, 2, \ldots, I. \tag{1}$$

The axial diffusion relative to a molar-average plug flow velocity $u = \bar{u} = \sum_{i=1}^{I} (u_i C_i)$ is accounted for by means of Fick's law such that

$$u_i C_i = uC_i - \mathcal{D}_{ij} \, dC_i/dx, \; i = 1, 2, \ldots, I \tag{2}$$

where the mole fraction of specie i is

$$C_i = \nu_i/\nu = P_i/P = P_i/P_o \tag{3}$$

so that $\sum_{i=1}^{I} C_i = 1$ using $P = P_o = \sum_{i=1}^{I} P_i = \sum_{i=1}^{I} P_{io}$. The coordinate x is measured along the bore from the open end or root of the permeable tube. The assumptions of continuum, fully developed, laminar bore flow of perfect gases through an approximately straight tube with nearly uniform bore temperature and pressure have been used.

(iii) Diffusion Coefficient (Gas Phase)

The mutual diffusion coefficient $\mathcal{D}_{ij}$ depends on the total (as opposed to partial not static) pressure P and temperature T and can be written

$$\mathcal{D}_{ij} = \mathcal{D}_r \ (T/T_r)^N \ (P_r/P) \tag{4}$$

in terms of reference values, subscript r. The temperature exponent N is usually narrowly bounded $1.63 \leq N \leq 1.76$ for many common gas combinations and for most purposes can be taken to be $N \simeq 1.7$. The reference diffusion coefficient $\mathcal{D}_r = \mathcal{D}_r \ (P_r, T_r)$ is evaluated at the reference pressure and temperature which are conveniently chosen to be 1 atm and 300°K here. From Weissman (1971), Weissman and Mason (1962), and Annis, Humphreys and Mason (1969) typical values for $\mathcal{D}_r$ in cm^2/sec units are (H_2 - Xe) 0.61, (H_2 - Ar) 0.82, (H_2 - Ne) 1.17, (H_2 - He) 1.59, (H_2 - H_2) 1.47, (H_2 - D_2) 1.27, (H_2 - T_2) 1.18, (H_2 - O_2) 0.81, (H_2 - N_2) 0.76, (H_2 - CO) 0.77, and (H_2 - CH_4) 0.74 cm^2/sec which indicates that a value of about 1 cm^2/sec is often not a bad approximation. Usually $\mathcal{D}_{ij} \simeq \mathcal{D}_{ji}$ is a good assumption, and if more than two species are involved then j is usually taken to be the

combination of all species except i as an approximation. Since the bore pressure and temperature are approximately uniform, $\mathcal{D}_{ij}$ via (4) is a constant parameter in (2) here.

(iv) Permeation Rate (Wall Diffusion)

The term r_i on the right of (1) is the local molar source rate for specie i due to wall permeation per unit of bore cross sectional area $\pi D^2/4$ per unit of tube length L all divided by the total molar density ν_o in the vent volume. In general r_i is extremely complex and requires extensive numerical calculations to properly determine accurate values under arbitrary conditions. Even for relatively simple initial and boundary conditions for cylindrical, thick-walled tubes the solution (Jost, 1960, and Carslaw, 1959) involves zero order Bessel's functions of the first kind. However many problems of interest are operating most of the time in a quasi-steady or quasi-equilibrium mode such that r_i can be expressed approximately by*

$$r_i \simeq r_{ie} = r_i \ (t \to \infty) = \omega_{ie} \ (C_{i\infty} - C_i) \tag{5}$$

where $C_{i\infty} = P_{i\infty}/P_o$ does not represent a mole fraction, but only a pseudo-mole fraction due to the normalization by the vent volume total pressure, $\sum_{i=1}^{I} C_{i\infty} \neq 1$ necessarily. The parameter ω_{ie} is related to the wall material permeability coefficient K_i for specie i by

$$\omega_{ie} = (8 \ K_i \ RT/A_v)/D^2 \ell n \ (1+2h/D) \tag{6}$$

*This expression requires modification if the total pressure significantly exceeds the 100 atmosphere limit imposed here, and also for metal tubes permeated by polyatomic gas species.

for a tube of inside diameter D and wall thickness h, which reduces to that for a slab when $h/D << 1$. The parameters in (6) and their units are defined in the Appendix near equations (A19) and (A20). Actually (5) is a good approximation whenever the time measured from an abrupt reservoir concentration or temperature change exceeds t_w given by (A19) since $t_w = h^2/2D_i$ crudely estimates the time necessary to establish quasi-steady conditions following such a change. This can be demonstrated by the simple special case where $h/D << 1$ when the tube bore and wall initially have zero concentration of a specie and that in the bore remains nearly zero for all time, while the exterior of the tube is exposed to a concentration of unity at $t = 0$ and remains nearly unity for all time t. The solution (Jost, 1960) for r_i can then be expressed

$$r_i/r_{ie} = \left[1 + 2 \sum_{n=1}^{\infty} (-1)^n \exp\left(-\pi^2 n^2 D_i t/h^2\right)\right] \tag{7}$$

which gives the values $r_i/r_{ie} = 0.55$ at $t = 0.3\ t_w$, 0.90 at $t = 0.6\ t_w$, and 0.99 at $t = t_w = h^2/2D_i$ so that actually anytime $t > t_w/2$ the expression (5) is a reasonable approximation for r_i. This result remains valid for general cases where rapid reservoir concentration or temperature changes rather than unity step changes are present as well as cases where the thin wall approximation $h/d << 1$ is not true. Of course gradual changes are no problem since (5) remains valid for all time t if the rate change of the wall surface concentration is much smaller than the wall concentration differential divided by t_w, $\partial C_i/\partial t << |\Delta C_i/t_w|$. If the concentration change is due to a temperature change via the solubility coefficient temperature dependence, then the rate change of temperature is restricted such that

$$\partial T/\partial t << \left|(\Delta C_i/C_i)(T/t_w)(1 + E_s/R_c T)^{-1}\right| \tag{8}$$

in order that (5) hold for all time, where (8) is expressed in terms of quantities defined near (A19) and (A20). Representative values for t_w given following (A19) for a variety of examples demonstrate that it can easily vary in magnitude from a few seconds to many years without being unrealistic due to strong dependence on temperature, wall material and gas specie as well as wall thickness. Thus the restriction that $t > t_w$ for (5) to hold when rapid concentration or temperature changes exist may or may not be a problem. The same thing can be said about (8) if it is necessary that (5) be valid for all time when cases involving temperature variation are being investigated. In any event, if either $t > t_w$ or (8) is true, then (5) is valid, and it represents the final assumption for the work which follows. When (5) is valid, it is only necessary to use the correct local value for temperature to evaluate $K_i = K_i(T)$ in (6) and the proper local values for $C_{i\infty}$ and C_i. In regions where (5) is not valid, elaborate numerical calculations are necessary to determine r_i.

(v) Boundary Conditions and Combined Auxiliary Equations

When (1), (2) and (5) are combined using the auxiliary equations

$$\sum_{i=1}^{I} C_i = 1 \qquad \text{and} \tag{9}$$

$$du/dx = r_e = \sum_{i=1}^{I} r_{ie} = \sum_{i=1}^{I} \omega_{ie} \, (C_{i\infty} - C_i) \tag{10}$$

and $\mathcal{D}_{ij}$ is considered to be a nearly constant parameter

$$\mathcal{D}_{ij} \; (d^2 \, C_i/dx^2) - u \; (dC_i/dx) - r_e \, C_i + r_{ie} = 0 \tag{11}$$

results, which is a coupled set of (I - 1 using $\sum_{i=1}^{I} C_i = 1$) non-linear, second-order, ordinary differential equations. However due to the split boundary conditions,

$$\left.\begin{aligned} & C_i = C_{io} \text{ at } x = 0 \\ \text{and} \quad & u = 0, \; dC_i/dx = 0 \text{ at } x = L, \end{aligned}\right\} \tag{12}$$

the use of (9) - (11) is not as convenient as the set of first-order differential equations, (1) and (2) with boundary conditions (12).

(vi) Non-Dimensional Governing Equations

It is best to non-dimensionalize (1) and (2) before examining their mathematical nature; to do this x is normalized by the tube length L

$$X = x/L \tag{13}$$

and the dependent variable M_i is introduced such that

$$M_i = u_i \; C_i/L \; \omega_{ie} \; (C_{io} - C_{i\infty}) \tag{14}$$

which means physically that $u_i\ C_i$ has been normalized by its corresponding value for specie i at X = 0 when perfect mixing ($\mathcal{D}_{ij} \to \infty$) is approached; thus in the perfect mixing limit, as will be shown later, $C_i = C_{io}$ and $M_i(X = 0) = M_{io} = 1$. The resulting governing equations have a deceptively simple appearance

$$dM_i/dX = (C_i - C_{i\infty})/(C_{i\infty} - C_{io}) \tag{15}$$

$$dC_i/dX = \Phi_{ij}\ C_i + \Theta_{ij}\ M_i,\ i = 1, 2, \ldots, I \tag{16}$$

where

$$\Phi_{ij} = uL/\mathcal{D}_{ij} = -\ \delta_{ij}^{-1} \sum_{i=1}^{I} (\delta_{ij}\ \Theta_{ij}\ M_i) \tag{17}$$

$$\Theta_{ij} = \beta_{ij}^2\ (C_{i\infty} - C_{io}) \tag{18}$$

$$\delta_{ij} = \mathcal{D}_{ij}/\mathcal{D}_{1j} \qquad j \neq i \tag{19}$$

$$\beta_{ij}^2 = (L^2\ \omega_{ie}/\mathcal{D}_{ij}). \tag{20}$$

The boundary conditions for (15) and (16) are

$$\left.\begin{aligned} M_i(1) &= 0 \quad \text{at } X = 1 \\ C_i(0) &= C_{io} \quad \text{at } X = 0 \end{aligned}\right\} \tag{21}$$

where for numerical purposes $M_i(1) << M_i(0) = M_{io}$ is adequate. The parameter Φ_{ij} is the diffusion Péclét number N_{Pe} (L/D) based on tube length which carries the same sign as the global or net flow velocity $\dot{u}$ and whose magnitude indicates the relative (axial) diffusive ($\Phi_{ij} << 1$) or convective ($\Phi_{ij} >> 1$) nature of the bore flow; the word convective is used to denote plug flow here rather than in the pure sense discussed in the Appendix. That is the velocity profile is not really flat, but can be regarded as being such only for the purposes of analyzing specie transport in the bore with the assumptions listed in Table I. The sign of Θ_{ij} indicates the individual specie flow direction if perfect mixing ($\mathcal{D}_{ij} \to \infty$) were present, while the sign of $\Theta_{ij} M_i$ is the same as that of u_i for the general problem with arbitrary $\mathcal{D}_{ij}$ magnitude. Thus if M_i is positive, the specie velocity in the bore has the same direction as would be present in the perfect mixing case, while negative M_i indicates that they are opposite. Of course the local sign of $(C_i - C_{i\infty})$ gives the direction of flow of specie i through the wall which is not necessarily the same as that in the bore.

II. Results

The solutions of (15) and (16) are extremely complicated and display widely varying physical and mathematical modes for the boundary conditions (21) and the defining equations (6), (14) and (17)-(20) even when I = 2 but especially when more than two species are present I > 2. The governing equations (15) and (16) consist of 2I coupled, first-order, non-linear ordinary differential equations which are certainly tractable via numerical methods. In addition the auxiliary algebraic equation $\sum_{i=1}^{I} C_i = 1$ can be used to reduce the governing differential equations to a set of (2I-1) first-order equations. However

even if the δ_{ij} are taken to be approximately unity, which may not always be a good approximation, then the (3I-1) independent dimensionless parameters in the form of β_i^2, $C_{i\infty}$ and C_{io}, using $\sum_{i=1}^{I} C_{io} = 1$, must be specified to identify a given solution. In order to properly understand the wide variety of numerical results produced in this manner, some framework must be established whereby classes of solutions with similar characteristics can be identified and analyzed separately prior to investigating general cases which may not clearly display any particular feature which is physically or mathematically unique. This framework is best established by means of a series of limiting solutions to (15) and (16) using (21) where the number of species is progressively increased and the diffusive nature of both the tube wall and the bore flow are taken to extreme limits.

(i) Limiting Solutions

The limiting solutions to (15) and (16) using (9) and (21) will be increased in complexity by increasing the number of species I present, starting with the single specie case.

I = 1 (SINGLE SPECIE)

When I = 1 the identity (9) determines C_1

$$C_1 = C_{10} = 1 \tag{22}$$

and (15) gives M_1

$$M_1 = 1 - X \tag{23}$$

so that $u_1 = u = \omega_{1e} (1 - C_{1\infty})(L - x)$ (24)

which merely shows, as was already known, that the assumptions, analyzed in the Appendix, eliminated all resistance to the flow of a single specie gas down the bore.

I = 2 (BINARY MIXTURE)

When two species are present and the assumption that $\mathcal{D}_{12} = \mathcal{D}_{21}$ is used, then $\delta_{12} = \delta_{21} = 1$ and $\phi = \Phi_{12} = \Phi_{21} = -(\Theta_{12} M_1 + \Theta_{21} M_2)$ where $\Theta_{12} = \beta_{12}^2 (C_{1\infty} - C_{10})$ and $\Theta_{21} = \beta_{21}^2 (C_{2\infty} - C_{20})$. If the auxiliary equation $C_2 = 1 - C_1$ is used to eliminate one differential equation, the three governing differential equations

$$dM_1/dX = (C_1 - C_{1\infty})/(C_{1\infty} - C_{10}) \tag{25}$$

$$dM_2/dX = (1 - C_{2\infty} - C_1)/(C_{2\infty} + C_{10} - 1) \tag{26}$$

$$dC_1/dX = \Theta_{12} M_1 (1 - C_1) - \Theta_{21} M_2 C_1 \tag{27}$$

describe the problem with boundary conditions (21).

Perfect Filter $\Theta_{21} = 0$

In the limit where only specie 1 permeates the tube wall, $\Theta_{21} = 0$ and (26) is eliminated so that

$$dM_1/dX = (C_1 - C_{1\infty})/(C_{1\infty} - C_{10}) \tag{28}$$

$$dC_1/dX = \Theta_{12} M_1 (1 - C_1) \tag{29}$$

which can be combined to give

$$d^2 \ln (1 - C_1)/dX^2 = \beta_{12}^2 (C_{1\infty} - C_1). \tag{30}$$

Letting $(\ )' = d(\ )/dX$ and $y = \ln (1 - C_1)$, (30) becomes

$$y'' = \beta_{12}^2 (C_{1\infty} - 1 + e^y). \tag{31}$$

Equation (31) can be formally integrated to give

$$y' = \phi = uL/\mathcal{D}_{12} = \left\{2\beta_{12}^2 \left[e^y + (C_{1\infty} - 1)\, y\right] + A_0\right\}^{1/2} \tag{32}$$

and

$$X = x/L = \int \left\{2\beta_{12}^2 \left[e^y + (C_{1\infty} - 1)\, y\right] + A_0\right\}^{-1/2} dy + B_0 \tag{33}$$

where A_0 and B_0 are integration constants. Unfortunately, due to the nature of the boundary conditions, A_0 and B_0 cannot be explicitly evaluated except in special cases. To obtain general results, one can use a numerical procedure to determine A_0 and B_0 from (32) and (33) or one can return to (28) and (29) and use a standard scheme to integrate a system of first-order differential equations. However, a great deal of information can be obtained from special, limiting solutions of these equations.

Diffusion Dominated Limit

First consider the special case of perfect mixing ($\mathcal{D}_{12} \to \infty$) so that $\Theta_{12} \to 0$ and $dC_1/dX = 0$ with the result that

$$C_1 = C_{10} \tag{34}$$

$$M_1 = 1 - X \tag{35}$$

giving

$$M_{10} = M_1(0) = 1 \tag{36}$$

so that

$$u_{10}\, C_{10} = L\omega_{1e}\, (C_{10} - C_{1\infty}) \tag{37}$$

implying, as it should, that no flow resistance effects are present. Actually, if this limit is approached by decreasing the total pressure, Knudsen flow will occur before it is reached, however proper behavior is displayed in the continuum sense even if it is idealized.

For finite $\mathcal{D}_{12}$ the problem is diffusion dominated if $|u| << |u_1|$ so that $|C_1\, \Phi_{12}| << |\Theta_{12}\, M_1|$; but since $\phi = \Phi_{12} \to -\Theta_{12}\, M_1$ or $u = C_1\, u_1$

when $\Theta_{21} = 0$, this limit can only be approached if $C_1 << 1$ implying that $C_{10} << 1$ and also $C_{1\infty} + (C_{10} - C_{1\infty})/\cosh \beta_{12} << 1$ via (38) so that only a trace of specie 1 is present in the tube compared to the concentration of specie 2 which is stagnant in the tube bore in this case, $C_2 = 1 - C_1$. Equation (30) then becomes $d^2C_1/dX^2 = \beta_{12}^2 (C_1 - C_{1\infty})$ the solution (well known due to the analogy to the familiar thin, finite-length-fin, heat-transfer problem) of which is

$$(C_1 - C_{1\infty})/(C_{10} - C_{1\infty}) = [\cosh \beta_{12} (1 - X)]/\cosh \beta_{12} \tag{38}$$

so that C_1 varies exponentially between the limits of C_{10} and $C_{1\infty} + (C_{10} - C_{1\infty})/\cosh \beta_{12}$ at $X = 0$ and $X = 1$, respectively. To complete the solution, M_1 is obtained from (28) using (38)

$$M_1 = [\sinh \beta_{12} (1 - X)]/\beta_{12} \cosh \beta_{12} \tag{39}$$

which has the value

$$M_{10} = C_{10}\, u_{10}/L\, \omega_{1e} (C_{10} - C_{1\infty}) = \tanh \beta_{12}/\beta_{12} \tag{40}$$

at $X = 0$. Note that M_1 is always bounded $0 \leq M_1 \leq 1$ for all X and β_{12}, and in fact $0 \leq M_1 < \beta_{12}^{-1}$ for $\beta_{12} > 1$. From (40) it can be seen that only for $\beta_{12} << 1$ giving $M_{10} \to 1$ is the flow of specie 1 virtually unrestricted. In fact the perfect mixing case (34) - (36) is recovered as a special case from (38) - (40) when $\beta_{12} << 1$. On the other hand, when $\beta_{12} >> 1$ (actually $\beta_{12} > 3$) $M_{10} \to \beta_{12}^{-1}$ where $\beta_{12}^{-1} = (\mathcal{D}_{12}/\omega_{1e} L^2)^{1/2}$ so that the flow of specie 1 is almost stopped compared to the perfect mixing value. Such a phenomenon

occurs in this limit for high pressure and/or long tubes where the magnitudes necessary are controlled by the ω_{1e} value. Thus when $\beta_{12} >> 1$, increasing L does not increase the flow rate of specie 1 significantly since the β_{12}^{-1} decrease of M_{10} is due to the increase in the perfect mixing limit which has been used to normalize M_{10}. Of course these results are valid for flow in either direction indicated by the sign of $(C_{10} - C_{1\infty})$. The value of M_{10} from (40) is plotted versus β_{12} in Figure 2, where it is the lowest curve among the family of curves shown schematically there.

Notice that

$$\phi = uL/\mathcal{D}_{12} = \beta_{12}\ (C_{10} - C_{1\infty})[\sinh \beta_{12}(1-X)]/\cosh \beta_{12} \tag{41}$$

is in this case much smaller than unity over most of the tube length even for large β_{12}. This result can be arrived at using the fact that $|C_{1\infty} - C_{10}| << \cosh \beta_{12}/(\cosh \beta_{12} - 1)$ when $C_1 << 1$ so that $|\phi| << \beta_{12}\ [\sinh \beta_{12}(1-X)]/[\cosh \beta_{12} - 1]$ which yields $|\phi| << 5$ if $\beta_{12} < 5$ and $|\phi| << (eX)^{-1}$ for $\beta_{12} \geq 5$. Thus in this special case, the condition necessary for the diffusion dominated solution to hold $u << u_1$, implies that $|\phi| << 5$ for $0.074 \leq X \leq 1$ which accounts for a majority of the tube length. It will become clear later that $|\phi| = |\Phi_{12}| << 1$ over the majority of the tube length L in any case where at least some of the species are in the diffusion dominated region. The rather loose bounds established above are adequate here but in each specific case they can be significantly lowered.

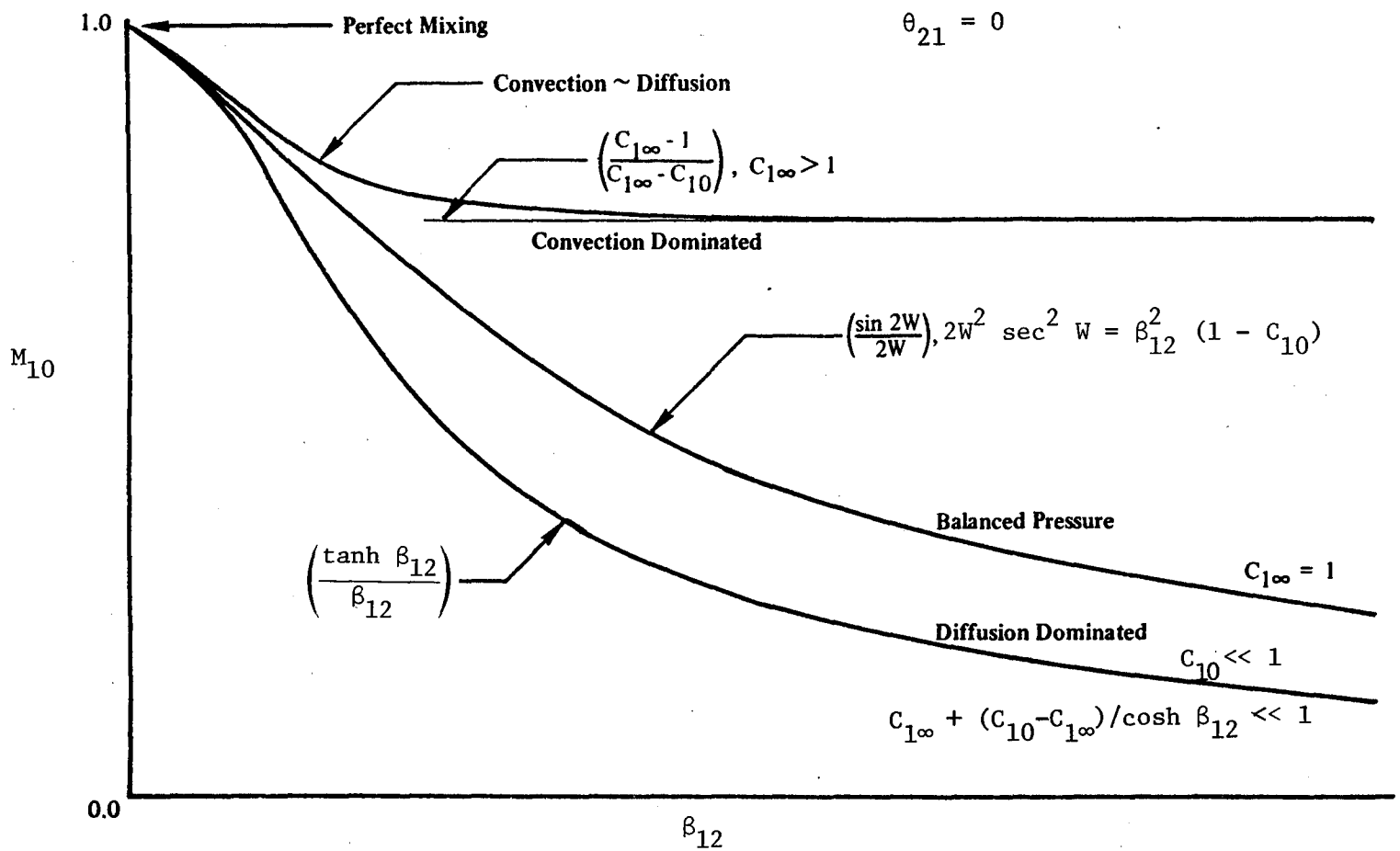

Figure 2. Root Mass Flow Ratio Versus β_{12} (Limiting Cases Schematic Diagram) For Binary Mixture, Perfect Filter, $\theta_{21} = 0$, Examples

Convection Dominated Limit

The other extreme, where the convection current (actually plug flow here due to the complete radial mixing) dominates the axial diffusion current and there is no axial mixing in tube bore, is obtained via $\mathcal{D}_{12} \to 0$ so that $u_1 = u_2 = u$ from (2). From (1) and the boundary condition at $X = 1$, an algebraic equation determines the value of C_1 at $X = 1$, $C_{11} = C_1(1)$, so that

$$(C_{11} - C_{1\infty})(C_{11} - 1) = 0 \tag{42}$$

and since in this limit (perfect filter and convection dominated) no mechanism exists which can allow a concentration gradient, the two cases

$$C_1 = C_{11} = C_{1\infty} \qquad M_1 = 0 \tag{43}$$

and $$C_1 = C_{11} = 1 \qquad M_1 = (1 - X)(C_{1\infty} - 1)/(C_{1\infty} - C_{10}) \tag{44}$$

result from (28) - (30). The trivial solution (43) valid for $C_{1\infty} \leq 1$ results for zero $C_{1\infty} = C_{10}$ or initially positive $C_{1\infty} < C_{10}$ velocity (flow into the tube at its open end or root) since specie 2 will just collect until C_1 is reduced to $C_{1\infty}$ and all flow stops, as well as some initially negative velocity cases where $C_{10} < C_{1\infty} \leq 1$. The non-trivial solution (44) valid for $C_{1\infty} > 1$ is for negative velocity (flow out at the root) since the non-permeating specie 2 is completely forced out of the tube bore due to the lack of a mixing mechanism. As opposed to the diffusion dominated case, the non-trivial convection dominated case (44) depends only on the pressure ratios $C_{1\infty}$ and C_{10} so that additional tube length always increases the flow rate via the u_o linear dependence on L

$$M_{10} = u_o/L\omega_{1e}\ (C_{10} - C_{1\infty}) = (C_{1\infty} - 1)/(C_{1\infty} - C_{10}) \tag{45}$$

which is shown schematically in Figure 2 as the family of horizontal lines labeled by M_{10} values less than unity, since (45) is independent of β_{12}. Therefore in this flow regime M_{10} is independent of all the physical uncertainties in the parameters contained in β_{12}. Figure 3 shows this perfect filter convection dominated case as a plot of M_{10} versus C_{10} with $C_{1\infty}$ as the parameter. Notice that

$$\phi = uL/\mathcal{D}_{12} = - \beta_{12}^2 \, (C_{1\infty} - 1)(1 - X) \tag{46}$$

for this case, so that $\beta_{12}^2 \, (C_{1\infty} - 1) >> 1$ is generally necessary; this results because it will become clear later that $|\phi| = |\Phi_{12}| >> 1$ is required over the majority of the tube length L (actually this is expected since $\mathcal{D}_{12} \to 0$ but $u = 0$ in general only at $X = 1$) in order that the convection dominated limit occur.

Balanced Pressure Limit

The two very different types of behavior exhibited by the diffusion limit (M_{10} dependent only on β_{12}) and the convection limit (M_{10} dependent only on C_{10} and $C_{1\infty}$) represent identifying characteristics of two classes of solutions $C_{1\infty} \lessgtr 1$ contained in the general perfect filter equations (28) - (33) which are separated (see Figure 2 schematic diagram) by a very special case, $C_{1\infty} = 1$, which implies $P_{1\infty} = P_o$ and thus is called the "balanced pressure" case here. In this limit the constants A_o and B_o in (32) and (33) can be determined via the boundary conditions (21) so that

$$(C_1 - 1)/(C_{10} - 1) = [\sec^2 W(1 - X)]/\sec^2 W \tag{47}$$

where W is an integration constant given in transcendental form as

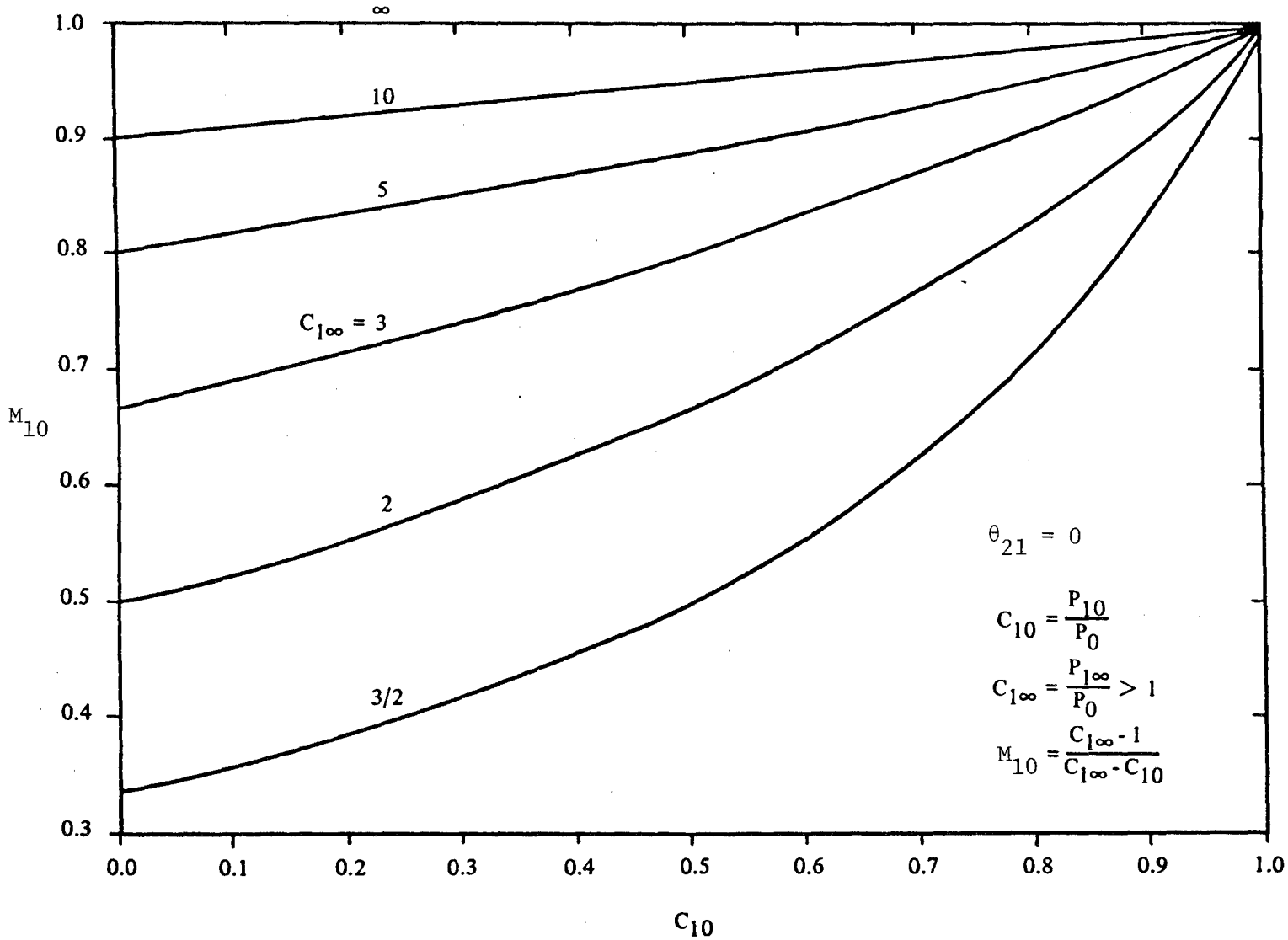

Figure 3. Root Mass Flow Ratio Versus C_{10} with $C_{1\infty} > 1$ Parameter (No Mixing $u_1 = u$) For Binary Mixture, Perfect Filter, $\theta_{21} = 0$, Example

$$2W^2 \sec^2 W = (\beta_{12})^2 \ (1 - C_{10}) \tag{48}$$

in terms of the parameters β_{12} and C_{10}. The solution for M_1 is

$$M_1 = [\tan W(1 - X)]/W \sec^2 W \tag{49}$$

which has the value

$$M_{10} = \sin 2 W/2 W \tag{50}$$

at X = 0 and showing the β_{12}^{-1} decay as β_{12} becomes large so that adding tube length does not increase the flow rate. This M_{10} depends on both β_{12} and C_{10} and it is plotted on Figure 4 versus β_{12} with C_{10} as the parameter. Notice that the family of curves is closely grouped for $0 \leq C_{10} \leq 0.6$ but rapidly fan out as C_{10} approaches unity. Also for the special example, the specific values for which are shown on the figure, the square root pressure scale for P_o in atmospheres is shown above the β_{12} scale to give an idea of the amount of reduction in M_{10} from unity (perfect mixing) which can occur. Note that since $C_{1\infty} = 1$ and $0 \leq C_{10} \leq 1$, then only negative velocity (flow out at the root) cases can occur in this limit. Also notice that

$$\phi = uL/\mathcal{D}_{12} = \beta_{12}^2 \ (1 - C_{10}) \ M_1 \tag{51}$$

for this case, which has no magnitude limitation since only $C_{1\infty} = 1$ is required.

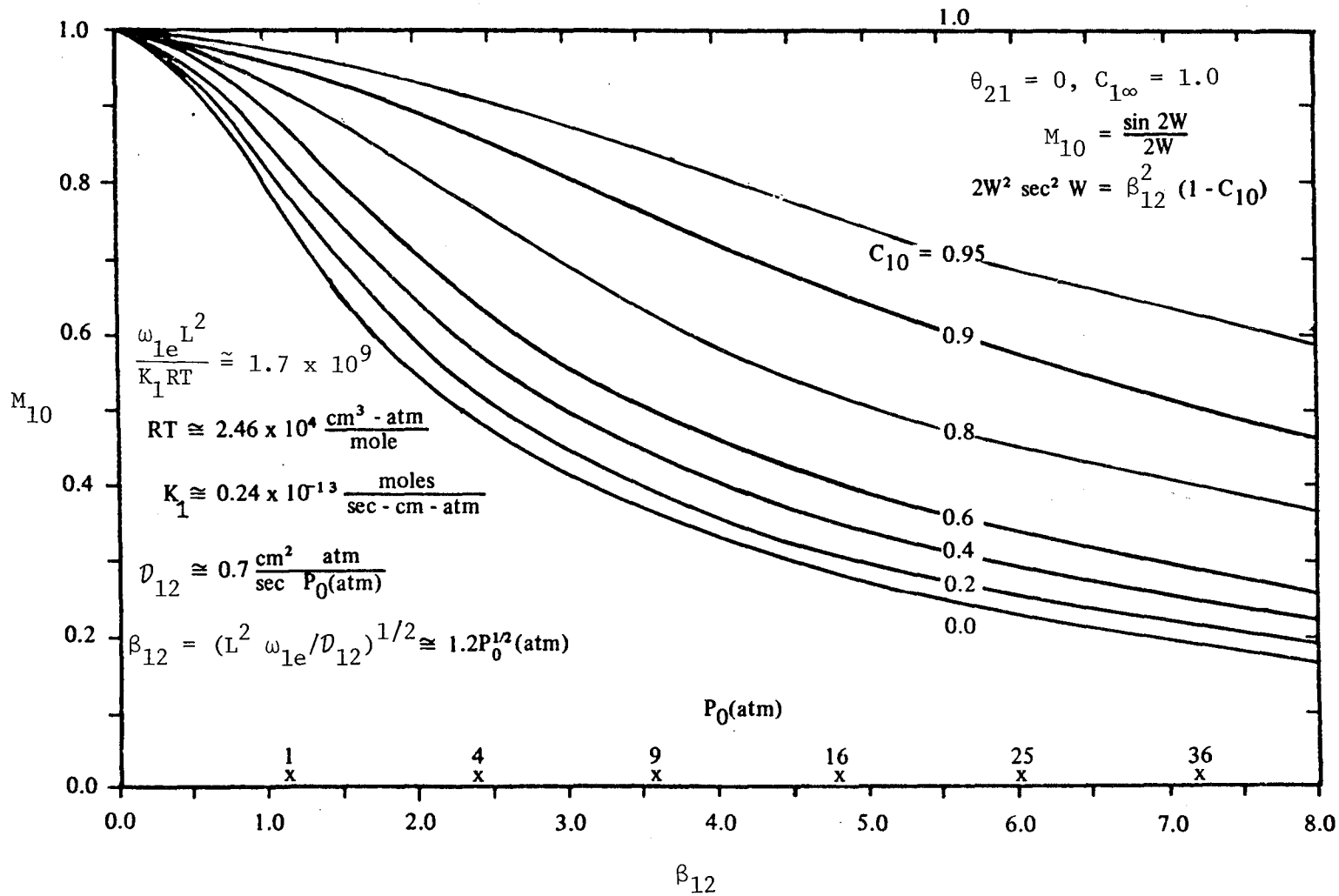

Figure 4. Root Mass Flow Ratio Versus β_{12} with C_{10} Parameter and $C_{1\infty} = 1$ (Balanced Pressure) For Binary Mixture, Perfect Filter, $\theta_{21} = 0$, Example

Real Filter $\Theta_{21} \neq 0$

When both species permeate the tube walls, (25) - (27) with boundary conditions (21) govern the problem. It is then of interest to re-examine the limiting solutions with $\Theta_{21} \neq 0$.

Diffusion Dominated Limit

The perfect mixing case ($\mathcal{D}_{12} \to \infty$) implies that $\Theta_{12} = \Theta_{21} \to 0$ and $dC_1/dX = dC_2/dX = 0$ so that

$$C_1 = 1 - C_2 = C_{10} \tag{52}$$

$$M_1 = M_2 = 1 - X \tag{53}$$

similar to (34) and (35).

For finite $\mathcal{D}_{12}$ the conditions and solutions (38) - (40) are the same for specie 1 as in the perfect filter limit, except the magnitude of C_1 is no longer restricted to be much less than unity; instead

$$C_1 \, |1 + \Theta_{21} \, M_2/\Theta_{12} \, M_1| \ll 1 \tag{54}$$

is required in order that $|u| \ll |u_1|$ be true. For specie 2, if $|u| \ll |u_2|$ so that $|C_2 \, \Phi_{21}| \ll |\Theta_{21} \, M_2|$, it is required that

$$C_2 \, |1 + \Theta_{12} \, M_1/\Theta_{21} \, M_2| \ll 1 \tag{55}$$

with the result that the diffusion dominated limit is approached and

$d^2 C_2/dX^2 = \beta_{21}^2 (C_2 - C_{2\infty})$. The mole fraction of specie 2 is

$$(C_2 - C_{2\infty})/(C_{20} - C_{2\infty}) = [\cosh \beta_{21} (1 - X)]/\cosh \beta_{21} \tag{56}$$

similar to (38) and M_2 is

$$M_2 = [\sinh \beta_{21} (1 - X)]/\beta_{21} \cosh \beta_{21} \tag{57}$$

similar to (39). Note that (54) reduces to $C_1 << 1$ if $\Theta_{21} = 0$ so that the limits on C_{10}, $C_{1\infty}$ and β_{12} given previously are obtained. Similarly (54) and (55) used with (38), (39), (56), and (57) determine the limits on C_{10}, C_{20}, $C_{1\infty}$, $C_{2\infty}$, β_{12} and β_{21} required if both species are in the diffusion dominated regime; it is important to recognize, however, that it is possible for only one of the two species (say specie 1) to be in the diffusion dominated regime so that (38) and (39) hold, but the solution for the other specie (specie 2) must be determined from (26) using $C_2 = 1 - C_1$. In such a case it is the M_2 from (26) not (57) which is used in (54) to determine the parameter limitations and of course (55) is dropped. The special case $\Theta_{21} = 0$ is an example of such a situation but where the solution for M_2 is not even needed as it is zero. Another special case where both (54) and (55) are satisfied via $u \to 0$, so that there is no restriction on C_1 and C_2 other than $C_1 + C_2 = 1$, results when $\Theta_{21} M_2 = - \Theta_{12} M_1$ so that

$$\beta_{12} (C_{1\infty} - C_{10}) \cosh \beta_{21} \sinh \beta_{12} (1 - X)$$

$$= \beta_{21} (C_{20} - C_{2\infty}) \cosh \beta_{12} \sinh \beta_{21} (1 - X) \tag{58}$$

gives the parameter limitations. Since (58) can be satisfied for all X only if $\beta_{12} = \beta_{21}$ with the result that $(C_{1\infty} - C_{10}) = (C_{20} - C_{2\infty})$, the very special nature of this case is evident.

Due to the similarity of (56) and (57) to (38) and (39) no further discussion or plots for this case are required. On the other hand, it is of interest to briefly examine the magnitude of $\phi = uL/\mathcal{D}_{12}$ when $\Theta_{21} \neq 0$. When $|u| << |u_1|$, ϕ can be written

$$\phi = (-u/u_1)(dC_1/dX)(C_1)^{-1} \tag{59}$$

and since

$$dC_1/dX = (C_{1\infty} - C_{10})\ \beta_{12}\ [\sinh \beta_{12}\ (1 - X)]/\cosh \beta_{12} \tag{60}$$

one can show that $|dC_1/dX| < 5$ for $0.074 \leq X \leq 1$ using $0 \leq C_1 \leq 1$ and the same reasoning given below (41). These loose bounds imply that $|\phi| << 5/C_1$ which is an adequate indication that $|\phi|$ must be small over most X values in this limit except when C_1 is very small. Since (59) can be written

$$\phi = (dC_1/dX)(1 + C_1\ u_1/C_2\ u_2) \tag{61}$$

then in the limit of small C_1 ($C_1 \to 0$), ϕ approaches dC_1/dX which can be shown to be small over most X values via the same reasoning following (41).

Thus if either or both of the species are in the diffusion dominated regime, it appears that ϕ must be small compared to unity over most of the tube length; the fact that ϕ is small does not, however, imply that all the species are in the diffusion dominated regime. Again notice that the

diffusion dominated solution is valid for flow in either direction depending on the signs of $(C_{1\infty} - C_{10})$ and $(C_{2\infty} - C_{20})$ for the individual species and the sign of $u = \sum_i C_i u_i$ for the net flow which, of course, has been restricted to be much smaller than u_1 or u_2 in this limit.

Convection Dominated Limit

When $\Theta_{21} \neq 0$ the convection limit is very complex compared with the $\Theta_{21} = 0$ case. In the limit $\mathcal{D}_{12} \to 0$, $u_1 = u_2 = u$ and

$$M_1 = C_1 \, u/L\omega_{1e} \, (C_{10} - C_{1\infty}) = M_2 \, (\Theta_{21}/\Theta_{12}) \, C_1/(1 - C_1) \tag{62}$$

via (2) or (27), giving the governing differential equations.

$$dM_1/dX = (C_{1\infty} - C_1)/(C_{10} - C_{1\infty}) \tag{63}$$

$$M_1 dC_1/dX = C_1 \, (1 - C_1)(C_{1\infty} - C_1)/(C_{10} - C_{1\infty})$$

$$+ (\Theta_{21}/\Theta_{12}) \, C_1^2 \, (C_1 + C_{2\infty} - 1)/(C_{10} + C_{2\infty} - 1) \tag{64}$$

from (25) and (26). Equations (63) and (64) have solutions of vastly different nature depending on the flow direction, which is due in part at least to the flow direction dependence of the C_1 boundary condition at $X = 0$ in this limit. For this reason there is considerable value in applying the C_1 boundary condition at $X = 1$ where it can be determined by solving the algebraic (quadratic if $I = 2$) expression obtained from (64) when it is set equal to zero. In other words, since $M_{11} = M_1(X = 1) = 0$

$$C_{11} = C_1(1) = \left[- b \pm \sqrt{b^2 - 4\ ac}\right] \Big/ 2a \leq 1 \tag{65}$$

where

$$\left.\begin{aligned} a &= (1 - \omega_{2e}/\omega_{1e}) = (1 - \Omega_2), \\ b &= [\Omega_2\ (1 - C_{2\infty}) - (1 + C_{1\infty})], \\ c &= C_{1\infty} \end{aligned}\right\} \tag{66}$$

which indicate that the value of C_{11} is independent of C_{10} in this limit. Figure 5 gives the results from (65) via C_{11} versus $C_{1\infty}$ with $\Omega_2 = \omega_{2e}/\omega_{1e}$ and $C_{2\infty}/C_{1\infty}$ as parameters. The diagonal line passing through the origin is the no flow $C_{11} = C_{1\infty}$ line and all values above it, selecting the sign in (65) giving $C_{11} \leq 1$, are for positive velocity while those below $C_{11} = C_{1\infty}$ and $C_{11} = 1$ are for negative velocity. It is evident that the nature of the two regions varies considerably.

This difference carries forward into the solutions of (63) and (64); one class of solutions is obtained when $dC_1/dX = 0$, which contains all negative velocity cases (flow out of tube open end) as well as the no flow limit, and results when $C_{1\infty} + C_{2\infty} \geq 1$ so that

$$C_1 = C_{11} = 1 - C_2 \tag{67}$$

$$M_1 = (1 - X)(C_{1\infty} - C_{11})/(C_{1\infty} - C_{10}) \tag{68}$$

where M_2 is determined from (62) and C_{11} is obtained from (65) which reduces to the perfect filter solution if $\Omega_2 \to 0$. Since $C_{11} \leq 1$, then the perfect filter M_1 from (44) is never greater than the real filter M_1 from (68) (see Fig. 6). Note that (67) and (68) are just slightly modified from (44) to account via

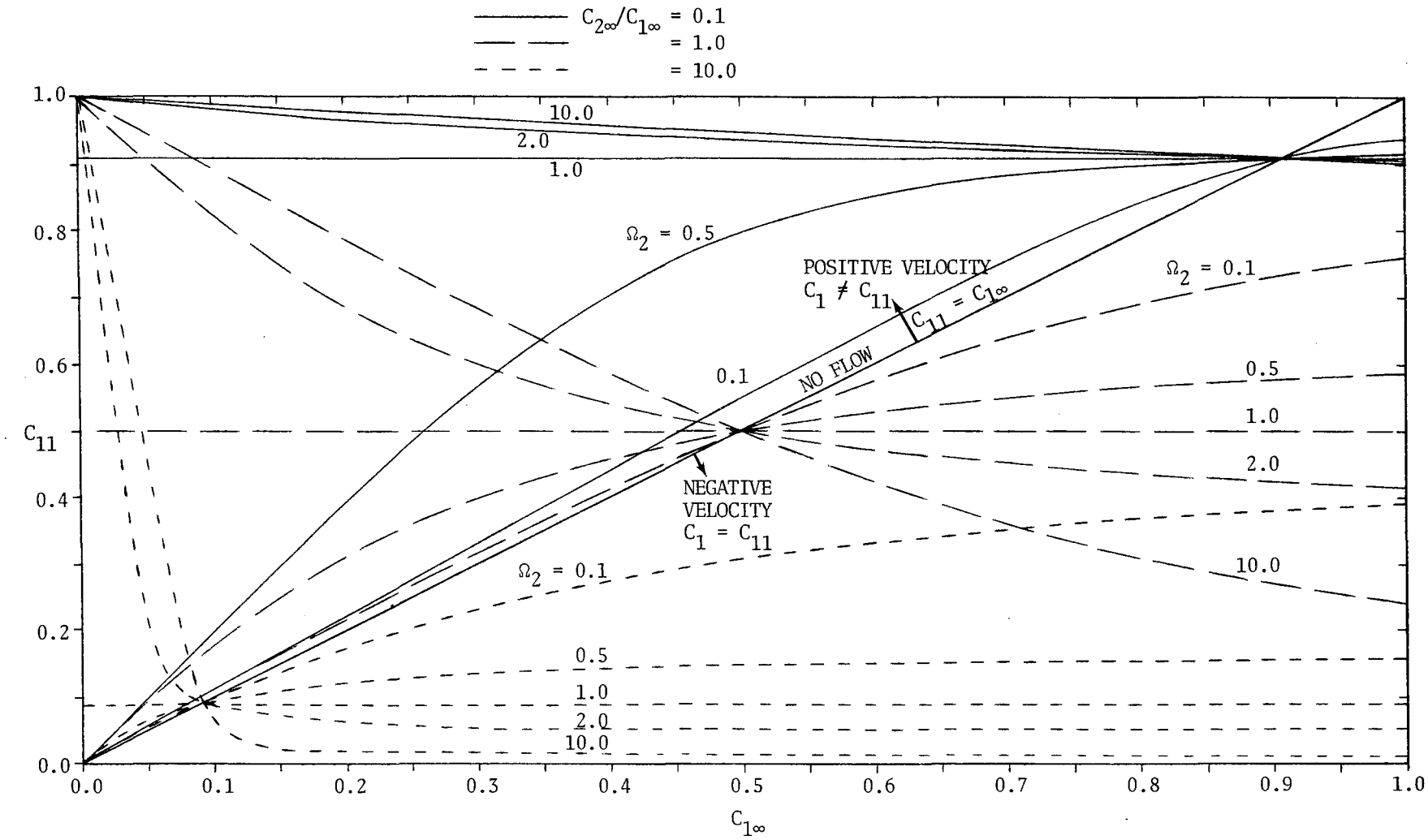

Figure 5. Convection Dominated Limit for Binary Mixture and Real Filter

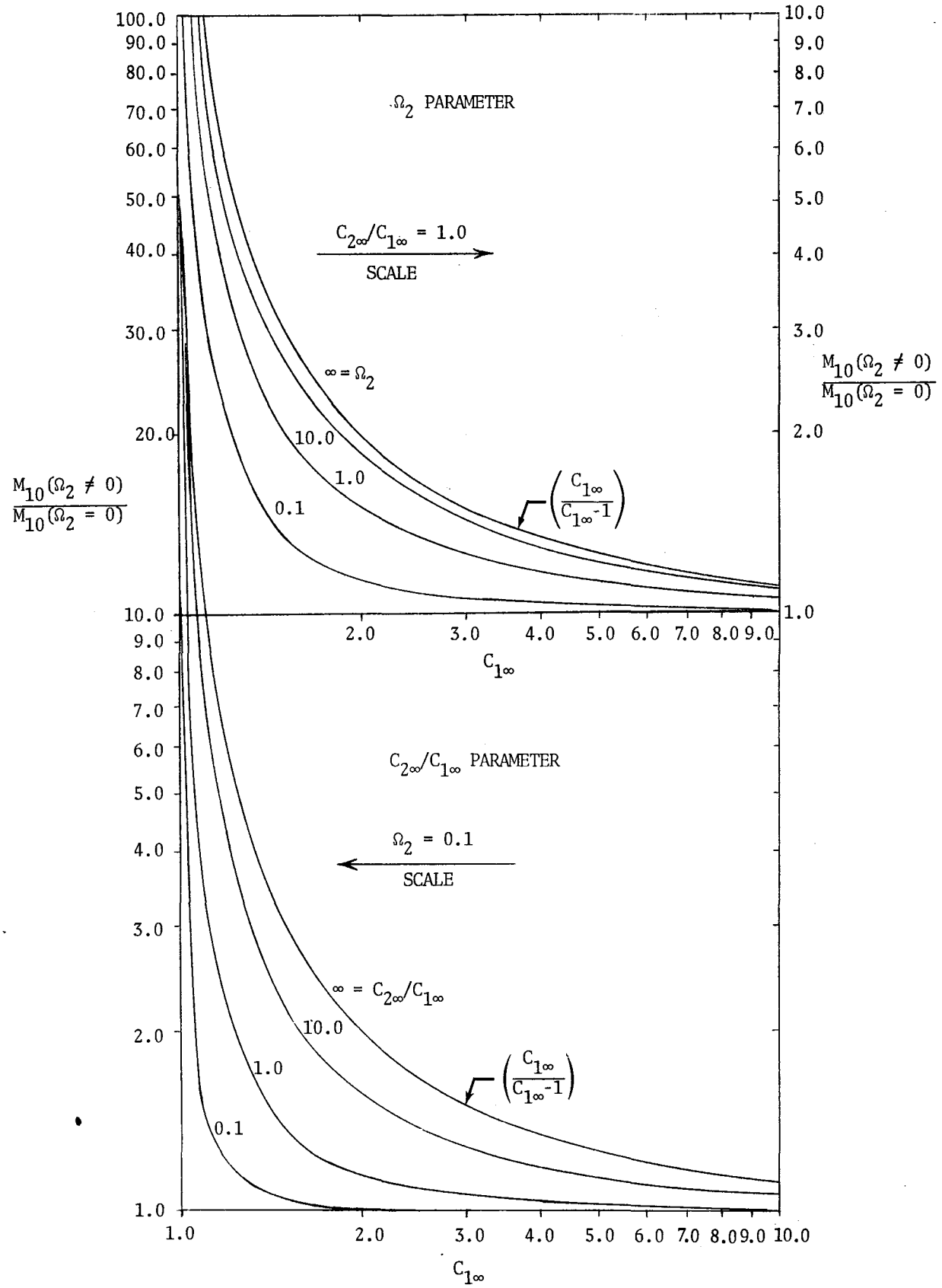

Figure 6. Real to Perfect Filter Flow Rate Ratio in Convection Limit

$C_{11} \neq 1$ for the proper mixture permeating the tube walls which then flushes all except that mixture from the tube due to the lack of a mixing mechanism. The solution becomes independent of the boundary condition $C_1 = C_{10}$ at $X = 0$ in this limit, which in fact is no longer valid as is shown by (67). Also observe that in this limit

$$\phi = - \beta_{12}^2 \, (C_{1\infty} - C_{11})(1 - X)/C_{11} \tag{69}$$

which is slightly modified from (46) to account for $C_{11} \neq 1$ when $\Theta_{21} \neq 0$. Although the appearance of (67) - (69) is very similar to (44) - (46), to which they reduce when $C_{11} \to 1$ as $\Theta_{21} \to 0$, this is somewhat deceptive since (67) - (69) can display much different physical behavior from that shown by (44) - (46). Equations (44) - (46) are valid for $C_{1\infty} > 1$ so that $C_{1\infty} > C_{10}$ and M_1 is positive and narrowly bounded $0 \leq M_1 \leq 1$ with $\beta_{12}^2 \, (C_{1\infty} - 1) >> 1$ being required to guarantee that the convection dominated limit holds. Equations (67) - (69) are valid for $C_{1\infty} + C_{2\infty} \geq 1$ where $C_{11} \leq C_{1\infty}$ but $C_{11} \lesseqgtr C_{10}$ and $C_{1\infty} \lesseqgtr C_{10}$ so that $- \infty < M_1 < \infty$ with $\beta_{12}^2 \, (C_{1\infty}/C_{11} - 1) >> 1$ being required to guarantee that the convection dominated limit holds. The physical meaning of this greatly expanded M_1 range is discussed briefly following the derivation of the other class of solutions.

The other class of solutions contained in (63) and (64) besides (67) and (68) is obtained when $dC_1/dX \neq 0$, which holds for all positive velocity cases (flow into open end of tube), and results when $C_{1\infty} + C_{2\infty} < 1$. In this case the differential equation obtained from (63) and (64)

$$f(d^2 \, C_1/dX^2) + F(d \, C_1/dX)^2 = 0 \tag{70}$$

must be solved using

$$\left.\begin{aligned} f = f\ (C_1) &= a\ C_1^2 + b\ C_1 + c \\ \text{and} \qquad & \\ F = F(C_1) &= -\ (1 + 2b + 3aC_1) \end{aligned}\right\} \tag{71}$$

where a, b and c are given by (66). After much manipulation the solution to (70) can be expressed

$$X = x/L = [1 - (Z/Z_o)(Y/Y_o)^{\alpha+1/2}] \tag{72}$$

which gives for M_1

$$M_1 = K(1 - X)\ C_1 \left(2a\ C_1 + b - 2\alpha\sqrt{b^2 - 4ac}\right)^{-1} \tag{73}$$

where the boundary conditions (21) have been applied and the subscript o on Z and Y indicates X = 0 values. The functions $Y = Y(C_1)$ and $Z = Z(C_1)$ (not to be confused with the compressibility factor) are defined as

$$Y = \left(2a\ C_1 + b + \sqrt{b^2 - 4ac}\right) \Big/ \left(2a\ C_1 + b - \sqrt{b^2 - 4ac}\right) \tag{74}$$

$$Z = \left(2a\ C_1 + b - 2\alpha\sqrt{b^2 - 4ac}\right) \Big/ \left(2a\ C_1 + b + \sqrt{b^2 - 4ac}\right) \tag{75}$$

and the constants K (not to be confused with the permeability coefficient) and α are

$$K = (b^2 - 4ac)(0.5 - 2\alpha^2)(C_{10} - C_{1\infty})^{-1} \tag{76}$$

$$\alpha = [\Omega_2 (1 - C_{2\infty}) + (1 - C_{1\infty})]/2\sqrt{b^2 - 4ac} \tag{77}$$

where using (66)

$$b^2 - 4ac = \{\Omega_2^2 (1 - C_{2\infty})^2 + (1 - C_{1\infty})^2 + 2\Omega_2 [C_{2\infty} (1 + C_{1\infty}) + (C_{1\infty} - 1)]\}. \tag{78}$$

Although the negative velocity cases given by (67) and (68) using (65) and (66) are very simple (aside from the wide M_1 range discussed below) due to C_1 being constant and M_1 being linear, the positive velocity cases given by (72) - (78) are more complex and need further discussion. Figures 7 and 8 give a specific example where $\omega_{2e} = 2\omega_{1e}$ or $\Omega_2 = 2$ and where $C_{1\infty} = C_{2\infty} = 0.15$. Figure 7 gives C_1 versus X with C_{10} as the parameter while Figure 8 gives M_1 versus X with C_{10} as the parameter. For the set of parameter values selected, Figure 5 or (65) and (66) indicate that $C_{11} = C_1$ (X = 1) = 0.75 in all cases no matter what value of C_{10} is used; also note that C_{11} depends on only the ratio of ω_{2e} and ω_{1e} not their magnitude. Figure 7 shows that C_1 may either decrease or increase from C_{10} to that C_{11} value depending on C_{10} being greater or less than C_{11}, respectively. Physically the V_o mixture identified by C_{10} is carried into the tube at X = 0 and must adjust to the C_{11} value at X = 1 which is compatible with the tube wall characteristics and the V_∞ mixture but independent of C_{10}. Figure 8 shows that M_1 (similar to the negative velocity case) has a wide range $-\infty < M_1 < \infty$, although the velocity for this example is always positive [the M_1 sign change is due to the sign change of $(C_{1\infty} - C_{10})$]. Notice that at X = 0, $dM_1/dX = -1$ and that $M_{11} = M_1(1) = 0$ for all C_{10} values; however, $M_{10} = M_1(0)$ must be adjusted until the latter condition is true so that M_{10} is different for each C_{10} value. In fact this procedure, which is automatically accomplished via (72) - (78), not only

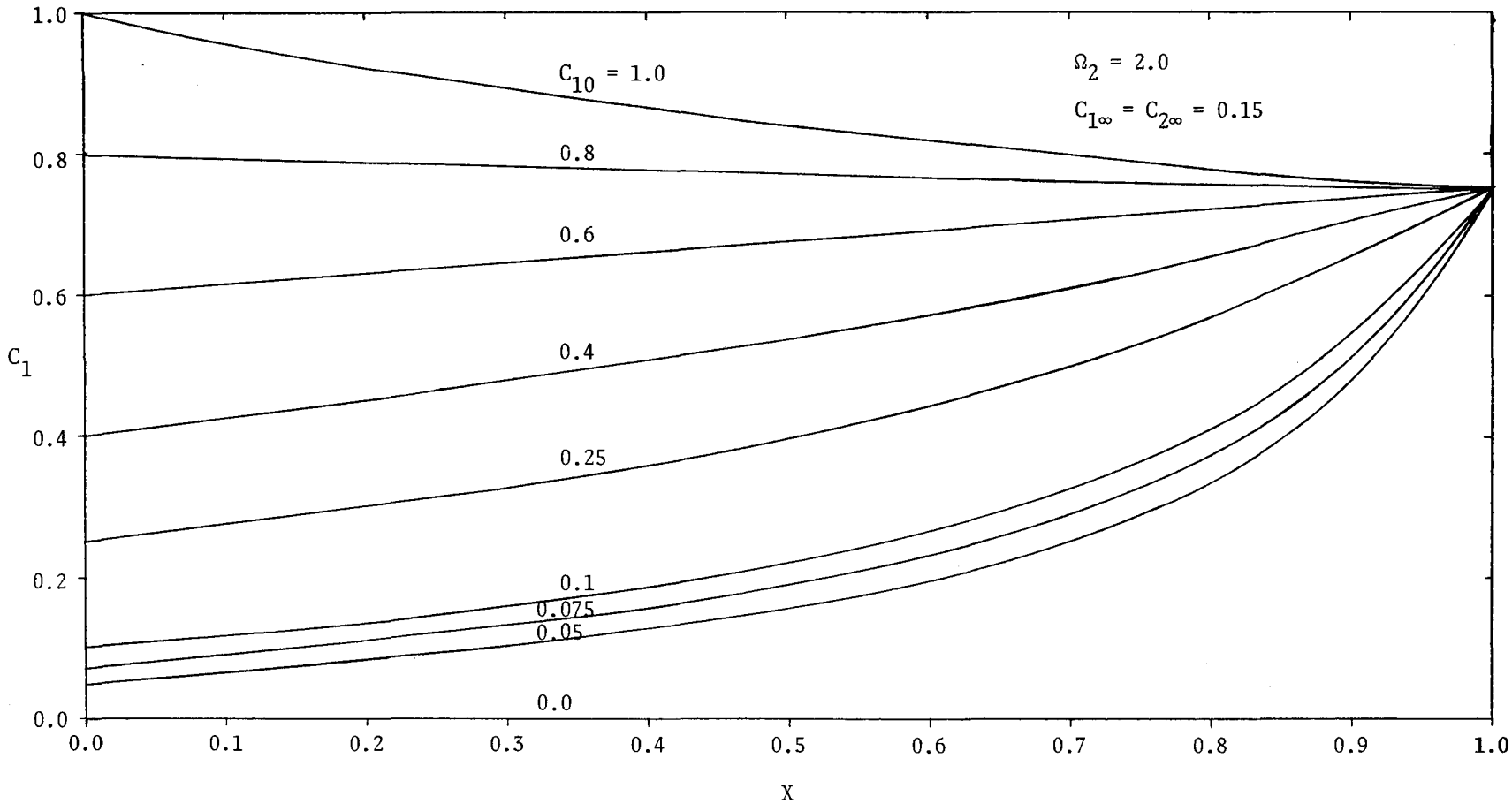

Figure 7. Convection Example with Positive Velocity, C_1 versus X

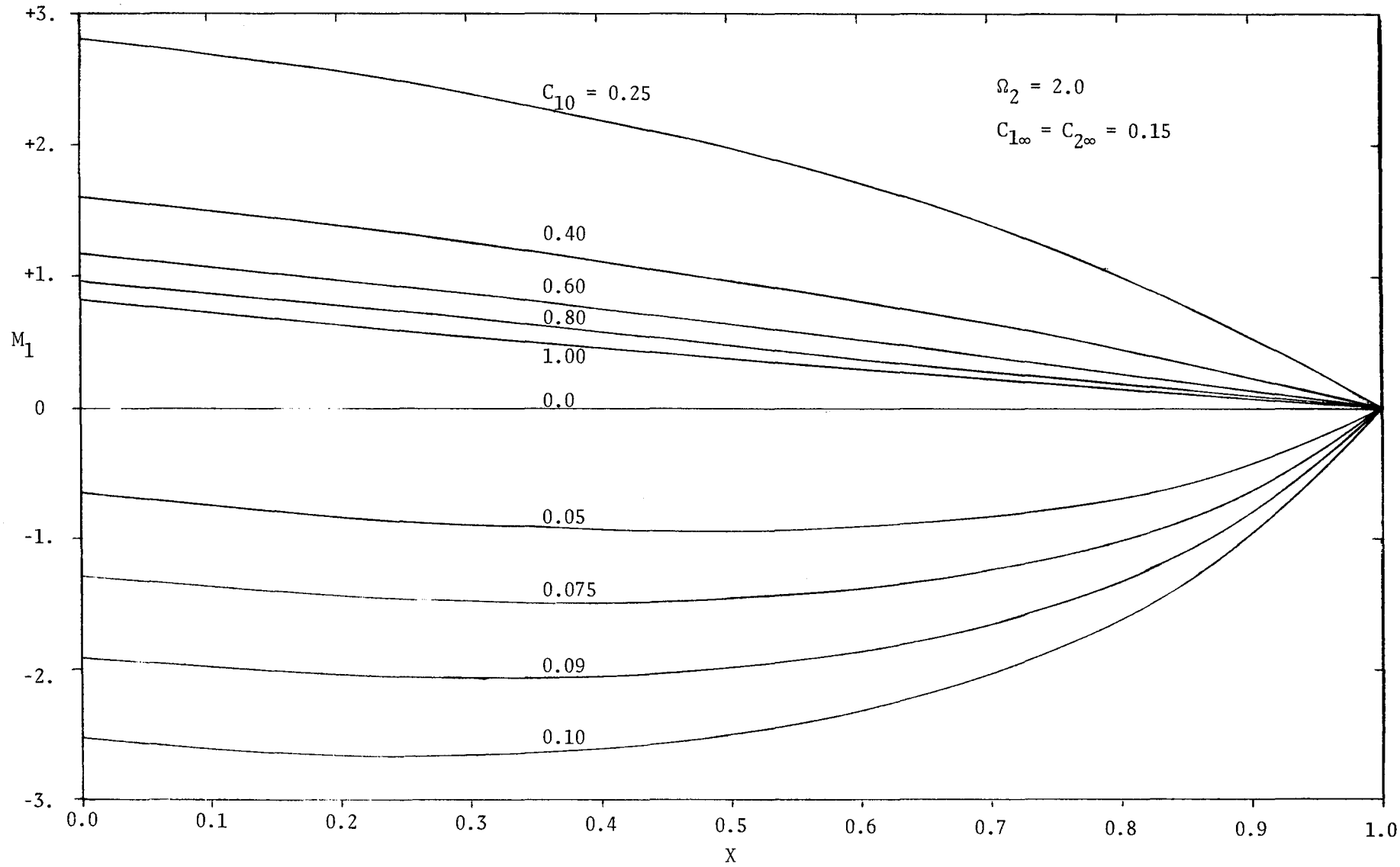

Figure 8. Convection Example with Positive Velocity, M_1 versus X

yields some negative values for M_1 which must exhibit a minimum where $dM_1/dX = 0$ at some $0 \leq X \leq 1$ but also yields values greater than unity. The physical meaning of both of these phenomena are discussed at great length later as well as possible means of exploiting these effects in applications. A brief indication of their physical meaning is given here, however. Negative M_1 values indicate that the actual flow direction of specie 1 (which in this limit $\mathcal{D}_{12} \to 0$ is the same for all species) is opposite to that which would exist if perfect mixing $\mathcal{D}_{12} \to \infty$ were present. Values of M_1 greater than unity at $X = 0$ $[M_1(0) = M_{10} > 1]$ indicate that the flow rate of specie 1 is greater than the perfect mixing $(\mathcal{D}_{12} \to \infty)$ flow rate. The physical reason that these phenomena can occur in the convection dominated limit (or near this limit), while M_1 is always narrowly bounded $0 \leq M_1 \leq 1$ in the diffusion dominated limit, is that as $\mathcal{D}_{12} \to 0$, $u_1 = u_2 = u$; thus when specie 2 is the controlling specie, it determines both the sign and magnitude of velocity for specie 1 independent of those for perfect mixing which have been used for normalization because that limit is the most common assumption.

$I \geq 3$ (TERNARY MIXTURE OR GREATER NUMBER OF SPECIES)

The general governing equations (15) - (21) do not lend themselves to extensive simplification when $I \geq 3$, although the use of $\sum_{i=1}^{I} C_i = 1$ does reduce the differential equations to a set of (2I - 1) first-order equations. Even if the δ_{ij} are taken to be approximately unity, then (3I - 1) independent dimensionless parameters in the form of $\beta_{ij}^2, C_{i\infty}$ and C_{io} using $\sum_{i=1}^{I} C_{io} = 1$ must be specified to identify a particular solution. Some limiting solutions can be obtained, however, and they help a great deal in understanding the general results generated numerically later in this report.

Diffusion Dominated Limit

As before, first consider the perfect mixing ($\mathcal{D}_{ij} \to \infty$) special case which implies that $dC_i/dX = 0$ so that

$$C_i = C_{io}, \quad i = 1, 2, \ldots, I \tag{79}$$

$$M_i = 1 - X \tag{80}$$

similar to (52) and (53).

For finite $\mathcal{D}_{ij}$ the problem is diffusion dominated for a specie i if $|u| << |u_i|$ so that $|C_i \Phi_{ij}| << |\Theta_{ij} M_i|$ giving the governing differential equation

$$d^2 C_i/dX^2 = \beta_{ij}^2 (C_i - C_{io}). \tag{81}$$

Equation (81) yields the mole fraction C_i for specie i

$$(C_i - C_{i\infty})/(C_{io} - C_{i\infty}) = [\cosh \beta_{ij} (1 - X)]/\cosh \beta_{ij} \tag{82}$$

and the M_i expression follows from (15)

$$M_i = [\sinh \beta_{ij} (1 - X)]/\beta_{ij} \cosh \beta_{ij} \tag{83}$$

which are both bounded between zero and unity ($0 \leq C_i \leq 1$, $0 \leq M_i \leq 1$).

Equations (82) and (83) display the same mathematical characteristics which were discussed following (38) and (40). It is possible for some species to be in the diffusion dominated region where (82) and (83) hold $|u| << |u_i|$, while other species are not in that region so that for those species (15) - (20)

must be used. The fact that $\phi = \Phi_{ij} = uL/\mathcal{D}_{ij}$ must be small in order for any of the species to be in the diffusion dominated regime can be shown via generalizations of (59) and (60)

$$\phi = (-\ u/u_i)(d\ \ell n\ C_i/dX) \tag{84}$$

$$(d\ C_i/dX) = (C_{i\infty} - C_{io})\ \beta_{ij}\ [\sinh \beta_{ij}\ (1 - X)]/\cosh \beta_{ij} \tag{85}$$

valid for $|u| << |u_i|$, so that following the reasoning below (41) and (60) one can show that $|\phi| << 5/C_i$ over most of the tube length. Similarly the generalization of (61)

$$\phi = (-dC_j/dX)\left[1 + \sum_{\substack{i=1 \\ i\neq j}}^{I} (C_i\ u_i/C_j\ u_j)\right] \tag{86}$$

can be used in the limit of very small C_i to show that $|\phi|$ must remain small even in that limit. As stated before, small ϕ is a necessary but not sufficient condition for a specie to be in the diffusion dominated region. For any specie i it is sufficient that $|\sum_{i=1}^{I} C_i\ u_i| << |u_i|$ in order that (82) and (83) hold; this condition can be expressed analogous to (54) and (55) as $|C_i\ \Phi_{ij}| << |\Theta_{ij}\ M_i|$ or

$$C_j\ \left|1 + \sum_{\substack{i=1 \\ i\neq j}}^{I} (\Theta_{ik}\ M_i/\Theta_{jk}\ M_j)(\delta_{ik}/\delta_{jk})\right| << 1 \tag{87}$$

which determines the limits on C_{io}, $C_{i\infty}$, β_{ij} and δ_{ij} when used with the appropriate C_i and M_i values. When (87) holds M_i is mathematically (via 83) bounded, $0 \leq M_i \leq 1$. Equation (82) mathematically bounds C_i to be between C_{io} and $C_{i\infty} + (C_{io} - C_{i\infty})/\cosh \beta_{ij}$ when (87) holds, but by definition C_i is bounded

also $0 \leq C_i \leq 1$ so that the mathematical bounds from (82) must not violate this definition or the physical bound established by (87).

Convection Dominated Limit

In the limit $\mathcal{D}_{ij} \to 0$, $u_i = u$ and (actually it is sufficient if $|u| >> |\mathcal{D}_{ij}\ d\ \ell n\ C_i/dx|$)

$$M_i = M_j (\Theta_{jk}/\Theta_{ik})(C_i/C_j)(\delta_{jk}/\delta_{ik}) \tag{88}$$

so that the governing equations are greatly simplified. Perhaps this is most clearly observed from (1) and (2). Equation (2) yields nothing but $u_i = u$ and (1) can be written (note $M_i = C_i\ u/L\omega_{ie}(C_{io} - C_{i\infty})$ here)

$$(u/L\omega_{1e})(dC_i/dX) = \Omega_i\ (C_{i\infty} - C_i) - C_i \sum_{i=1}^{I} \Omega_i\ (C_{i\infty} - C_i) = A_i \tag{89}$$

where

$$d\ (u/L\omega_{1e})/dX = \sum_{i=1}^{I} \Omega_i\ (C_{i\infty} - C_i) = B_i \tag{90}$$

and

$$\Omega_i = \omega_{ie}/\omega_{1e}. \tag{91}$$

Therefore, as in the binary mixture case, it can be expected that very different results will be obtained depending on the sign of u. Notice that by definition $\Omega_1 \equiv 1$ in (89) - (91).

Again, as in the binary case, it is of value to consider the C_i boundary condition at X = 1 which is determined in this limit by setting A_i from (89) equal to zero. Thus the $C_{i1} = C_i$ (X = 1) are obtained by solving the algebraic equations

$$C_{i1} = \Omega_i \ (C_{i\infty} - C_{i1}) / \sum_{i=1}^{I} \Omega_i \ (C_{i\infty} - C_{i1}) \tag{92}$$

which reduce to a quadratic equation using $\sum_{i=1}^{I} C_{i1} = 1$ when $I = 2$ giving the solution (65). Generally (92) must be solved numerically for the C_{i1} values as a function of the parameters Ω_i and $C_{i\infty}$, but this is a straightforward task which is easily accomplished. The results are very similar to the binary case in that the regions of positive velocity and negative velocity are separated by the no flow case $\sum_{i=1}^{I} C_{i\infty} = 1$.

In the negative velocity case as well as the no flow limit $d\,C_i/dX = 0$ and $\sum_{i=1}^{I} C_{i\infty} \geq 1$ with the results that, similar to (67) and (68),

$$C_i = C_{i1} = C_i \ (X = 1) \tag{93}$$

$$M_i = (1 - X)(C_{i\infty} - C_{i1})/(C_{i\infty} - C_{io}) \tag{94}$$

where the C_{i1} are obtained from (92). Obviously nothing fundamentally new is introduced by (91) - (94) over that already given by (65) - (68) for $I = 2$, except additional mathematical complexity which is easily handled via numerical calculations. Thus no further analysis is required at this point for the negative velocity case.

In the positive velocity case $dC_i/dX \neq 0$ and $\sum_{i=1}^{I} C_{i\infty} < 1$ so that (89) and (90) combine to give

$$A_i \ (d^2C_i/dX^2) - (dA_i/dX)(dC_i/dX) + B_i \ (dC_i/dX)^2 = 0 \tag{95}$$

which can be rewritten

$$A_i \; (d^2C_i/dX^2) + (\Omega_i + 2B_i)(dC_i/dX)^2 - C_i \; (dC_i/dX) \sum_{i=1}^{I} \Omega_i \; (dC_i/dX) = 0 \qquad (96)$$

the solution of which is needed only for i = 1, 2, . . ., I-1 since $\sum_{i=1}^{I} C_i = 1$. It appears, except for the exact solution (72) - (78) already given for the I = 2 case, that (96) must be solved by numerical techniques as will be done in the following pages.

That $\Phi_{ij} = uL/\mathcal{D}_{ij}$ from (17) must in general be large in order for the convection dominated regime to occur can be shown via (2). From (2) it can be seen that $u_i \simeq u$ if $|u| >> |\mathcal{D}_{ij} \; d \; \ell n \; C_i/dx|$ which can be expressed $|\Phi_{ij}| >> |C_i^{-1} \; dC_i/dX|$. Of course the Φ_{ij} are about the same $\phi = \Phi_{ij}$ for all species if the $\mathcal{D}_{ij}$ are about the same magnitude. The criteria stated above must hold for most of the X range $0 \leq X \leq 1$ if a specie is to be considered in the convection regime. Thus for $|\phi| >> 1$ to be used as a necessary and sufficient condition specifying the convection regime, it must be shown that $C_i^{-1} \; dC_i/dX$ is bounded over most X values between zero and unity. The examples given in this work adequately demonstrate that $C_i^{-1} \; dC_i/dX$ is bounded except near X = 0 for negative u and near X = 1 for positive u values. In fact for negative velocity, the C_i become constant (93) over most X so that dC_i/dX approaches zero in that convection limit. Such is not the case for positive velocity, however examples like the one shown on Figure 7 are ample proof that $C_i^{-1} \; dC_i/dX$ is well bounded except near X = 1. Hence $|\phi|>>1$ can serve as both the necessary and sufficient condition that the convection limit is present.

As a final point, it should be noted that the balanced pressure limiting solution given by (47) - (50) for I = 2 and $\Theta_{21} = 0$, apparently has no useful meaning for more general cases; hence it is not examined as a limiting case beyond that special case which was meaningful.

(ii) Numerical Results (Arbitrary C_{i0}, $C_{i\infty}$, β_{ij}, δ_{ij})

The limiting solutions (22)-(96) are valid only for special sets of the determining parameters C_{i0}, $C_{i\infty}$, β_{ij}, δ_{ij} which yield either $u_i \to u$ or $|u_i| >> |u|$, except for the one balanced pressure case where $C_{1\infty} = 1$ when $I = 2$ and $\Theta_{21} = 0$. These limiting solutions provide the framework needed to understand the results obtained by numerical integration of (15) and (16) with boundary conditions (21) for arbitrary C_{i0}, $C_{i\infty}$, β_{ij} and δ_{ij} values. The numerical results generated for each set of controlling parameters consist of C_i, M_i and Φ_{ij} plotted versus X, although in some cases a plot of M_{i0} versus a parameter such as β_{ij} for various C_{i0} and $C_{i\infty}$ values is adequate.

Prior to examining specific examples, it is worth briefly reviewing the physical information carried by C_i, M_i, and Φ_{ij}. First notice that the sign of $(C_{i0} - C_{i\infty})$ indicates the flow direction (wall and bore) for specie i in the perfect mixing limit, $\mathcal{D}_{ij} \to \infty$. The sign of $(C_i - C_{i\infty})$ indicates the local wall flow direction for specie i for arbitrary $\mathcal{D}_{ij}$. It is found that C_i may either increase or decrease from C_{i0} at $X = 0$ and that $(C_i - C_{i\infty})$ may in fact change sign for some $0 \leq X \leq 1$, so that a "<u>wall stagnation point</u>" exists locally for specie i when $C_i = C_{i\infty}$. Since M_i is $u_i C_i$ normalized by its corresponding root $(X = 0)$ value when perfect mixing $(\mathcal{D}_{ij} \to \infty)$ is approached, the value of M_i at the root, M_{i0}, is an important overall performance indicator as was shown in Figures 2-6. Thus $M_{i0} < 1$ or $M_{i0} > 1$ indicates dehancement or enhancement, respectively, of the total flow for specie i compared to the perfect mixing case. Also $M_{i0} < 0$ indicates that the other species are controlling the problem to the extent that specie i is flowing in the opposite direction at the root compared to that indicated

by $(C_{i0} - C_{i\infty})$ for perfect mixing. Even more physical information is carried by the local value of M_i as was shown in Figure 8. Of course $dM_i/dX = 0$ indicates that a local "wall stagnation point" exists since dM_i/dX is proportional to $(C_i - C_{i\infty})$. In addition, if $M_i = 0$ at some $0 \leq X \leq 1$, then a local "bore stagnation point" for specie i exists and the bore flow direction for that specie is different on opposite sides of that point. Of course in this application $M_i = 0$ at $X = 1$ via the boundary conditions (21). The "wall" and "bore" stagnation points are different physically and must not be confused. The sign of Φ_{ij} gives the net or global flow direction, which may or may not coincide with the flow direction of the individual species; whether it does or not depends in part at least on the flow regime present over most of the tube length (the relative amount of diffusion compared to convection). A necessary and sufficient condition for $u_i \to u$ (convection regime) is $|\Phi_{ij}| >> 1$, so that the magnitude of Φ_{ij} is a valuable indicator of flow regime. Small Φ_{ij} is a necessary (but not sufficient) condition for $|u_i| >> |u|$, (diffusion regime). Of course $\Phi_{ij} = 0$ indicates a global flow stagnation point, one of which is always present at $X = 1$. Another parameter which is sometimes useful in analysis of numerical examples is an "effective separation ratio" defined as

$$\Omega_{\text{eff } i} = \Omega_i \ (M_{i0}/M_{10}) \tag{97}$$

where Ω_i is the wall material separation ratio defined by (91). Equation (97) gives the apparent separation ratio which appears to exist for the wall material if one is not aware of the effects which the tube geometry and associated fluid mechanics can have on the problem when gas mixtures are involved. In general it is found that either $\Omega_{\text{eff } i} > \Omega_i$ or $\Omega_{\text{eff } i} < \Omega_i$ is possible and in fact $\Omega_{\text{eff } i} < 0$ can also occur.

The same format followed for the limiting solutions is also useful here, starting with the two specie case as the most simple non-trivial example.

I = 2 (BINARY MIXTURE)

In addition, as before, the binary mixture case is divided into the perfect filter cases where $\Omega_2 = 0$ and the real filter cases where $\Omega_2 \neq 0$.

Perfect Filters, $\Omega_2 = 0$

The schematic diagram on Figure 2, and Figures 3 and 4 describe the limiting case behavior of M_{10} for a perfect filter, $\Omega_2 = 0$. Figure 9 gives a specific example corresponding to the illustration shown on Figure 2 and includes not only the limiting cases but also the results between such special solutions. Figure 9 is for the case where specie 1 is absent in the receiver, $C_{10} = 0$, and $C_{1\infty}$ is used as the parameter; since $C_{1\infty} \geq C_{10}$ and $\Omega_2 = 0$, the entire family of curves shown on Figure 9 is for negative global velocity (flow out at the root). Note that $0 \leq M_{10} \leq 1$ here, and since $\Omega_2 = 0$ the value of M_{20} is irrelevant. However if this case is regarded as representative of the limit $\Omega_2 << 1$, then M_{20} is of interest too and it is found to be greater than unity, in some instances at least, since in the convection limit $M_{20} = (1 - C_{2\infty}^{-1})^{-1}$. The result is that $\Omega_{eff\ 2} \geq \Omega_2$ since in the convection limit $\Omega_{eff\ 2} = \Omega_2\ (1 - C_{1\infty}^{-1})^{-1}\ (1 - C_{2\infty}^{-1})^{-1}$ and $C_{1\infty} + C_{2\infty} \geq 1$. It should be observed from Figure 9 that when $C_{1\infty} > 1$, the convection dominated solutions (horizontal lines) apply to an increasingly broad range of β_{12} values as $C_{1\infty}$ increases. In Figure 9 all of the solutions for

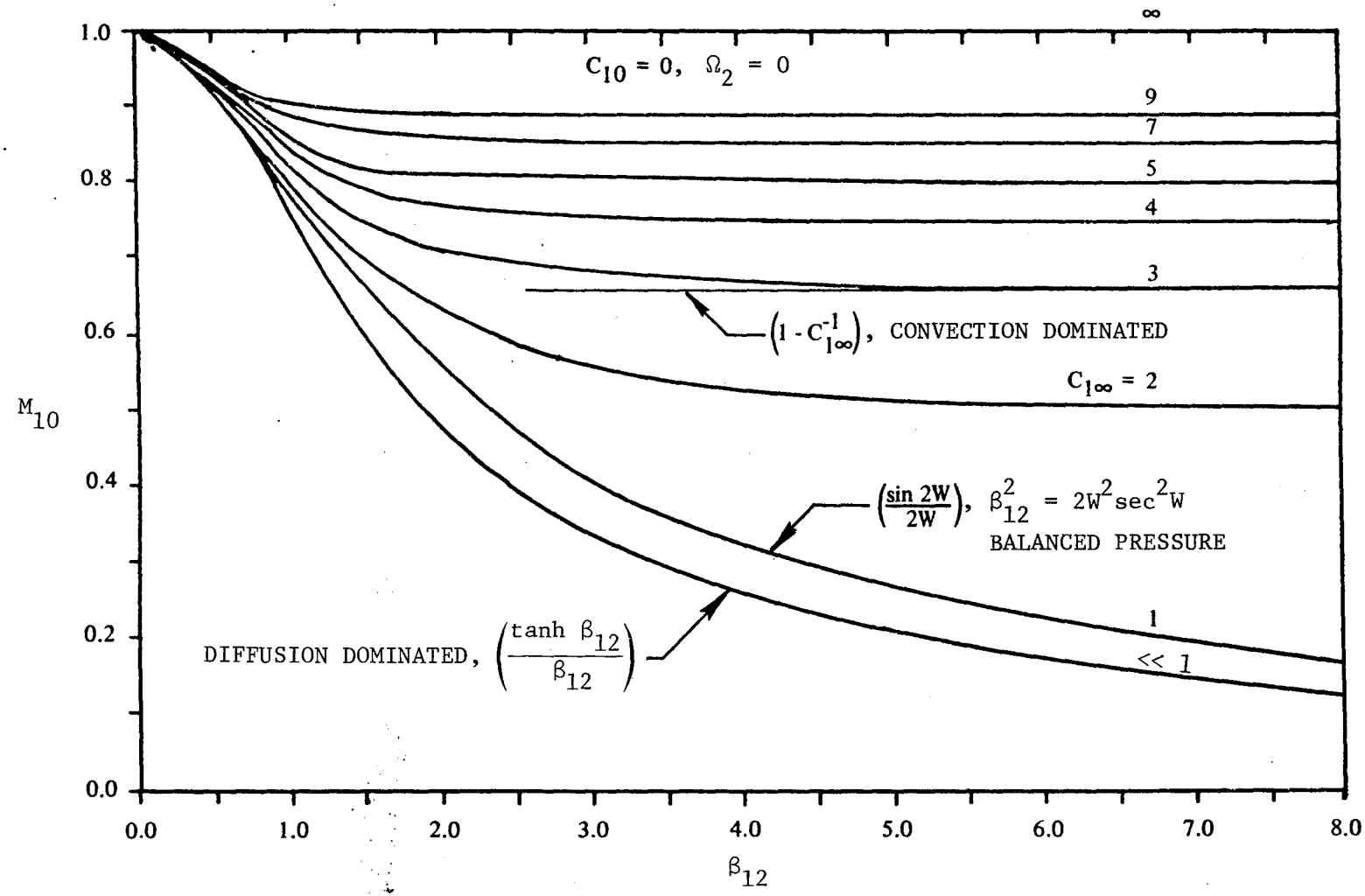

Figure 9. Root Mass Flow Ratio Versus β_{12} with $C_{1\infty}$ Parameter and $C_{10} = 0$ For Binary Mixture, Perfect Filter, $\Omega_2 = 0$, Example

$0 < C_{1\infty} < 1$ occupy the narrow region between the balanced pressure and the diffusion dominated solutions. This region is not so narrow for other values of C_{10} because the balanced pressure curve moves up, shrinking the $C_{1\infty} > 1$ region to nothing as C_{10} approaches unity, see Figure 4. Actually Figure 9 represents the worst perfect filter case (smallest M_{10}) since for $0 < C_{10} \leq 1$, the entire family of curves is shifted upward toward unity as is shown in Figures 10 and 11. Figure 10 gives another perfect filter example, but where $C_{1\infty}$ is fixed at 0.1 and C_{10} is the parameter. Here the entire family of curves, except the lowest one, is for positive global velocity (flow in at the root). The family of horizontal curves seen in Figure 9 for the convection limit is not present in Figure 10 because for positive velocity and $\Omega_2 = 0$, the convection limit yields $M_{10} = 0$ via (43). Figure 11 gives another perfect filter example where $C_{10} = 0.95$ and $C_{1\infty}$ is the parameter; here the lower three curves are for positive global velocity while the rest are for negative velocity. Notice that no solutions exist for this case which are near the diffusion dominated solution $\tanh \beta_{12}/\beta_{12}$. Figure 12 is a plot of M_1 versus X for this case. Notice that M_1 is linear with X for large $C_{1\infty}$ but becomes less and less linear as $C_{1\infty}$ becomes small. Figure 13 gives C_1 versus X and shows both increasing and decreasing C_1 distributions with $C_2 = 1 - C_1$ being the opposite; at this point little can be gained from additional perfect filter examples per se, although many others are required in the real filter analysis.

Real Filters, $\Omega_2 \neq 0$

The real filter solutions are best discussed by means of comparisons with perfect filter solutions. Figures 14-16 give one such example consisting of plots for M_i, C_i and $-\phi$ versus X. Curves are given for $\Omega_2 = 0$, 0.1

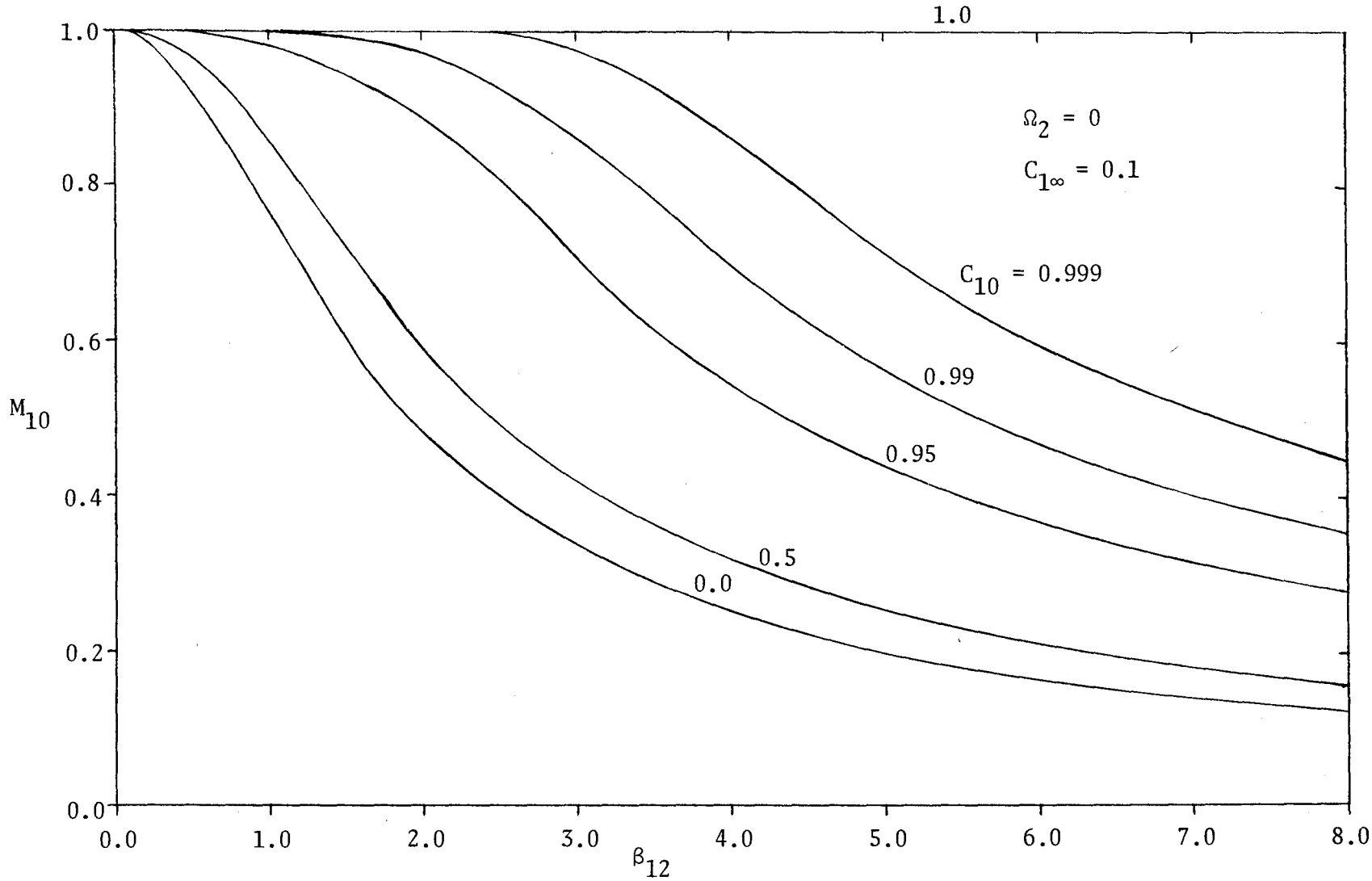

Figure 10. Root Mass Flow Ratio versus β_{12} with C_{10} Parameter and $C_{1\infty} = 0.1$ for Binary Mixture, Perfect Filter, $\Omega_2 = 0$, Example

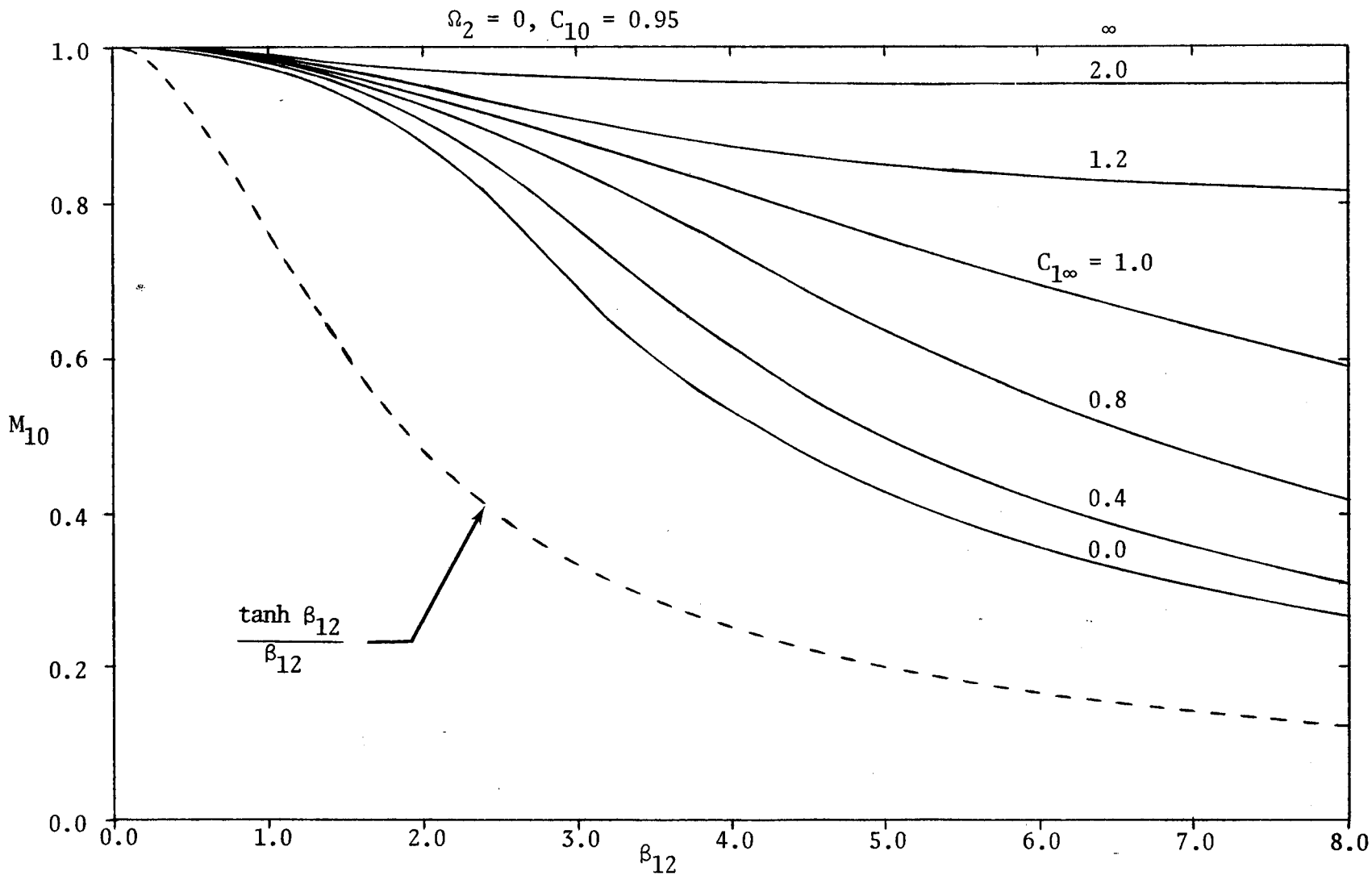

Figure 11. Root Mass Flow Ratio versus β_{12} with $C_{1\infty}$ Parameter and $C_{10} = 0.95$ for Binary Mixture, Perfect Filter, $\Omega_2 = 0$, Example

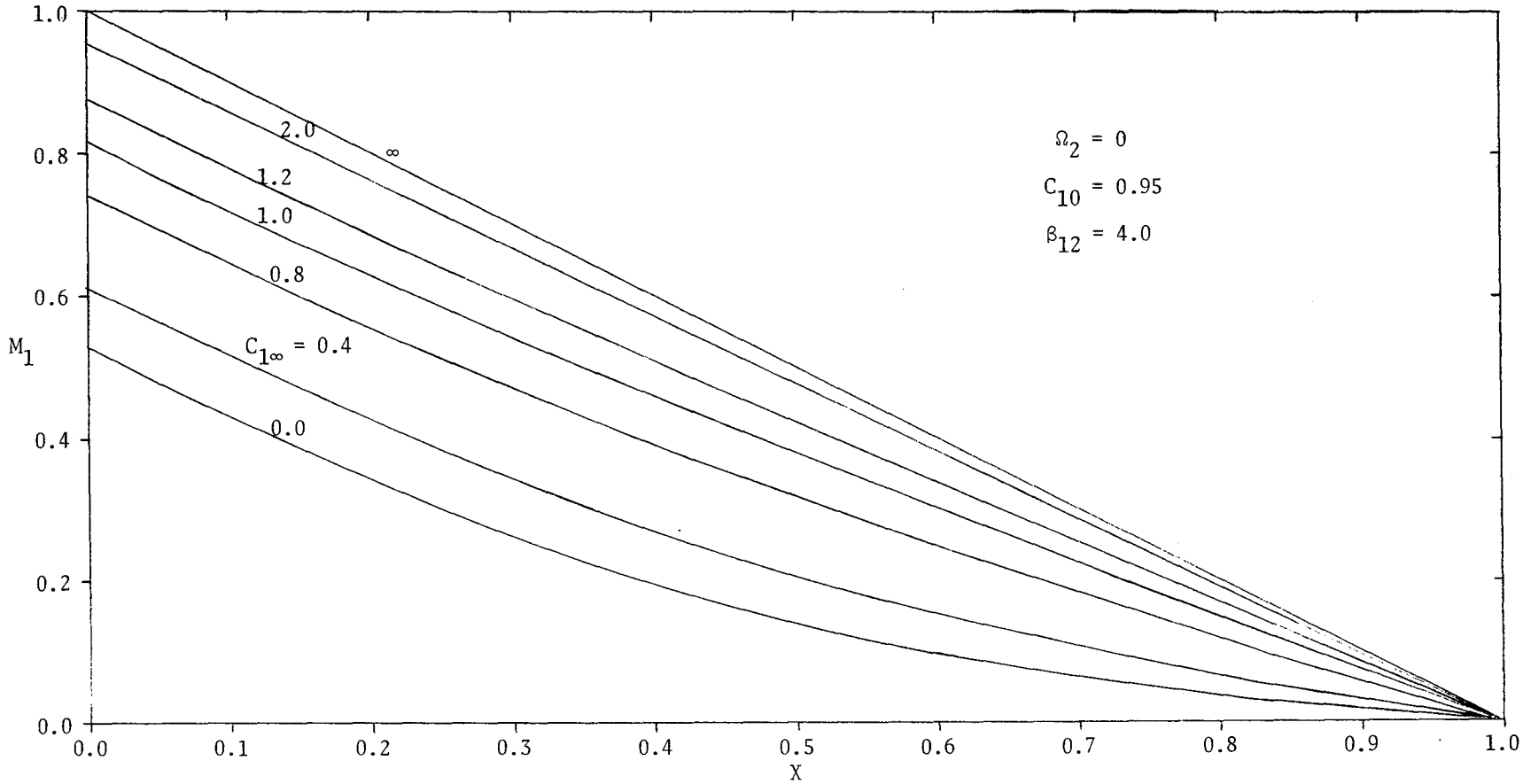

Figure 12. Binary Mixture, Perfect Filter Example with C_{10} = 0.95 and β_{12} = 4.0, M_1 versus X

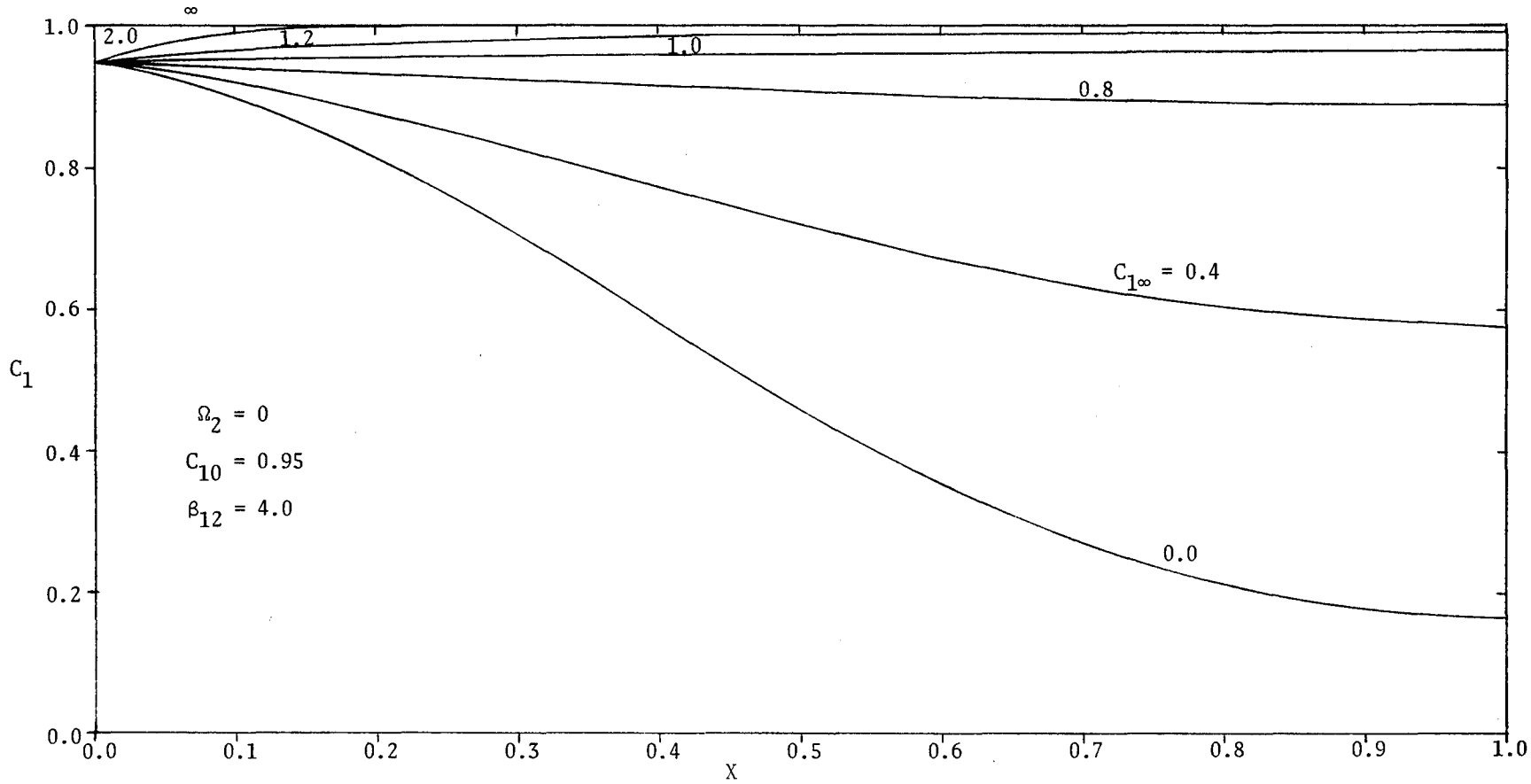

Figure 13. Binary Mixture, Perfect Filter Example with C_{10} = 0.95 and β_{12} = 4.0, C_1 versus X

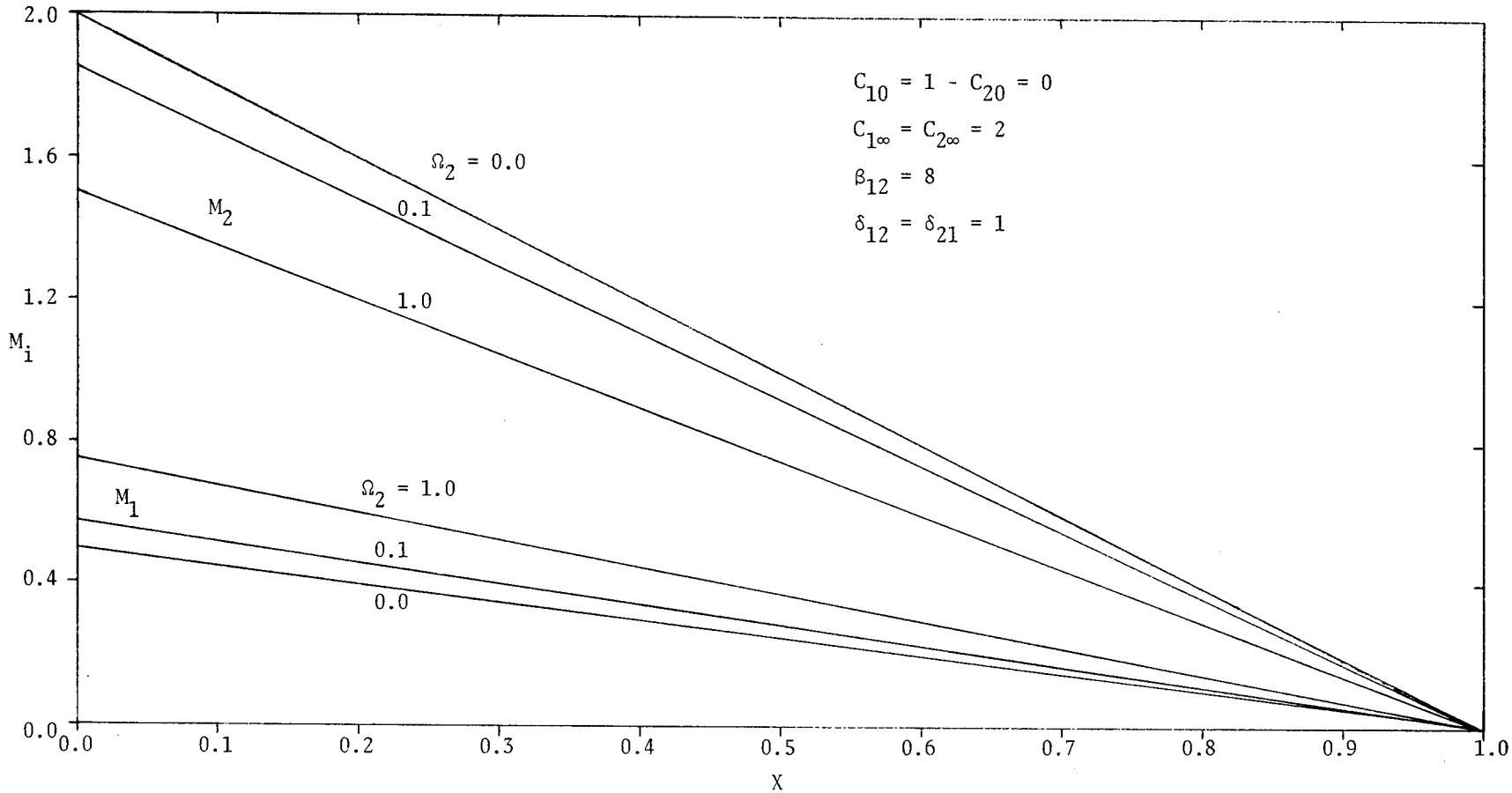

Figure 14. Binary Mixture, Real Filter Example, $C_{10} = 0$, $\beta_{12} = 8$, $C_{1\infty} = C_{2\infty} = 2$, M_i versus X

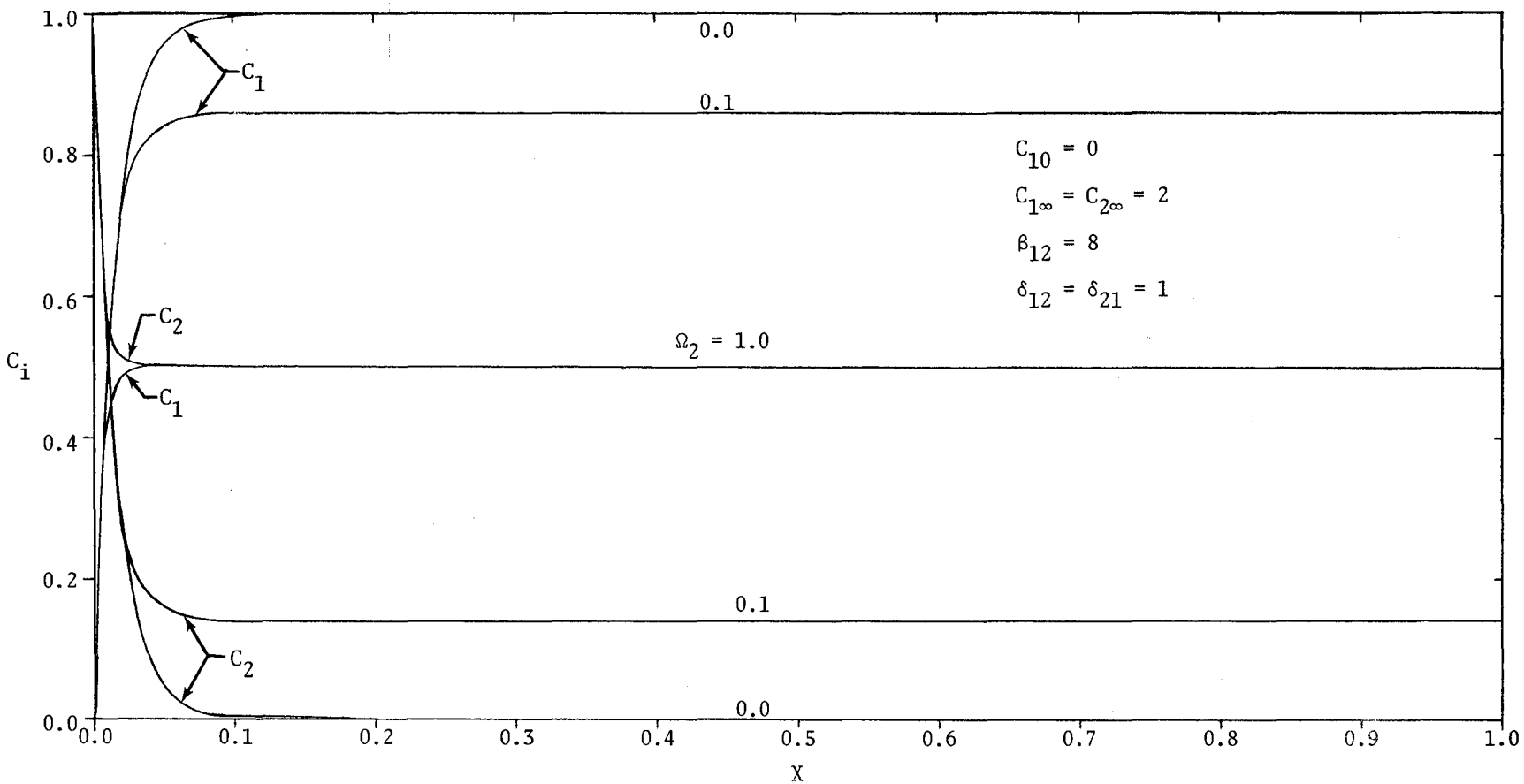

Figure 15. Binary Mixture, Real Filter Example, $C_{10} = 0$, $\beta_{12} = 8$, $C_{1\infty} = C_{2\infty} = 2$, C_i versus X

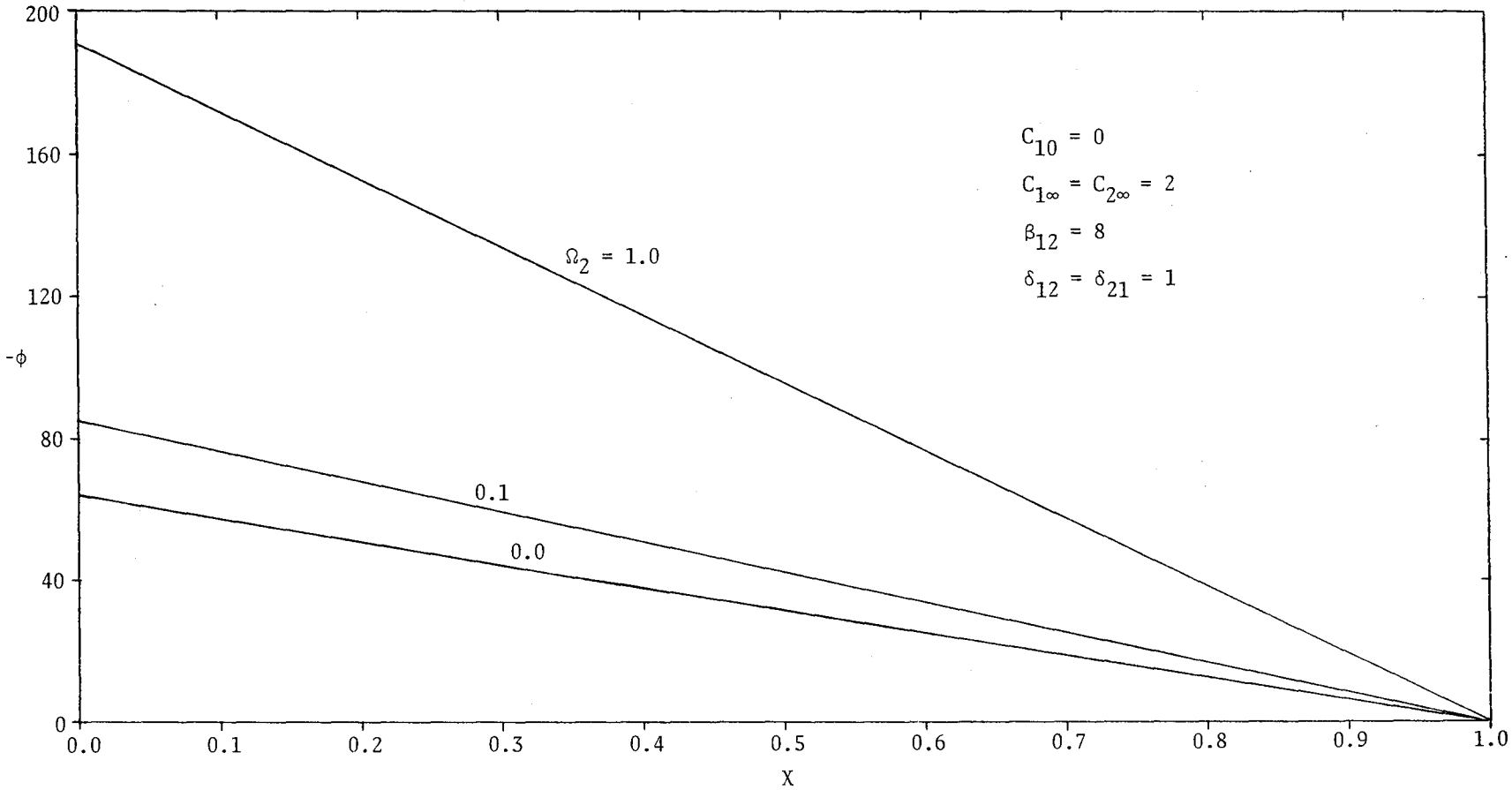

Figure 16. Binary Mixture, Real Filter Example, $C_{10} = 0$, $\beta_{12} = 8$, $C_{1\infty} = C_{2\infty} = 2$, $-\phi$ versus X

and 1.0, all of which yield negative velocity cases since ϕ is negative, Figure 16. The flat C_i distributions (Figure 15) and large $|\phi|$ values (Figure 16) indicate that this example is convection dominated. The perfect filter case here is one of the examples shown on Figure 9 where $M_{10} = 0.5$ and specie 1 is absent in the vent volume. Notice that M_2 is also shown on Figure 14 and that $M_{20} > 1$. Increasing separation ratio Ω_2 tends to force $M_{i0} \rightarrow 1$ in this case. It can be observed that the perfect filter case $\Omega_2 = 0$ is certainly representative of all $\Omega_2 << 1$ cases. The effective separation ratio $\Omega_{eff\ 2}$ is greater than Ω_2, $\Omega_{eff\ 2} > \Omega_2$ for this case, and it may be greater or less than unity depending on the value of Ω_2. For large Ω_2 the effective separation ratio approaches Ω_2.

To show the effects of reduced convection domination, the preceding example is repeated in Figures 17-19 but with β_{12}^2 reduced from 64 to 6.4. From Figures 18 and 19 one can observe that for each of $\Omega_2 = 0$, 1 and 10 negative velocity exists; for $\Omega_2 = 0$ the problem is not convection dominated although for $\Omega_2 = 1$ it is near the convection regime and for $\Omega_2 = 10$ it is convection dominated. This result is physically caused by the additional flow of specie 2 as Ω_2 increases. The behavior of M_i in Figure 17 is similar to that already discussed and shown in Figure 14 for the preceding example.

As a final negative velocity, two specie example consider the case given by Figures 20-22. As can be seen from Figures 21 and 22, the $\Omega_2 = 0$ case is not convection dominated while the $\Omega_2 = 2.25$ case is nearly convection dominated. Figure 21 shows the interesting result that for $\Omega_2 = 0$, C_1 increases with X and C_2 decreases while for $\Omega_2 = 2.25$ the opposite is true. Also Figure 20 shows that for $\Omega_2 = 0$, $M_{20} > 1$ and $M_{10} < 1$ while for $\Omega_2 = 2.25$ the opposite is true. The power of one specie to control the characteristics of the flow of another specie is therefore beginning to emerge as a potentially useful method of operation. That is, in Figures

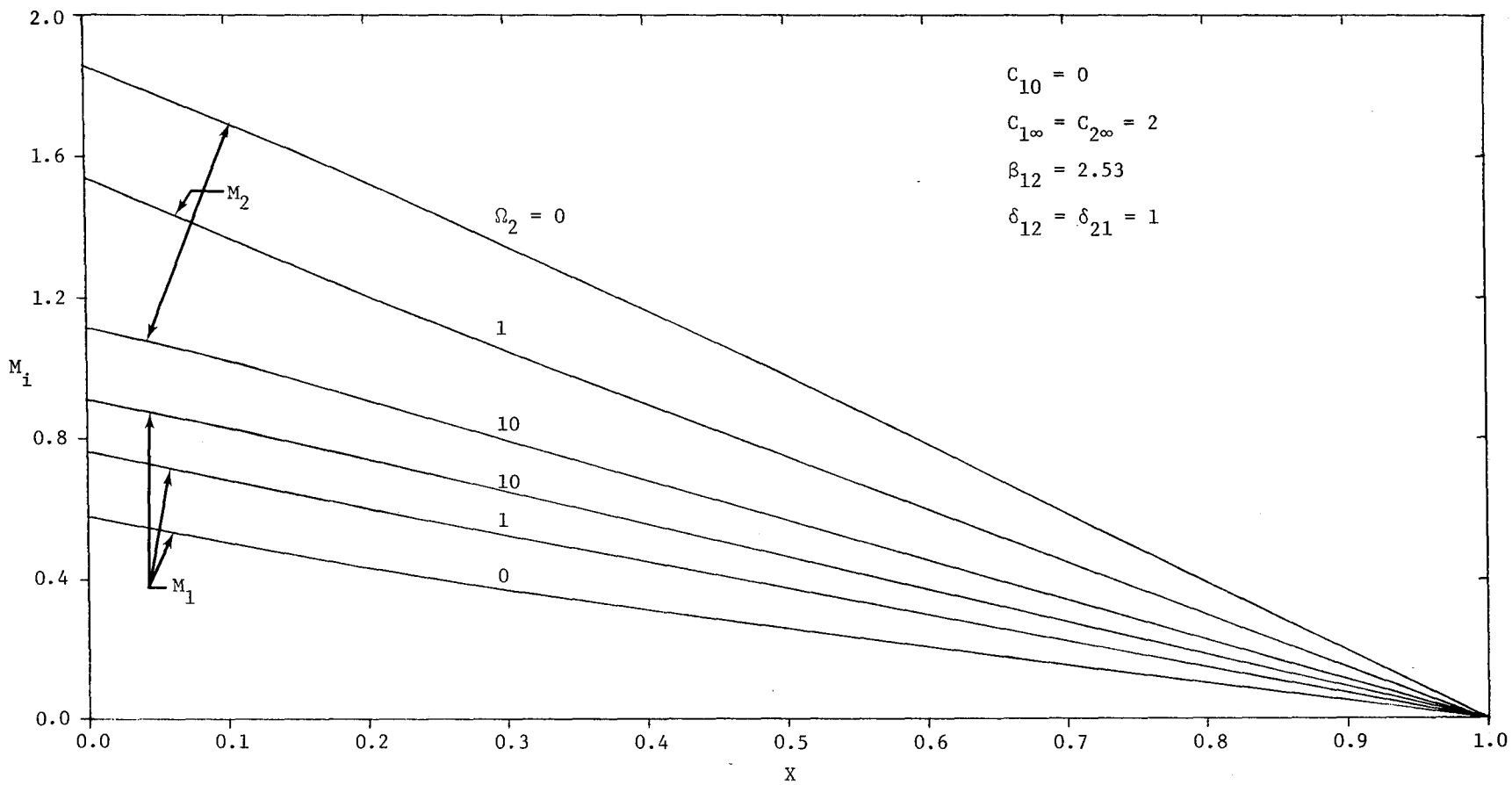

Figure 17. Real Filter Example, $C_{10} = 0$, $C_{1\infty} = C_{2\infty} = 2$, $\beta_{12} = 2.53$, M_i versus X

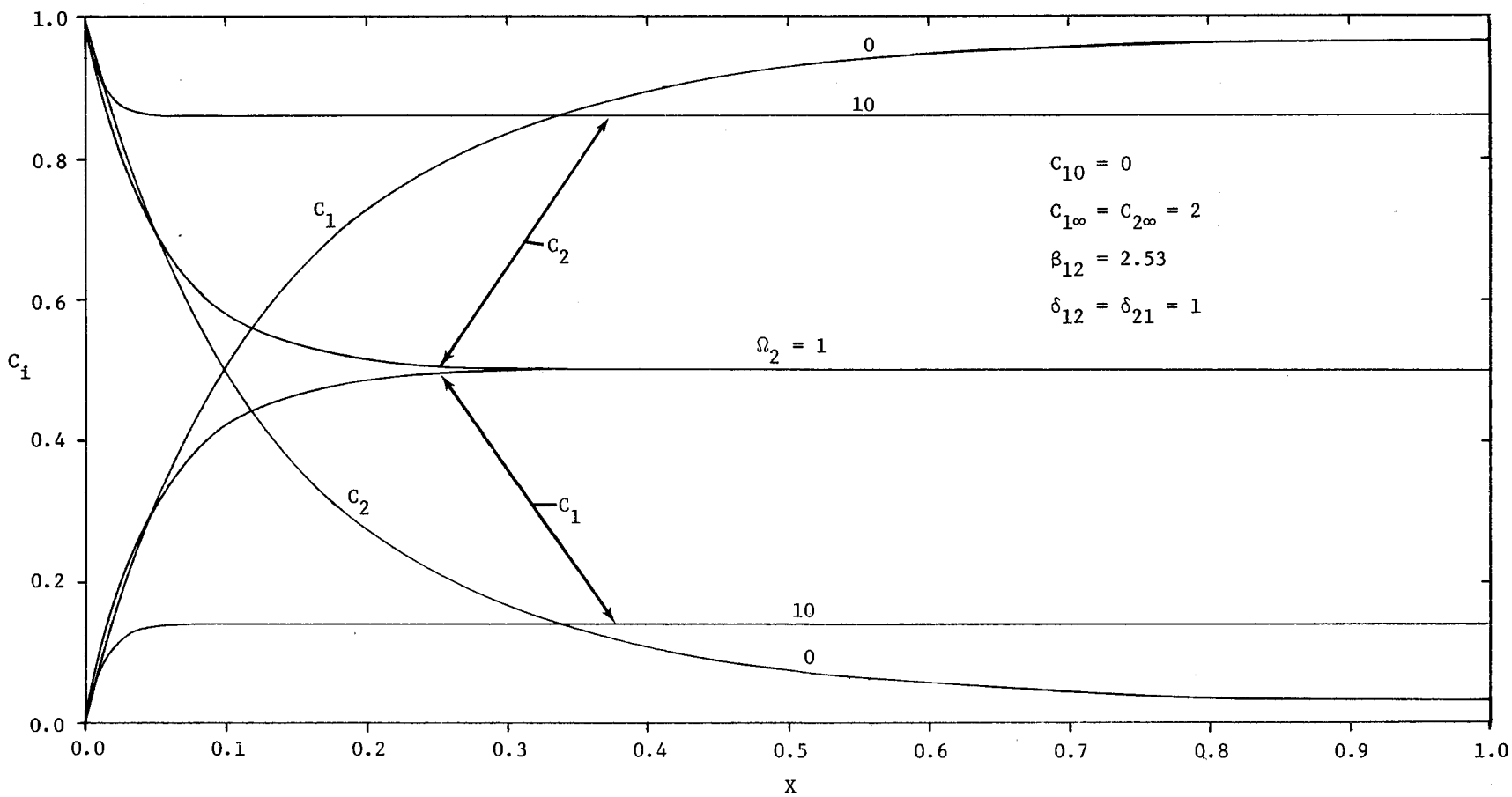

Figure 18. Real Filter Example, $C_{10} = 0$, $C_{1\infty} = C_{2\infty} = 2$, $\beta_{12} = 2.53$, C_i versus X

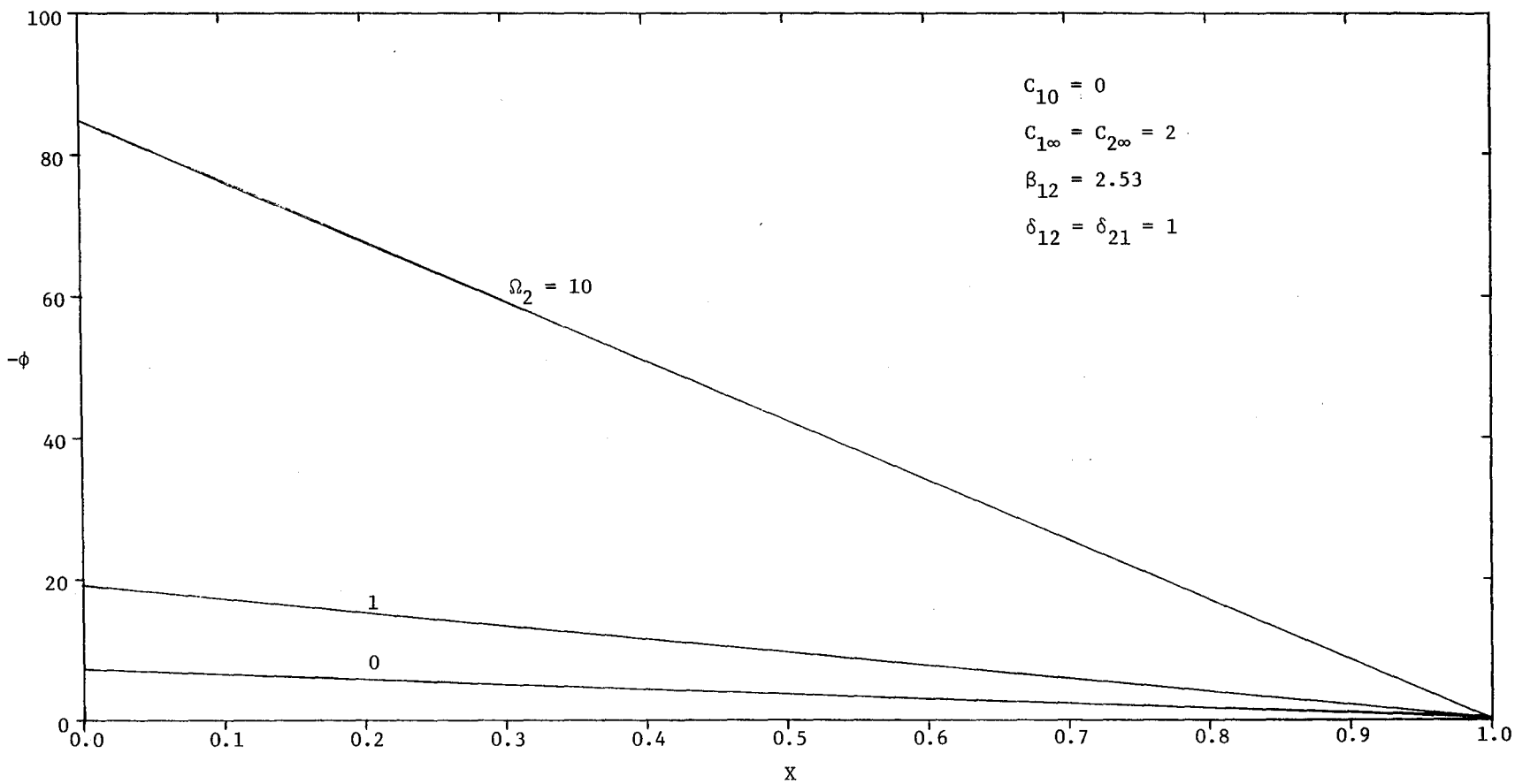

Figure 19. Real Filter Example, $C_{10} = 0$, $C_{1\infty} = C_{2\infty} = 2$, $\beta_{12} = 2.53$, $-\phi$ versus X

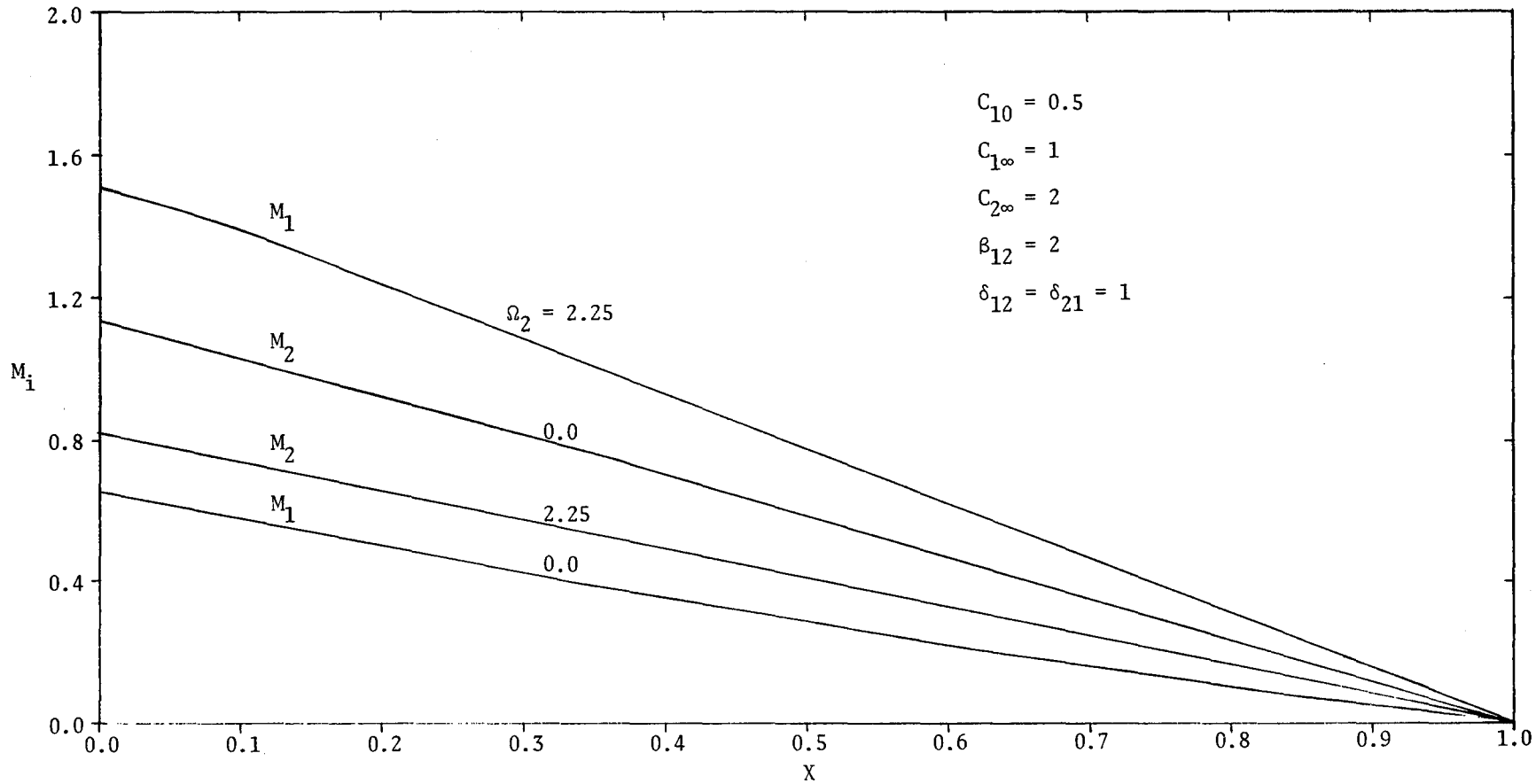

Figure 20. Real Filter Example, $C_{10} = 0.5$, $C_{1\infty} = 1$, $C_{2\infty} = 2$, $\beta_{12} = 2$, M_i versus X

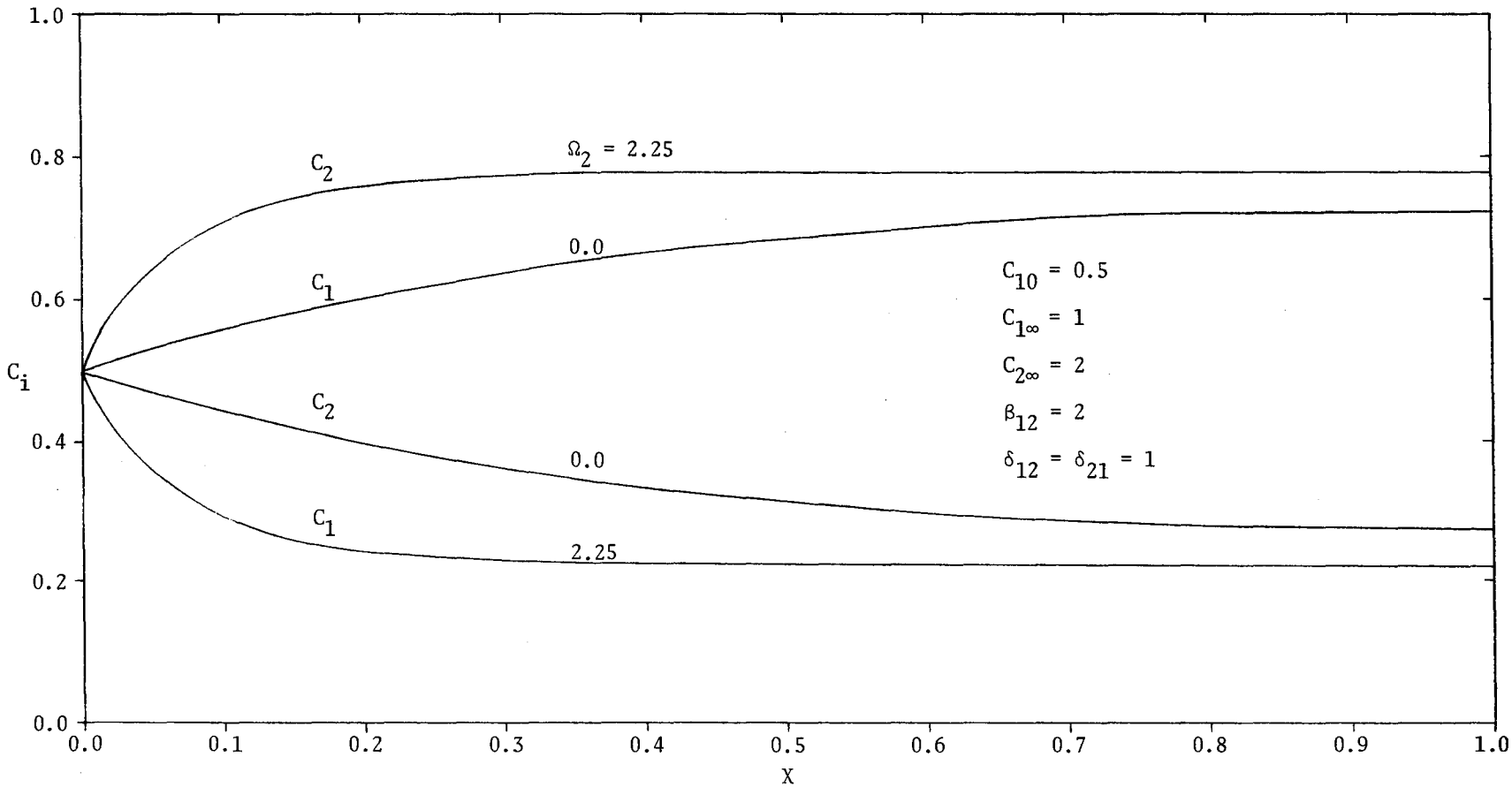

Figure 21. Real Filter Example, $C_{10} = 0.5$, $C_{1\infty} = 1$, $C_{2\infty} = 2$, $\beta_{12} = 2$, C_i versus X

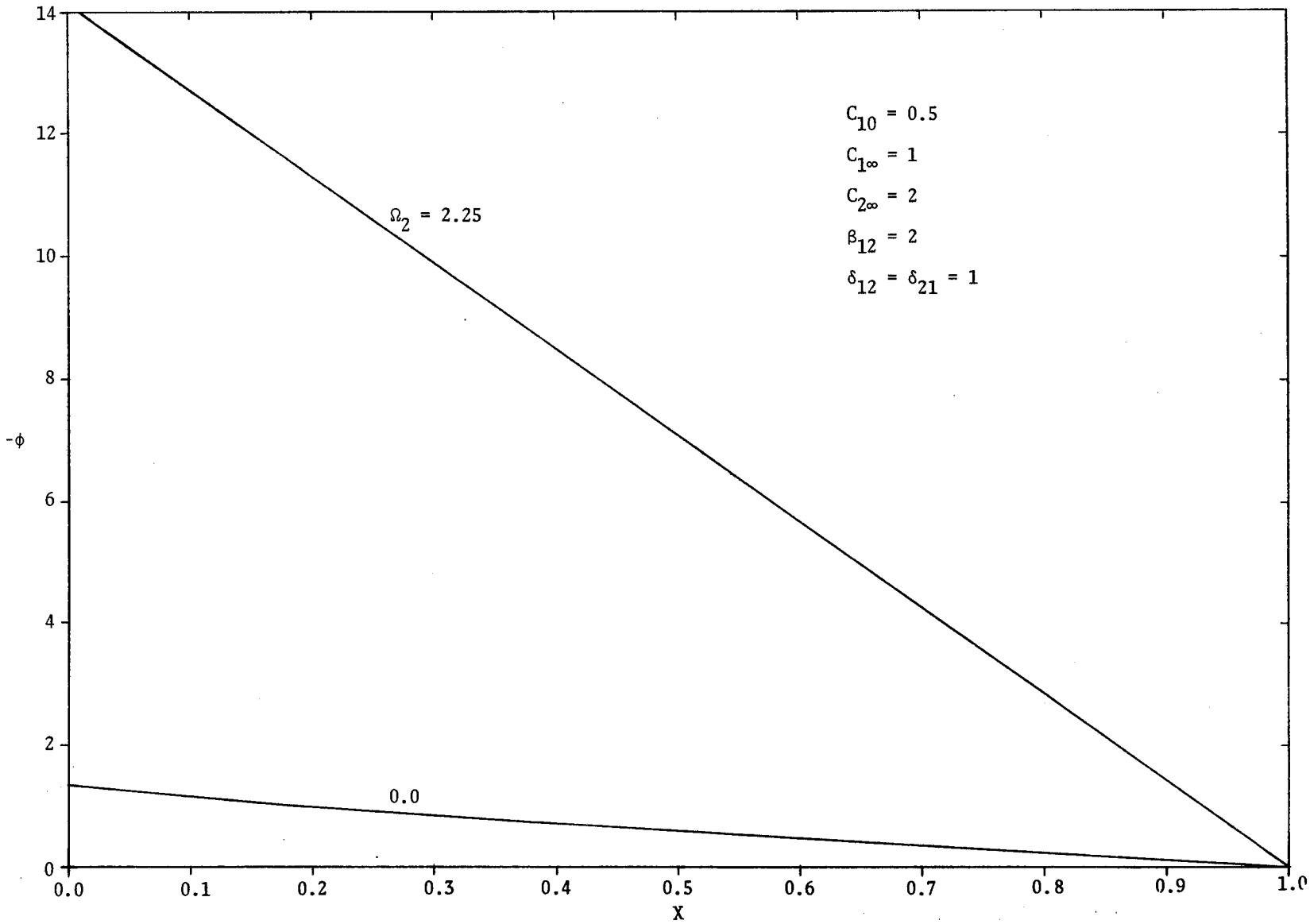

Figure 22. Real Filter Example, $C_{10} = 0.5$, $C_{1\infty} = 1$, $C_{2\infty} = 2$, $\beta_{12} = 2$, $-\phi$ versus X

14-19 the use of another permeating specie $\Omega_2 > 0$ for specie 2 tended to eliminate via $M_{10} \to 1$ the initial $\Omega_2 = 0$ dehanced flow of specie 1, $M_{10} < 1$, but never enhanced it above the normalizing limiting case. However the example given by Figures 20-22 in fact shows that the $\Omega_2 = 0$ dehanced flow of specie 1 becomes enhanced $M_{10} > 1$ when a faster permeating specie $\Omega_2 = 2.25$ is used for specie 2. Also notice that while $\Omega_{eff\ 2} > \Omega_2$ for the examples in Figures 14-19, for the example in Figures 20-22 $\Omega_{eff\ 2} < \Omega_2$; this shows that $\Omega_{eff\ 2}$ too can be altered in a potentially useful way.

Figures 23-25 give an example where the so called "driver volume" is evacuated so that the global velocity must be positive, see Figure 25. The perfect filter result is not very near to the convection dominated case, while the $\Omega_2 = 2$ case is in the near convection regime. Of course since the global flow velocity is positive, the convection regime is no longer characterized by flat C_i profiles. However, as in the preceding negative velocity case, the C_i and M_i curves show a reversal, so that phenomenon is not limited by the flow direction. Figures 26-28 are for a similar, but somewhat modified, positive velocity case with evacuated driver volume. The reduced β_{12} value shifts both the $\Omega_2 = 0$ and $\Omega_2 = 2$ results away from convection domination. Note, on the other hand, that the C_i and M_i curves still display the potentially useful reversal of roles, indicating that it is not necessary to fully enter the convection regime in order to obtain such an effect.

Figures 29-46 give a series of examples closely related to the positive velocity, convection dominated examples given in Figures 7 and 8. Among other things, this allows some information to be obtained about the parameter values necessary to produce the convection dominated solutions for positive velocity cases; the flat C_i profiles present for negative

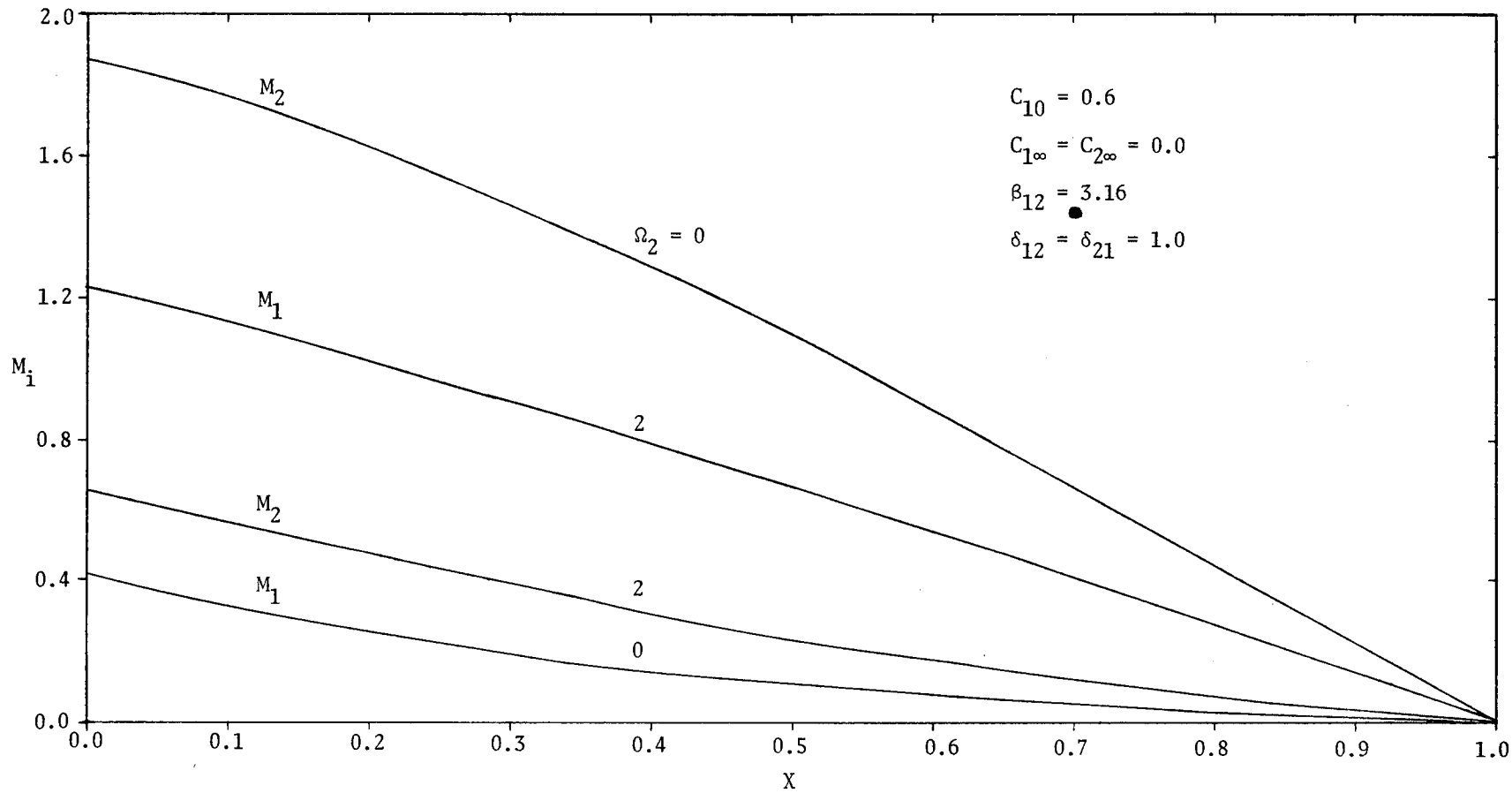

Figure 23. M_i versus X, $C_{10} = 0.6$, $C_{1\infty} = C_{2\infty} = 0$, $\beta_{12} = 3.16$

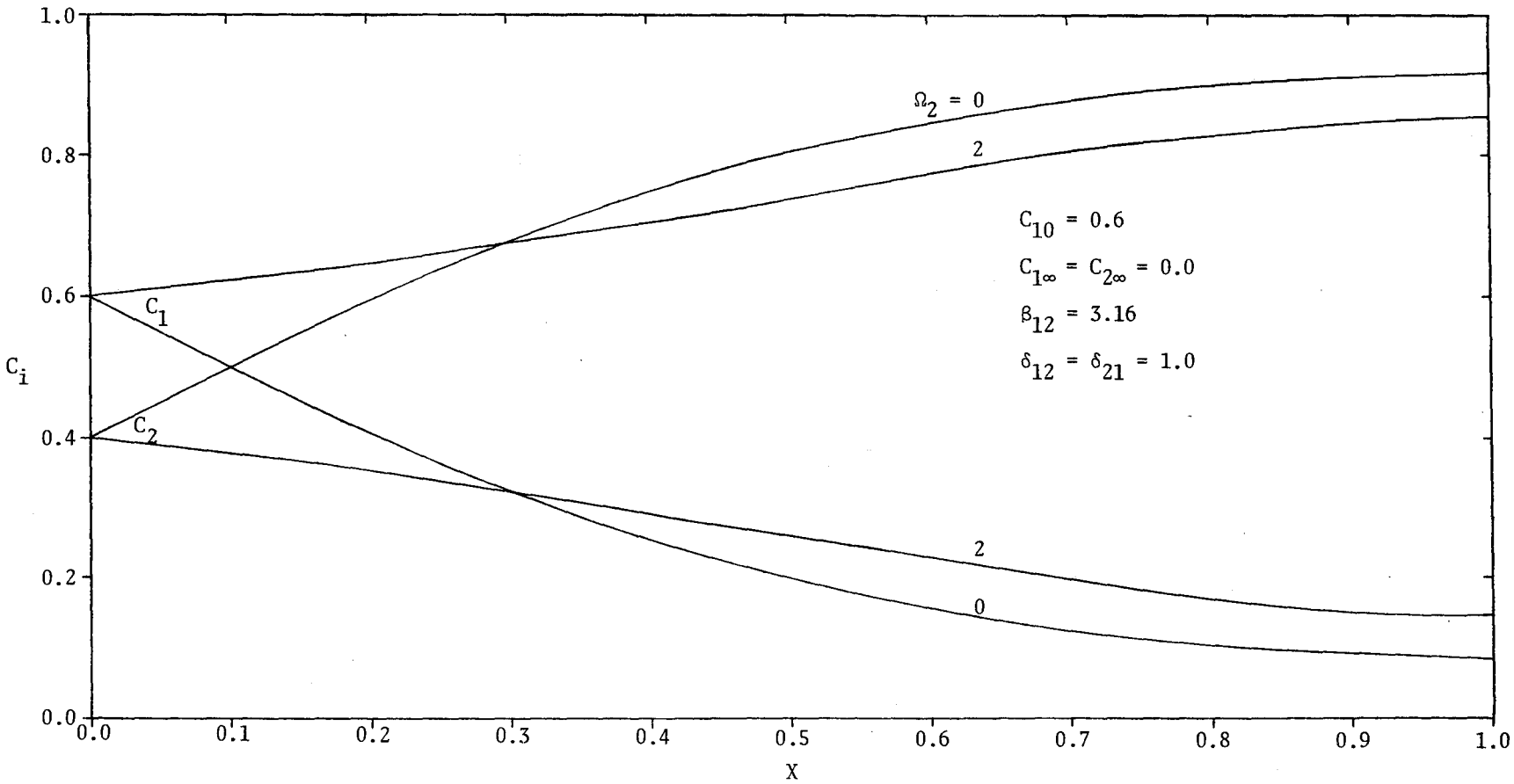

Figure 24. C_i versus X, $C_{10} = 0.6$, $C_{1\infty} = C_{2\infty} = 0$, $\beta_{12} = 3.16$

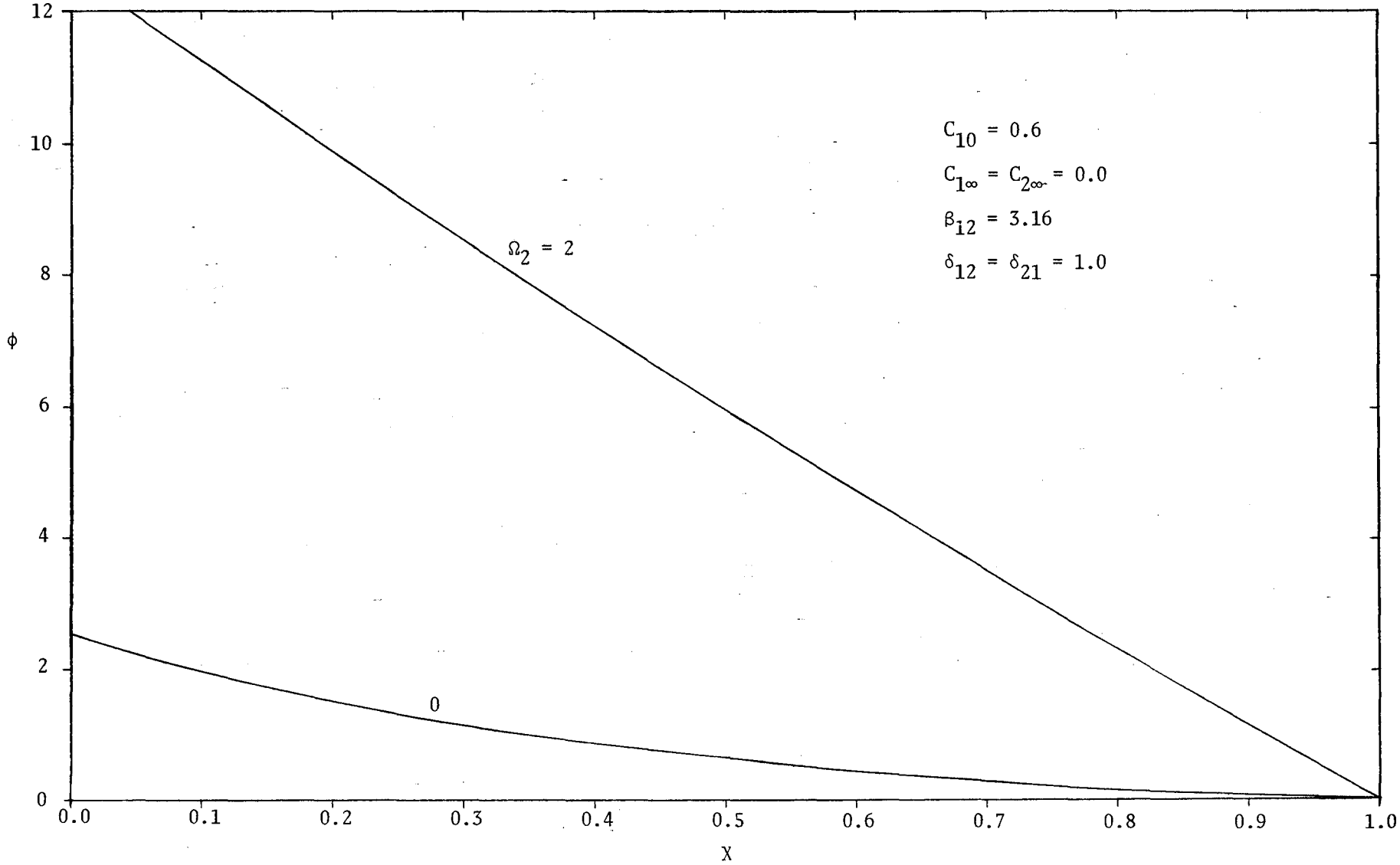

Figure 25. ϕ versus X, $C_{10} = 0.6$, $C_{1\infty} = C_{2\infty} = 0$, $\beta_{12} = 3.16$

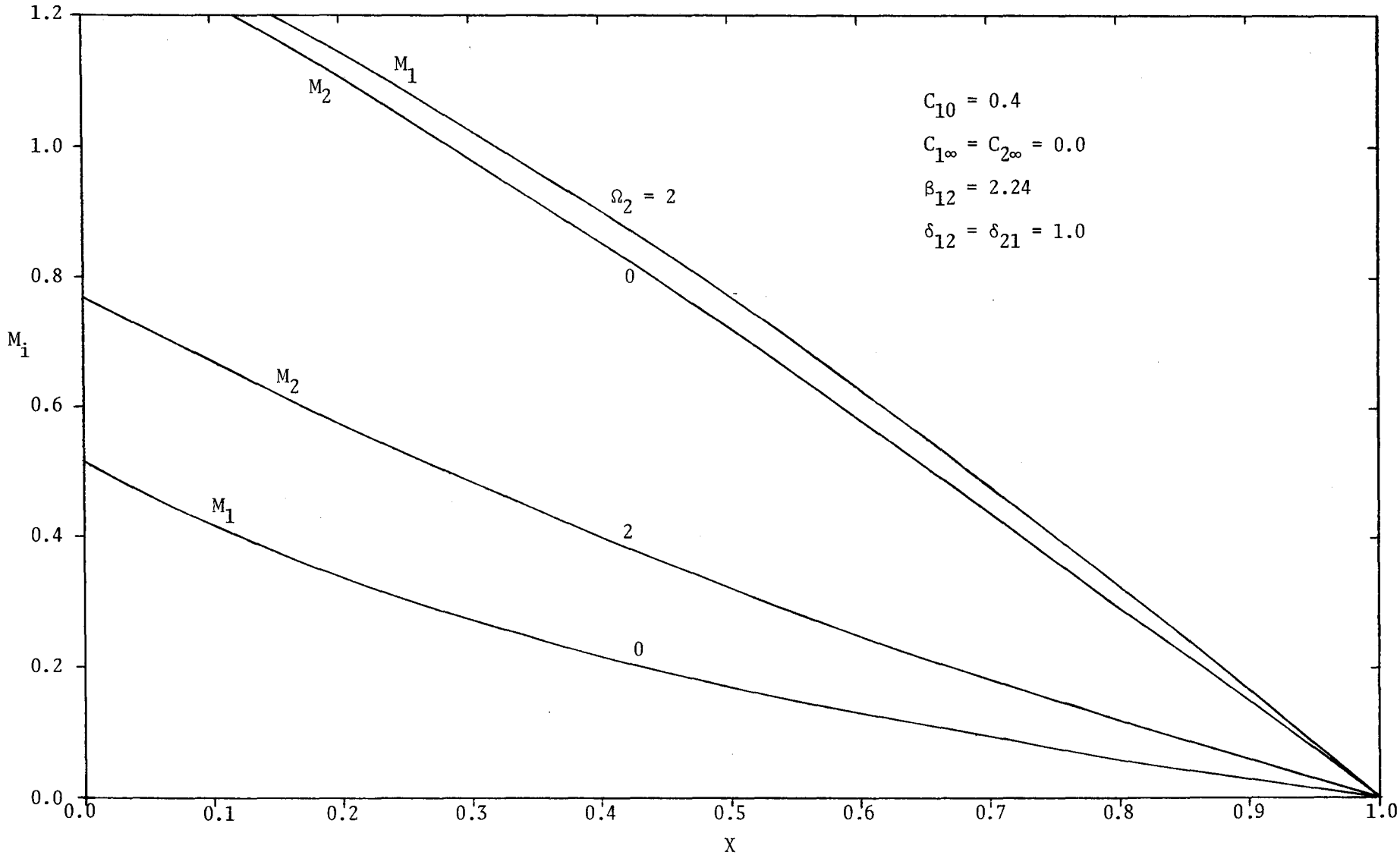

Figure 26. M_i versus X, $C_{10} = 0.4$, $C_{1\infty} = C_{1\infty} = 0$, $\beta_{12} = 2.24$

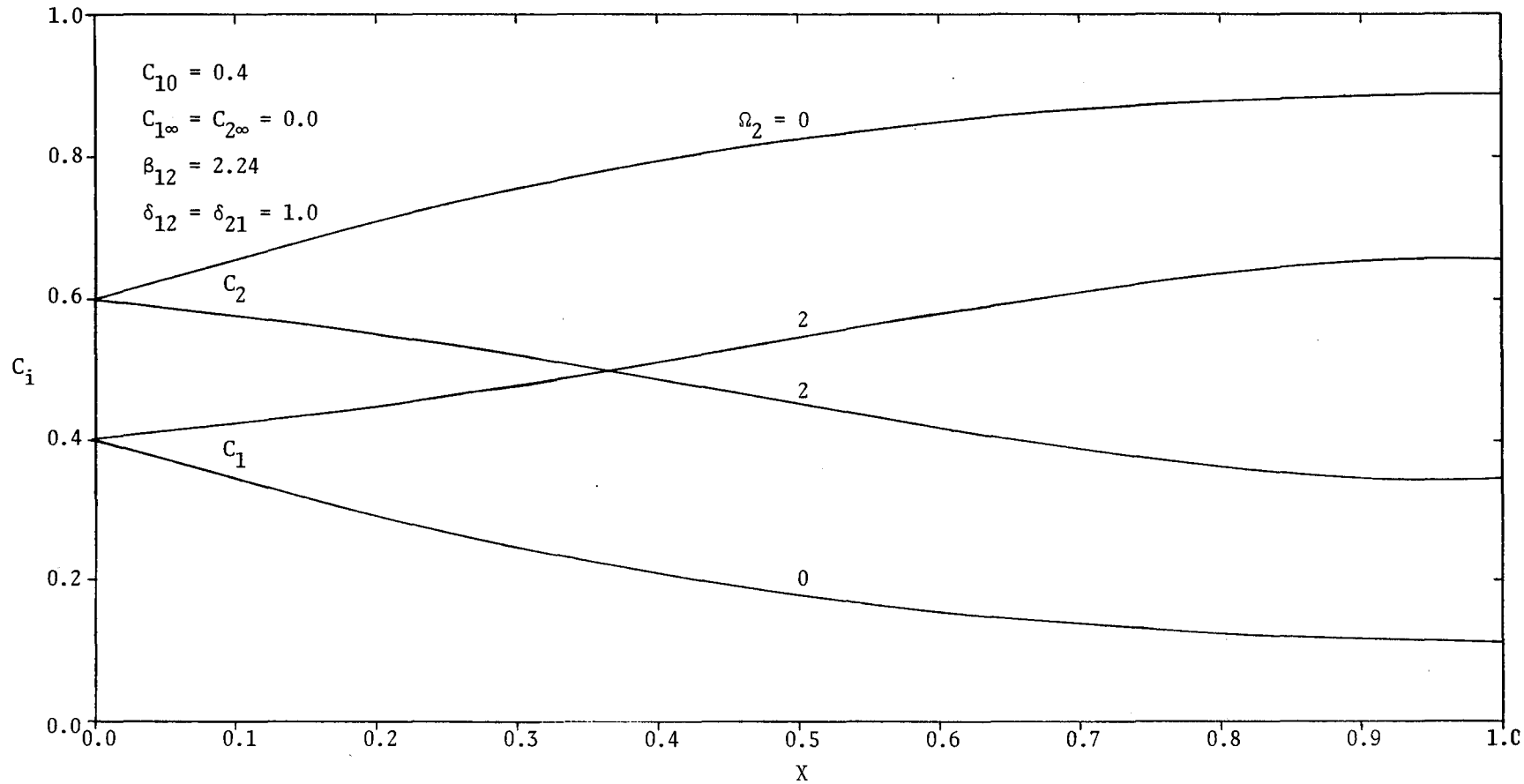

Figure 27. C_i versus X, C_{10} = 0.4, $C_{1\infty}$ = $C_{2\infty}$ = 0, β_{12} = 2.24

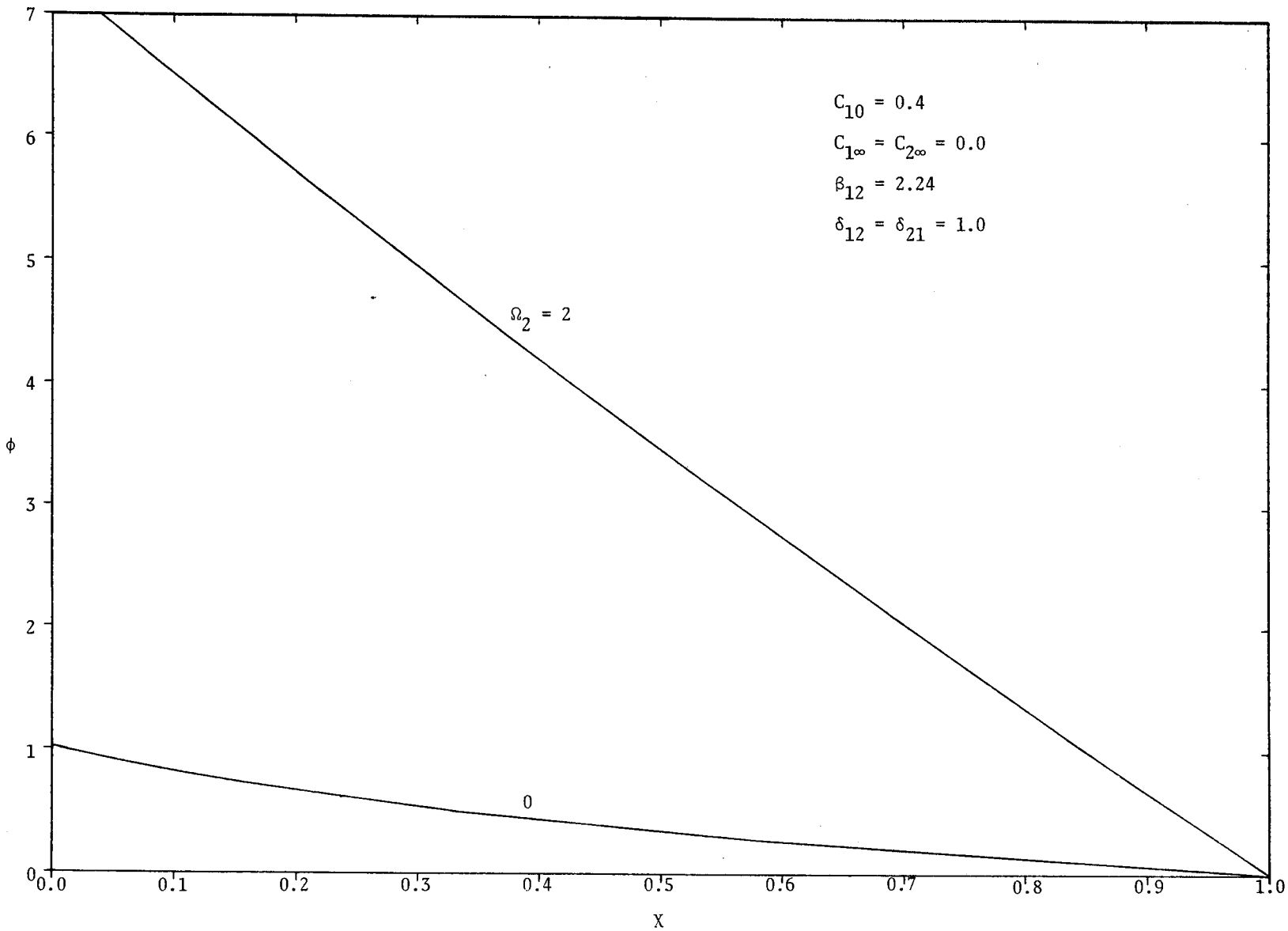

Figure 28. ϕ versus X, $C_{10} = 0.4$, $C_{1\infty} = C_{2\infty} = 0$, $\beta_{12} = 2.24$

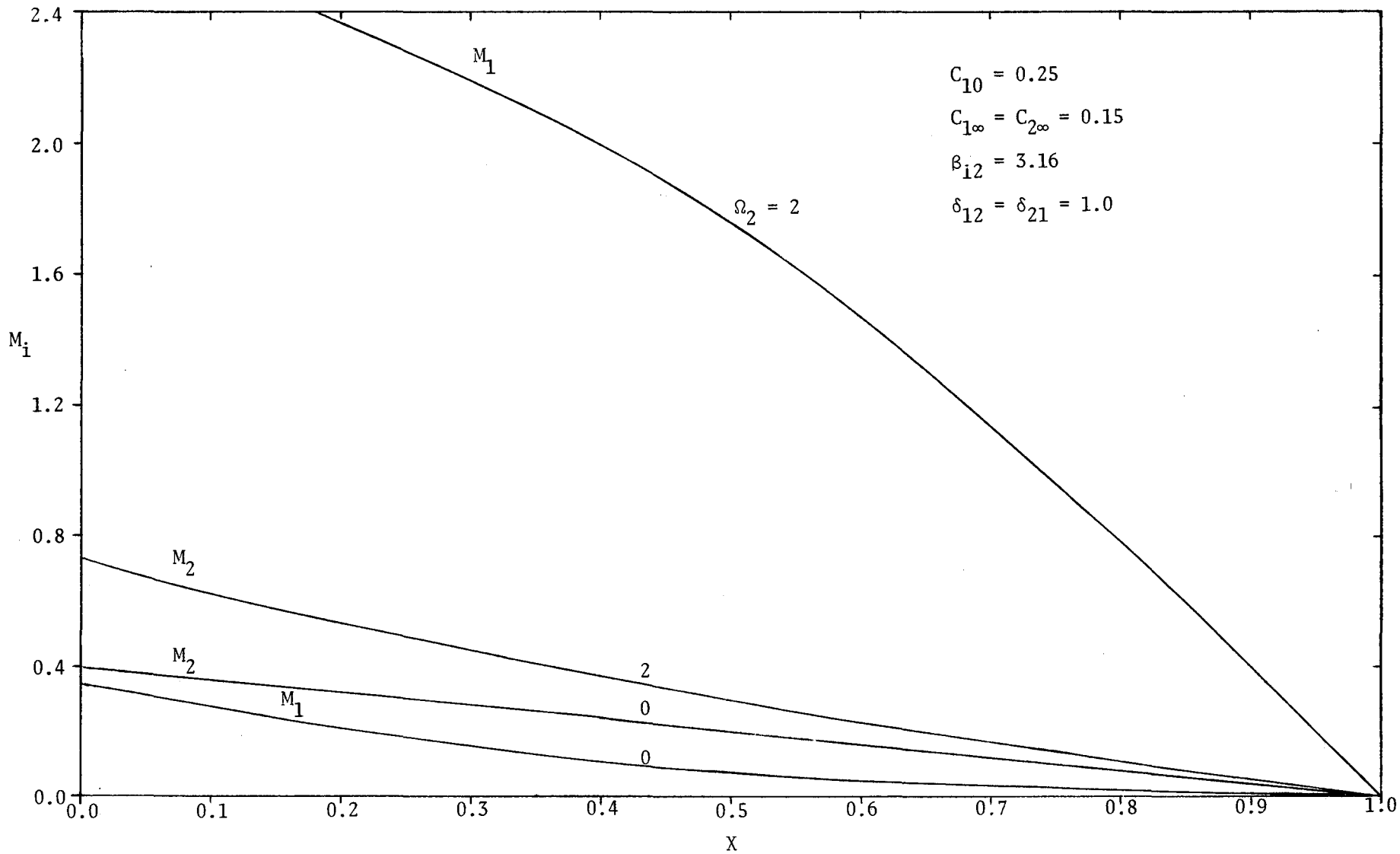

Figure 29. M_i versus X, $C_{10} = 0.25$, $C_{1\infty} = C_{2\infty} = 0.15$, $\beta_{12} = 3.16$

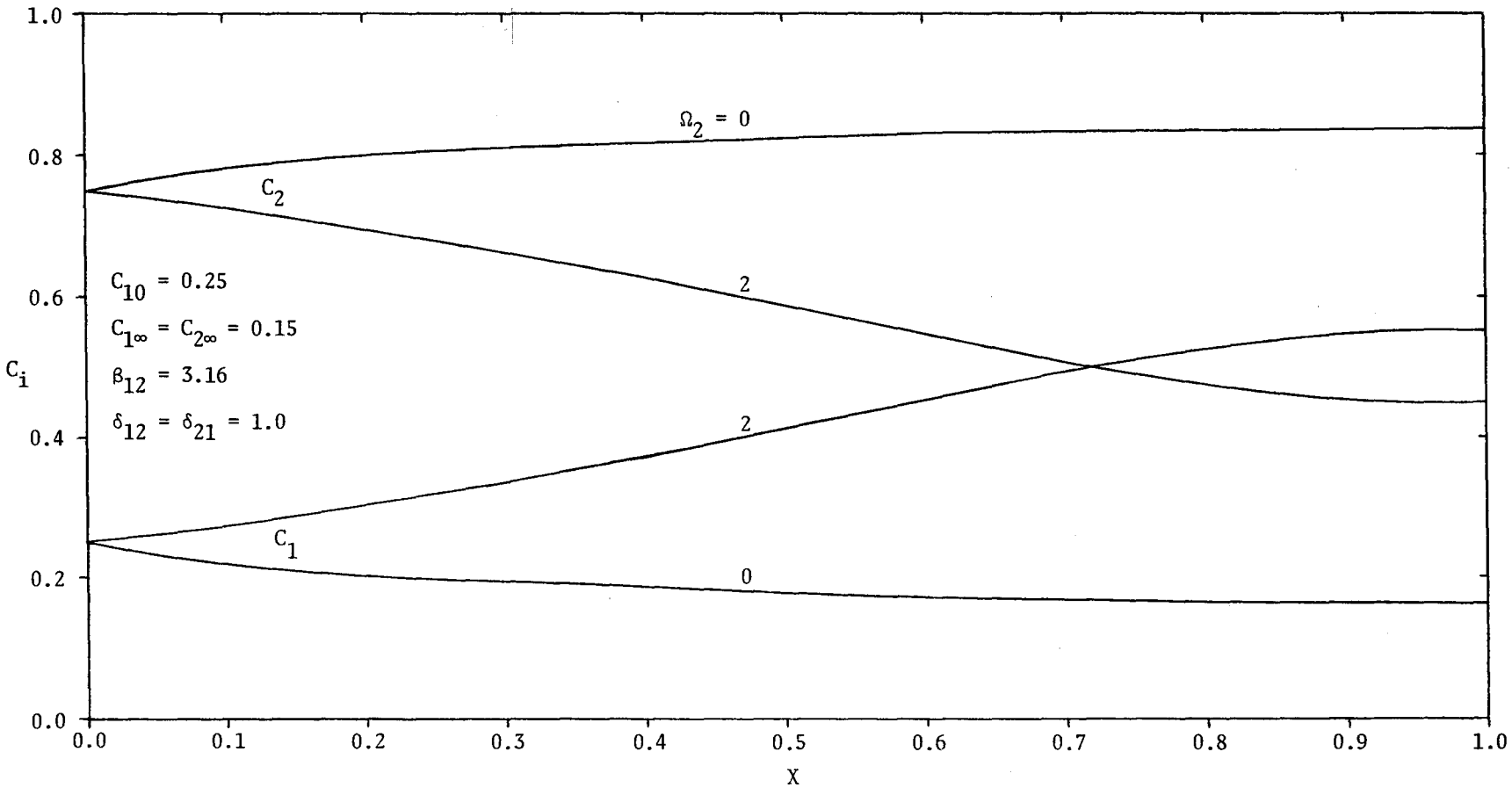

Figure 30. C_i versus X, $C_{10} = 0.25$, $C_{1\infty} = C_{2\infty} = 0.15$, $\beta_{12} = 3.16$

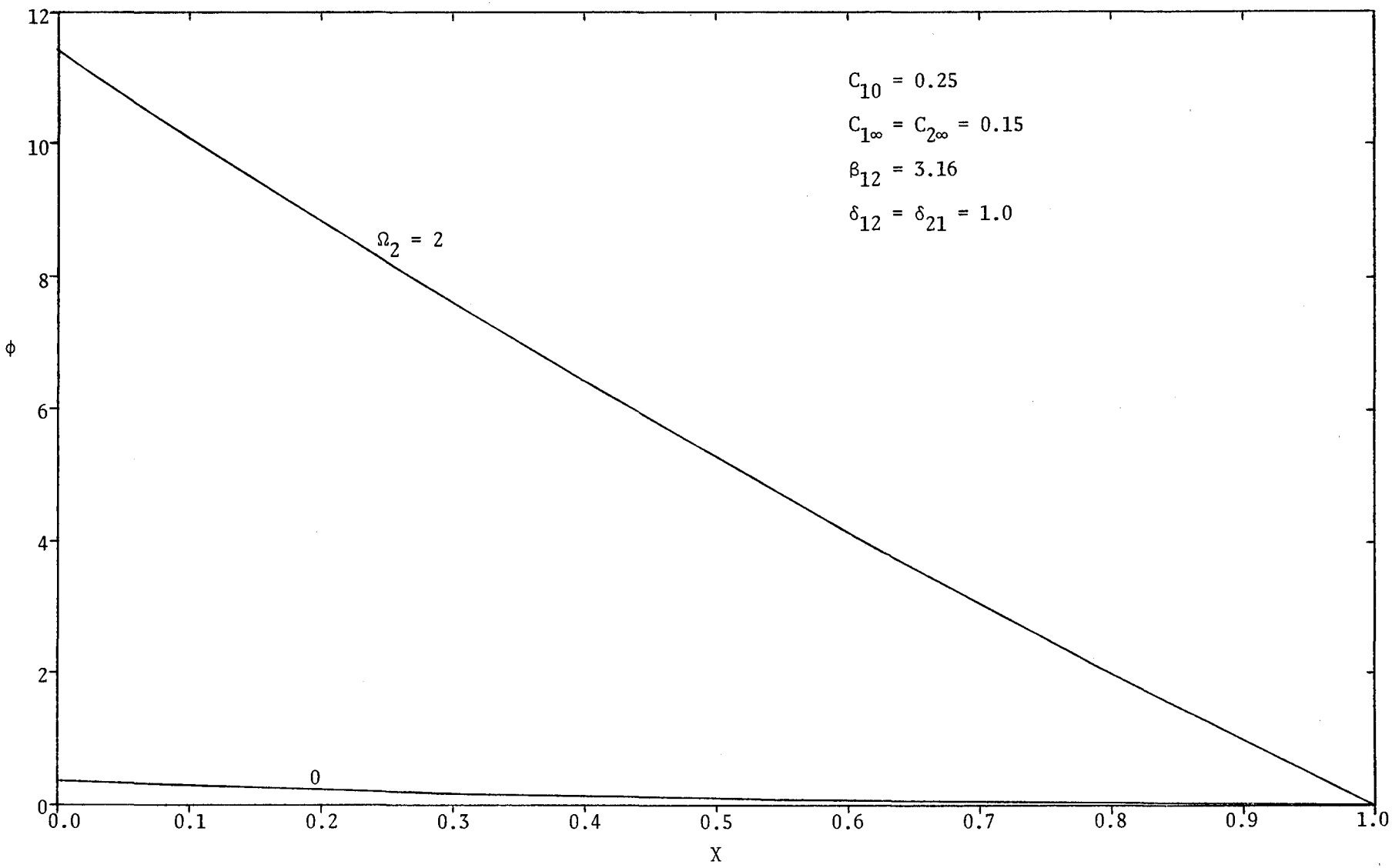

Figure 31. ϕ versus X, $C_{10} = 0.25$, $C_{1\infty} = C_{2\infty} = 0.15$, $\beta_{12} = 3.16$

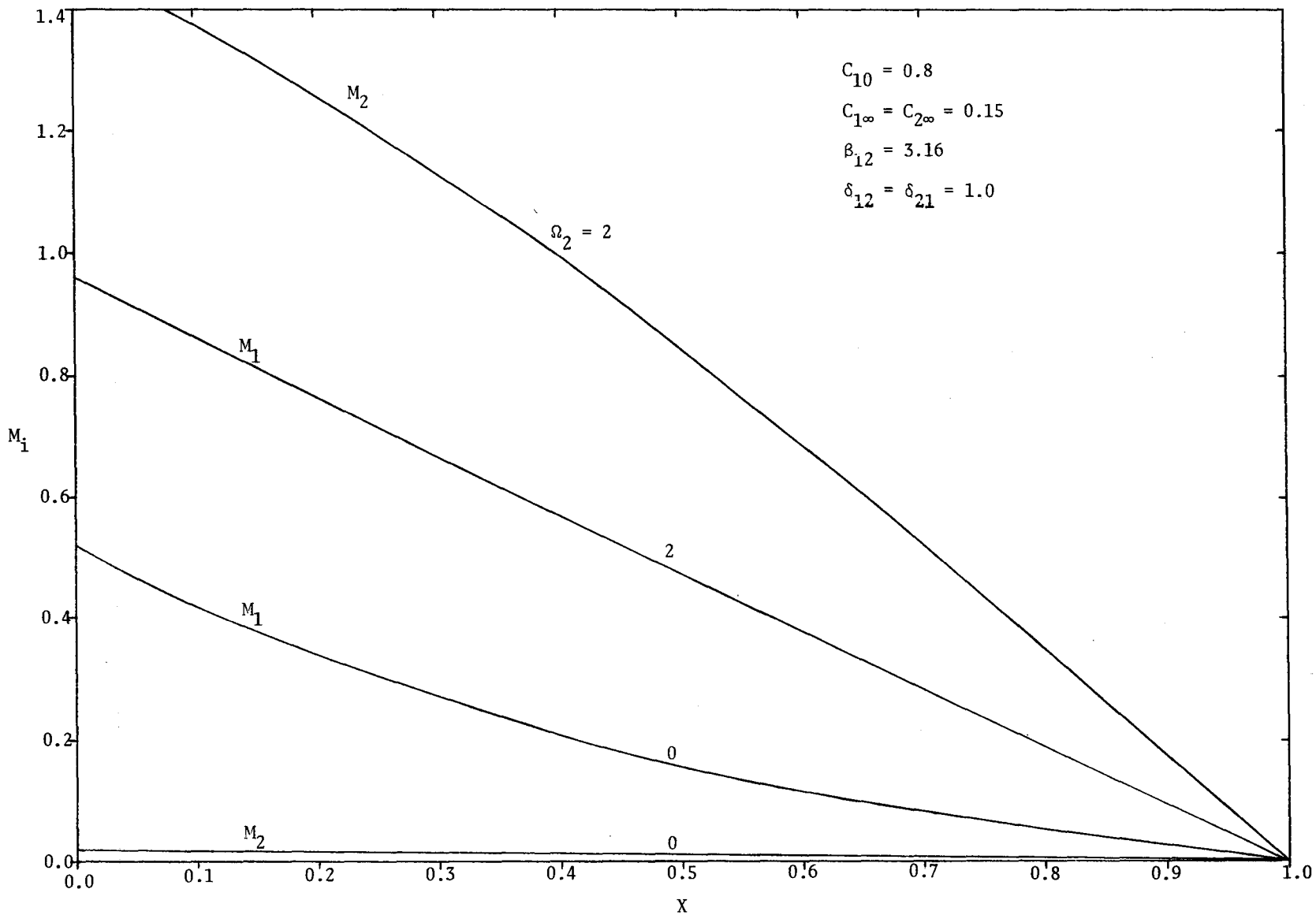

Figure 32. M_i versus X, $C_{10} = 0.8$, $C_{1\infty} = C_{2\infty} = 0.15$, $\beta_{12} = 3.16$

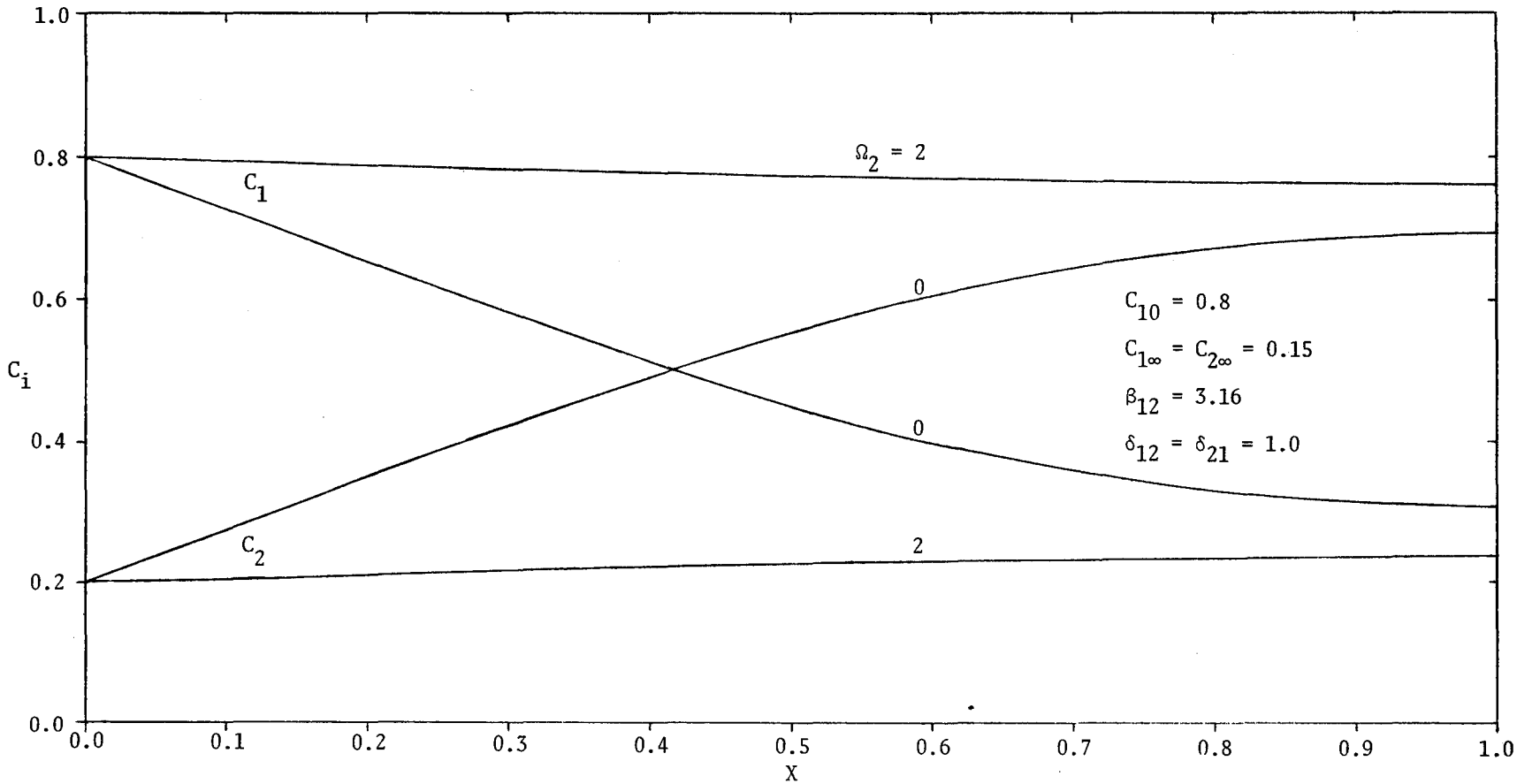

Figure 33. C_i versus X, $C_{10} = 0.8$, $C_{1\infty} = C_{2\infty} = 0.15$, $\beta_{12} = 3.16$

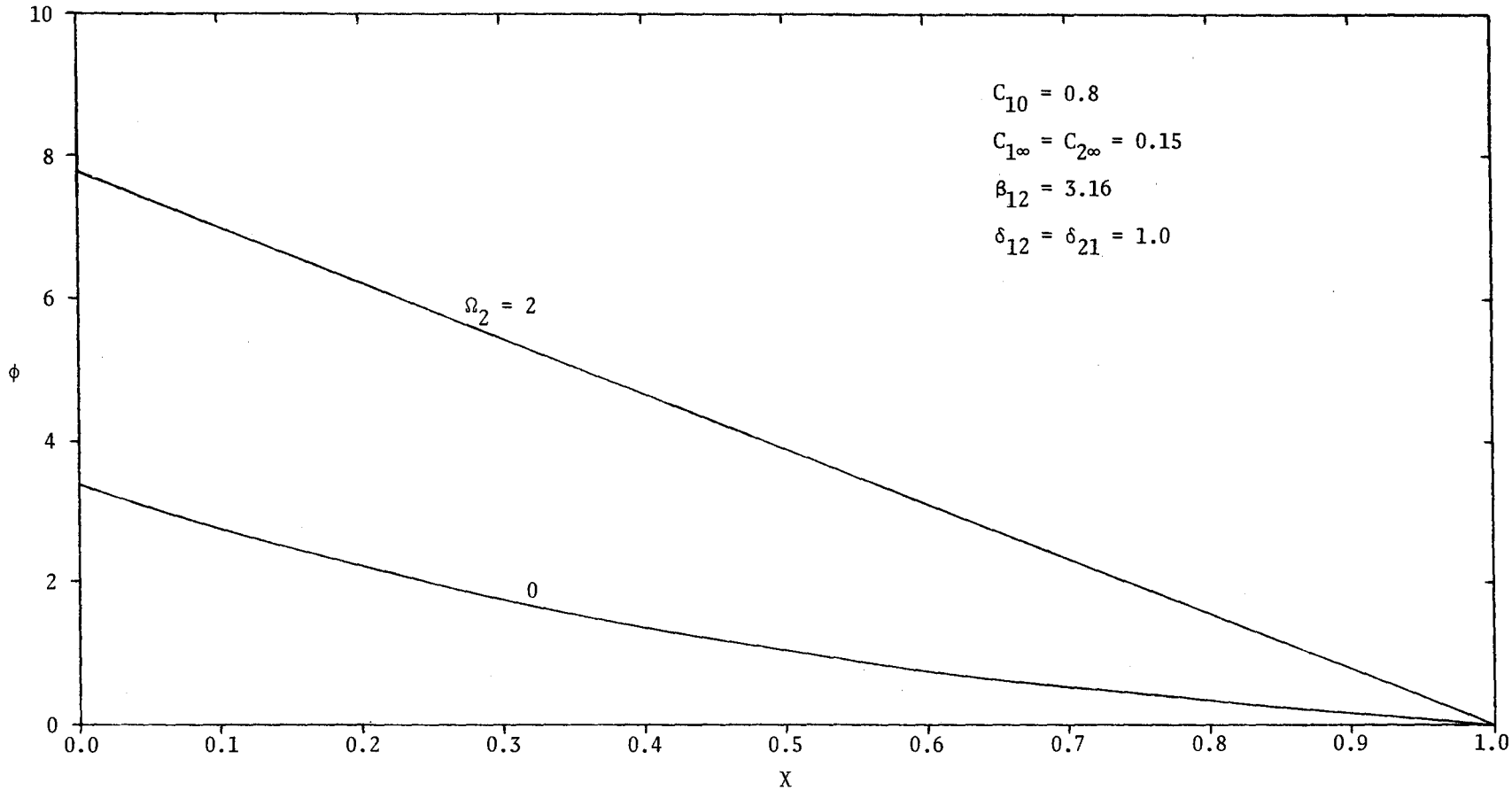

Figure 34. ϕ versus X, $C_{10} = 0.8$, $C_{1\infty} = C_{2\infty} = 0.15$, $\beta_{12} = 3.16$

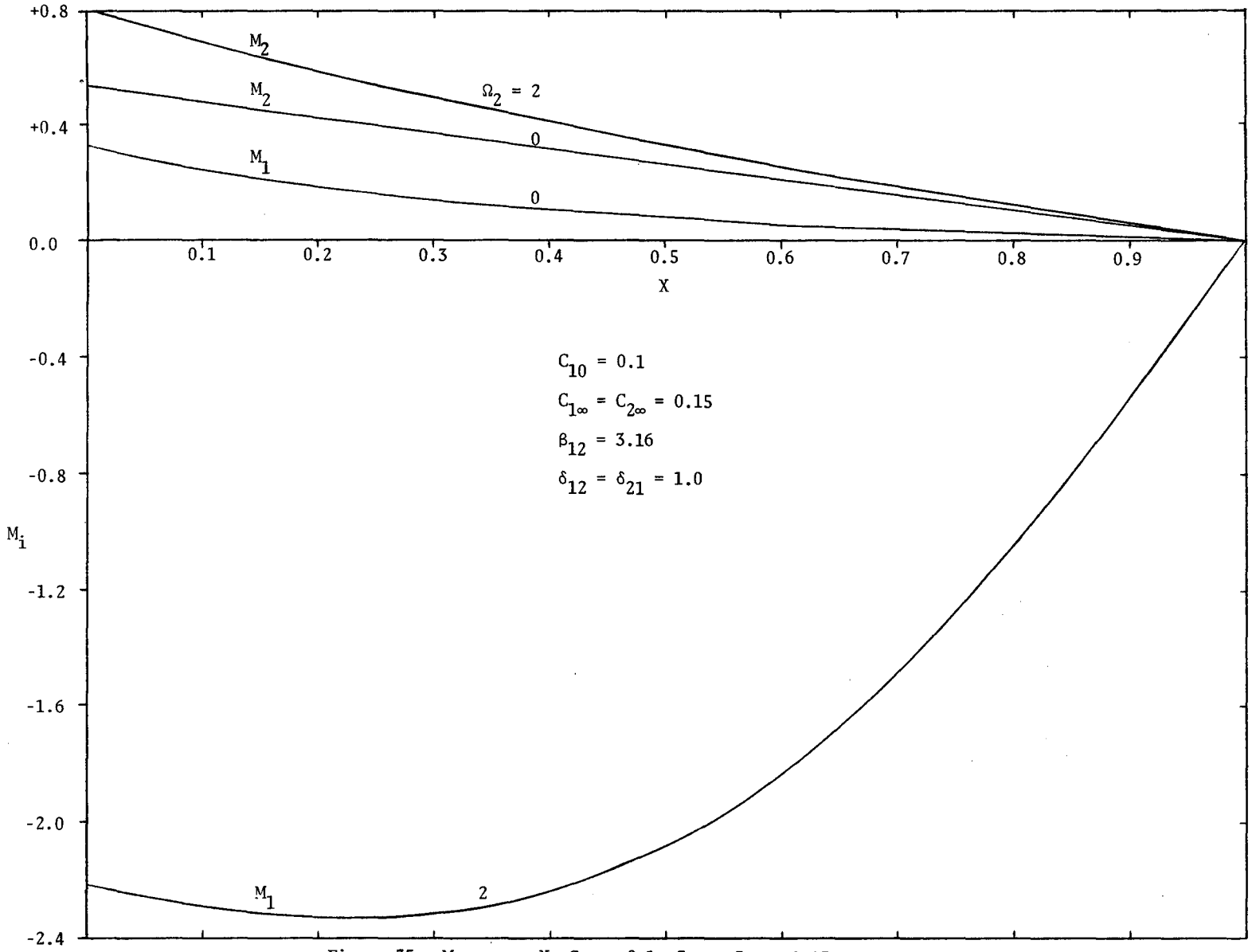

Figure 35. M_i versus X, $C_{10} = 0.1$, $C_{1\infty} = C_{2\infty} = 0.15$, $\beta_{12} = 3.16$

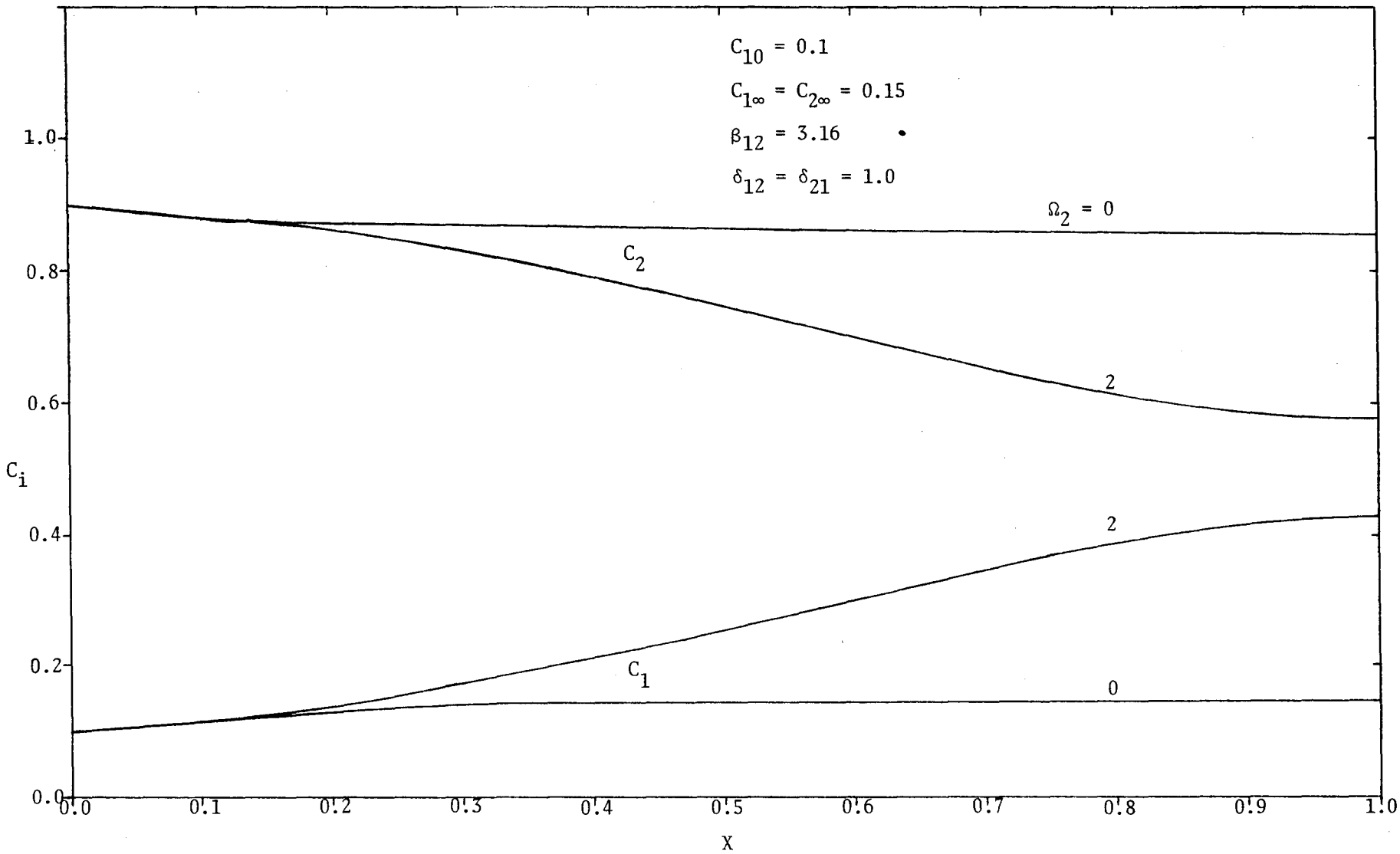

Figure 36. C_i versus X, $C_{10} = 0.1$, $C_{1\infty} = C_{2\infty} = 0.15$, $\beta_{12} = 3.16$

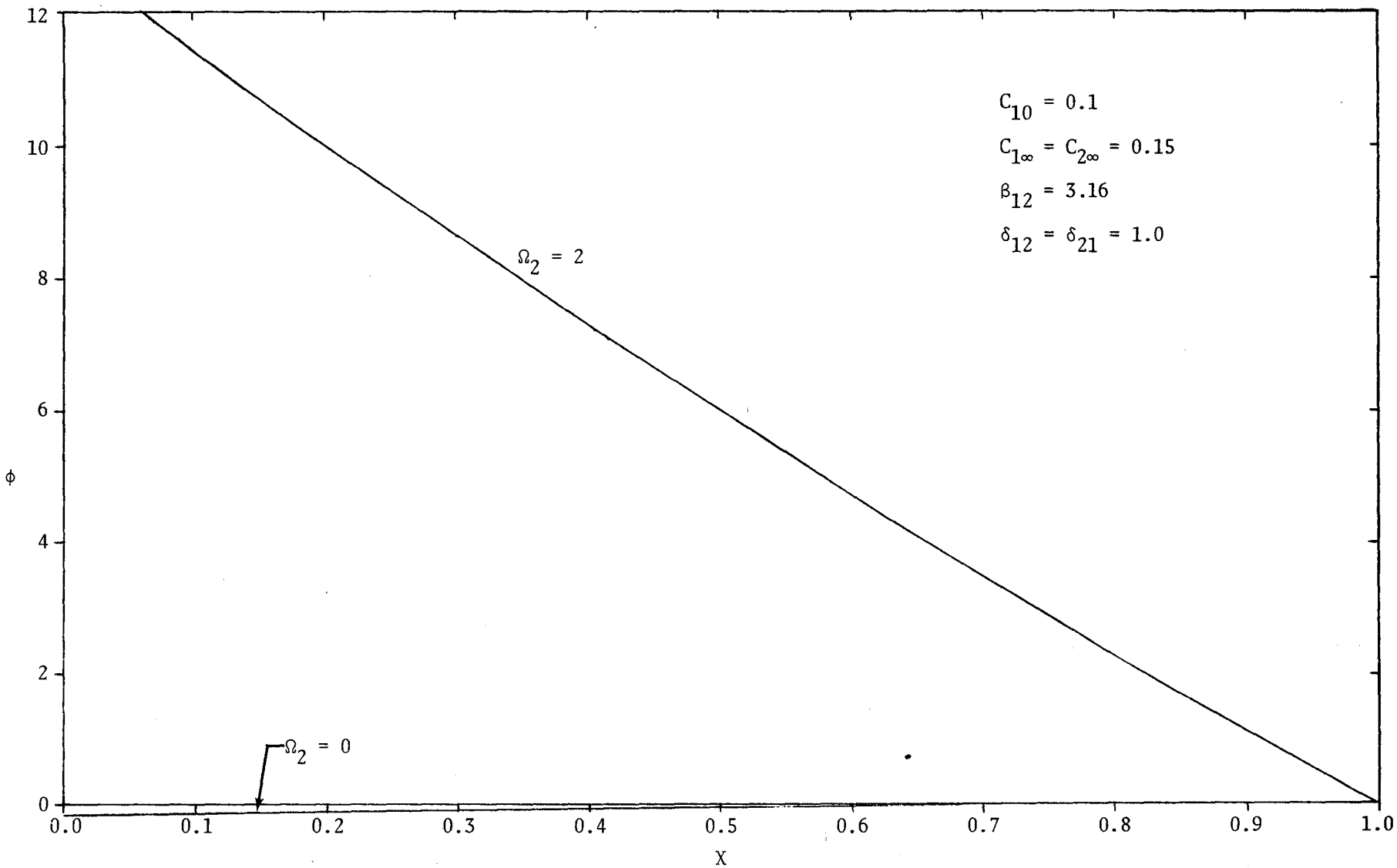

Figure 37. ϕ versus X, $C_{10} = 0.1$, $C_{1\infty} = C_{2\infty} = 0.15$, $\beta_{12} = 3.16$

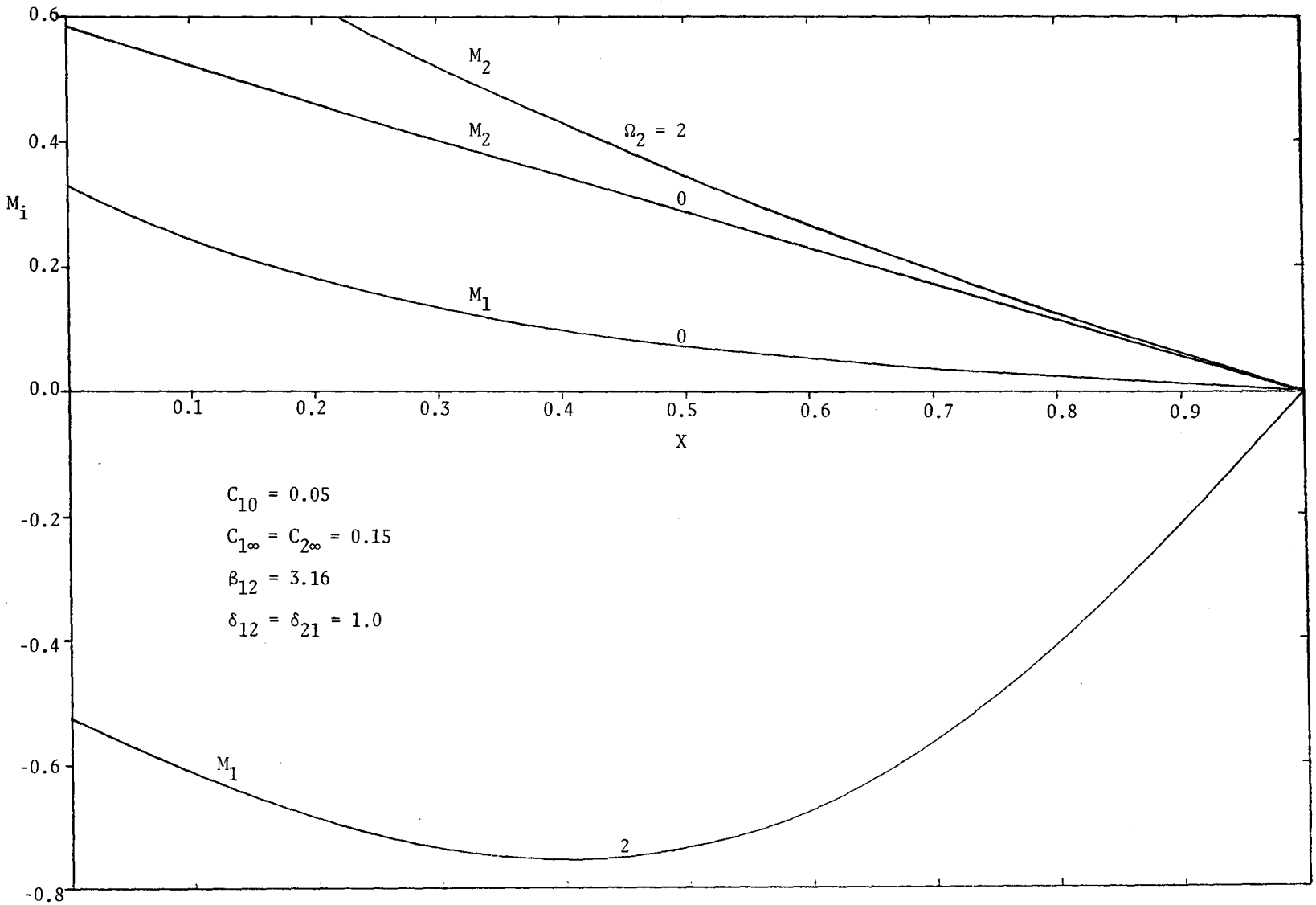

Figure 38. M_i versus X, $C_{10} = 0.05$, $C_{1\infty} = C_{2\infty} = 0.15$, $\beta_{12} = 3.16$

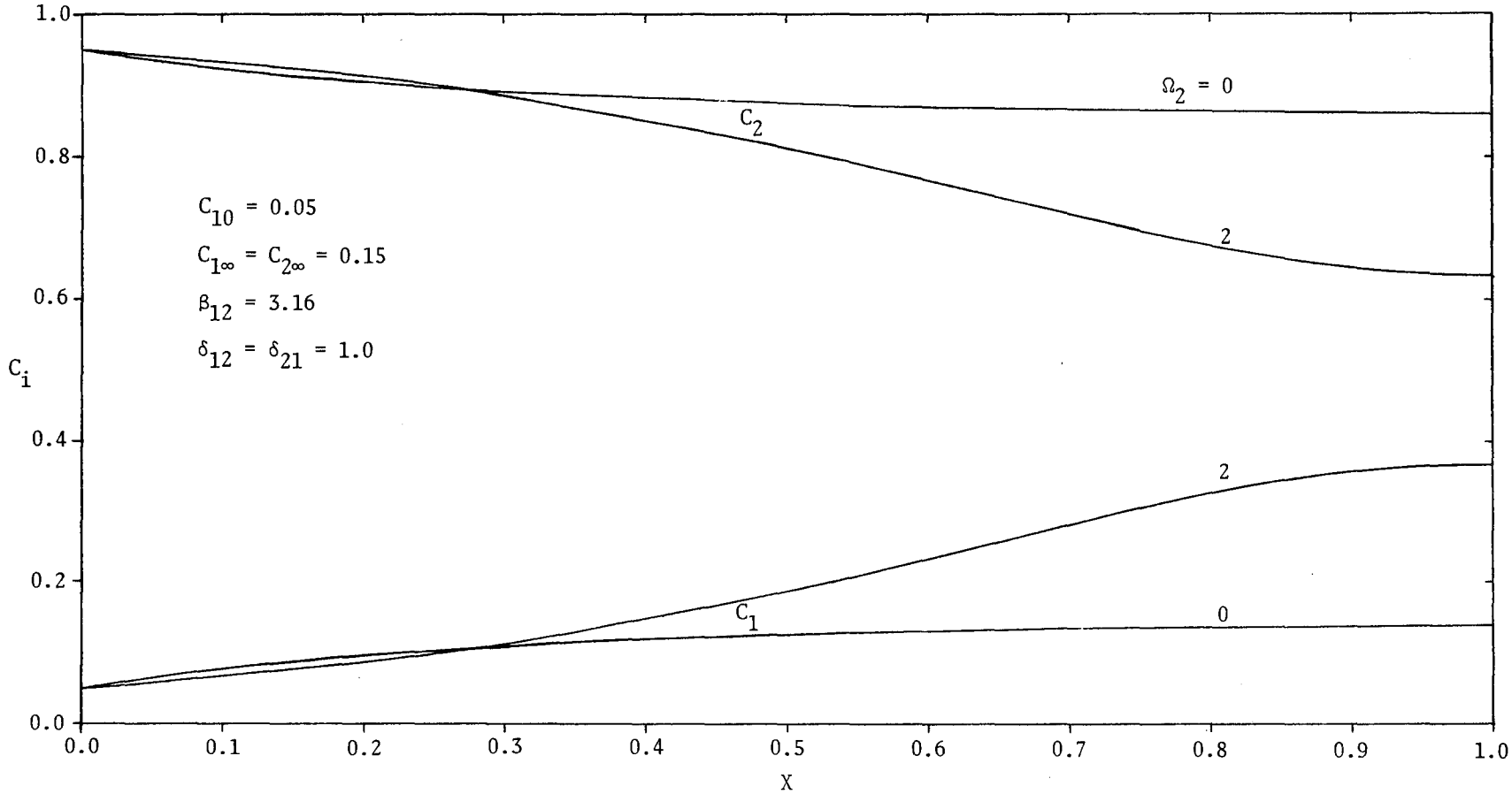

Figure 39. C_i versus X, $C_{10} = 0.05$, $C_{1\infty} = C_{2\infty} = 0.15$, $\beta_{12} = 3.16$

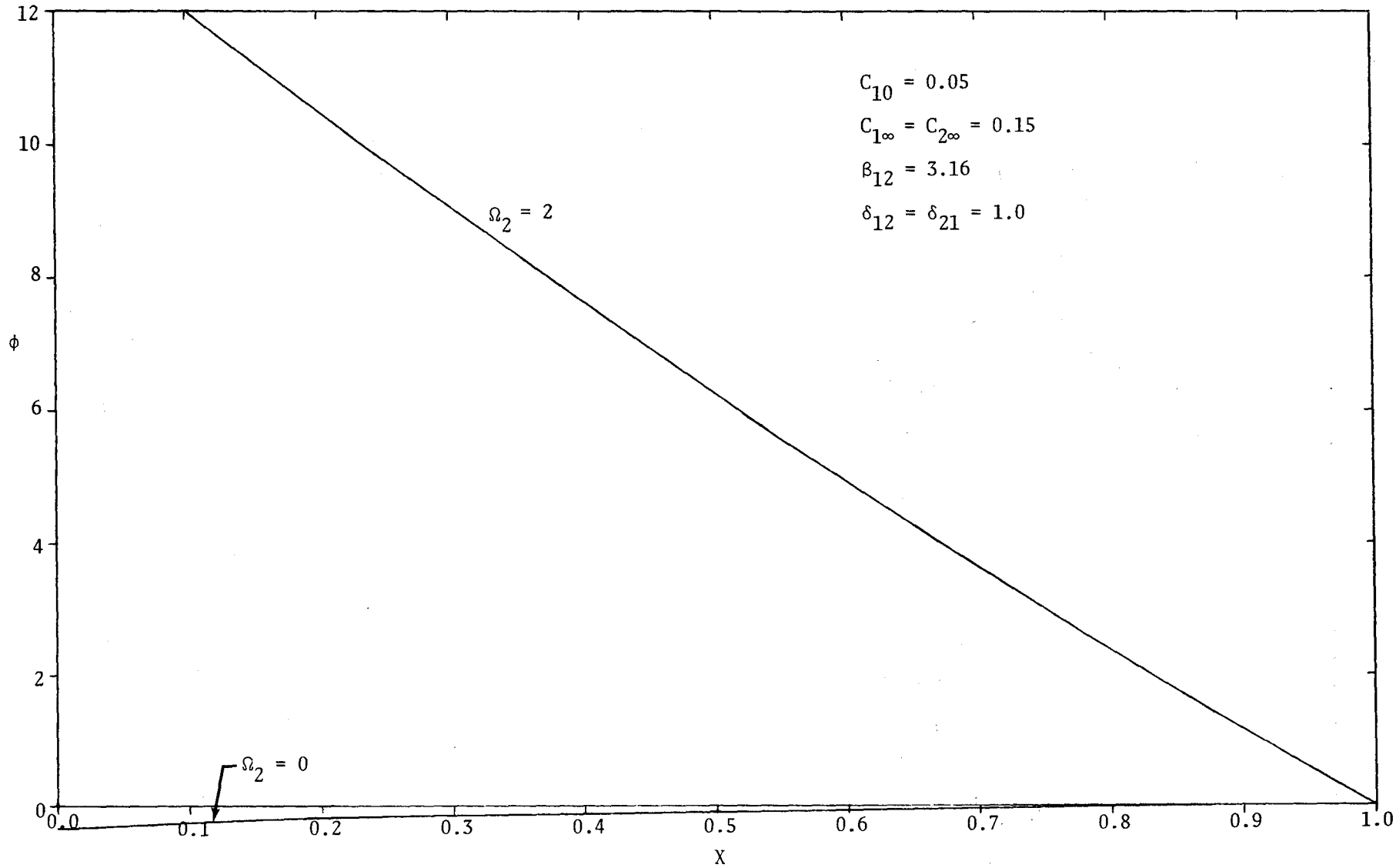

Figure 40. ϕ versus X, C_{10} = 0.05, $C_{1\infty}$ = $C_{2\infty}$ = 0.15, β_{12} = 3.16

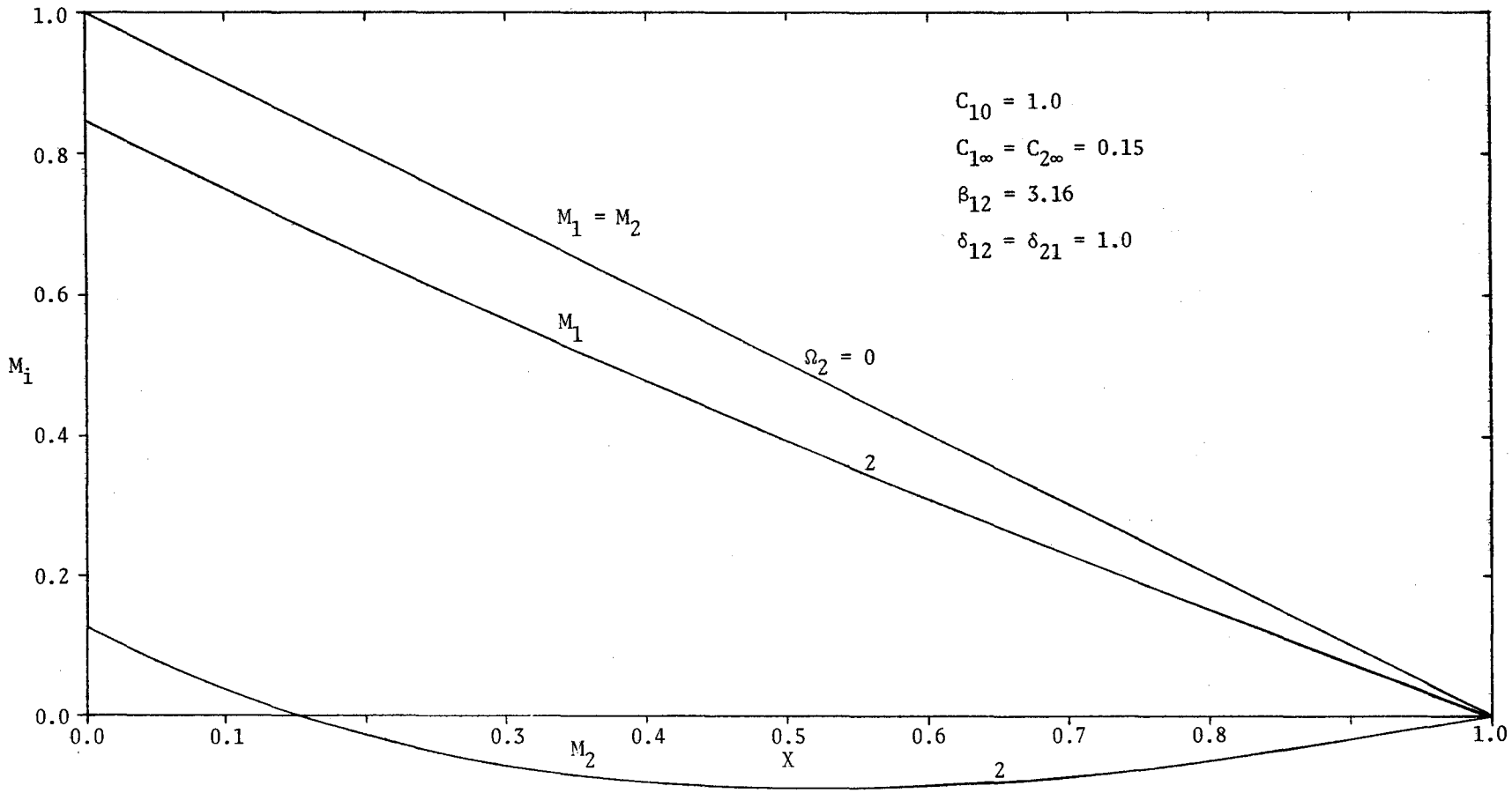

Figure 41. M_i versus X, C_{10} = 1.0, $C_{1\infty}$ = $C_{2\infty}$ = 0.15, β_{12} = 3.16

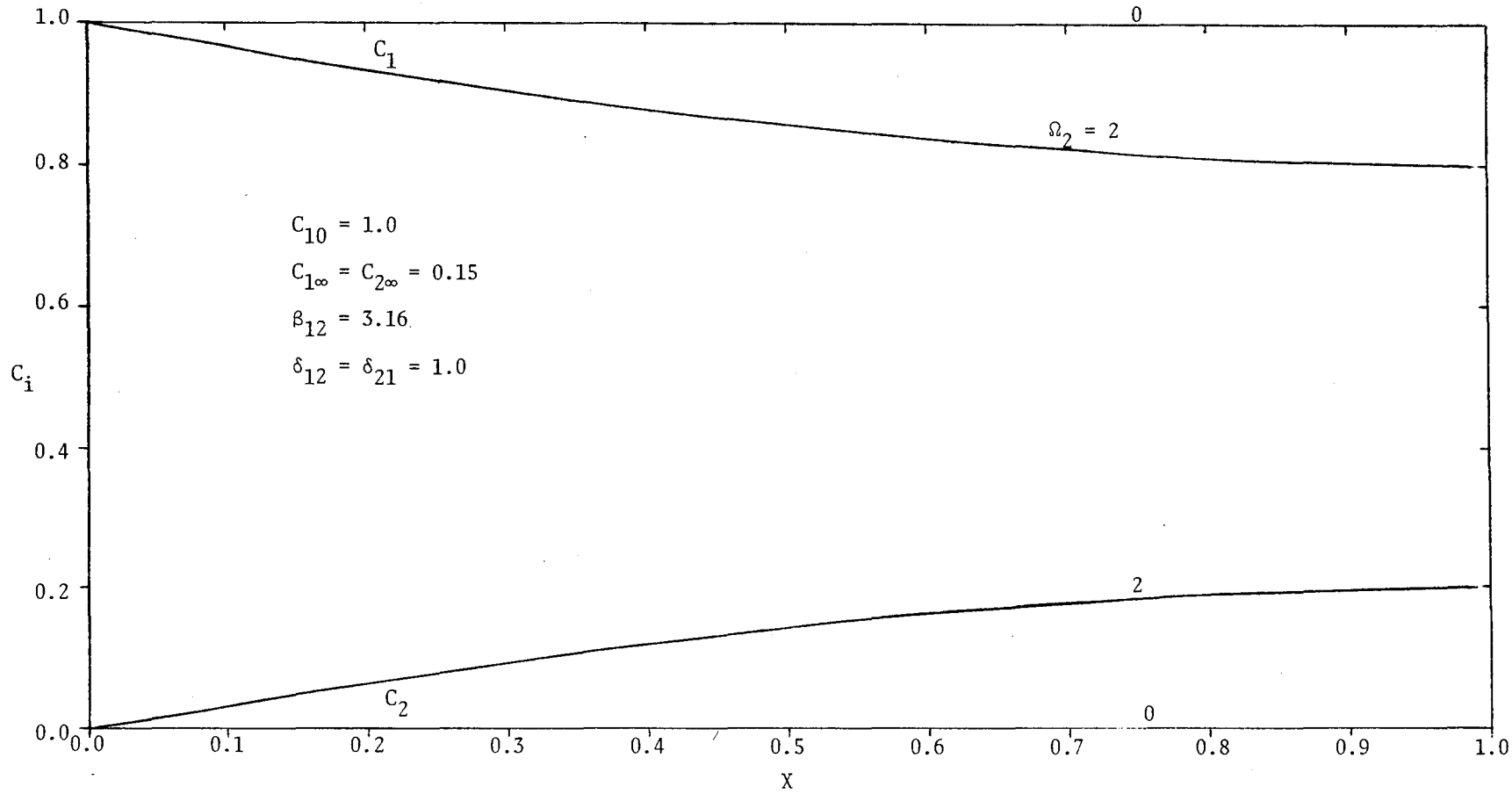

Figure 42. C_i versus X, $C_{10} = 1.0$, $C_{1\infty} = C_{2\infty} = 0.15$, $\beta_{12} = 3.16$

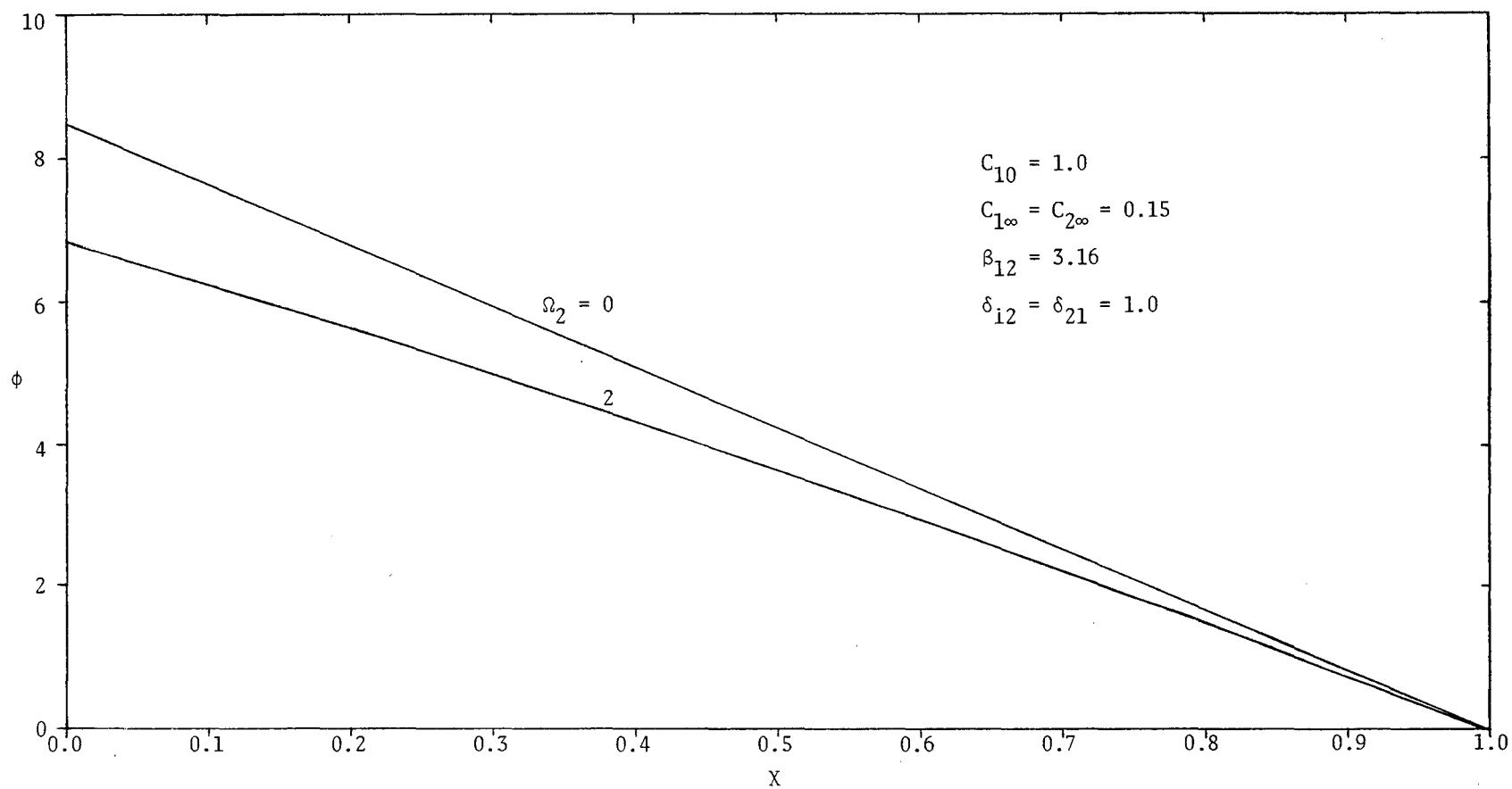

Figure 43. ϕ versus X, C_{10} = 1.0, $C_{1\infty}$ = $C_{2\infty}$ = 0.15, β_{12} = 3.16

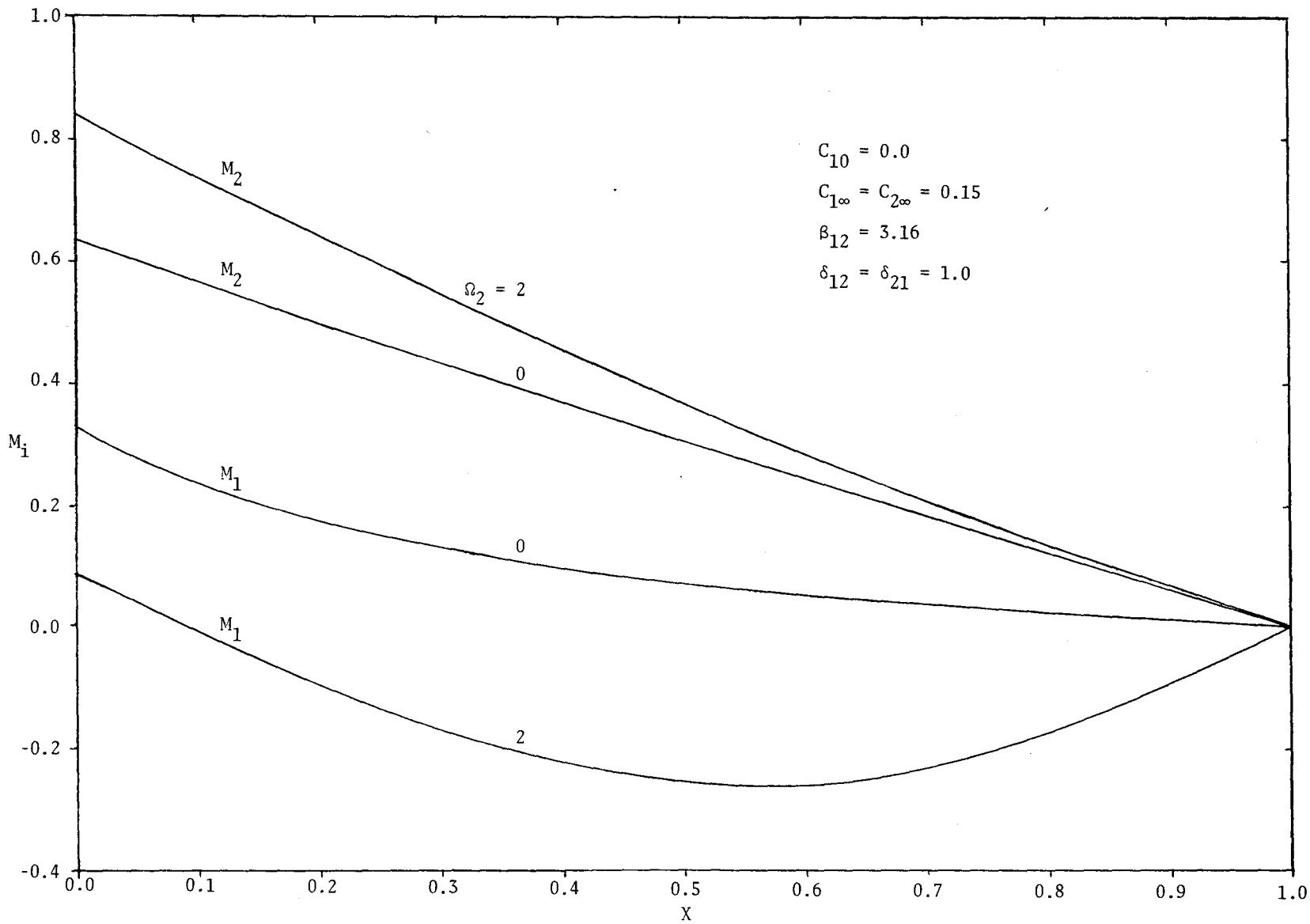

Figure 44. M_i versus X, $C_{10} = 0.0$, $C_{1\infty} = C_{2\infty} = 0.15$, $\beta_{12} = 3.16$

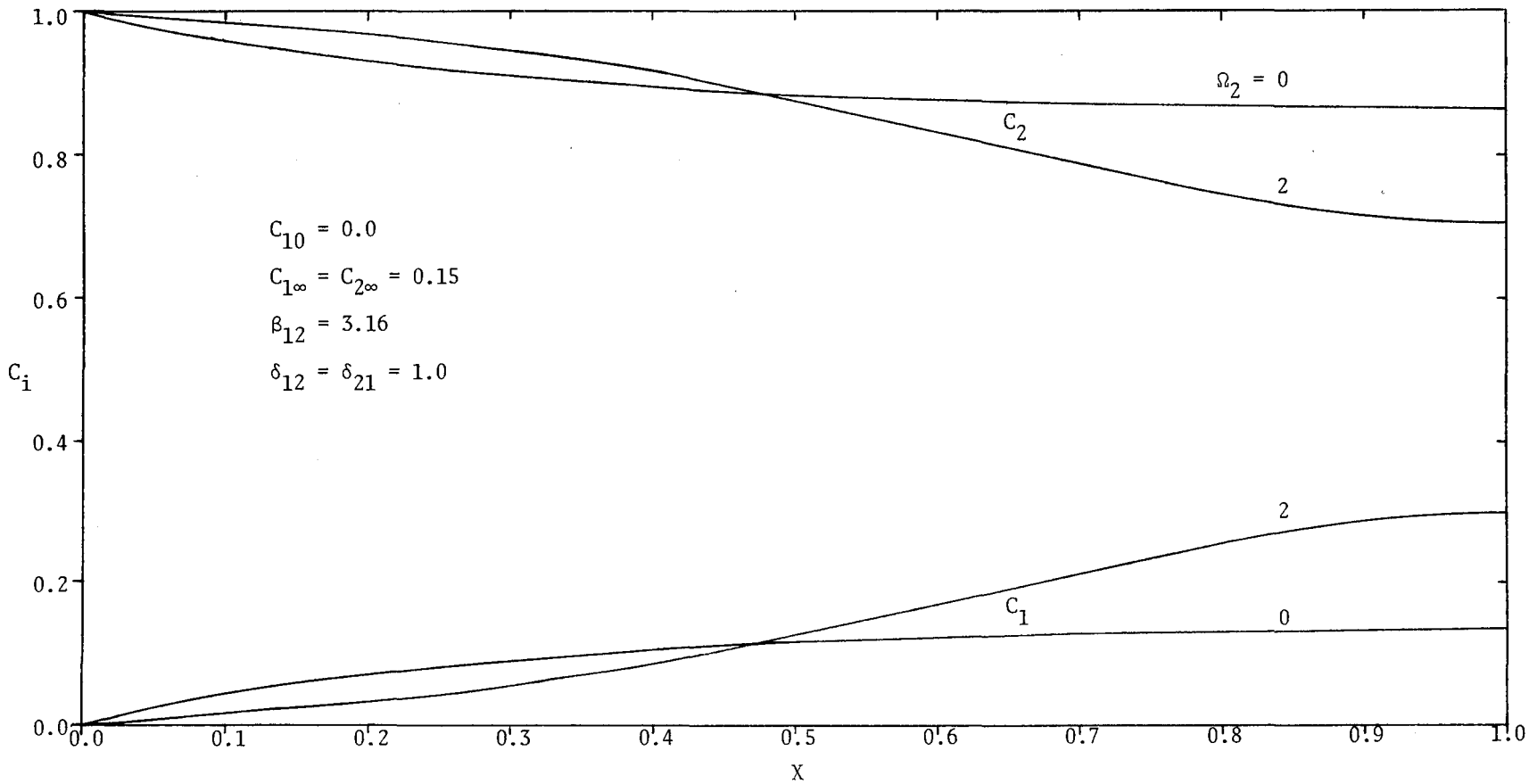

Figure 45. C_i versus X, $C_{10} = 0.0$, $C_{1\infty} = C_{2\infty} = 0.15$, $\beta_{12} = 3.16$

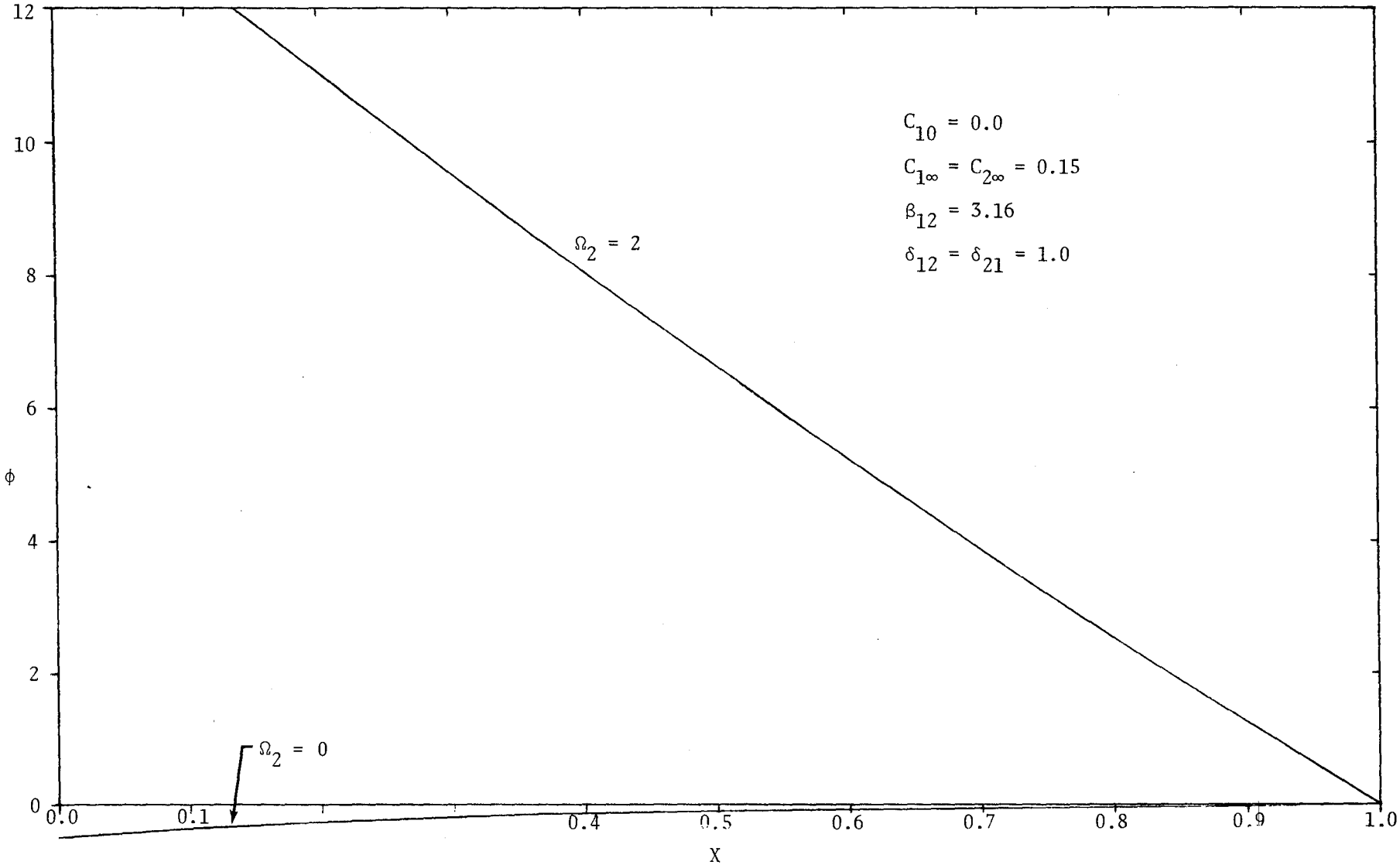

Figure 46. ϕ versus X, $C_{10} = 0.0$, $C_{1\infty} = C_{2\infty} = 0.15$, $\beta_{12} = 3.16$

velocity convection cases do not occur here and provide such an easily identified characteristic. Figures 29-46 are all for the case $C_{1\infty} = C_{2\infty} = 0.15$, $\beta_{12}^2 = 10$ and $\Omega_2 = 2$ and 0. The value of $C_{10} = 1 - C_{20}$ is varied to illustrate a number of new features not present in the other examples. Figures 29-31 are for $C_{10} = 0.25$. The $\Omega_2 = 0$ case is not near the convection dominated limit, however when $\Omega_2 = 2$ then $\phi_0 = \phi(X = 0) > 11$. That this $\Omega_2 = 2$ case is somewhat near the convection limit is shown by the fact that from Figures 7 and 8 $M_{10} = 2.8$ and $M_{20} = 0.7$ while $C_{11} = 0.75$ at that limit. Notice that $\Omega_{eff\ 2} < \Omega_2$ for this case. Figures 32-34 are for $C_{10} = 0.8$ and the results for $\Omega_2 = 2$ appear to be closer to the convection limit than the previous case even though ϕ is a little less than 8 at $X = 0$. In this case $\Omega_{eff\ 2} > \Omega_2$. Figures 35-37 are for $C_{10} = 0.1$ and show vastly different results from the preceding two examples. First, observe that specie 2 is controlling the problem when $\Omega_2 = 2$ to the extent that specie 1 has been reversed in flow direction from that which would exist for perfect mixing. In fact it is flowing at more than twice the rate of, as well as in the opposite direction from, that expected for perfect mixing. Furthermore specie 1 has a wall stagnation point at about $X = 0.24$ where $dM_1/dX = 0$ so that specie 1 flows from the bore for $X > 0.24$ and to the bore for $X < 0.24$. In addition, Figure 37 shows that the perfect filter case $\Omega_2 = 0$ has negative global velocity while the $\Omega_2 = 2$ case has positive global velocity. Of course negative M_{10} causes $\Omega_{eff\ 2}$ to be negative as well. Figures 38-40 are for $C_{10} = 0.05$ and show much the same behavior as seen in Figures 35-37 with the minimum in M_1 when $\Omega_2 = 2$ being even more pronouned and moving out to about $X = 0.41$. As before, the $\Omega_2 = 2$ case is somewhat near the convection limit but not completely in that regime as is seen by comparison with Figures 7 and 8.

Figures 41-43 are for $C_{10} = 1.0$, so that the vent volume contains only specie 1. This is one of the most interesting examples given here. First notice that for the perfect filter $\Omega_2 = 0$, $M_{10} = M_{20} = 1.0$ and $C_1 = C_{10} = 1.0$ so that the tube geometry does not contribute anything. However when $\Omega_2 = 2$, M_2 exhibits a sign change at about $X = 0.16$ as well as a minimum at about $X = 0.53$. Thus both bore and wall stagnation points are present. At the root specie 2 flows from the bore, but for $X > 0.16$ specie 2 flows away from the root. Also specie 2 flows into the bore via the wall for $X < 0.53$, while it flows from the bore for $X > 0.53$. The net or global velocity is positive for both $\Omega_2 = 0$ and $\Omega_2 = 2$. The effective separation ratio is greatly reduced from Ω_2, $\Omega_{eff\ 2} < \Omega_2$ when $\Omega_2 = 2$.

The final example given by Figures 44-46 is for $C_{10} = 0.0$; at first it appears to be very similar to the preceding case even though in this example the vent volume contains none of specie 1 compared to only specie 1 there. However in this example the global velocity is negative for $\Omega_2 = 0$ and positive for $\Omega_2 = 2$. Also in this case it is specie 1, as should be expected, which displays the bore and wall stagnation points when $\Omega_2 = 2$. Here the effective separation ratio is greatly increased over Ω_2, $\Omega_{eff\ 2} > \Omega_2$.

The two specie cases have exhibited a wide variety of behavior; this behavior can involve flow regime variation between the diffusion and convection limits, either positive or negative flow velocity for individual species as well as the global flow, and local specie wall and bore stagnation points. This behavior is controlled by the values of C_{i0}, $C_{i\infty}$, β_{ij} and δ_{ij} which depend on the diffusive and permeating properties of the gases and wall materials, respectively, the particular gas mixtures present in each reservoir, the total pressure in the vent volume, the system temperature, and the tube geometry in the form of length, diameter, and wall thickness.

$I \geq 3$ (TERNARY MIXTURE OR GREATER NUMBER OF SPECIES)

Since most of the possible physical behavior can be and has been illustrated by means of two specie examples, only a few examples with more species are needed.

The first example is given by Figures 47-49 and consists of a case where equal molar amounts of five different species are placed in each reservoir with the driver volume having a total pressure five times that of the vent volume. Thus a negative velocity case results. The δ_{ij} values are all taken to be unity, and the separation ratios Ω_i for the respective species are 1.0, 0.25, 0.0225, 0.0025 and 0.0, with $\beta^2_{1j} = 4.0$. Figure 47 shows that the fast permeating species 1 and 2 have dehanced flow rates compared to perfect mixing, $M_{10} < 1$ and $M_{20} < 1$, while species 3, 4 and 5 are enhanced $M_{i0} > 1$. Physically this occurs because species 1 and 2 build up in the tube due to the difficulty that they experience in diffusing through the nearly stagnant species 3, 4 and 5. This is shown by Figure 48 and the magnitude of ϕ from Figure 49.

Another type of example is given by Figures 50-52, where the equi-molar mixture is maintained for the five species in the vent volume, but the driving pressures of the species are different, $C_{i\infty} = 10$, 5, 2, 0.5 and 0.2001, respectively. Here all species have essentially equal permeating properties, $\Omega_i = 1$ and $\beta^2_{ij} = 4$. This example is nearly in the convection regime as is shown by the flat C_i profiles and the magnitude of ϕ in Figures 51 and 52, respectively. Notice that species 1 and 2 are dehanced in flow rate from the perfect mixing case while species 3, 4 and 5 are enhanced. For specie 5 the enhancement is very large, $M_{50} = 1.86 \times 10^3$, since in the perfect mixing case it would hardly flow at all due to the small value for $(C_{5\infty} - C_{50}) = 10^{-4}$. This results because the fast

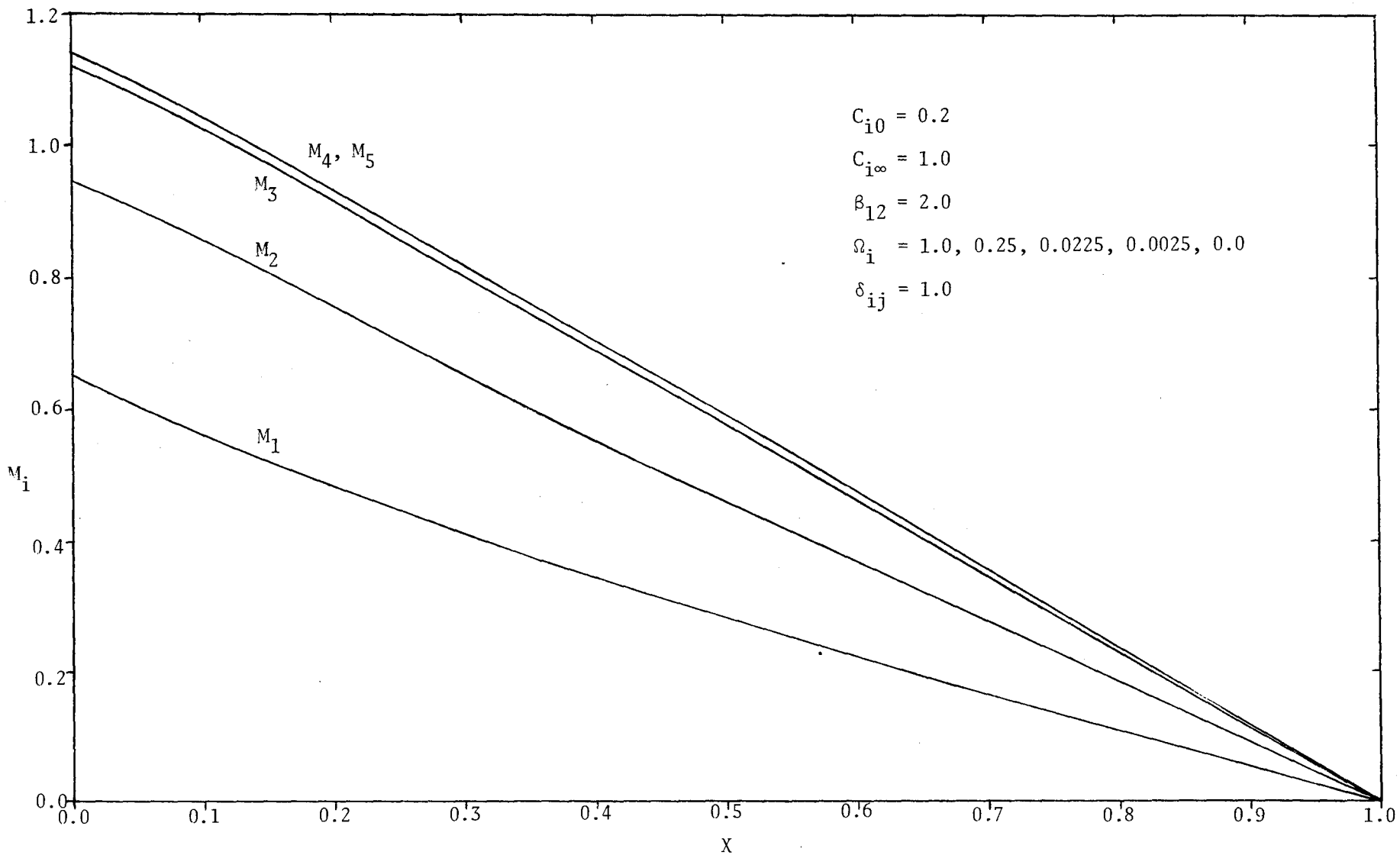

Figure 47. M_i versus X, Five Species, C_{i0} = 0.2, $C_{i\infty}$ = 1.0, β_{12} = 2.0, Ω_i = 1.0, 0.25, 0.0225, 0.0025, 0.0

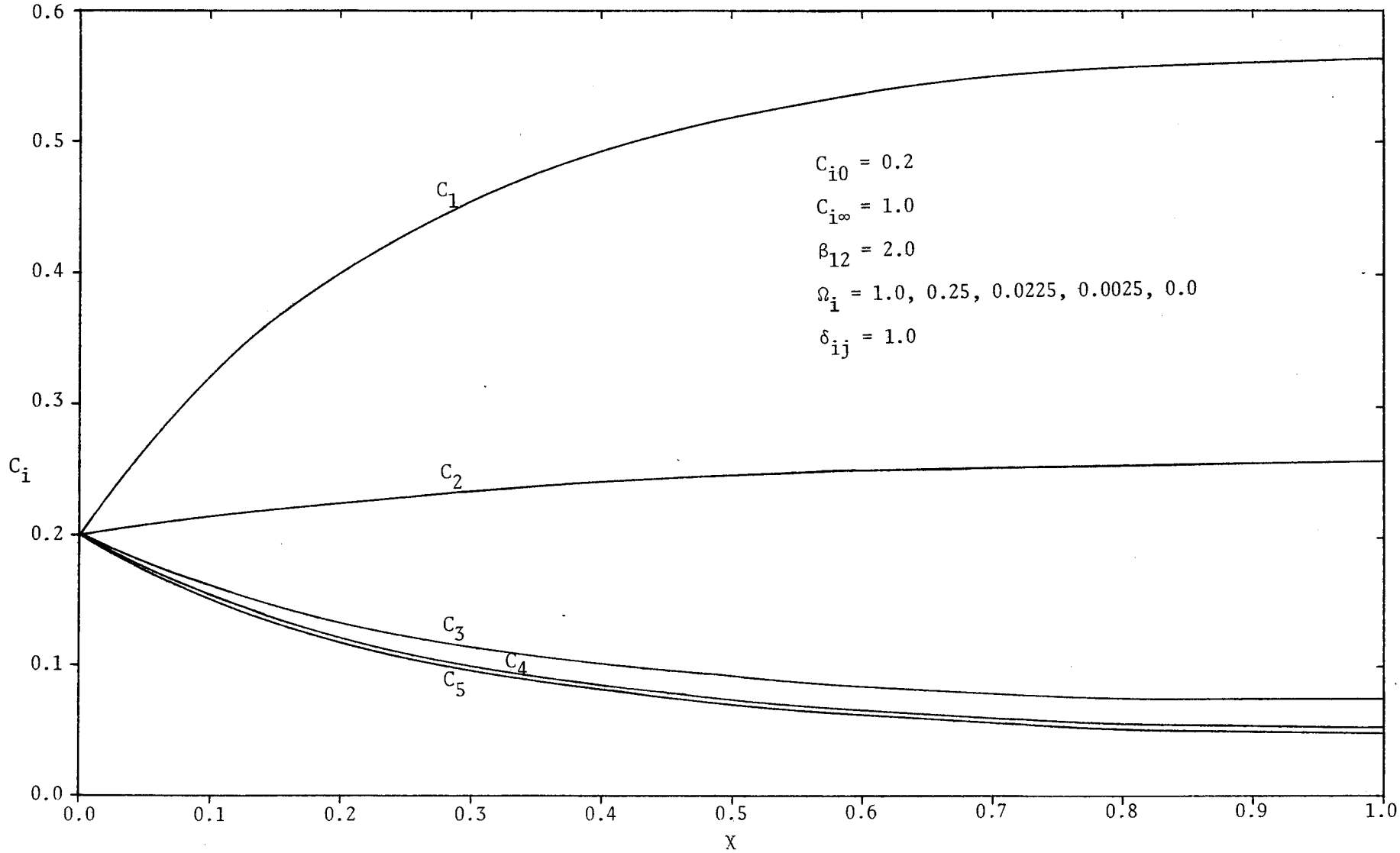

Figure 48. C_i versus X, Five Species, C_{i0} = 0.2, $C_{i\infty}$ = 1.0, β_{12} = 2.0, Ω_i = 1.0, 0.25, 0.0225, 0.0025, 0.0

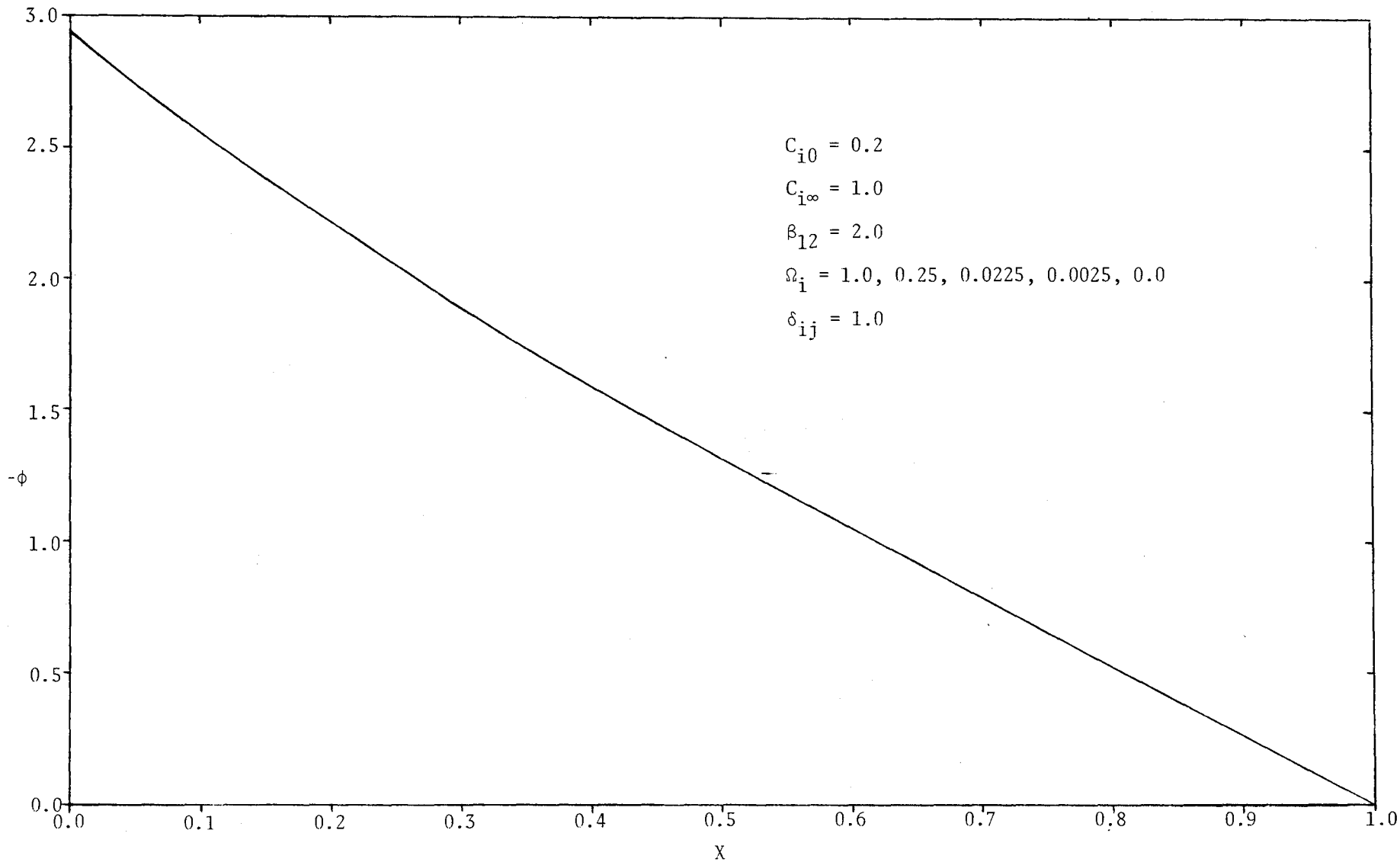

Figure 49. $-\phi$ versus X, Five Species, $C_{i0} = 0.2$, $C_{i\infty} = 1.0$, $\beta_{12} = 2.0$, $\Omega_i = 1.0, 0.25, 0.0225, 0.0025, 0.0$

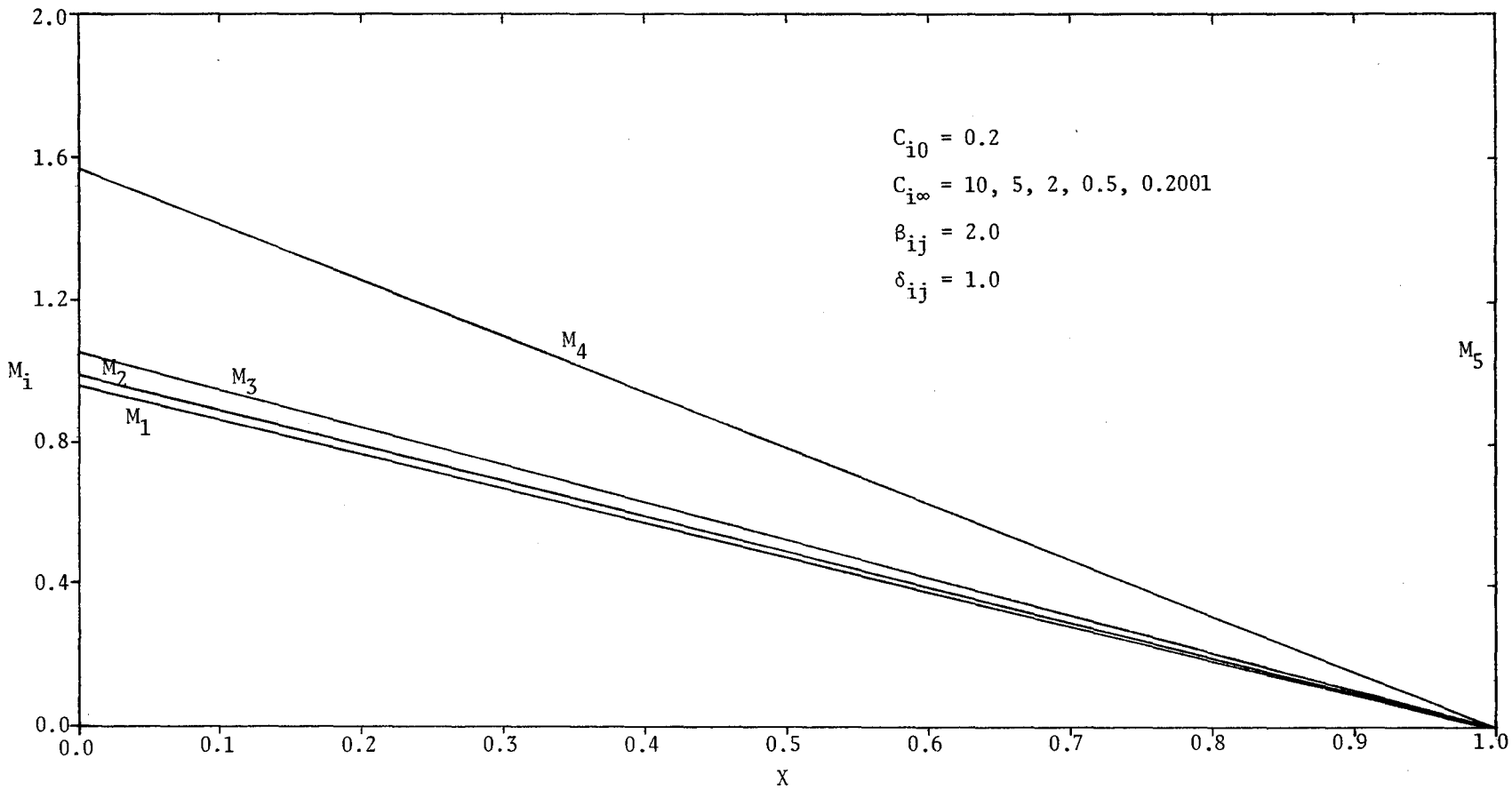

Figure 50. M_i versus X, Five Species, C_{i0} = 0.2, $C_{i\infty}$ = 10, 5, 2, 0.5, 0.2001, β_{ij} = 2.0

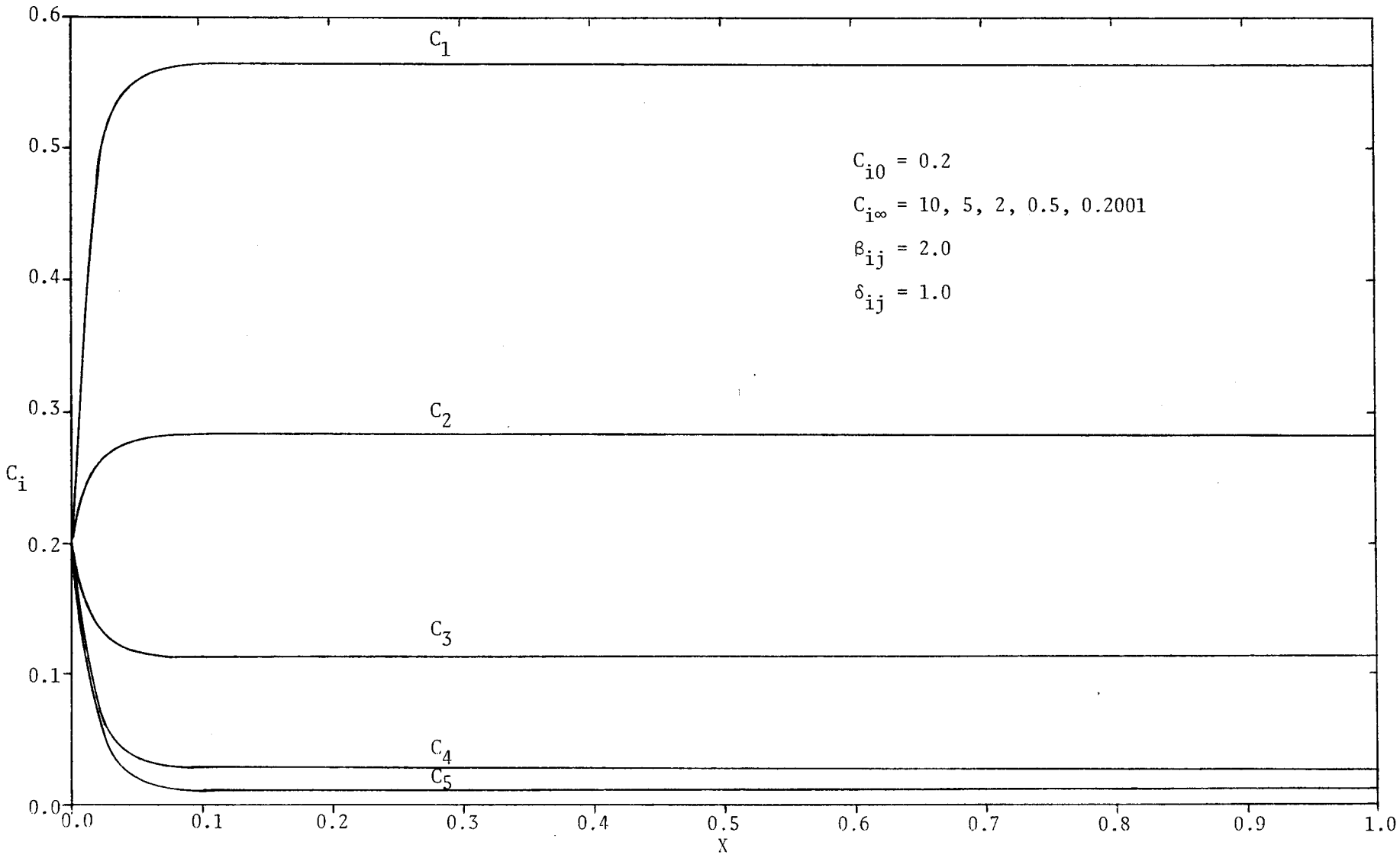

Figure 51. C_i versus X, Five Species, C_{i0} = 0.2, $C_{i\infty}$ = 10, 5, 2, 0.5, 0.2001, β_{ij} = 2.0

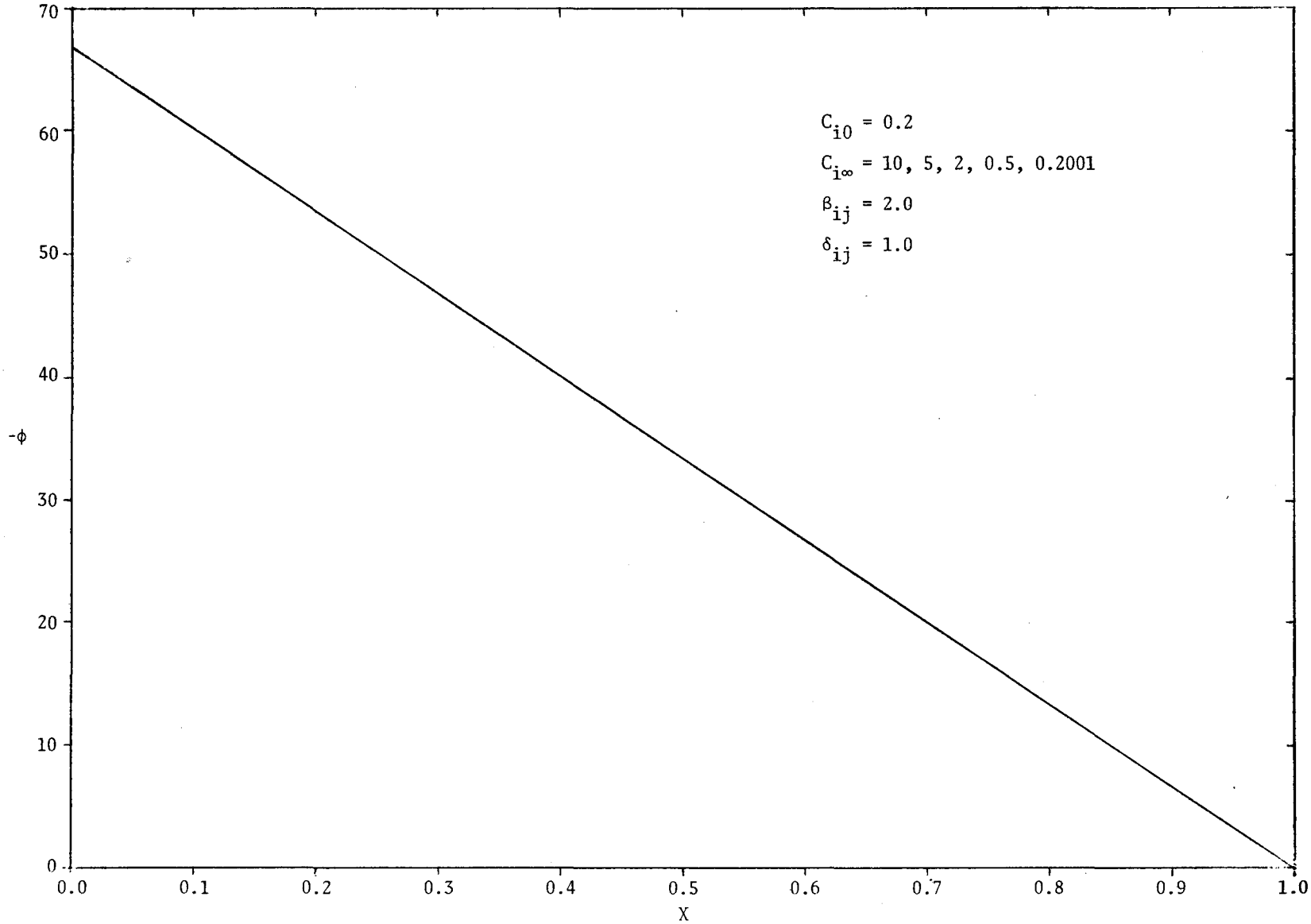

Figure 52. -ϕ versus X, Five Species, C_{i0} = 0.2, $C_{i\infty}$ = 10, 5, 2, 0.5, 0.2001, β_{ij} = 2.0

permeating species displace specie 5 from the tube so that the local driving force $C_{5\infty} - C_5$ is greatly increased over $C_{5\infty} - C_{50}$.

An example where the mixture is different in each reservoir is given by Figures 53-55; the C_{i0} values are 0.0, 0.1, 0.2, 0.3 and 0.4, while the $C_{i\infty}$ values are 2, 10^0, 10^{-1}, 10^{-2} and 10^{-4}, respectively. The δ_{ij} and Ω_i values are all unity and $\beta_{ij}^2 = 4$. Figures 54 and 55 show that the net velocity is negative and that the example is not convection dominated. Figure 53 shows that all five specie flow rates are dehanced in magnitude from their perfect mixing values. Species 1 and 2 dominate the problem since they both have negative velocity and M_i is positive for all X. Specie 3 also has negative velocity for all X, but this is caused by the specie 1 and 2 domination since M_3 is negative indicating that it would have positive velocity in the perfect mixing limit; specie 3 has a wall stagnation point near X = 0.11. Specie 4 has a wall stagnation point near X = 0.56 and a bore stagnation point near X = 0.33, so that it has positive bore velocity only for X < 0.33. Finally, specie 5 has positive bore velocity for all X. Thus the specie 1 and 2 domination is not sufficient to change the flow direction of specie 5 although such is the case for specie 3.

As a final five specie example, Figures 56-58 give the case identical to that given by Figures 47-49 except that the non-permeating specie 5, $\Omega_5 = 0$, is replaced by a very fast permeating specie, $\Omega_5 = 4$. From Figures 57-58 versus 48-49 it is evident that such a change shifts the flow regime much nearer to the convection dominated regime. Also it is apparent from Figure 56 versus Figure 47 that the flow rates of species 1-4 are increased, since the M_{i0} are increased, although the flow of specie 5 itself is greatly dehanced from the perfect mixing limit. More will be said about the potential for exploitation of some of these phenomena in the following discussion.

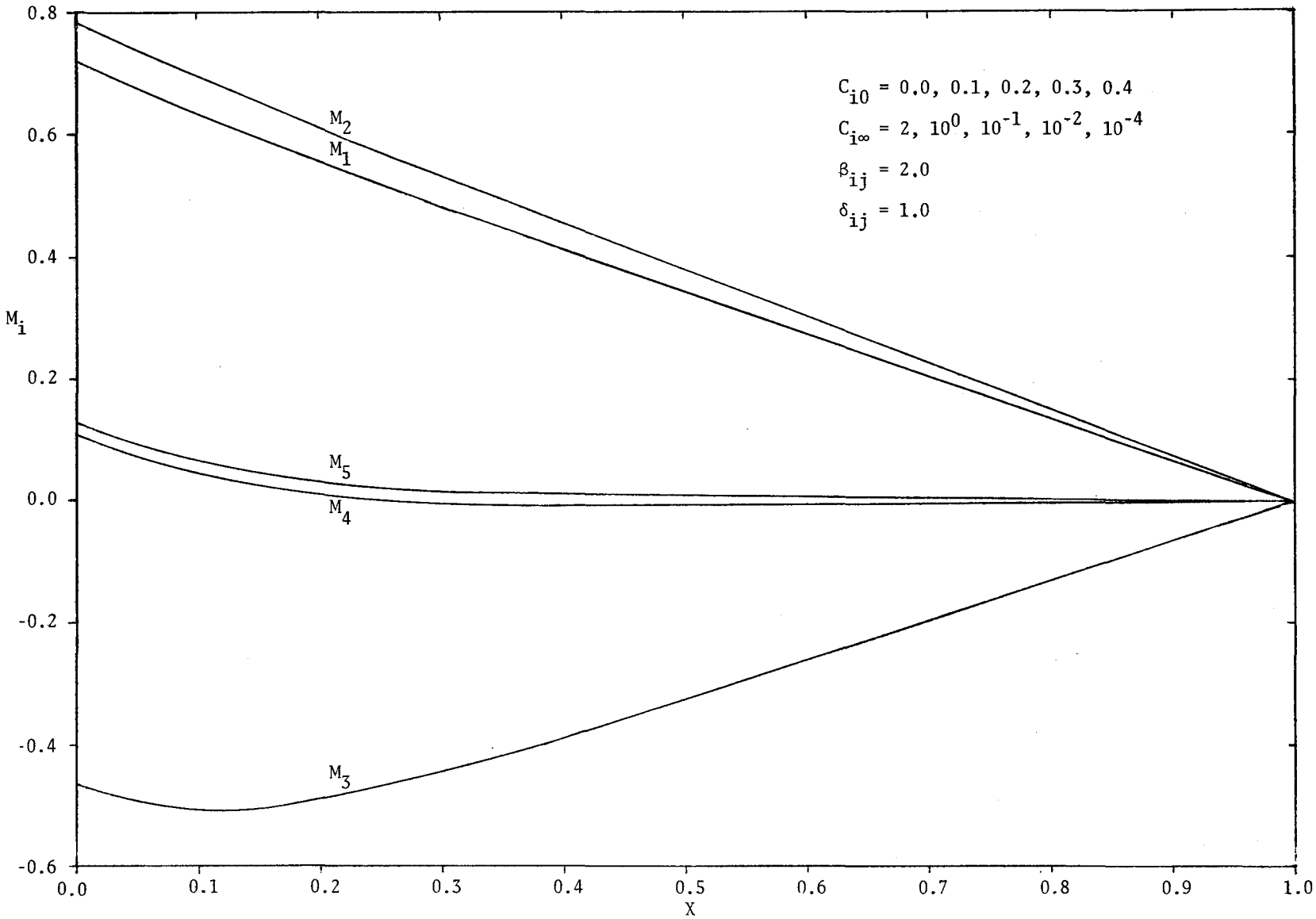

Figure 53. M_i versus X, Five Species, C_{i0} = 0.0, 0.1, 0.2, 0.3, 0.4, $C_{i\infty}$ = 2, 10^0, 10^{-1}, 10^{-2}, 10^{-4}, β_{ij} = 2.0

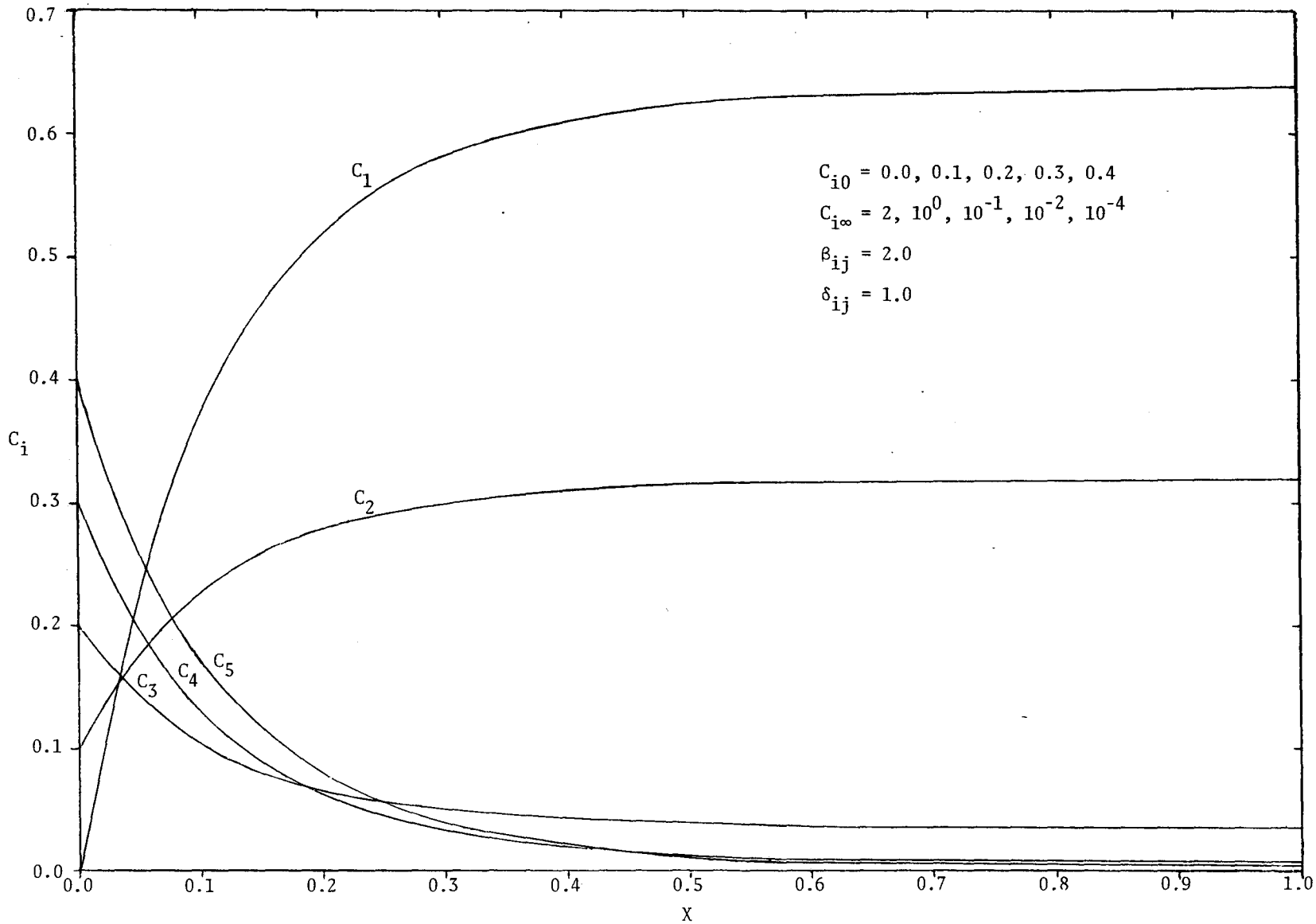

Figure 54. C_i versus X, Five Species, C_{i0} = 0.0, 0.1, 0.2, 0.3, 0.4, $C_{i\infty}$ = 2, 10^0, 10^{-1}, 10^{-2}, 10^{-4}, β_{ij} = 2.0

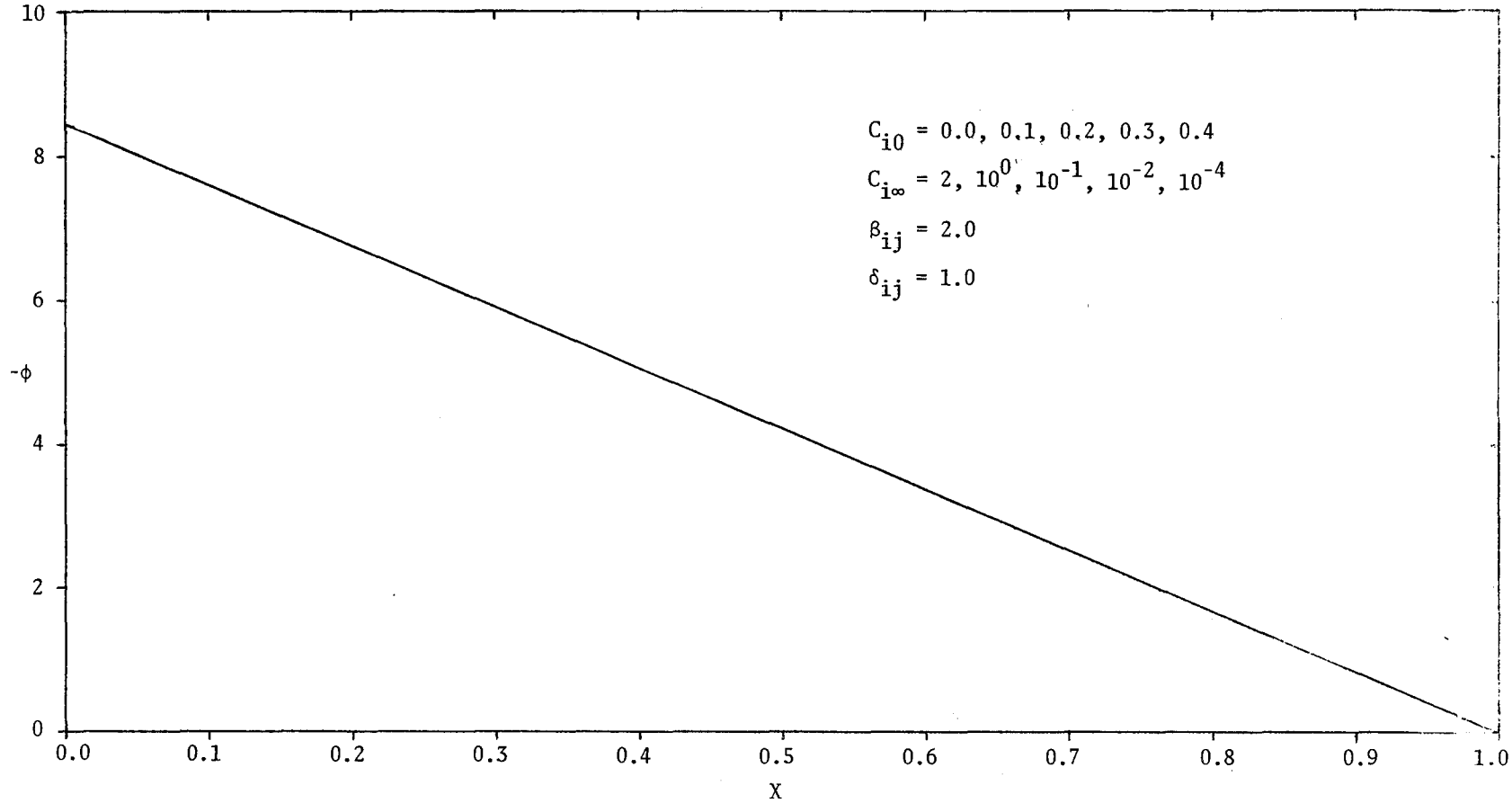

Figure 55. -ϕ versus X, Five Species, C_{i0} = 0.0, 0.1, 0.2, 0.3, 0.4, $C_{i\infty}$ = 2, 10^0, 10^{-1}, 10^{-2}, 10^{-4}, β_{ij} = 2.0

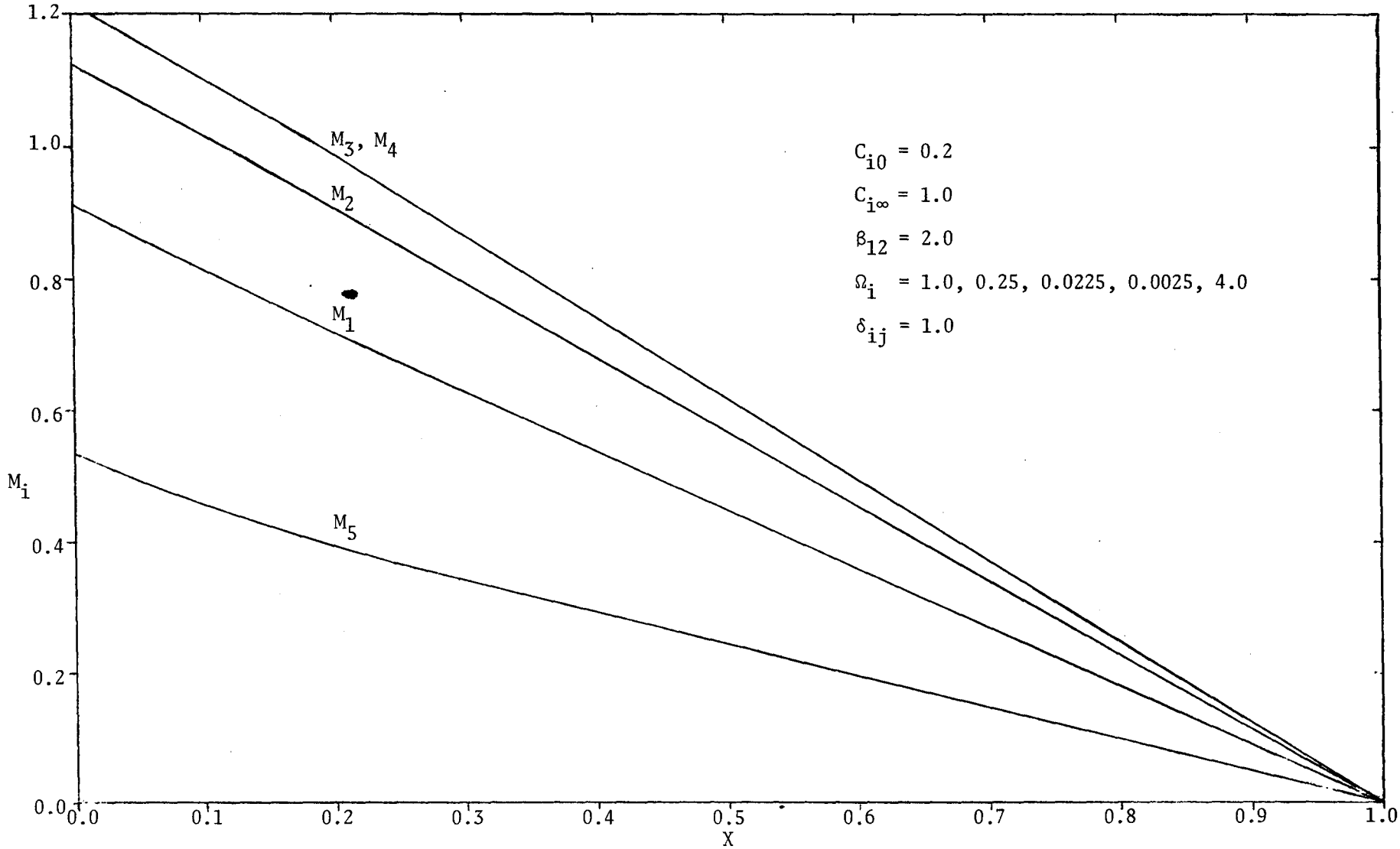

Figure 56. M_i versus X, Five Species, $C_{i0} = 0.2$, $C_{i\infty} = 1.0$, $\beta_{12} = 2.0$, $\Omega_i = 1.0, 0.25, 0.0225, 0.0025, 4.0$

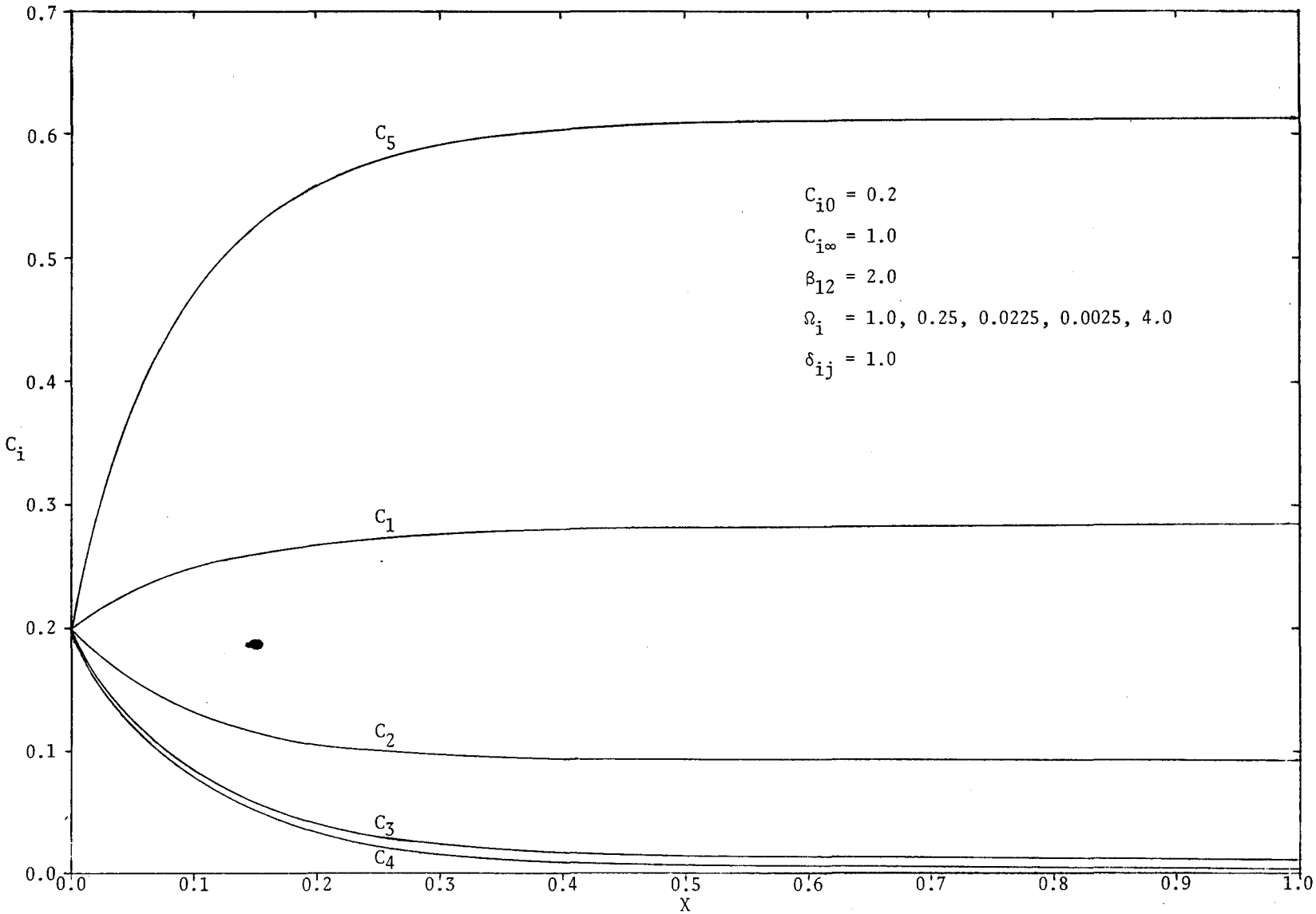

Figure 57. C_i versus X, Five Species, C_{i0} = 0.2, $C_{i\infty}$ = 1.0, β_{12} = 2.0, Ω_i = 1.0, 0.25, 0.0225, 0.0025, 4.0

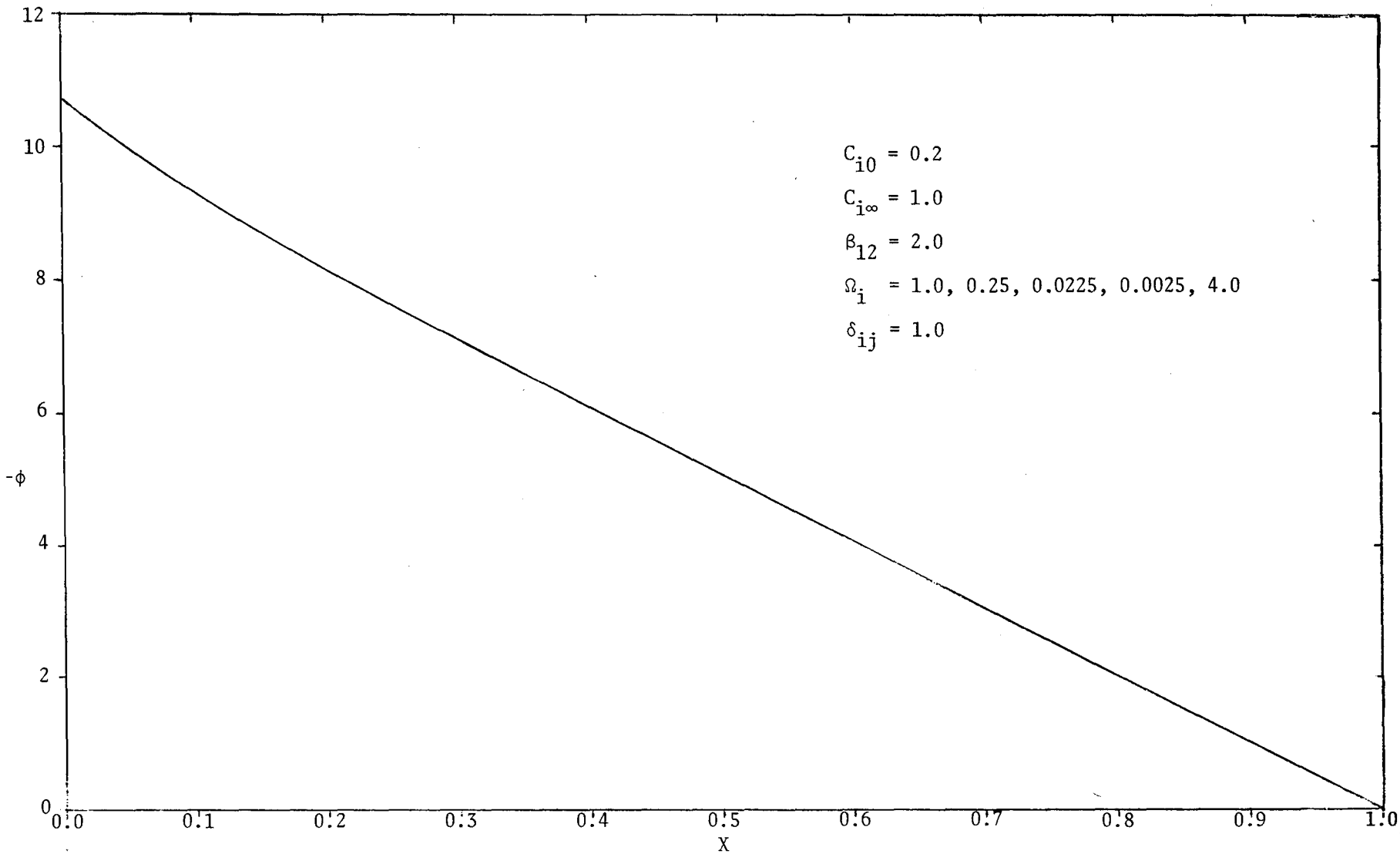

Figure 58. $-\phi$ versus X, Five Species, $C_{i0} = 0.2$, $C_{i\infty} = 1.0$, $\beta_{12} = 2.0$, $\Omega_i = 1.0, 0.25, 0.0225, 0.0025, 4.0$

(iii) Special Modes of Operation

The preceding examples have brought several interesting operational features forward which require some additional discussion. These include the possible beneficial effects of immersing the tube in the other reservoir (reverse the driver and vent volumes with no other change) so that the differences between positive and negative velocity cases can be exploited. Also of interest are the effects of adding an additional specie (or species) to one or both reservoirs in order to favorably influence the results for the original species in cases where such a tactic does not have other detrimental physical effects on the related processes; alternately, the exchange of a specie of secondary importance already present in one or both reservoirs for one which exercises more favorable control over the primary species is of interest.

Reservoir Switch

Within the assumptions applied to the current model, the results are identical in the perfect mixing limit regardless of which reservoir the permeable tube is immersed in. For finite $\mathcal{D}_{ij}$ the fluid mechanical coupling can be greatly different for positive and negative velocity cases so that some consideration must be given to which is the best for a particular application. Due to the fact that the tube bore is exposed to different total pressure and different gas concentrations when the reservoirs are switched, some care must be taken when comparisons are made. The controlling parameters C_{i0}, $C_{i\infty}$ and β_{ij}^2 are different for the two cases; the new ones (primed) are related to the old ones via

$$\left.\begin{aligned} C'_{i0} &= C_{i\infty} \Big/ \sum_{i=1}^{I} C_{i\infty} \\ C'_{i\infty} &= C_{i0} \Big/ \sum_{i=1}^{I} C_{i\infty} \\ \beta^{2'}_{ij} &= \beta^{2}_{ij} \sum_{i=1}^{I} C_{i\infty} \end{aligned}\right\} \tag{98}$$

so that usually the M'_{i0} and M_{i0} comparisons, or the $\Omega'_{\text{eff } i}$ versus $\Omega_{\text{eff } i}$ comparisons via (97) allow one to decide which is the best for the application under consideration.

All of the examples given cannot be evaluated here via (98), but it is possible to give an example to illustrate what has been said. Consider the perfect filter limit $\Omega_2 << 1$ for the example given by Figures 41-43 where $C_{10} = 1.0$, $C_{20} = 0.0$, $C_{1\infty} = C_{2\infty} = 0.15$ and $\beta^2_{12} = 10$ so the gas in the vent volume is nearly all specie 1. The result is that positive global velocity is present and there is no effect, $M_{10} = 1.0$. Now since $\sum_{i=1}^{2} C_{i\infty} = 0.3$, then $C'_{10} = C'_{20} = 0.5$ and $C'_{1\infty} = 3.333$, $C'_{2\infty} = 0$, $\beta^{2'}_{12} = 3.0$. The result is that $M'_{10} = 0.854$ so that almost 15 percent dehancement of the total flow rate for specie 1 is obtained if the negative velocity flow direction is selected for the permeable tube. This result can be easily predicted for this special case on simple physical grounds but such is not always the case, and it is often worth comparing the positive and negative velocity modes of operation. Of course there are many cases where negative velocity flow is better than the positive velocity direction.

Addition of Control Species

If additional species are introduced for the purposes of improving the flow of some or all of the original species, the original (unprimed) governing parameters are changed so that

$$\left.\begin{aligned} C'_{i0} &= C_{i0} \sum_{i=1}^{I} P_{i0} \Big/ \sum_{i=1}^{I'} P_{i0} \\ C'_{i\infty} &= C_{i\infty} \\ \beta^{2'}_{ij} &= \beta^{2}_{ij} \sum_{i=1}^{I} P_{i0} \Big/ \sum_{i=1}^{I'} P_{i0} \end{aligned}\right\} \tag{99}$$

where $I' = I + N$ and N is the number of control species added. Again through comparisons of the M'_{i0} and M_{i0} values or the $\Omega'_{eff\ i}$ and $\Omega_{eff\ i}$ values one can decide if an improvement has been obtained. Since all pure gas flows, $I = 1$, give $M_{10} = 1$ here, then all of the $I \geq 2$ cases (actually $I' \geq 2$ where $N \geq 1$) can be regarded as special examples of this procedure; thus whenever $M'_{10} > 1$ is obtained, the flow rate of specie 1 has been increased due to the presence of the other specie (or species). Of course many cases occur where $M'_{10} < 1$ so that care must be taken to alter the flow regime in a manner where favorable effects are in fact obtained.

Substitution for Secondary Species

If a specie having different permeation characteristics is substituted for a secondary specie already present in the same amount

$$\left.\begin{aligned} C'_{i0} &= C_{i0} \\ C'_{i\infty} &= C_{i\infty} \\ \beta^{2'}_{ij} &= \beta^{2}_{ij}\ (\Omega'_i/\Omega_i)(\delta_{ij}/\delta'_{ij}) \end{aligned}\right\} \tag{100}$$

where Ω_i is defined by (91). All of the examples displaying the effects of different Ω_2 values when I = 2 (Figures 14-46) as well as the I = 5 cases shown in Figures 47-49 and 56-58 where Ω_5 was changed from 0 to 4, assuming $\delta_{ij} \simeq \delta'_{ij}$, illustrate the effects of substituting another specie for one already present but having different permeation properties. These examples are ample evidence that large effects can be obtained by such a tactic, often as a result of changing the flow regime indicated by the change in magnitude of ϕ.

III. Experimental Data

R. J. Page (8157) conducted some experiments a number of years ago in order to determine the possible extent of the physical effects as well as the validity of some of the modeling assumptions used here. The experiments involved two dead-ended SiO_2 tubes, each with nominal ID of 1.8×10^{-2} cm and nominal OD of 3×10^{-2} cm; one tube was approximately 2×10^3 cm in length, while the other tube was about a factor of ten shorter. The tubes were immersed in helium filled driver volumes large enough such that no significant pressure changes resulted from permeation effects; the vent or receiver volumes initially contained only nitrogen at pressures equal to or less than those of the helium driver volume.

(i) Perfect Filter Limit

Since helium permeates SiO_2 several orders of magnitude faster than nitrogen, (see Barrer, R. M., Diffusion in and through Solids, Cambridge, 1941, pp 133-141) only negative velocity cases resulted from such experiments, and essentially the perfect filter limit was being tested. The receiving volumes were small enough so that significant changes in total pressure occurred due to helium permeation; the resulting pressure (differential) histories for various initial nitrogen pressures allow the relative permeation rates to be estimated and show to what extent the presence of nitrogen affected the flow rate of helium. Figure 59 gives a schematic diagram of the experimental setup.

Figure 60 shows pressure versus time curves for the 2×10^3 cm tube when the helium driver pressure is about 69 atmospheres, while the initial receiver nitrogen pressure is 1, 18, 35 and 69 atm, respectively. After

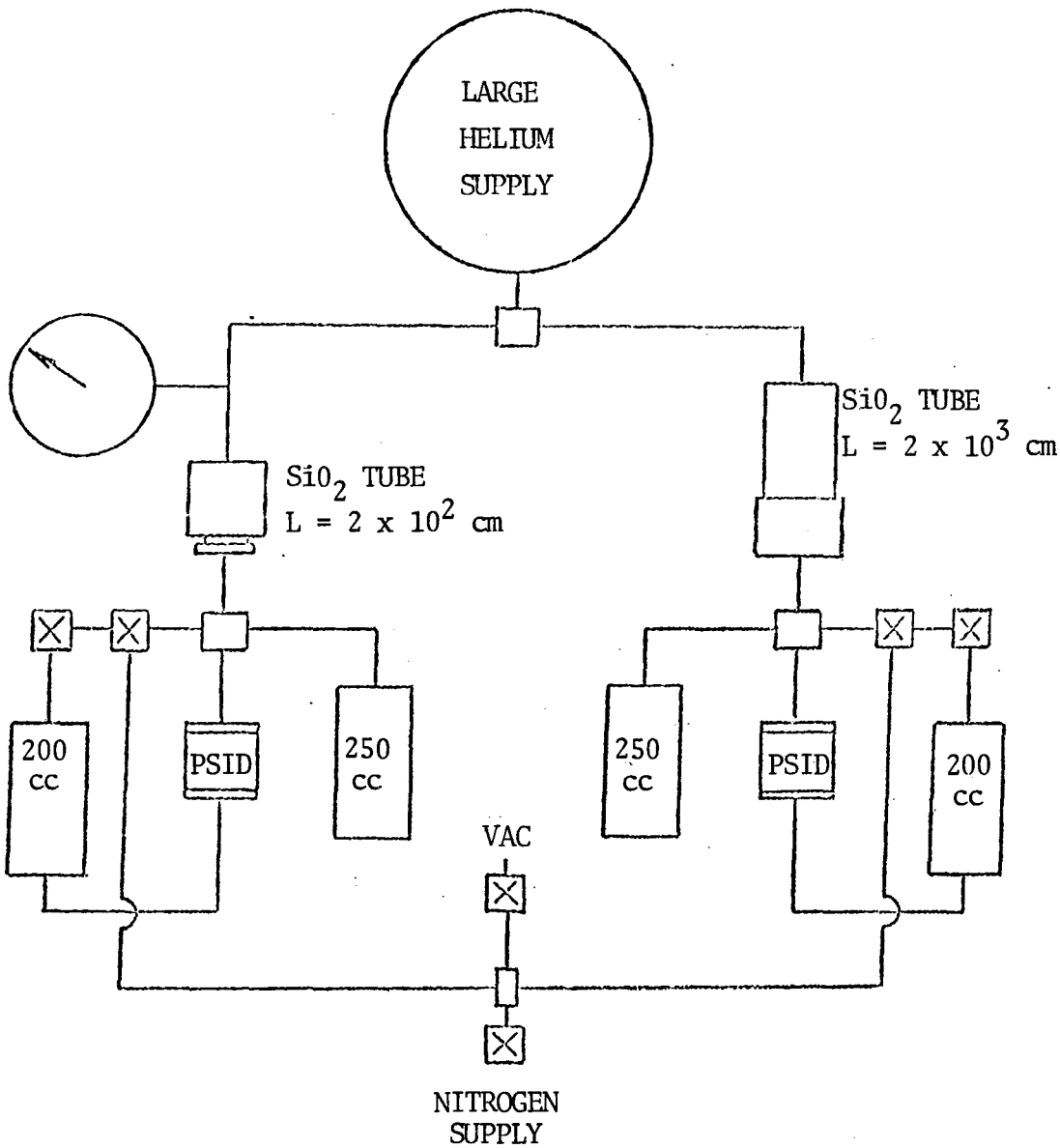

Figure 59. Schematic Diagram of Experimental Setup

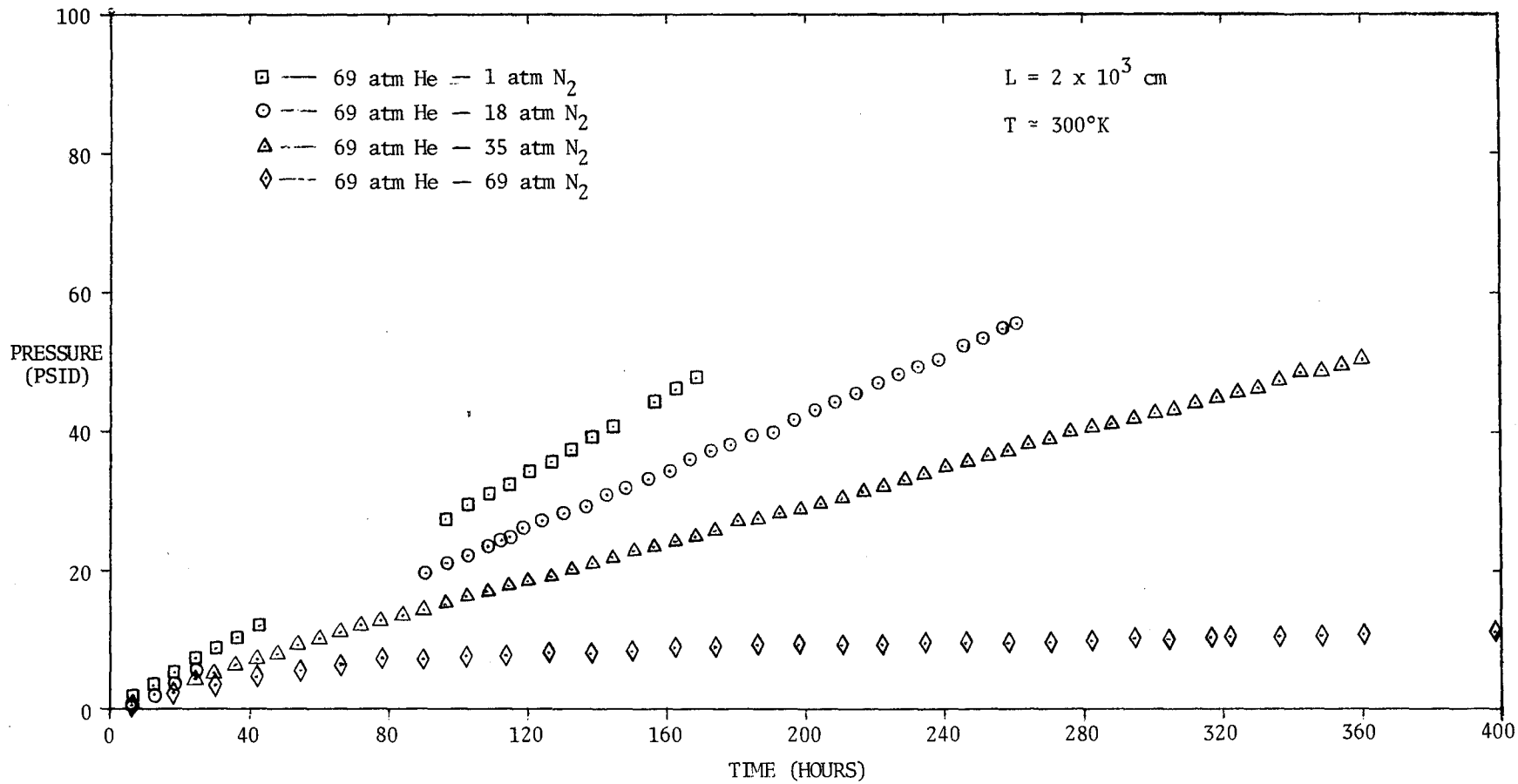

Figure 60. Receiver Pressure Differential versus Time for Various Initial N_2 Pressures, L = 2 x 10^3 cm.

the initial transient, the nearly linear pressure-time slopes indicate the relative flow rates when the four cases are compared. One can immediately observe that large effects are obtained over this pressure range. Figure 61 shows three cases where the helium driver pressure and the initial nitrogen receiver pressure are equal at 69.0, 55.4 and 14.6 atm, respectively. These cases were run to test the balanced pressure limiting solution. Figure 62 shows results for the 2×10^2 cm tube with helium driver pressure of 69 atm and initial nitrogen pressures of 1, 18 and 35 atmospheres, respectively.

Figure 62 shows effects similar to those shown on Figure 60; in fact, since the ordinate scale is exactly a factor of ten smaller on Figure 62 than on Figure 60, the nearly identical results for initial N_2 pressures of 1, 18 and 35 atm, except for the scale factor equal to the tube length ratio, are indicative of other physical significance. From the preceding analysis it is known that such a phenomenon can exist only near the convection dominated limit. When the M_{10} for cases with initial N_2 pressures of 1, 18 and 35 atm are first calculated via the general perfect filter equations (28) and (29), and then are calculated via the convection dominated solution, equation (45), the results agree to within 3%. This verifies that these cases are convection dominated and therefore are nearly independent of β_{12}. The results of these calculations compared to the measured M_{10} obtained directly from the linear pressure-time slope ratios are given in Table II. Considering the difficulty in obtaining accurate slopes from the data, the agreement must be concluded to be good. Also shown in Table II are balanced pressure calculations (here strong dependence on β_{12} is present while $C_{1\infty}$

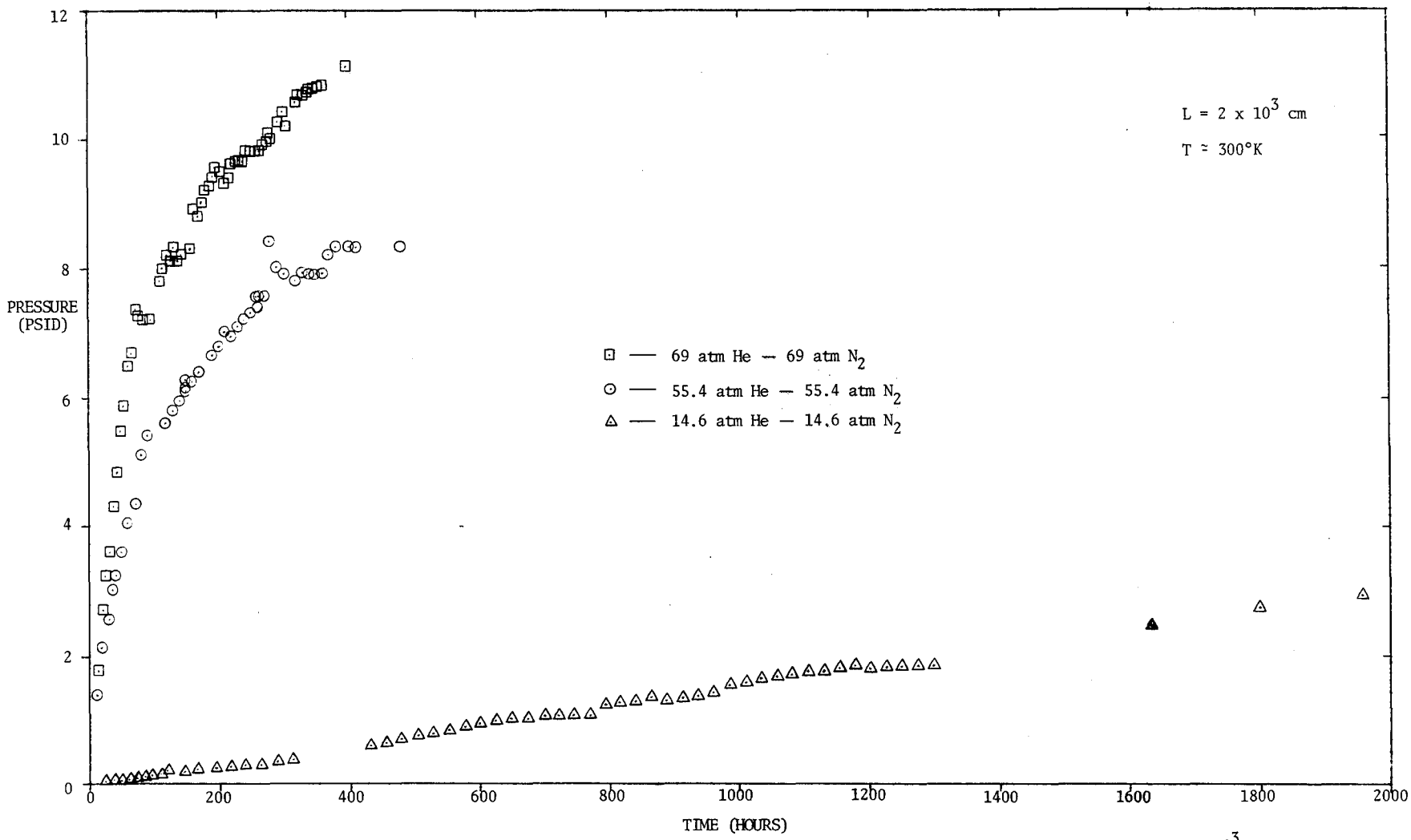

Figure 61. Receiver Pressure Differential versus Time for Various Initially Balanced He — N_2 Pressures, $L \approx 2 \times 10^3$ cm.

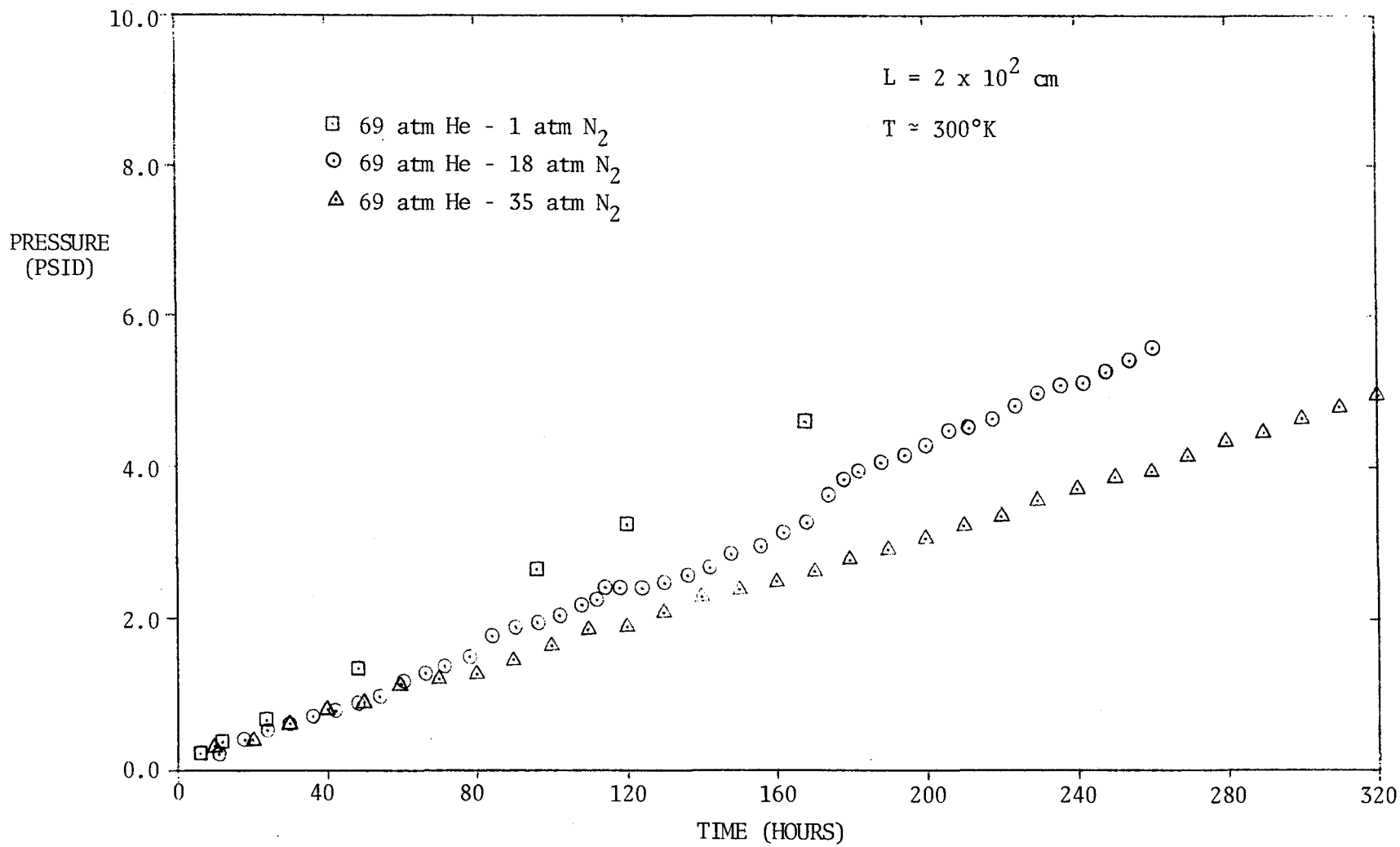

Figure 62. Receiver Pressure Differential versus Time for Various Initial N_2 Pressures, $L = 2 \times 10^2$ cm

L(cm)	He $P_{1\infty}$(atm)	INITIAL N_2 P_{20}(atm)	AFTER STEADY-STATE P_o(atm)	$C_{1\infty}$	C_{10}	β_{12}	M_{10}(meas)	Eqs(28)-(29) M_{10}(calc)	FLOW REGIME
2×10^3	69.0	1.0	3.7	18.5	0.73	23.2	0.98	0.985	conv.
2×10^3	69.0	18.0	20.7	3.33	0.13	54.7	0.74	0.728	conv.
2×10^3	69.0	35.0	38.1	1.81	0.08	74.1	0.44	0.468	conv.
2×10^3	69.0	69.0	69.8	0.99	0.01	100.2	0.017	0.0140	bal. press.
2×10^3	55.4	55.4	56.0	0.99	0.01	89.8	0.015	0.0156	bal. press.
2×10^3	14.6	14.6	15.5	0.95	0.055	47.2	0.026	0.0285	bal. press.
2×10^3	55.4	1.0	3.1	18.1	0.67	21.0	0.98	0.981	conv.
2×10^2	69.0	1.0	1.3	53.4	0.21	1.36	0.99	0.985	conv.
2×10^2	69.0	18.0	18.3	3.77	0.015	5.13	0.77	0.742	conv.
2×10^2	69.0	35.0	35.3	1.95	0.0087	7.13	0.55	0.502	conv.
2×10^2	55.4	1.0	1.2	45.3	0.17	1.33	0.98	0.981	conv.

TABLE II

DATA/ANALYSIS COMPARISONS

is near unity) which also agree with the limiting solution given by equations (48)-(50) within 3%. The pressure-time slopes are even more difficult to extract from data here, but reasonable agreement is still present.

The calculated and experimental M_{10} values are plotted versus C_{10} with either $C_{1\infty}$ or β_{12} as the parameter, respectively, in Figure 63 to show the relatively wide range of parameters covered by the experiments as well as the magnitude of the effects observed. It can be concluded that the presence of N_2 in the receiver for these nearly perfect filter cases induced very significant effects on the He permeation rate. Also the analytical model formulated here seems to adequately describe these effects.

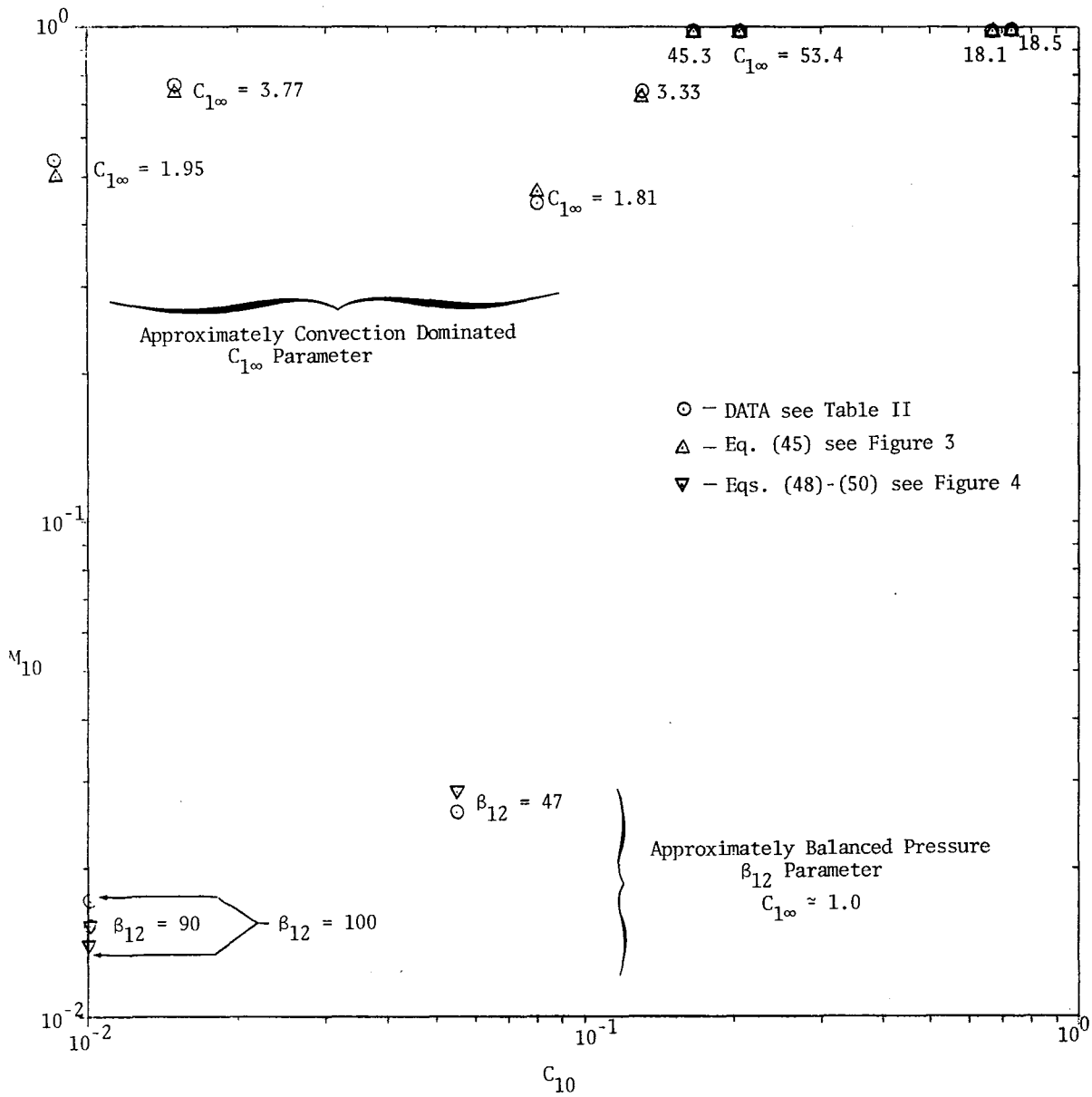

Figure 63. Data--Analysis Comparisons

CONCLUSIONS

The transport of gaseous species in dead-end tubes having selectively permeating walls has been investigated. The assumptions of continuum, quasi-steady, fully developed, laminar bore flow of perfect gases which behave like an axially diffused plug flow through an approximately straight tube with nearly uniform bore temperature and pressure were used; the supply and receiving reservoirs were assumed to be well mixed so that uniform reservoir temperature and concentrations existed. The limits of validity for these assumptions were established and were given in terms of a series of inequalities involving the key parameters.

Detailed results were generated via exact physically limiting solutions as well as numerical integration of the governing equations for cases involving up to five species. Both positive and negative global velocity cases were examined and were used to show that better results can sometimes be obtained if the tube is immersed in the opposite reservoir. Tube materials having specie separation ratios varying from unity (non-selective) to very large or very small values (near perfect filters) were included in the study. It was shown that the flow of a given specie can be either enhanced or dehanced, and even reversed in direction, relative to the corresponding perfect mixing value due to the presence of other species. This led to the definition of an effective separation ratio for specie flow from the tube which may be greater or less than that of the tube material in slab form which is approached in the perfect mixing limit. It was also shown

that in certain cases an individual specie can exhibit wall and bore stagnation points at different locations where the flow direction changes for that specie. From the consideration of such phenomena it was demonstrated, as a possible mode of operation, that secondary control species having very large or very small permeation rates can be used to favorably alter the flow characteristics of primary species.

Finally, some experimental data was given to verify the large effect which the presence of a low permeating specie in the tube bore can have on the flow of another specie which readily permeates the tube walls. It was shown in the near perfect filter limit, that the mathematical model given here properly describes the effects obtained in both the balanced pressure and the convection dominated experimental limits.

The information contained in this document eliminates the need to operate such dead-end tubes with selectively permeating walls near the perfect mixing limit to avoid unknown effects; this is true because these effects are now predictable and well enough understood so that they can even be exploited to produce favorable effects in some cases.

REFERENCES

0. Annis, B. K., Humphreys, A. E. and Mason, E. A., "Nonisothermal, Non-Stationary Diffusion," Phys. Fluids (1969) Vol. 12, No. 1, pp. 78-83.

1. Aris, R., "On the Dispersion of a Solute in a Fluid Flowing Through a Tube," Proc. Roy. Soc., Vol. A235, 1956, p. 67.

2. Bird, R. B., Stewart, W. E., and Lightfoot, E. N., Transport Phenomena, Wiley & Sons, New York, 1960, p. 47, 126-130.

3. Bournia, A., et al., "Dispersion of Gases in Laminar Flow Through a Circular Tube," Proc. Roy. Soc., Vol. A261, 1961, p. 227.

4. Carslaw, H. S., and Jaeger, J. C., Conduction of Heat in Solids, Oxford at the Clarendon Press, Second Edition, 1959, pp. 96, 388, 391.

5. Chenoweth, D. R., "Isothermal Viscous/Knudsen Blowdown of a Container with Nearly Constant Outgassing and Back-Pressure," Sandia Laboratories Report, SCL-RR-72-0350, December 1972. Also see Analysis in SCL-RR-710022, March 1971.

6. Cramer, J. D., "The Compressibility of Gaseous Mixtures of Helium-Nitrogen and Helium-Deuterium at High Pressures," Los Alamos Scientific Laboratory Report (LA-3250-MS), March 1965.

7. Dayan, J. and Levenspiel, O., "Longitudinal Dispersion in Packed Beds of Porous Adsorbing Solids," Chemical Engineering Science, 1968, Vol. 23, pp. 1327-1334.

8. Dushman, S., Scientific Foundations of Vacuum Technique, ed. by J. M. Lafferty, Wiley & Sons, New York, 1962.

9. Evans, E. V., et al., "Gaseous Dispersion in Laminar Flow Through a Circular Tube," Proc. Roy. Soc., Vol. A284, 1965, p. 540.

10. Gill, W. N., et al., A.I.Ch.E.J., "Laminar Dispersion in Capillaries:"
I, Vol. 11, "Mathematical Analysis," 1965, p. 1063;
II, Vol. 12, "Effect of Inlet Boundary Conditions," 1966, p. 906;
III, Vol. 12, "Experiments in Horizontal Tubes," 1966, p. 916;
IV, Vol. 13, "The Slug Stimulus," 1967, p. 801;
V, Vol. 14, "Dispersion in Developing Velocity Fields," 1968, p. 939.

11. Ginzburg, I. P., Applied Fluid Dynamics, Leningrad State University, 1958. (Translated from Russian, 1963, published for the National Science Foundation by the Israel Program for Scientific Translation.)

12. Hirschfelder, J. O., et al., Molecular Theory of Gases and Liquids, Wiley & Sons, New York, 1954.

13. Huang, J. C. P., and Yu, H. S., "Pressure Distributions in Porous Ducts of Arbitrary Cross Section," Transactions of the ASME, J. Fluids Eng. 1973, Sept., p. 342.

14. Jordan, K. C., Blanke, B. C., and Dudley, W. A., "Half-Life of Tritium," J. inorg. nucl. Chem., 1967, Vol.29, pp. 2129 to 2131.

15. Jost, W., "Diffusion in Solids, Liquids, Gases," Academic Press, Inc., Publ., N.Y. (1960).

16. Kreith, E. F., "Principles of Heat Transfer," International Textbook Co., Scranton, 1958.

17. Libby, P. A., Liu, T. M., and Williams, F. A., "Flow Development in a Tube with Injection of a Light or Heavy Gas," J. Heat Mass Transfer, 1969, Vol. 12, p. 1267.

18. Michels, A., et al., "Compressibility Isotherms," (He) Vol. 8, 1941, pp. 923-32; (Ar) Vol. 15, 1949, pp. 627-633; (N_2) Vol. 17, 1951, pp. 801-816; (H_2) Vol. 25, 1959, pp. 25-42; (Ne) Vol 26, 1960, pp. 539-543.

19. Nunge, R. J., Lin, T. S., and Gill, W. N., "Laminar Dispersion in Curved Tubes and Channels," J. Fluid Mech. (1972), Vol. 51, Part 2, pp. 363-383.

20. Schlichting, H., Boundary Layer Theory, translated by J. Kestin, McGraw-Hill, New York, 1955.

21. Shapiro, A. H., Compressible Fluid Flow, Vol. I, Ronald Press, New York, 1953, pp. 982-6.

22. Shelby, J. E., "A Comprehensive Review of Gas Permeation, Diffusion and Solubility in Inorganic Glasses," Sandia Laboratories Report, SLL-73-0259, Aug. 1973.

23. Taylor, G. I., "Dispersion of Soluble Matter in Solvent Flowing Slowly Through a Tube," Proc. Roy. Soc., Vol. A219, 1953, p. 186.

24. Taylor, G. I., "Diffusion and Mass Transport in Tubes," Proc. Phys. Soc. London, Vol. 67, 1954, p. 857.

25. Truesdell, L. C., Jr., and Adler, R. J., "Numerical Treatment of Fully Developed Laminar Flow in Helically Coiled Tubes," AIChE Journal, Vol. 16, No. 6, Nov. 1970, pp. 1011.

26. Weissman, S., and Mason, E. A., "Determination of Gaseous-Diffusion Coefficients from Viscosity Measurements," J. Chem. Phys. (1962), Vol. 37, No. 6, pp. 1289-1300.

27. Weissman, S., "Mutual Diffusion Coefficients for the He-H_2 System," J. Chem. Phys. (1971) Vol. 55, No. 12, pp. 5839-5840.

APPENDIX

A description of each major assumption and its physical relation to the particular problem of interest here are given below. Some of the assumptions listed do not directly enter the resulting analytical model, but instead they enter indirectly via the physical justification of other assumptions which do have explicit influence on the final governing equations.

Continuum Flow [Kn]

Continuum flows are usually distinguished from free molecular flows (Dushman, 1962; Chenoweth, 1972) by considering the magnitude of the dimensionless parameter called the Knudsen number. This basic parameter Kn is defined as the ratio of the molecular mean free path λ to a characteristic flow length, in this case the bore diameter D. In continuum fluid mechanics

$$\lambda/D << 1 \tag{A1}$$

so that the density is high enough for intermolecular collisions to dominate over collisions with the boundaries. For most common gases the mean free path λ in centimeters (Hirschfelder, et al., 1954; Chenoweth, 1972) is of the order of

$$\lambda(\text{cm}) \simeq 10^{-7}\ T(°K)/3P(\text{atm}) \tag{A2}$$

in terms of the gas temperature T in degrees Kelvin and the pressure P in atmospheres. Therefore in order for continuum flow to be assured for this

application it is sufficient for the inequality

$$D(\text{cm})\ P(\text{atm}) > 10^{-5}\ T(°K) \tag{A3}$$

to be satisfied. For a gas or a mixture of gases at ten atmospheres and 300°K the bore diameter must exceed 3×10^{-4} cm as an example.

Perfect Gases [Z]

Each gas specie is assumed to behave as a thermally-perfect gas so that $P_i = \nu_i RT$, where the molar gas constant $R = 82.06\ cm^3$ atm/mole °K; similarly $P = \sum_i P_i = RT \sum_i \nu_i = \nu RT$ for the mixture, where $C_i = \nu_i/\nu = P_i/P$ defines the mole fraction of species i in the mixture. If the compressibility factor

$$P/\nu RT = Z = Z(P,T,C_i) \tag{A4}$$

is near unity

$$0.94 \leq Z \leq 1.06 \tag{A5}$$

then generally the perfect gas assumption is adequate; if this is not true due to one or more species with non-negligible mole fractions exhibiting compressibility effects, then these results may require alteration. For most purposes (Michels, et al., 1941-1960) mixtures of common gases can be treated as thermally-perfect gases at 300°K if the total pressure remains less than about 100 atm.

$$P < 100 \text{ atm} \tag{A6}$$

For example, at 300°K and 100 atm the pure gases He, Ar, N_2, H_2 and Ne have compressibility factors Z (He) = 1.047, Z (Ar) = 0.953, Z (N_2) = 1.005, Z (H_2) = 1.060 and Z (Ne) = 1.049. Note, however, that the method of partial volumes, Amagat's law $Z = \sum_i C_i Z_i$, is not always adequate (Cramer, 1965) to determine mixture compressibility factors.

Fully Developed Laminar Bore Flow [Re, L/D]

First consider the case where the flow is through a pipe with non-permeable walls, rather than the more complex case where virtually all of the flow enters via the pipe walls. The conditions required for these assumptions to hold involve the magnitude of the familiar dimensionless parameter (Bird, et al., 1960; Ginzburg, 1958; Schlichting, 1955) Re called the Reynolds number, a measure of the ratio of inertia forces to viscous forces. When the velocity profile is fully developed in a spacial sense (the temporal development of the velocity profile is considered later) a Reynolds number based on pipe diameter is more meaningful than one based on axial distance since the boundary layer has spread to the center line of the pipe and no longer continues to increase in thickness.

(i) Laminar Flow

Since transition to turbulent flow can sometimes occur if the Reynolds number based on diameter (Bird, 1960) exceeds about 2000, it is sufficient to require

$$Re = \rho \bar{u} D/\mu = 4\,\dot{m}/\pi D \mu < 2000 \qquad \text{(A7)}$$

in order to ensure laminar flow, where the mass flow rate $\dot{m} = \pi D^2 \rho \bar{u}/4$ has been introduced. Thus, the mass flow rate must remain less than $500\ \pi D\mu$

$$\dot{m} < 500\ \pi D\mu \tag{A8}$$

to ensure laminar flow. For example, if the bore diameter $D \simeq 2 \times 10^{-2}$ cm and the viscosity coefficient $\mu \simeq 1.5 \times 10^{-4}$ g/cm sec, then $\dot{m} < (3\pi/2) \times 10^{-3}$ g/sec is required.

(ii) Fully Developed Flow

The entrance length required to establish laminar fully developed (paraboloidal) velocity profiles spacially is (Bird, et al., 1960)

$$L_e \simeq 0.035\ DRe \tag{A9}$$

and no corrections are required to account for such a region if the pipe length greatly exceeds this length, $L \gg L_e$, for example $L > 10\ L_e$. Thus the length to diameter ratio is restricted

$$L/D > 0.35\ Re \tag{A10}$$

so that the bulk of the pipe flow is fully developed. Since $Re < 2000$ has already been imposed via (A7) then (A10) is always satisfied if $L/D > 700$. In dimensional form a further restriction on the mass flow rate has therefore been established.

$$\dot{m} < 0.7\ \pi D\mu\ (L/D) \tag{A11}$$

For the same values used above and $L/D = 10^4$, then $\dot{m} < 2.1\ \pi\ 10^{-2}$ g/sec is required. The application of these results in an approximate local sense to tubes with permeable walls is discussed later.

Uniform Bore Temperature and Pressure [M, γ]

The physical mechanisms by which non-uniform temperature and pressure distributions can be created are considered in order to bound the uniform distribution assumption.

(i) Uniform Bore Temperature

Both gas reservoirs, including the one in which the permeable tube is immersed, are assumed to be at nearly the same temperature which must therefore be restricted to change slow enough with time so that the system is maintained at nearly uniform temperature. The criteria for the existence of uniform reservoirs are derived later.

Under these conditions the gas flow in the bore can only attain a non-uniform radial and axial distribution of temperature via conversion of thermal energy to kinetic energy (neglecting for the moment frictional effects which are considered in the following section). The worst situation then occurs under near adiabatic flow conditions where $T/T_o = \left[1 + \frac{\gamma-1}{2} M^2\right]^{-1}$ is the ratio of static to stagnation temperature (Shapiro, 1953) expressed in terms of γ, the ratio of specific heats and M, the local Mach number (the ratio of local velocity to local sound speed). Since γ is physically bounded, if the local Mach number (which is maximum at the axis of the pipe near the pipe exit into the vent reservoir) is less than 0.3

$$M < 0.3$$
$$1 < \gamma \leq 5/3 \tag{A12}$$

then $0.97 \leq T/T_o \leq 1.0$ even for $\gamma = 5/3$. Since $M_{\mathbb{G}} = 2\overline{M} = 2\overline{u}/[1.0133 \times 10^6\ \gamma RT/W]^{1/2}$ then $M < 0.3$ implies that

$$\dot{m}(g/sec) < 37.5\ \pi\gamma^{1/2}\ D^2(cm^2)\ P(atm)\ W^{1/2} \left(\frac{g}{g\text{-mole}}\right)^{1/2} \left[T(°K)\ R\left(\frac{cm^3\ atm}{g\text{-mole}°K}\right)\right]^{-1/2} \tag{A13}$$

giving another restriction on maximum flow rate allowed. For example using the gas molecular weight $W = 2$ g/g-mole, $\gamma = 7/5$, $P = 10$ atm, $D = 2 \times 10^{-2}$ cm, $T = 300°K$ and $R = 82.06\ \frac{cm^3\ atm}{g\text{-mole}°K}$ gives $\dot{m} < 1.60\ \pi\ 10^{-3}$ g/sec as the upper limit on total mass flow rate. Of course this assumption essentially eliminates the conservation of energy equation from further consideration since viscous effects are considered in the following analysis of the uniform pressure assumption.

(ii) Uniform Bore Pressure

Again, first consider the case where the flow is through a pipe with non-permeable walls rather than the more complex case where virtually all of the flow enters via the pipe walls. The effect of permeable walls on flow in a dead-end tube is examined later.

Since the strongest pressure-temperature coupling occurs for isentropic flow where $P/P_o = (T/T_o)^{\frac{\gamma}{\gamma-1}}$ the previous Mach number restriction ($M < 0.3$) also implies that dynamic pressure effects (differences between static and stagnation pressures) are negligibly small ($0.93 \leq P/P_o \leq 1.0$) even for $\gamma = 5/3$. Therefore the bore pressure will be nearly uniform and equal to

the receiving volume pressure unless significant pressure losses occur due to viscous (frictional) effects. The Poiseuille flow formula (Schlichting, 1955; Ginzburg, 1963) can be used to estimate (actually overestimate) this effect if one assumes that all of the flow (which is flowing at the open end) enters a capillary with non-permeable walls at the closed end rather than being added through the walls along its entire length; since fully developed laminar incompressible flow is present due to previous restrictions the pressure loss due to friction

$$\Delta P/P = 32 \ (L/D)(\gamma \overline{M}^2/Re) << 1 \tag{A14}$$

is sufficient to assure uniform pressure. Equation (A14) can be rewritten

$$\Delta P/P = (\dot{m}/W)(128 \ \mu LRT/\pi D^4 P^2) << 1 \tag{A15}$$

which yields the dimensional inequality

$$\dot{m} < 10^{-4} \pi D^4 P^2 W/\mu LRT \tag{A16}$$

restricting mass flow rate. As an example when $\mu = 1.5 \times 10^{-10}$ atm-sec, $P = 10$ atm, $T = 300°K$, $D = 2 \times 10^{-2}$ cm, $L/D = 10^4$, $W = 2$ g/g-mole and $R = 82.06$ cm^3 atm/mole °K then $\dot{m} < 4.3 \ \pi \ 10^{-6}$ g/sec is required by (A16). The modified form of (A14) resulting when permeable walls exist is given later. Of course this assumption essentially eliminates the momentum equation from further consideration in this work except where it is needed to examine other assumptions.

Quasi-Steady, Axially-Diffused Plug Flow

$$[N_{Pe},\ h/D,\ V_o/V_\infty,\ V',\ D_i',\ \alpha',\ S_i']$$

These assumptions are the most important of the many assumptions made to derive the approximate governing equations for this problem. At the same time, extremely involved physical reasoning and very detailed analysis must be applied in order to establish the many new independent dimensionless parameters and the restrictions required on their magnitudes. First, a description is given of the nature of the results desired; then these results are derived with heavy reliance on the large body of related literature available; finally, the results are summarized, with special emphasis placed on establishing the dimensionless and dimensioned inequalities required by these assumptions, similar to the resulting restrictions derived for the other assumptions.

The flow in the capillary bore is assumed to be quasi-steady with respect to the rest of the problem which is inherently transient. This means that steady flow results are used for the bore flow at any instant of time; only the transient boundary conditions determined from the related parts of the problem are allowed to control the time-dependent behavior of the flow in the capillary bore which is assumed to respond instantaneously to the boundary condition changes. In order for this to be a valid approach it must be shown that the characteristic times describing the other transient aspects of the problem are much larger than those describing the time to establish both radial and axial profiles for velocity and concentration in the capillary bore.

$$t_{system}/t_{bore} \gg 1 \tag{A17}$$

First, consider the characteristic times controlling the transient behavior of the rest of the problem. We are concerned here only with the case where specie concentration differences are the driving forces for gas transfer between reservoirs via diffusion or permeation through the wall material (many materials, Jost, 1960, exhibit such characteristics). If instead it was the total pressure differential, then the following analysis would require some modification to allow for global flow through porous wall material for instance. The permeation of gases through the capillary walls is altered then by changes in reservoir concentrations or by changes in the capillary wall diffusion coefficients controlling the transfer. It is assumed that the reservoirs comprise a closed system in that no gas is added or removed from the constant volume system during operation. The gas composition can thus be changed in a reservoir only by transfer between reservoirs or by chemical and physical changes in the gas within a reservoir. It is assumed that chemical reactions between gas species are not present; this is primarily because an analysis of various chemically reacting situations is beyond the scope of this work due to their possible complex and widely varying nature. On the other hand radioactive decay is a physical change which can be used to illustrate the nature of such effects in a simple way.

(i) Decay

Therefore if a gas specie is a radioactive isotope undergoing decay (for example, beta decay) such that $\nu_i/\nu_i(0) = \exp(-\alpha t)$ then the decay constant α^{-1} (which is indicative of the time for 63% decay) can be regarded as the characteristic time for that physical phenomenon. For example, the decay constants for ${}_1H^3$, ${}_{86}Rn^{222}$, ${}_{36}Kr^{85}$, ${}_{17}C\ell^{36}$ and ${}_{35}Br^{82}$ with half lives of

12.35 yr (Jordan, 1967), 3.82 da, 10.8 yr, 3.1 x 10^5 yr and 35.5 hr, respectively, (CRC Handbook of Chemistry and Physics, 50th Edition, Table of Isotopes) are

$$\alpha^{-1} = t_d = - t_{1/2}/\ln (1/2) = 17.8 \text{ yr}, 5.51 \text{ da}, \quad 15.6 \text{ yr}, 4.5 \times 10^5 \text{ yr and } 51.2 \text{ hr, respectively.} \tag{A18}$$

(ii) Wall Diffusion

The characteristic times (Jost, 1960) which measure the times to re-establish steady-state diffusion rates (like 98.6% of steady state) after a change in temperature or concentration for a slab of thickness h are

$$t_w = h^2/2D_i \tag{A19}$$

where D_i is the wall material diffusion coefficient to gas specie i and depends strongly on temperature (many materials, Jost, 1960, allow such selective permeation to various gas species). Often (Shelby, 1973) D_i is expressed in terms of temperature T as $D_i = D_o T \exp(-E_d/R_c T)$, $R_c = 1.987$ cal/mole °K where at 300°K, SiO_2-He has $t_{SiO_2\text{-He}} = 13.4$ min using $D_o = 3.3 \times 10^{-7}$ cm^2/sec°K, $E_d = 4945$ cal/mole, D_{He} (300°K) = 2.5 x 10^{-8} cm^2/sec and h = 6.4 x 10^{-3} cm. Similarly for SiO_2-D_2, using $D_o = 1.5 \times 10^{-7}$ cm^2/sec °K and $E_d = 8540$ cal/mole, D_{D_2} (300°K) = 2.7 x 10^{-11} cm^2/sec, one obtains $t_{SiO_2\text{-}D_2} = 1.23$ wk with the same h value. Analogous calculations for SiO_2-Ne, D_{Ne} (300°K) = 3.5 x 10^{-12} cm^2/sec gives $t_{SiO_2\text{-Ne}} = 2.2$ mo

while for SiO_2-Ar, D_{Ar} (300°K) = 4.9×10^{-25} cm^2/sec resulting in $t_{SiO_2\text{-}Ar} \simeq 1.3 \times 10^{12}$ yr. This characteristic time is strongly dependent on temperature, wall material and gas specie as well as wall thickness. For example, if $h = 10^{-3}$ cm, then $t_{SiO_2\text{-}He} = 20$ sec while $h = 10^{-1}$ cm gives 55 hr showing the influence of the h^2 wall thickness dependence. Comparative values for the wall diffusion coefficient can be obtained from Jost; for example, with vulcanized Neoprene D_{N_2} (27.1°C) $\cong 1.9 \times 10^{-7}$ cm^2/sec, D_{H_2} (17.0°C) $\cong 1.03 \times 10^{-6}$ cm^2/sec and D_{Ar} (36.1°C) $\cong 3.3 \times 10^{-7}$ cm^2/sec while for Palladium D_{H_2} (272°C) $\simeq 2 \times 10^{-5}$ cm^2/sec.

(iii) Finite Volumes

For diffusion controlled transfer between two finite volumes (Chenoweth, 1971) the characteristic time for substantial change (63% vented if $V_o \to \infty$) in gas composition due to gas transfer between reservoirs is

$$t_{FV} = (h/A_s)\,(A_V/D_i S_i RT)\; V_o\, V_\infty/(V_o+V_\infty) \qquad \text{(A20)}$$

where $A_V = 0.6 \times 10^{24}$ molecules/mole and A_s is the effective surface area roughly approximated by $\pi L(h+D)$. The vent volume is V_o and the driver volume is V_∞ and $S_i = S_o \exp(-E_s/R_c T)$ is the solubility coefficient such that $K_i = S_i D_i$ is the permeability coefficient for gas specie i at temperature T (Shelby, 1973). Therefore if $A_s \simeq 17$ cm^2 and $V_\infty = 10^2$ cm^3 while $V_o = 10^3$ cm^3, the finite volume characteristic times for the SiO_2 - gas combinations given above can be easily calculated. For SiO_2-He, $S_o = 2 \times 10^{17}$ molecules/cm^3 atm and $E_s = -625$ cal/mole so that at 300°K, $t_{FV} = 1.8$ yr while for SiO_2-D_2,

$S_o = 1.4 \times 10^{17}$ molecules/cm^3 atm and $E_s = -1160$ cal/mole so that $t_{FV} = 0.96 \times 10^3$ yr. Similarly for SiO_2-Ne, $t_{FV} = 8.9 \times 10^3$ yr and for SiO_2-Ar, $t_{FV} = 1.7 \times 10^{15}$ yr using data from Shelby, 1973. Again strong dependence on temperature, wall material and gas specie is evident.

In summary (A18)-(A20) give the characteristic times for the phenomena which control the transient nature of the system. In order for the bore flow to be quasi-steady the times given by (A18)-(A20) must be much larger $t_{system}/t_{bore} >> 1$ than those describing the time to establish both radial and axial profiles for velocity and concentration in the capillary bore during normal system operation or following external control changes in system temperature or reservoir concentrations.

(iv) Radial Profiles

First consider the startup problem (a comparable adjustment must be made after any change in boundary conditions) for laminar flow in a circular tube (Bird, et al., 1960) with non-permeable walls. Note that since the flow has already been taken to be fully developed in the spacial sense, then sufficient length of tube is available so that the flow can also become fully developed in a temporal sense. Physically the steady-state radial dependence of the velocity is established (95% of steady-state paraboloid) as soon as wall effects have had time to diffuse sufficiently to the tube axis, so that roughly

$$t_{VR} = D^2/8\nu \qquad \text{(A21)}$$

where $\nu = \mu/\rho$ is the kinematic viscosity; eq (A21) is exactly analogous to (A19) if h is replaced by the pipe radius D/2 and D_i is replaced by ν. Similarly the radial dependence of the concentration profiles approaches steady-state in times of the order

$$t_{CR} = D^2/8\mathcal{D}_{ij} \tag{A22}$$

where $\mathcal{D}_{ij}$ is the mutual diffusion coefficient. Note that $t_{CR} = t_{VR}$ Sc where $Sc = \nu/\mathcal{D}_{ij} = N_{Pe}/Re$ is the Schmidt number. The Schmidt number for gas flows is usually of the order of unity, especially if the specie molecular weights are not vastly different, and $\mathcal{D}_{ij}$ has inverse pressure dependence with the one atmosphere, room temperature value near 1 cm^2/sec. Thus as an example, at 10 atmospheres and 300°K, $t_{VR} \simeq t_{CR} \simeq 5 \times 10^{-4}$ sec if D is taken as before to be 2×10^{-2} cm.

(v) Axial Profiles

Due to the interactions between axial and radial diffusion and axial convection, the characteristic times associated with the approach to steady-state flow in the axial direction is more difficult to estimate than the simple diffusion estimates for radial profiles.

Velocity Profiles

However, the axial velocity profile develops in a convection dominated flow in roughly five traversals of sound waves at the initial sound speed (Shapiro, 1953)

$$t_{VA} = 5L/c_{oi} \tag{A23}$$

where the initial sound speed is c_{oi}(cm/sec) = 10^3 $(\gamma RT/W_i)^{1/2}$ using the same definitions and units used previously for γ, R, W_i and T. Thus for $\gamma = 7/5$, $W_i = 2$ g/g-mole, T = 300°K, R = 82.06 cm^3 atm/mole°K, L/D = 10^4 and D = 2×10^{-2} cm one obtains $t_{VA} = 0.76 \times 10^{-2}$ sec. Obviously the development of the radial and axial velocity profiles take place simultaneously and in some cases where nearly pure convection is not present considerable interaction takes place. However the sum (sequential development) of the orders of magnitudes established by (A21) and (A23), and the larger of the two (assuming the fastest one is instantaneous) should always bound the combined velocity field development times

$$(\text{greater of } t_{VR} \text{ and } t_{VA}) \leq t_{combined} \leq (t_{VR} + t_{VA})$$

even when the wave effects and frictional effects are interacting.

Concentration Profile via Convection

As before, first consider the case of flow through a straight tube with non-permeable walls. In the absence of all molecular diffusion effects, the paraboloidal velocity profile (laminar, fully developed both spacially and temporally) will stretch a radially uniform front marking an axial step change in gas composition into a paraboloid; this distributes the concentration behind the front linearly with axial distance, where the vertex of the paraboloid moves at the velocity $2\bar{u}$ (e.g., $x_{vertex} = x_{2\bar{u}} = 2\bar{u}t$) and $\bar{u}$ denotes the average axial velocity over the pipe cross-section (Taylor, 1953-4). Thus a section of pipe of length L is 95% flushed by such a convective process in approximately

$$t_{2\bar{u}} = 5L/\bar{u} \tag{A24}$$

which crudely represents a measure of the time to establish a new quasi-steady axial concentration profile by convection alone, while effects are first felt (break-through) at x = L when

$$t = L/2\bar{u} \tag{A25}$$

The conditions under which nearly pure convection can exist are derived in the following discussions of axial and radial diffusion effects; they are found to be controlled by the diffusion Péclét number N_{Pe} based on D and a reduced time variable τ_D measuring time from the instant that a step concentration profile existed such that the inequalities

$$\tau_D = 4\mathcal{D}_{ij}\ t/D^2 \leq 0.05 \tag{A26}$$

$$N_{Pe} = \bar{u}D/\mathcal{D}_{ij} \geq 50/\tau_D^{1/2} \tag{A27}$$

limit the magnitudes of the dimensionless parameters τ_D and N_{Pe}. Hence a region of nearly pure convection exists under laminar and fully developed conditions only if $(50/N_{Pe})^2 \leq (\tau_D)_{2\bar{u}} \leq 0.05$ so that $N_{Pe} \geq 224$ is required. This is shown on Figure A1 which is a plot of N_{Pe} versus τ_D. In order to establish a quasi-steady concentration profile by means of convection, the convection region must exist at least as long as $t_{2\bar{u}} = 5L/\bar{u}$ so that $(\Delta\tau_D)_{2\bar{u}} \geq t_{2\bar{u}}\ (4\mathcal{D}_{ij}/D^2)$ or $0.05 - (50/N_{Pe})^2 \geq (4\mathcal{D}_{ij}/D^2)(5L/\bar{u}) = 20(L/D)/N_{Pe}$ with the result that the tube length to diameter ratio must be restricted to be

$$L/D \leq (N_{Pe}/400 - 125/N_{Pe}), \quad N_{Pe} \geq 224 \tag{A28}$$

which is shown on Figure A2, a plot of L/D versus N_{Pe}. Notice that (A10) can be written

$$L/D \geq 0.35\ Re = 0.35\ N_{Pe}/Sc$$

which completely excludes (A28) since $Sc \simeq 1$. Therefore the previous assumption that the velocity entrance region effects be negligible which resulted in (A10) prevents the quasi-steady axial concentration profile from being established by nearly pure convection mechanisms in laminar fully developed flow as the present model assumes.

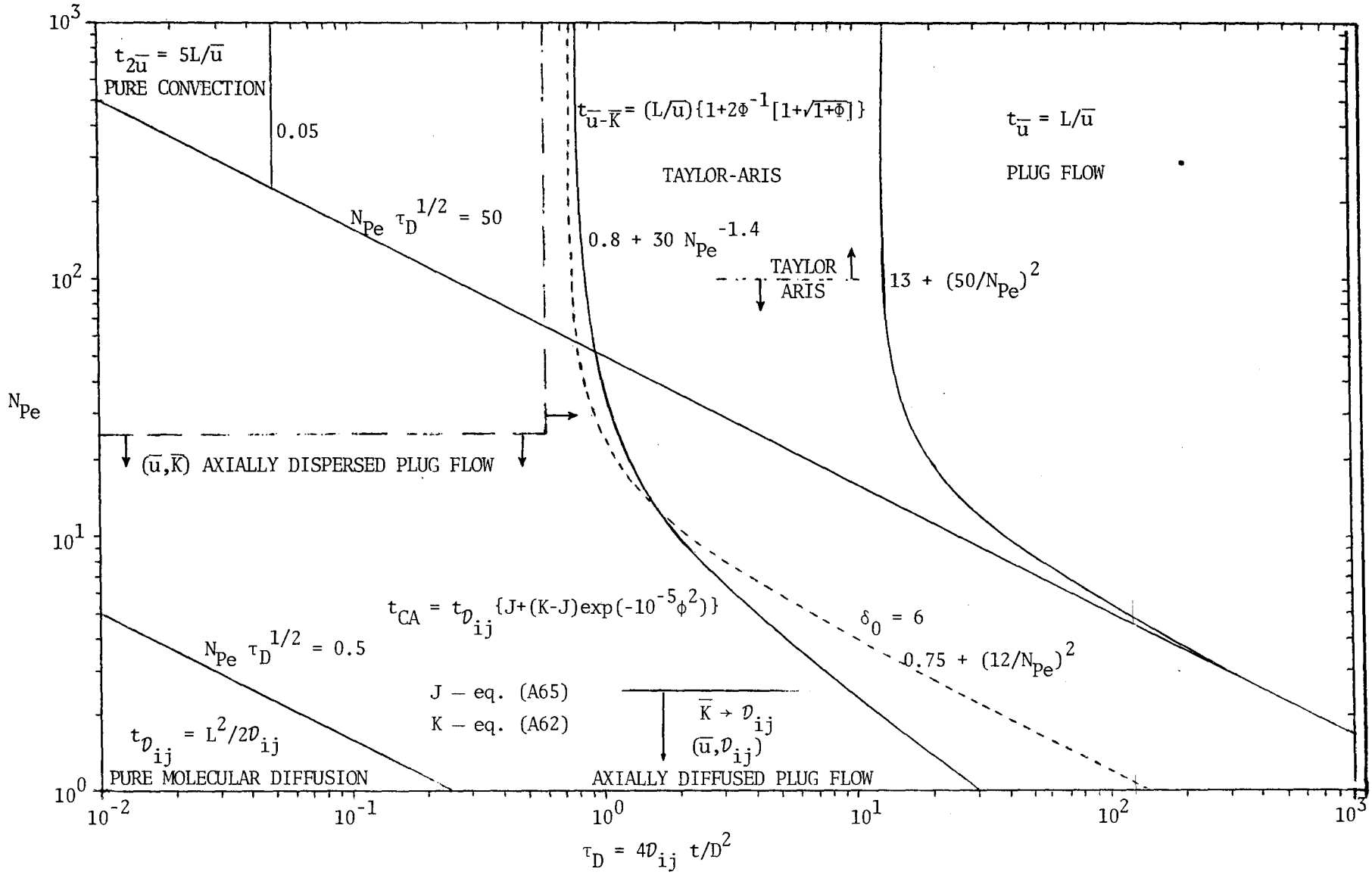

Figure A1. Flow Regions for Axial Dispersion (Initial Step Profile in Concentration at Tube Inlet Set Into Motion at Zero Time).

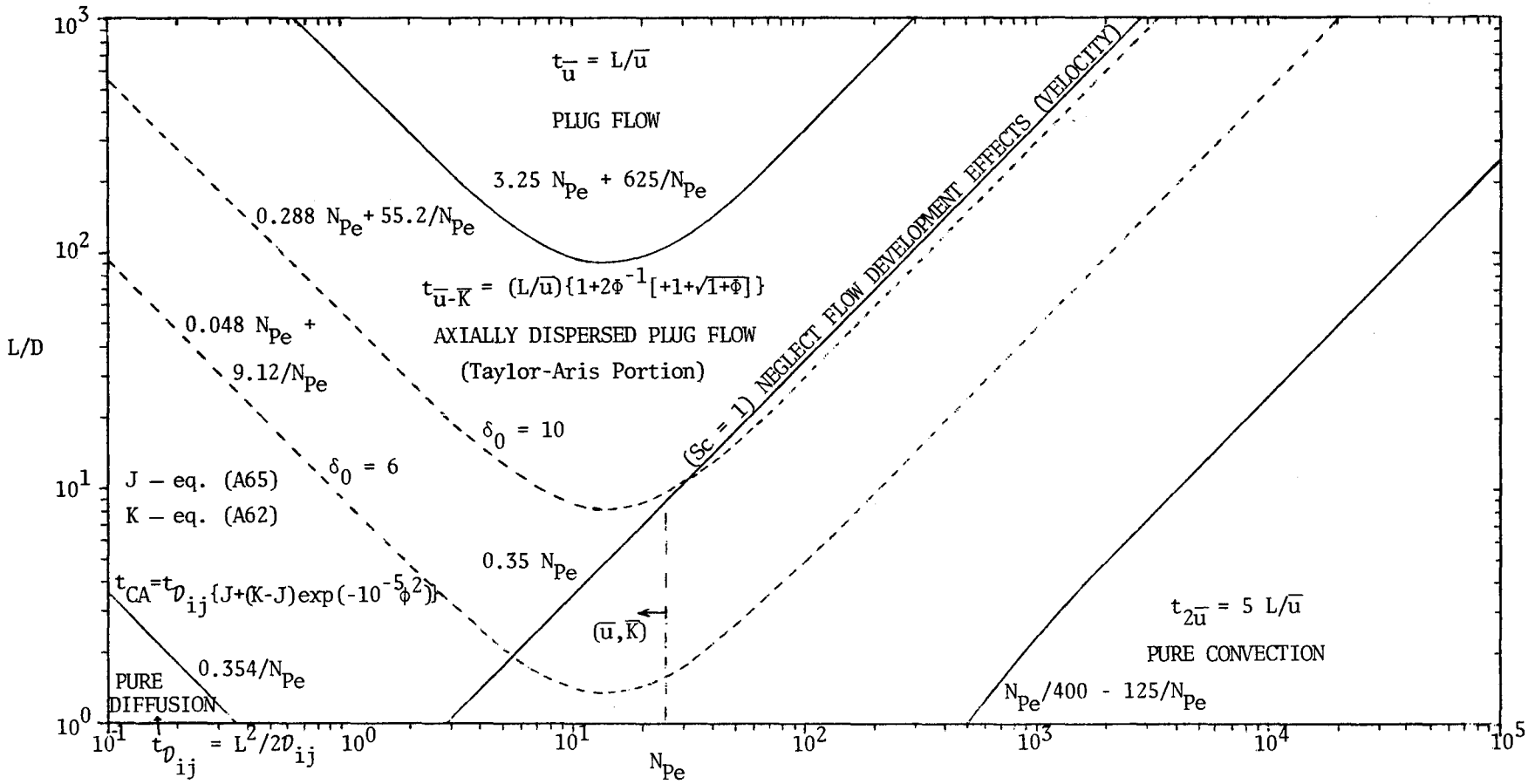

Figure A2. Requirements for Quasi-Steady Axial Concentration Profiles in Various Flow Regions

Concentration Profile via Axial Diffusion

Within the restrictions already imposed, the gas behind the front can exceed the vertex of the paraboloid created by convection only by axial molecular diffusion. This phenomenon in fact always occurs at early times since the root-mean-square displacement due to planar molecular diffusion is proportional to the square root of time (Jost, 1960) $x_{rms} = \sqrt{2\mathcal{D}_{ij}t}$ ($\sqrt{4\mathcal{D}_{ij}t}$ and $\sqrt{6\mathcal{D}_{ij}t}$ for radial cylindrical and spherical diffusion, respectively, although such geometric differences will be ignored here for order of magnitude estimates) compared with the linear dependence of convection, where $\mathcal{D}_{ij}$ is the mutual diffusion coefficient at the prevailing local pressure and temperature. A length more indicative of the distance over which most of the concentration change is occurring via diffusion is

$$x_{\Delta c} = \sqrt{20\mathcal{D}_{ij}t} \tag{A29}$$

Thus the first significant effects (time of break-through) are felt at a distance $x_{\Delta c} = L$ from an initial step change in concentration in times of the order of

$$t = L^2/20\mathcal{D}_{ij} \tag{A30}$$

while a new quasi-steady axial concentration profile is established via diffusion over that tube length in times of the order of

$$t_{\mathcal{D}_{ij}} = L^2/2\mathcal{D}_{ij} \tag{A31}$$

estimated by taking $x_{rms} = L$. By comparing pure axial diffusion concentration changes with those for pure convection, the ratio of lengths

$$x_{2\bar{u}}/x_{\Delta c} = N_{Pe}\ \tau_D^{1/2}/\sqrt{20} \tag{A32}$$

indicates that nearly pure axial diffusion can be expected to exist if $N_{Pe}\ \tau_D^{1/2} = \phi\ \tau_L^{1/2} << 1$ and can be expected to remain dominant if

$$N_{Pe}\ \tau_D^{1/2} < 0.5 \tag{A33}$$

a result derived by Gill (1965), see Figure A1; the parameters τ_D and τ_L are related by $\tau_D = \tau_L\ (L/D)^2$ and $\phi = N_{Pe}\ (L/D)$ relates the length and diameter based diffusion Péclét numbers. Note that ϕ is a measure of the ratio of axial convective mass transport to that for axial diffusion (the maximum possible); also since $t_{\mathcal{D}_{ij}}/t_{2\bar{u}} = \phi/10$ one can see that the magnitude of ϕ gives a measure of the relative amounts of time required to obtain either break-through or quasi-steady concentration profiles for these two pure physical mechanisms which of course occur simultaneously for real physical conditions with considerable modifying interaction that is later investigated.

First the conditions under which nearly pure axial diffusion can be expected to establish a quasi-steady axial concentration profile are determined. Since the diffusion dominated region must exist for at least as long as it takes to establish the quasi-steady concentration profile, then using (A31) and (A33)

$$t_{\mathcal{D}_{ij}} = L^2/2\mathcal{D}_{ij} \leq (2N_{Pe})^{-2}\ (D^2/4\mathcal{D}_{ij})$$

which yields the inequality

$$L/D \leq 0.354/N_{Pe}$$

which is shown on Figure A2. Notice that in this case the limit on L/D caused by the neglect of velocity entrance region effects excludes only part of the diffusion dominated region as opposed to all of the convection dominated region. That is the model being formulated here can actually operate (is valid) in a diffusion dominated region provided N_{Pe} is less than unity ($N_{Pe} \leq 1$).

Radial Diffusion Effects

After the time of axial diffusion domination has been exceeded, $N_{Pe}\ \tau_D^{1/2} > 0.5$, the effects of convection begin to disperse the gas initially behind the front toward a paraboloidal shape (except for the distortions caused by the early axial diffusion) resulting as was noted earlier in a nearly linear axial distribution of concentration when convection is dominant. From (A32) it appears that, if the tube is long enough, eventually convection always dominates axial diffusion effects when

$$N_{Pe}\ \tau_D^{1/2} >> 1$$

and usually

$$N_{Pe}\ \tau_D^{1/2} \geq 50 \qquad \text{(A34)}$$

is an adequate indication of convection domination. Long before this point is reached strong radial concentration gradients have often been created by the convective effects. These gradients drive radial diffusion which can only be ignored prior to diffusive break-through to the tube center-line,

so that only for $\tau_D << 1$ or from (A30)

$$\tau_D \leq 0.05 \tag{A35}$$

does nearly pure convection exist. Thus the pair of inequalities (A26) and (A27), which were previously used in the convection discussion, have been established and they require that $N_{Pe} \geq 224$. When $\tau_D > 0.05$ and $N_{Pe}\ \tau_D^{1/2} > 0.5$ the effects of radial diffusion on axial dispersion must be included.

The effect of radial molecular diffusion is the opposite of axial diffusion in that it allows gas from the high velocity region of the paraboloid to diffuse into the low velocity region nearer the walls; hence radial diffusion tends to create a concentration front which is more uniform or flat than the paraboloid and moving at the velocity $\bar{u}$ if radial diffusion is effective even though the velocity remains paraboloidally distributed with a maximum velocity of $2\bar{u}$ at the tube axis of symmetry. From (A22) it is obvious that radial diffusion can be expected to be effective in establishing a quasi-steady radial concentration profile if $\tau_D \geq 0.5$. [Gill (1965) numerically arrives at $\tau_D \geq 0.6$.] Thus radial diffusion inhibits axial dispersion due to convection and axial diffusion so that eventually $\tau_D \geq 0.5$ a quasi-steady state is approached where most of the radial concentration gradients are eliminated and axial mass transport behaves as if there is a plug flow at the average velocity $\bar{u}$ but dispersing relative to $\bar{u}$ [called "axially dispersed plug flow"] with some axial dispersion coefficient $\bar{K}$ (effective axial diffusivity) which is greater than the molecular value $\mathcal{D}_{ij}$, $\bar{K} \geq \mathcal{D}_{ij}$, even though the velocity profile remains essentially paraboloidal. Gill (1965) has numerically determined that the $(\bar{u}, \bar{K})$ model holds approximately for all τ_D if $N_{Pe} \leq 25$, while for $N_{Pe} > 25$ it holds only if

$\tau_D \geq 0.6$. The amount by which $\overline{K}$ exceeds $\mathcal{D}_{ij}$ indicates the effects which the paraboloidal velocity profile has had on axial dispersion via interaction with radial diffusion. A large body of literature exists (Taylor, 1953-4; Gill, 1965-8; Aris, 1956; Bournia, 1961; Evans, 1965) which is concerned with the determination, both analytically and experimentally, of $\overline{K}$ under a wide variety of initial and boundary conditions. Typically the form which $\overline{K}$ usually takes can be expressed

$$\overline{K} = \mathcal{D}_{ij} \; (1 + S \; N_{Pe}{}^2) \quad . \tag{A36}$$

For example, if an initial step profile in concentration at the inlet to a straight tube from a well mixed reservoir is set into motion with a uniform axial velocity at $t = 0$, then for $N_{Pe} < 25$ it is found that (Gill, 1965) S is bounded such that $0 \leq S(t) \leq 1/192$; in fact $S \simeq 1/192$ for all N_{Pe} values after about $\tau_D \geq 0.6$ where radial concentration profiles are fully developed. Obviously for large N_{Pe} values, $N_{Pe} > 25$, considerable enhancement of the effective axial diffusion coefficient $\overline{K}$ is obtained due to the interaction of convection and radial diffusion. On the other hand if $N_{Pe} < 1$ no significant enhancement is obtained for this case. The upper limit on S depends considerably on the boundary conditions but appears to remain small compared to unity. For example it increases to 11/192 in capillary systems with high adsorption on the walls or in the limit of infinite ratio of stagnant pore volume to capillary flow volume for porous wall cases with a straight tube (Dayan and Levenspiel, 1968). Also for straight channels with non-permeable and non-adsorbing walls the upper limit on S appears to be 8/945. In any event these cases seem to show that any time $N_{Pe} < 1$ the enhancement of $\overline{K}$ above $\mathcal{D}_{ij}$ can be neglected.

In the "axially dispersed plug flow region" where $\bar{u}$ and $\bar{K}$ can be used to describe the concentration profile, expressions analogous to (A24) - (A32) can be written

$$x_{\bar{u}} = \bar{u}t \quad , \; t_{\bar{u}} = L/\bar{u} \tag{A37}$$

$$x_{rms} = \sqrt{2\bar{K}t} \; , \; t_{\bar{K}} = L^2/2\bar{K} \tag{A38}$$

$$x_{\Delta c} = \sqrt{20\bar{K}t}, \; t = L^2/20\bar{K} \tag{A39}$$

so that

$$x_{\bar{u}}/x_{\Delta c} = N_{Pe} \; \tau_D^{1/2} (\mathcal{D}_{ij}/\bar{K})^{1/2}/2\sqrt{20} \tag{A40}$$

and

$$t_{\bar{K}}/t_{\bar{u}} = (\phi/2)(\mathcal{D}_{ij}/\bar{K}). \tag{A41}$$

Thus the criterion for the neglect of dispersion relative to the plug motion at $\bar{u}$ is somewhat different than that for neglect of molecular diffusion relative to pure convection on the tube axis of symmetry at $2\bar{u}$; this is primarily due to the presence of $(\mathcal{D}_{ij}/\bar{K})$. Care must be exercised in the use of (A37) - (A41) since they are valid only in the "axially dispersed plug flow" region and under no circumstances should they be used for $\tau_D \lesssim 0.5$ even at high N_{Pe} values ($N_{Pe} >> 1$). Only if $N_{Pe} < 1$ is $\bar{K} \simeq \mathcal{D}_{ij}$ so that the criterion $N_{Pe} \; \tau_D^{1/2} > 50$ stated before (A34) as the criterion for convection domination becomes approximately valid here. More generally the near plug flow region can be specified by

$$N_{Pe} \; \tau_D^{1/2} \gtrsim 50 \; (\bar{K}/\mathcal{D}_{ij})^{1/2} \tag{A42}$$

so that if (A36) with S = 1/192 is used as an example then

$$\tau_D \geq 13 + (50/N_{Pe})^2 \tag{A43}$$

specifies that region in which (A37) or

$$t_{\bar{u}} = L/\bar{u} \tag{A44}$$

approximately estimates the time to establish a new axial concentration profile since in that time the tube is essentially flushed or swept clean by the plug motion. Since (A43) can be written

$$t \geq \frac{L}{\bar{u}} [3.25\ N_{Pe} + 625/N_{Pe}]/(L/D) \tag{A45}$$

and the flush or quasi-steady profile can occur only if

$$t \geq t_{\bar{u}} = L/\bar{u} \tag{A46}$$

then

$$L/D \geq [3.25\ N_{Pe} + 625/N_{Pe}] \tag{A47}$$

for $t_{\bar{u}} = L/\bar{u}$ to be a valid estimate of flushing time. This region is shown on both Figure A1 and Figure A2 where it is obvious that there is a large region between the regions where $t_{\bar{u}}$ and $t_{\mathcal{D}_{ij}}$ are valid as well as between $t_{\bar{u}}$ and the limit $L/D > 0.35\ N_{Pe}$ set by neglect of the velocity entrance region effects.

This gap can be partially bridged by deriving the analogous expression to $t_{\bar{u}}$ which is valid for much smaller τ_D and L/D values. Mathematically this

can be done by recognizing that after $\delta = \bar{u}\ (t/\bar{K})^{1/2}$ exceeds about 10 (actually 6 is probably adequate) then a similar solution (a function of η only) well known to hold for the infinite capillary case for the concentration

$$C = 0.5 \text{ erfc } \eta = 0.5\ (1 - \text{erf } \eta) \tag{A48}$$

becomes approximately valid for the semi-infinite capillary (Gill, 1965) more precisely described by

$$C = \frac{1}{2}\ \{\text{erfc}\, \eta + \exp\ [\delta(2\eta + \delta)]\ \text{erfc}\ (\eta + \delta)\}; \tag{A49}$$

this is because the boundary condition $C(x=0,t) = 1$ at the tube inlet no longer has a significant effect on the concentration profile since it is so far downstream of the inlet following the initial conditions $C(x<0,t=0) = 1$ and $C(x>0,t=0) = 0$. This region, which is within the axially dispersed plug flow region where a $\bar{K}/\mathcal{D}_{ij}$ model holds, is often called the Taylor-Aris region. Gill (1965) numerically determined that $\tau_D \geq 0.8 + 30\ N_{Pe}^{-1.4}$ (which is a crude fit of table values given by Gill) approximately bounds the Taylor-Aris region for the special case alluded to earlier where $\bar{K}/\mathcal{D}_{ij} = 1 + N_{Pe}^2/192$. The upstream boundary condition must be accounted for via (A49) or some other appropriate expression if another boundary condition is present, for smaller δ values and S in the $\bar{K}/\mathcal{D}_{ij}$ model must then be recognized to be possibly less than 1/192, $0 \leq S \leq 1/192$. Of course for finite length capillaries the downstream boundary condition may also be important and require a finite capillary solution which is discussed later. At this point only the Taylor-Aris region (infinite capillary solution) is investigated via $C = \frac{1}{2}$ erfc η. Thus the value of $\eta = \pm\sqrt{5}$ can be used to identify the head and tail of the concentration front respectively, via the + and - sign. Also since

$$\eta = (x - \bar{u}t)/2\sqrt{\bar{K}t} \tag{A50}$$

then

$$x = x_{\bar{u}} \pm x_{\Delta c} \tag{A51}$$

immediately indicates the physical interpretation regarding the head and tail of the profile relative to the plug motion. Hence for $x = L$ the $\pm$ signs indicate break-through and flushing, respectively. The solution of (A50) for t with $x = L$ therefore gives an estimate of the times at which these events occur. This solution is

$$t_{\bar{u}-\bar{K}} = (L/\bar{u}) \left\{1 - 2\,\Phi^{-1}\,[-1 \pm \sqrt{1 + \Phi}]\right\} \tag{A52}$$

where the $\pm$ signs still are related to the $\eta = \pm\sqrt{5}$ relation rather than the two roots of the quadratic, one of which has been eliminated on physical grounds. The parameter Φ can be written

$$\Phi = \phi(\mathcal{D}_{ij}/\eta^2\bar{K}) = N_{Pe}(L/D)(\mathcal{D}_{ij}/\bar{K})/5 \tag{A53}$$

which becomes

$$\Phi = N_{Pe}(L/D)/(5 + 0.026\,N_{Pe}^2) \tag{A54}$$

if (A36) and $S = 1/192$ are used as an example. Since $\bar{K} \to \mathcal{D}_{ij}$ if $N_{Pe} \lesssim 1$ then $\Phi \to \phi/5$ and

$$t_{\bar{u}-\mathcal{D}_{ij}} = (L/\bar{u}) \left\{1 - 10\,\phi^{-1}\,[-1 \pm \sqrt{1 + \phi/5}\,]\right\} \tag{A55}$$

where the - sign gives the time to a new steady-state concentration profile while the + sign is related to the break-through time. The solution $t_{\bar{u}-\bar{K}}$, (A52), extends to lower L/D than (A47) for $t_{\bar{u}}$. This approximate limit is controlled by the choice of the lower limit on $\delta = \bar{u}(t/\bar{K})^{1/2}$ given before to be 6 to 10 depending on how close the similar solution is approached before it is said to be valid. Since

$$\bar{u}(t/\bar{K})^{1/2} = N_{Pe}\ \tau_D^{1/2}\ (\mathcal{D}_{ij}/\bar{K})^{1/2}/2 \tag{A56}$$

then a lower limit δ_o on $\bar{u}(t/\bar{K})^{1/2}$ simply places a lower limit on τ_D of

$$\tau_o = \delta_o^2\ (\bar{K}/\mathcal{D}_{ij})(2/N_{Pe})^2 \tag{A57}$$

which is a little different than the expression fit to Gill's tabled data, although not greatly different when $\delta_o = 6$, since $\delta_o = 10$ is entirely within Gill's Taylor-Aris region. In any event using $t_{\bar{u}-\bar{K}}$ (- sign) with the requirement that it should be greater than the time t_o obtained from (A57), $\tau_o = 4\ t_o\ \mathcal{D}_{ij}/D^2$, $t_{\bar{u}-\bar{K}} \geq t_o$, gives the result

$$L/D \geq (\bar{K}/\mathcal{D}_{ij})(\delta_o/N_{Pe})(\delta_o - 4.48) \tag{A58}$$

in order for $t_{\bar{u}-\bar{K}}$ to be a valid estimate of time for quasi-steady concentration profile. If $\delta_o = 10$

$$L/D \geq (55.2/N_{Pe})(\bar{K}/\mathcal{D}_{ij}) \tag{A59}$$

while $\delta_o = 6$ gives

$$L/D \geq (9.12/N_{Pe})(\overline{K}/\mathcal{D}_{ij}) \tag{A60}$$

which are both shown on Figure A2 using $\overline{K}/\mathcal{D}_{ij} = 1 + N_{Pe}^2/192$ as an example. Several important results can be observed from Figure A2. One is that for large N_{Pe} values (greater than 5 to 25), the assumption of negligible velocity entrance region effects excludes all L/D values below the limits given above for $\delta_o = 6$ and 10 so that $t_{\overline{u}-\overline{K}}$ via (A52) using - sign is the only expression required here to estimate characteristic times to establish concentration profiles. For N_{Pe} below these values $\overline{K}$ rapidly approaches $\mathcal{D}_{ij}$ so that an additional expression is needed to bridge the gap between $t_{\mathcal{D}_{ij}} = L^2/2\mathcal{D}_{ij}$, valid for $\phi < 0.354$, and $t_{\overline{u}-\mathcal{D}_{ij}}$ given by (A55) which is approximately valid for $\phi > 55$ but good for crude estimates if $\phi > 10$. The region $0.354 \leq \phi \leq 55.2$ must therefore be examined. To properly cover this region neither the infinite nor the semi-infinite capillary solutions known for certain special cases are adequate; that is a solution for finite length capillary is required. The case where a capillary of length L joins two reservoirs (well mixed) located at x = 0 and x = L with the initial conditions $C(x < 0, 0) = 1$ and $C(x > 0, 0) = 0$ has a well known (Carslaw and Jaeger, 1959) solution for $C(x,t)$ with boundary conditions $C(0,t) = 1$ and $C(L,t) = 0$ when $\overline{u}$ and $\mathcal{D}_{ij}$ are constants. The best measure of the establishment of the quasi-steady concentration profile is when the transport rate past x = L of the specie behind the initial front approaches the well known steady-state value. This occurs when $t/t_{\mathcal{D}_{ij}} = t_{CA}/t_{\mathcal{D}_{ij}}$ satisfies

$$\left\{\left[\frac{e^{\phi/2}-e^{-\phi/2}}{\phi/2}\right]\sum_{n=1}^{\infty}(-1)^n\left[1+\left(\frac{\phi}{2\pi n}\right)^2\right]^{-1}\exp\left[\frac{-(n\pi)^2}{2}\left[1+\left(\frac{\phi}{2\pi n}\right)^2\right]\left(t_{CA}/t_{\mathcal{D}_{ij}}\right)\right]\right\}$$

$$= \varepsilon << 1 \tag{A61}$$

and it is found that the series converges rapidly for $\phi < 10^2$ since $t/t_{\mathcal{D}_{ij}}$ is not too small, $t/t_{\mathcal{D}_{ij}} > 2 \times 10^{-2}$. For small $t/t_{\mathcal{D}_{ij}}$ the series has poor convergence characteristics but since the equation for $t_{\bar{u}-\bar{K}}$ holds in that region it is of no concern here. If the small quantity ε is chosen to be $\varepsilon = 0.01438$, which implies that the transport rate at $X = L$ is 98.562% of steady-state, then the results for $t/t_{\mathcal{D}_{ij}}$ with ϕ values as large as 150 are shown on Figure A3 along with those calculated from (A55) $t_{\bar{u}-\mathcal{D}_{ij}}$ normalized by $t_{\mathcal{D}_{ij}}$. The results from the two different expressions are nearly asympototic around $\phi = 150$. The quantity $t/t_{\mathcal{D}_{ij}}$ simply represents the fraction of the time $t_{\mathcal{D}_{ij}} = L^2/2\mathcal{D}_{ij}$ for pure diffusion to reach 98.562% of the steady-state rate which is required to establish the concentration profile when convection $\bar{u} \neq 0$ is present. Notice that the transition from $t_{\mathcal{D}_{ij}} = L^2/2\mathcal{D}_{ij}$ to $t_{\bar{u}} = L/\bar{u}$ starts to be significant when ϕ reaches about 2 and is essentially complete when ϕ reaches about 2×10^3 as $t/t_{\mathcal{D}_{ij}}$ approaches the limit $2\phi^{-1}$ indicating $L/\bar{u}$ is being approached. The results below $\phi = 150$ obtained from (A61) can be represented by the fit

$$K = \left(t/t_{\mathcal{D}_{ij}}\right)_{\phi<150} = e^{-.03\phi^2} + 5.269\ \phi^{-1.15}\left(1 - e^{-.002\phi^3}\right) \quad \text{(A62)}$$

and since for large ϕ from (A55)

$$J = \left(t/t_{\mathcal{D}_{ij}}\right)_{\phi>>1} = 2\ \phi^{-1}\left\{1 + 10\ \phi^{-1}\ [1 + \sqrt{1 + \phi/5}\,]\right\} \quad \text{(A63)}$$

then it is possible to represent the entire ϕ region by

$$F = t_{CA}/t_{\mathcal{D}_{ij}} = J + (K - J)\ e^{-10^{-5}\phi^2} \quad \text{(A64)}$$

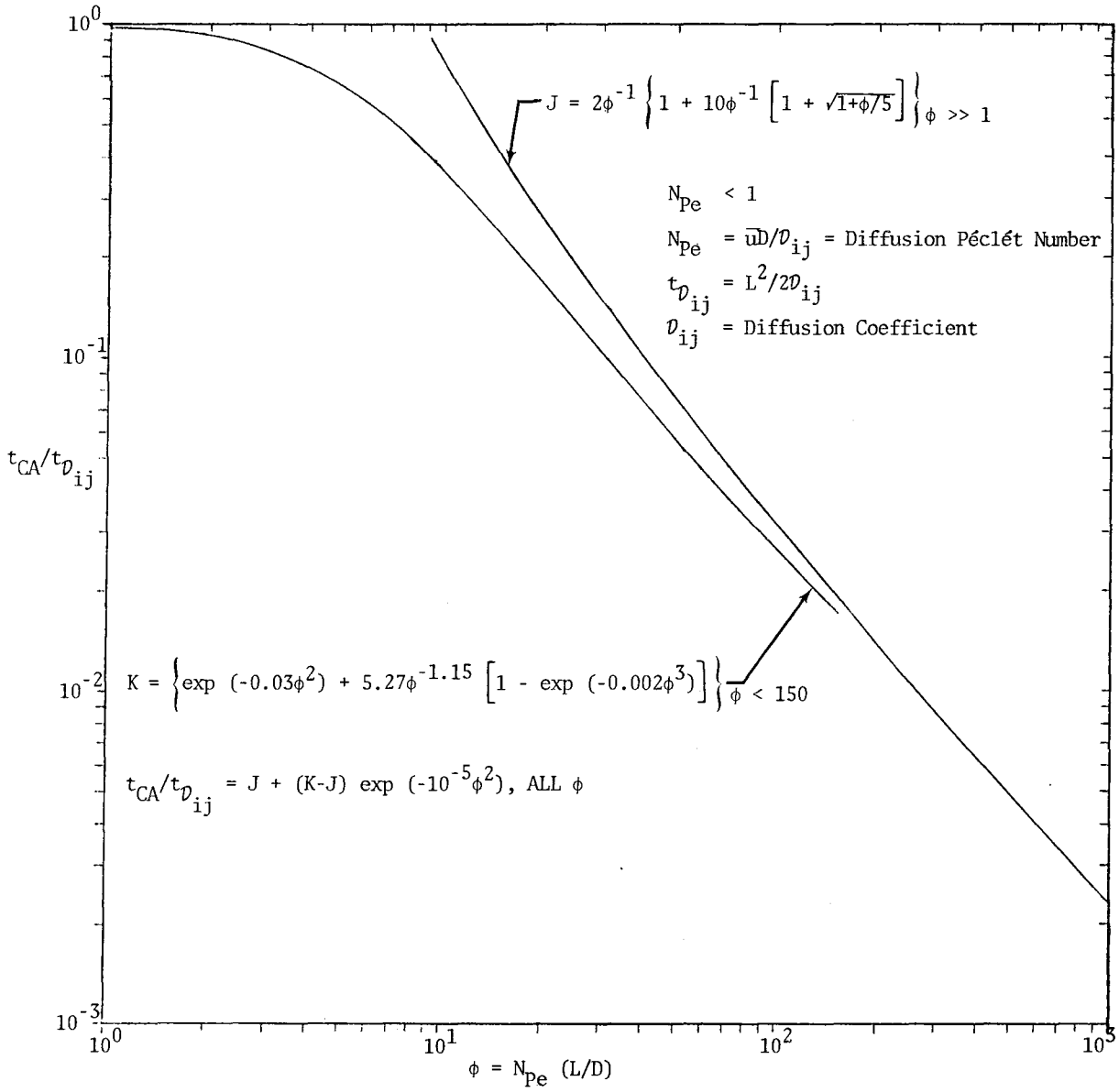

Figure A3. Time to Establish Axial Concentration Profiles, t_{CA}, in a Tube of Length L and Diameter D with Average Velocity $\bar{u}$, versus ϕ.

so that the desired results for small N_{Pe} values have been obtained. If J is replaced by a generalized expression obtained from (A52), valid for large N_{Pe},

$$J = 2\,\phi^{-1}\left\{1 + 10\,\phi^{-1}\,(\bar{K}/\mathcal{D}_{ij})\left[1 + \sqrt{1 + (\phi/5)/(\bar{K}/\mathcal{D}_{ij})}\,\right]\right\} \qquad \text{(A65)}$$

then (A64) is approximately valid over the entire region not already excluded by previous restrictions such as negligible velocity entrance region effects; note for large N_{Pe} values that both ϕ and N_{Pe} or N_{Pe} and L/D are required to calculate the fraction of $t_{\mathcal{D}_{ij}} = L^2/2\mathcal{D}_{ij}$ which is required to reach a new quasi-steady concentration profile while for small N_{Pe} values only ϕ is required. Of course for other initial conditions and other boundary conditions the results would be somewhat different than those on Figure A3, however since only an estimate of the characteristic time is needed here the result just derived should be more than adequate.

SUMMARY - Quasi-Steady, Axially-Diffused Plug Flow

The results of this section on the regions of validity of the quasi-steady and axially diffused plug flow ($\overline{u}$, $\mathcal{D}_{ij}$) assumptions need to be summarized due to their complicated nature. The previous six assumptions resulted in restrictions on the magnitudes of six independent non-dimensional parameters (Kn, Z, Re, L/D, M, γ) which were translated into six dimensional inequalities involving pressure, temperature, tube length and diameter, viscosity, and total mass flow rate. In this section it has been shown that seven more independent non-dimensional parameters (N_{Pe}, h/D, V_o/V_∞, V', D_i', α', S_i') are required, each of which is also restricted in magnitude via a complex set of twelve ratios of characteristic times, only seven of which are independent. Since all thirteen dimensioned parameters are involved in these ratios, the resulting dimensional inequalities number thirteen including an additional restriction resulting from the axially diffused plug flow assumption.

Axially Diffused Plug Flow

To be specific, Gill (1965) has shown that for $N_{Pe} \lesssim 25$ the axially dispersed plug flow ($\overline{u}$, $\overline{K}$) model is approximately valid for all τ_D values. However for $N_{Pe} > 25$ (really $25 < N_{Pe} < 2000$ when $Sc \simeq 1$ due to the previous $Re < 2000$ restriction) Gill concluded that the $\overline{u}$, $\overline{K}$ model was valid approximately only if $\tau_D > 0.6$ which is about the same as the $\tau_D > 0.5$

restriction arrived at here. This implies that $t > 0.5\ D^2/4\mathcal{D}_{ij}$ is necessary but since the profile does not remain in the tube unless $t < L/\bar{u}$ then

$$0.5\ D^2/4\ \mathcal{D}_{ij} < t < L/\bar{u}$$

so that in order that such a region exist at all

$$L/D > 0.125\ N_{Pe}$$

and in order that it exist over most of the tube length

$$L/D > 1.25\ N_{Pe} = 1.25\ Re\ Sc$$

or thereabouts. Notice that this result is comparable to the previous result

$$L/D > 0.35\ Re$$

required for the neglect of velocity entrance region effects, considering $Sc \simeq 1$, so that no new restriction has really been derived. In any event, the $N_{Pe} > 25$ results are not of interest here since

$$N_{Pe} < 1 \tag{A66}$$

in order for $(\bar{u}, \bar{K}) \rightarrow (\bar{u}, \mathcal{D}_{ij})$ so that the axially <u>diffused</u> plug flow model is valid; then one finds that

$$\dot{m} < \pi D\mu/4Sc \tag{A67}$$

which of course is much more restrictive than the previous inequality $\dot{m} < 500\ \pi D\mu$ derived from the Re < 2000 restriction and therefore should be used in its place. For the previous example with Sc = 0.75 one obtains $\dot{m} < \pi \times 10^{-6}$ g/sec.

Quasi-Steady Bore Flow

The characteristic time ratios required to be small

$$t_{bore}/t_{system} << 1 \tag{A68}$$

will be evaluated in detail using $t_{bore}/t_{system} < 0.2$ as the requirement for approximate validity of the quasi-steady assumption. The new dimensionless parameters N_{Pe}, h/D, V_o/V_∞, $V' = \pi D^2 L/4V_o$, $\alpha' = \alpha L^2/2\mathcal{D}_{ij}$, $D_i' = D_i/\mathcal{D}_{ij}$ and $S_i' = S_i RT/A_V$ are introduced. The constant A_V is Avogadro's number 0.6023×10^{24} and since V_o is the vent or receiving volume V' is the ratio of tube volume to the connected vent volume. Also from (A64)

$$F(L/D,\ N_{Pe}) = t_{CA}/t_{\mathcal{D}_{ij}} = 2\mathcal{D}_{ij}\ t_{CA}/L^2 \leq 1$$

is used to simplify terminology. The resulting twelve time ratios (seven of which are independent) are

$$t_{VR}/t_d = (t_{CR}/t_d)(t_{VR}/t_w)/(t_{CR}/t_w) \tag{A69}$$

$$t_{VA}/t_d = (t_{CR}/t_d)(t_{VA}/t_w)/(t_{CR}/t_w) \tag{A70}$$

$$t_{CR}/t_d = (\alpha D^2/8\mathcal{D}_{ij}) = [\alpha'/4(L/D)^2] \tag{A71}$$

$$t_{CA}/t_d = (\alpha L^2/2\mathcal{D}_{ij})\ F\ (L/D,\ N_{Pe}) = \alpha' F \tag{A72}$$

$$t_{VR}/t_w = (D_i D^2/4\nu h^2) = [D_i'/4(h/D)^2]\ (Re/N_{Pe}) \tag{A73}$$

$$t_{VA}/t_w = (10\ D_i L/c_o h^2) = [10\ D_i'/(h/D)^2](L/D)(M/N_{Pe}) \tag{A74}$$

$$t_{CR}/t_w = (D_i D^2/4\mathcal{D}_{ij} h^2) = [D_i'/4(h/D)^2] \tag{A75}$$

$$t_{CA}/t_w = (D_i L^2/\mathcal{D}_{ij} h^2)\ F = D_i' F(L/D)^2/(h/D)^2 \tag{A76}$$

$$t_{VR}/t_{FV} = (t_{VR}/t_w)(t_{CR}/t_{FV})/(t_{CR}/t_w) \tag{A77}$$

$$t_{VA}/t_{FV} = (t_{VA}/t_w)(t_{CR}/t_{FV})/(t_{CR}/t_w) \tag{A78}$$

$$t_{CR}/t_{FV} = \left(\frac{A_s}{h}\right)\left(\frac{V_o + V_\infty}{V_o\ V_\infty}\right)\left(\frac{D_i S_i RT}{A_v}\right)\left(\frac{D^2}{8\mathcal{D}_{ij}}\right)$$

$$= \left(1 + \frac{D}{h}\right)\left(1 + \frac{V_o}{V_\infty}\right) V' D_i' S_i'/2 \tag{A79}$$

$$t_{CA}/t_{FV} = (t_{CA}/t_d)(t_{CR}/t_{FV})/(t_{CR}/t_d) \tag{A80}$$

where (A69), (A70), (A77), (A78) and (A80) are written in terms of (A71) - (A76) and (A79) to emphasize the independence of only seven of these ratios.

In order that the quasi-steady assumption be approximately valid without any additional qualifying restrictions, each of (A69) - (A80) must at least be less than 1/5, an arbitrary small number stated earlier which may be

decreased if even stricter validity is required. Using the fact that $Sc = N_{Pe}/Re \simeq 1$ certain pairs of (A69) - (A80) become nearly identical; thus if (A69) and (A71) are less than 1/5 the inequality

$$D(cm) < 3 \times 10^4 \, [P(atm)]^{-1/2} \tag{A81}$$

results, as an example, when $\alpha^{-1} = 17.8$ yr, the decay constant for ${}_1H^3$ and $\mathcal{D}_{ij}(cm^2/sec) \simeq [P(atm)]^{-1}$, which is not very restrictive generally considering $P < 10^2$ atm here. Similarly (A73) and (A75) are less than 1/5 if

$$D(cm) < 0.9 \, h(cm) (\mathcal{D}_{ij}/D_i)^{1/2} \tag{A82}$$

where $\mathcal{D}_{ij}/D_i = [D_o(cm^2/sec°K) \, P(atm) \, T(°K)]^{-1} \exp (E_d/R_cT)$ which as an example for SiO_2 - He at 300°K and 10 atm has the value

$$\mathcal{D}_{ij}/D_i \simeq 4 \times 10^6 \text{ giving } D(cm) < 1.8 \times 10^3 \, h(cm)$$

which also is not very restrictive for most applications. In the same manner (A77) and (A79) yield

$$V' = (\pi D^2 L/4V_o) < 0.4 \left(1 + \frac{D}{h}\right)^{-1} \left(1 + \frac{V_o}{V_\infty}\right)^{-1} / D_i' S_i' = V_b' \tag{A83}$$

which, as an example, when $V_o/V_\infty \simeq 10$, $D/h \simeq 3.2$, $T = 300°K$ and $P = 10$ atm, then $V' < 1.5 \times 10^6$, for SiO_2 - He which is certainly not restrictive since $V' << 1$ for most applications. The inequalities (A81) - (A83) are for quasi-steady radial profiles in the bore of the tube.

The inequalities resulting for quasi-steady axial profiles in the bore of the tube are now examined. If (A70) is less than 1/5 then

$$L(\text{cm}) < 2 \times 10^{11} \left(\gamma T(°K)/W(\text{g/g-mole})\right)^{1/2} \tag{A84}$$

using α^{-1}=17.8 yr which is certainly not very restrictive for γ = 5/3 and W = 4 at 300°K or any other reasonable values for γ, W and T. Similarly (A72) yields

$$L(\text{cm}) < 1.5 \times 10^{4}\ F^{-1/2}\ [P(\text{atm})]^{-1/2} \tag{A85}$$

which under the worst conditions, F = 1 and P = 10^2 atm, results in $L < 1.5 \times 10^3$ cm; generally of course L can be much larger than this since $F \leq 1$ and $P \leq 10^2$ atm, however this is probably the most restrictive inequality derived up to this point. From (A74) one finds

$$L(\text{cm}) < 1.8 \times 10^{2}\ h^2(\text{cm}^2) \left(\gamma/T(°K)\ W(\text{g/g-mole})\right)^{1/2} \frac{\exp(E_d/RT)}{D_o(\text{cm}^2/\text{sec}°K)} \tag{A86}$$

which becomes $L(\text{cm}) < 0.76 \times 10^{11}\ h^2(\text{cm}^2)$ for the conditions used in earlier examples and indicates little problem. The analogous result from (A76) is

$$L(\text{cm}) < (5F)^{-1/2}\ h(\text{cm})\ (\mathcal{D}_{ij}/D_i)^{1/2} \tag{A87}$$

which becomes $L(\text{cm}) < 2 \times 10^3\ (5F)^{-1/2}\ h(\text{cm})$ for the conditions used earlier. To show that (A87) can be very restrictive, assume that $L/D = 10^4$ and $N_{Pe} = 10^{-2}$ so that $F = 2.4 \times 10^{-2}$ and let $h = 6.4 \times 10^{-3}$ cm with the result that L < 37 cm. This inequality will be discussed further later. In terms of V_b', given by (A83), (A78) yields

$$V' < V_b' \ (c_o D/\mathcal{D}_{ij})/40 \ (L/D) \tag{A88}$$

or

$$V' < (6.9 \times 10^3) \left(\gamma T(°K)/W(g/g\text{-mole})\right)^{1/2}$$

which becomes $V' < 7.5 \times 10^4$ for the conditions used earlier.

Finally from (A80) one obtains

$$V' < V_b'/4(L/D)^2 \ F \tag{A89}$$

which as an example becomes

$$V' < 0.16$$

using the conditions stated previously. This final inequality could be restrictive in some applications.

As stated earlier, if all of the inequalities (A81) - (A89) are satisfied, then the solutions derived in this report can be used under the prevailing local conditions in a quasi-steady fashion. If one (or more) of the inequalities is not satisfied then the converse is true unless the driving force for the particular physical phenomenon referred to in the inequality is not present in a significant amount. For instance, if the decaying specie is not present in significant amounts in the system, then the inequalities derived from (A69) - (A72) can be ignored. Also if the most rapidly permeating specie (largest $D_i S_i$) is not present in significantly different concentrations in one reservoir compared to the other volume, then its inequalities derived from (A77) - (A80) can be ignored in favor of those for a specie which is permeating in significant amounts. Similarly the

initial startup transients which occur following the filling of the reservoirs with the gas mixtures may occupy such an insignificant fraction of the total period of operation that they can be ignored; also the fact that some of the related inequalities are not satisfied becomes irrelevant unless there are other perturbing factors such as system temperature changes during the period of operation which are of interest. Thus if an inequality such as (A87) is not satisfied, and there are large and rapid system temperature changes, then the model being derived here cannot apply. If, however, the magnitude of the temperature changes or the rate of change of system temperature is controlled or restricted properly, then the model can still be applied with confidence. Specifically, this is true if the temperature change takes place over a period of time which is 5 or more times

$$t(\text{Temp. Change}) > 5t_{CA} \tag{A90}$$

larger than t_{CA} or ΔT is less than the amount which would cause $\Delta D_i/D_i$ to exceed 0.05 for example.

<u>Uniform Reservoirs</u> $[L/X_v,\ X_d/X_v,\ t_{stc}/t_{rc},\ \Delta T_{max}/T]$

Since a physical mechanism is not present which can maintain a significant gradient in total pressure in either reservoir, the uniformity of concentration and temperature are of primary concern.

Concentration

Each reservoir is assumed to be spherical in shape, so that in the vent volume (see Figure 1) the gas must mix well for a distance of the order of

the volume diameter $X_v = (6V_o/\pi)^{1/3}$, while in the driver volume mixing for a distance of the order of the volume radius $X_d = (3V_\infty/4\pi)^{1/3}$ is necessary. Due to the line source and point source nature of the problem, the time required to mix gases over these distances via molecular diffusion alone can be expressed [note that $(\mathcal{D}_{ij})_d \neq (\mathcal{D}_{ij})_v$ necessarily due primarily to different total pressure].

$$t_{X_d} \simeq X_d^2/4(\mathcal{D}_{ij})_d \tag{A91}$$

$$t_{X_v} \simeq X_v^2/6(\mathcal{D}_{ij})_v \tag{A92}$$

Equations (A91) and (A92) must be much smaller than the time required to transfer significant quantities of gas from one volume to the other volume t_{FV} estimated from (A20) for the dominant specie

$$t_{X_d}/t_{FV} = 0.12\ LV_\infty^{2/3}/V_o(V_b')_d << 1 \tag{A93}$$

$$t_{X_v}/t_{FV} = 0.32\ L/V_o^{1/3}(V_b')_v << 1 \tag{A94}$$

where V_b' is dimensionless and is given by (A83) and the fact that $(\mathcal{D}_{ij})_d \neq (\mathcal{D}_{ij})_v$ must be properly accounted for when it is evaluated. If these ratios are taken to be less than 10^{-2} the resulting length restrictions are

$$L < 0.083\ (V_b')_d V_o/V_\infty^{2/3} \tag{A95}$$

$$L < 0.031\ (V_b')_v V_o^{1/3} \tag{A96}$$

which gives as an example, respectively,

$$L < 0.29 \times 10^5 \text{ cm} \tag{A97}$$

$$L < 0.24 \times 10^5 \text{ cm} \tag{A98}$$

if the maximum driver pressure is 10^3 atm and the maximum vent pressure is 10^2 atm and $V_o \simeq 10^3$ cm^3, $V_\infty \simeq 10^2$ cm^3 using the other values given previously as examples for SiO_2-He. Of course the smaller the time ratio the more uniform the reservoirs are, so that if 10^{-4} is used in place of 10^{-2} above the length restrictions are reduced by a factor of 10^2 and the reservoirs are even more uniform.

Temperature

Two phenomena may cause reservoir thermal gradients; one is due to internal heat sources in the reservoir gas and the other is related to thermal lag in the reservoir gas if it cannot keep up with rapid temperature changes external to the system. The thermal lag can be analyzed using an expression analogous to (A92) for a spherical volume of radius $r_{res} = (3V_{res}/4\pi)^{1/3}$ if the diffusion coefficient is replaced by the gas thermal diffusivity $a = k/\rho C_p$ so that

$$t(\text{spherical res. conduction}) \simeq r_{res}^2/6a \tag{A99}$$

where it is assumed that the reservoir wall material has much greater thermal response rate than that of the gas and all convection mechanisms are neglected here. The reservoir gas will stay relatively uniform temperature wise if the temperature of the system is changed over a period greater than about five times that given by (A99)

$$t_{stc}/t_{rc} = t\ (\text{sys. temp. change})/t(\text{res. conduction}) > 5 \tag{A100}$$

so that

$$t(\text{sys. temp. change}) > 5\ r_{res}^2/6a \tag{A101}$$

results. The thermal diffusivity (Kreith, 1958) is generally between 4×10^{-3} cm^2/sec for gases like N_2 and O_2 and 6×10^{-2} cm^2/sec or less for gases like He and H_2 at 300°K and 1 atm and exhibits inverse pressure dependence. As an example, for a 1 liter reservoir volume and 10 atm of N_2 at 300°K, the time of temperature change should exceed 21 hr for conduction only; convection of course would lower this time by about an order of magnitude to around an hour at least.

The heat buildup due to internal heat sources uniformly distributed in a gas reservoir can also be analyzed using heat conduction only (no convection) and a constant heating rate per unit volume $\dot{q}$ so that (Kreith, 1958)

$$\Delta T_{max}/T = \dot{q}\ r_{res}^2/6kT \tag{A102}$$

is the maximum difference in temperature resulting at steady state between the center and surface of a spherical volume of gas. Since $\Delta T_{max}/T$ must be small

$$\Delta T_{max}/T < 10^{-1} \tag{A103}$$

for example

$$r_{res}^2 < 0.6\ kT/\dot{q}\ . \tag{A104}$$

As an example, the heating rate per unit volume for molecular ${}_1H^3$ is (Jordan, private communication, 0.324 watts/gm)

$$\dot{q}_{{}_1H^3}(\text{g-cal/sec/cm}^3) \simeq 0.467\ P_{{}_1H^3}(\text{atm})/RT(°K) \tag{A105}$$

so that at 300°K

$$\dot{q}_{{}_1H^3}(300°K) = 1.9 \times 10^{-5}\ P_{{}_1H^3}(\text{atm})\ \text{g-cal/sec/cm}^3$$

in terms of the partial pressure of molecular ${}_1H^3$. The conductivity times the temperature at 300°K is around 1.2×10^{-2} g-cal/sec/cm for gases like O_2 and N_2 while for gases like He and H_2 it is about 1.3×10^{-1} g-cal/cm/sec or less at 300°K. The worst case (most restrictive) is for ${}_1H^3$ to exist as a component in a mixture of low conductivity gases like O_2 and N_2 so that

$$r^2_{res}(\text{cm}^2) < 379/P_{{}_1H^3}(\text{atm}) \tag{A106}$$

which as an example yields $r_{res} < 10$ cm for 3.79 atm ${}_1H^3$ and $r_{res} < 1$ cm for 379 atm ${}_1H^3$. Reliable values comparable to (A105) - (A106) are not available for all of the isotopes listed in the decay section, however, a heating rate of 0.53 watts/gm for ${}_{36}Kr^{85}$ (Chart of Nuclides as Modified by Battelle Northwest, May 1969, 1970, Gov. printing off. #1970-O-389-841) can be used. The results are

$$\dot{q}_{Kr}\ (\text{g-cal/sec/cm}^3) = 10.8\ P_{Kr}(\text{atm})/RT(°K)$$

$$\dot{q}_{Kr}\ (300°K) = 4.4 \times 10^{-4}\ P_{Kr}(\text{atm})$$

$$r^2_{res}(cm^2) < 16.3/P_{Kr}(atm)$$

the last of which yields $r_{res} < 10$ cm for 0.163 atm $_{36}Kr^{85}$ and $r_{res} < 1$ cm for 16.3 atm $_{36}Kr^{85}$. These results are significantly different than those for $_1H^3$. Of course convection would increase greatly the limits on the reservoir radius, possibly as much as a factor of 3 to 5.

Straight Tube [d/D]

Many of the previous results are for straight tubes which may be impractical due to the lengths involved. It is therefore of interest to examine the effects of coiling the tube (small coiling pitch) with some coil diameter d. It is desired to determine what the minimum value of d is in order that no significant effects result from the coiling procedure.

Flow Rate

One possible effect results due to the altered velocity profile in the tube which increases the resistance to the flow such that a reduced flux or flow rate is obtained. This has been studied by Truesdell and Adler (1970) where fully developed laminar flow in helically coiled tubes (small coiling pitch) is investigated. The result is that for circular tubes, there is less than 1% effect on the volumetric flux if the ratio of the helical coil diameter to the tube inside diameter is greater than 10^{-2} Re^2

$$d/D > 10^{-2}\ Re^{2} \tag{A107}$$

where Re is the Reynolds number. It is obvious that this usually can be an important restriction only for large Re, Re >> 1 which is not the case here.

Dispersion

Another possible effect is the alteration of dispersion mechanisms along the tube bore. Two competing processes interact to determine this effect. Curvature increases the variation in residence time across the flow which in turn tends to increase the dispersion coefficient while the secondary flow which occurs in curved tubes creates a transverse mixing that tends to decrease the axial dispersion coefficient. Results are given for such an investigation by Nunge, et al. (1972) which indicate that the dispersion coefficient first increases and then decreases as the Reynolds number increases. For Schmidt numbers of the order of unity (actually Sc ≃ 0.75) those results indicate that there will be less than 5% effect on the axial dispersion coefficient if

$$d/D > 2.66\ Re^{1/8}\ (1 + 10^{-3}\ Re^{2}) \tag{A108}$$

which is usually not a significant restriction unless Re >> 1. Since Re < 1 is the region of general interest here, neither (A107) or (A108) usually need be considered a serious limit although in that region (A108) is always the most restrictive while for large Re, Re >> 1, (A107) is most restrictive.

Dead End Permeable Tube

Several of the previous assumptions were evaluated via results for flow through open ended tubes with impermeable walls. .These include the assumptions of fully developed laminar flow, uniform bore pressure, quasi-steady radial and axial profiles, and straight tubes. Obviously when the tube is dead ended with all the flow entering through permeable walls, the results can be vastly different. However there are conditions where the axial flow at a given location along the tube interacts very little with the mass addition at that location, but is primarily determined by the combined or integrated effects of everything both upstream and downstream of that location so that those boundary conditions are properly satisfied. This is not likely to be true, of course, near the closed end of the tube; but if it is true locally over most of the tube, then the assumption evaluations previously based on open ended tubes with impermeable walls can be expected to hold in local spacial application when properly interpreted.

One measure of the difference between the two cases (impermeable and permeable walls) is the pressure drop along the tube; the conditions under which the pressure drop can be ignored were determined previously using the viscous flow (Poiseuille flow formula) equation for impermeable walls because it was expected to be more severe than the permeable wall case. The nature of the relationship between the two cases is clearly determined by Huang and Yu (1973). That study is for steady, incompressible, laminar flow in a porous duct with uniform fluid addition or extraction along the

walls. The results adequately illustrate the physical fundamentals which are also involved for a nonuniform wall velocity v_w expected in this work. Using the nomenclature of Huang and Yu, the average velocity along the tube at any x coordinate location for uniform v_w is then

$$\bar{u}(x) = \bar{u}_o(1 - x/L) \tag{A109}$$

with x measured from the open end where $\bar{u} = \bar{u}_o$ and $\bar{u} = 0$ at the closed end, $x = L$ (or at least symmetry causes zero velocity there). For a circular tube the resulting approximate axial pressure change is then

$$\left[\frac{P(0) - P(x)}{\frac{1}{2}\rho\bar{u}_o^2}\right] = \left(\frac{64}{Re}\frac{x}{D}\right)\left(1 - 2\frac{Re_w}{Re}\frac{x}{D}\right)\left(1 - Re_w/3\right) \tag{A110}$$

in terms of the wall Reynolds number $Re_w = v_w D/\nu$; Huang and Yu showed that (A110) is an adequate approximation provided $Re_w/Re \ll 1$ and $|Re_w| \leq 1$ where $Re = \bar{u}_o D/\nu$ is the open end Reynolds number. Negative Re_w refers to blowing or fluid addition while positive Re_w refers to suction or fluid extraction. Since $Re_w = 0$ and $x/L \ll 1$ gives the case of an impermeable wall, the first factor on the right of (A110) is the familiar Poiseuille formula used earlier (A14) so that it introduces a linear axial dependence. The next factor on the right of (A110) accounts for the distributed mass addition or extraction and thus alters the axial dependence to quadratic as a first approximation. Since for a dead end permeable tube $Re/Re_w = \bar{u}_o/v_w = 4\ L/D$, the second factor becomes 1/2 at $x = L$ due to the average axial velocity being 1/2 of that at the open end; this substantiates the earlier statement about impermeable tube results being more severe than permeable results

since the pressure change along a dead end porous tube is 1/2 that which would occur if the open end flow passed through the entire length L of the impermeable tube (perhaps this is easier to observe if (A110) is rewritten)

$$\left[\frac{P(x) - P(L)}{\rho \bar{u}_o^2/2}\right] = (64\ L/ReD)(1/2)(1 - x/L)^2\ (1 - Re_w/3) \qquad \text{(A111)}$$

provided the effects of the last factor are negligible. The last factor weighs or measures viscous forces versus inertial forces normal to the wall as they interact via blowing or suction such that if they balance when $Re_w = Re_{wc} = 3$ (actually more exact results show $Re_{wc} \cong 2.6$) via suction, then no net pressure gradient results when the suction velocity is uniform. This factor becomes unity for all practical purposes when Re_w is small, say for example $|Re_w| \leq 0.03$. Although Huang and Yu only examined the single specie case, Libby, Liu and Williams (1969) confirm the wall Reynolds number criterion in the 2 specie case where the greatest effect on pressure gradient occurs for light gas injected into a heavy one. It would therefore appear that a local application of the Poiseuille flow formula is justified if

$$Re_w/Re << 1 \qquad \text{(A112)}$$

$$|Re_w| << 1 \qquad \text{(A113)}$$

which can be satisfied if

$$L > 10^2\ D \qquad \text{(A114)}$$

$$\dot{m} < 10^{-1}\ \mu L \tag{A115}$$

the last of which is of a similar form as (A11) but more restrictive. For the same example given previously (A114) and (A115) require that $L > 2$ cm and $\dot{m} < 3 \times 10^{-3}$ g/sec. The conditions stated above essentially allow the velocity profile to be approximated over most of the tube length, not too near the closed end, by a paraboloid whose peak value at the center line is determined by the local flow rate such that it is equal to $8\ \dot{m}(x)/\pi\rho D^2$. When interpreted in this manner, the previous evaluations of the assumptions of fully developed laminar flow, uniform bore pressure and straight tubes should certainly be adequate. The results of Libby, et al. (1969) confirm this via an investigation of the flow development region in the case of two species of considerably different molecular weights when either the heavy or the light one is injected uniformly. Also Gill, et al. (1968) note that the extent of dispersion is less in developing velocity fields than in those which are fully developed (the bulk of the tube here) because dispersion is enhanced by velocity differences (these are maximum when fully developed) normal to the main flow direction. Even in the fully developed region the velocity profile is closely coupled to concentration profiles so that one expects no great alteration of the concentration profiles via the small departures from the paraboloidal velocity profiles allowed under the restrictions imposed here. However the physical difference in boundary conditions in that a rich or lean mixture of gases is being added or removed radially at the tube walls rather than axially at the tube ends can be a significant effect on axial dispersion. Diffusion and convection tend to create radial uniformity very fast relative to the axial distribution because large L/D tubes are in general necessary in order to satisfy other assumptions. The

axial concentration profile, however, can be altered significantly by wall effects. This is, as was previously discussed, best treated via an axial dispersion coefficient (which includes radial effects). For example (Dayan and Levenspiel, 1968) an enhancement of the dispersion coefficient of over an order of magnitude has been reported for capillary systems with high adsorption on the walls or in the limit of infinite ratio of stagnant pore volume to capillary flow volume for porous wall cases. The existence of this effect, however, was previously taken into account when the bounds were established on several parameters in the radial diffusion effects treatment. Thus no further adjustments of the limiting inequalities are necessary here.

UNLIMITED RELEASE

INITIAL DISTRIBUTION:

EPA Technical Center
Research Triangle Park
North Carolina 27711
Attn: Dr. W. Herget, P-222

Air Force Aero Propulsion Laboratory
Wright-Patterson AFB, Ohio 45433
Attn: AFAPL/TBC
Dr. Kervyn Mach

NASA Ames Research Center
Deputy Chief Aeronautics Division
Mail Stop 27-4
Moffett Field, CA 94035
Attn: Mr. Edward W. Perkins

NASA Lewis Research Center
21000 Brookpark Road
Cleveland, OH 44135
Attn: D. Morris, Mail Stop 60-3

Naval Ordnance Laboratory Commander
White Oak
Silver Springs, MD 20910
Attn: Library

Naval Postgraduate School
Monterey, CA 93940
Attn: Library (Code 0212)

The Aerospace Corporation
P.O. Box 92957
Los Angeles, CA 90009
Attn: Mr. Alexander Muraszew

Ballistics Research Laboratory
Commanding Officer
Aberdeen Proving Ground, MD 21005
Attn: Library

Naval Weapons Center
Commander
China Lake, CA 93555
Attn: Technical Library

California Institute of Technology
Jet Propulsion Laboratory
4800 Oak Grove Drive
Pasadena, CA 91103
Attn: Library

University of California, San Diego
Dept. of Aerospace and Mechanical
Engineering
La Jolla, CA 92037
Attn: Prof. Paul Libby

University of California
School of Engineering & Applied Science
7513 Boelter Hall
Los Angeles, CA 90024
Attn: Engineering Reports Group

Georgia Institute of Technology
School of Aerospace Engineering
Atlanta, GA 30332
Attn: Dr. Ben T. Zinn

McDonnel Douglas Corporation
Project Propulsion Engineer
Dept. 243, Bldg. 66, Level 2S
P.O. Box 516
St. Louis, MO 63166
Attn: Mr. William C. Paterson

Massachusetts Institute of Technology
Room 10-408
Cambridge, MA 02139
Attn: Engineering Technical Reports

Purdue University
School of Mechanical Engineering
West Lafayette, IN 47907
Attn: Prof. V. W. Goldschmidt

Stanford University
Dept. of Aeronautics Astronautics
Stanford, CA 94305
Attn: Dr. Walter G. Vincenti

von Karman Institute for Fluid Mechanics
72 Chauseé de Waterloo
Rhode-St-Genése
Belgique

Presbyterian University Hospital
230 Lothrop Street, Room 2418
Pittsburg, PA 15213
Attn: Dr. David Powner

Battelle Memorial Institute
Pacific Northwest Laboratory
P.O. Box 999
Richland, WA 99352
Attn: Tech. Information Sect.

Harvard Medical School
Cambridge, MA 02138

Medical College of Wisconsin
Milwaukee, WI 53233

New York Medical College
Valhalla, NY 10595

New York University
School of Medicine
550 First Avenue
New York, NY 10016

Stanford University
School of Medicine
Stanford, CA 94305

Tulane University
School of Medicine
1430 Tulane Avenue
New Orleans, LA 70112

University of California at Los Angeles
School of Medicine
Los Angeles, CA 90024

University of Chicago
School of Medicine
920 East 58th Street
Chicago, IL 60637

University of Illinois
Department of Biochemistry
Urbana, IL 61801
Attn: Daniel Storm

University of Pennsylvania
School of Medicine
Johnson Research Foundation
Philadelphia, PA 19104

University of So. California
School of Medicine
2025 Zonal Avenue
Los Angeles, CA 90033

Vanderbilt University
Medical College
Nashville, TN 37232

University of Wisconsin at Madison
1215 Linden Drive
Madison, WI 53706

Washington University
School of Medicine
660 S. Euclid Avenue
St. Louis MO 63110

Washington University
School of Medicine
Seattle, WA 98195

R. M. Fulrath
Dept. of Materials Science & Engineering
College of Engineering
University of California
Berkeley, CA 94720

R. J. Nunge
Clarkson College of Technology
Potsdam, NY 13676

W. N. Gill
Clarkson College of Technology
Potsdam, NY 13676

U.S. Energy Research and Development Administration
Washington, D.C. 20545
Division of Military Applications
Attn: Col. Herbert McClammy

U.S. Energy Research and Development Administration
Washington, D.C. 20545
Division of Magnetic Fusion Energy
Attn: F. F. Coffman

U.S. Energy Research and Development Administration
Washington, D.C. 20545
Division of Physical Research
Attn: James S. Kane
Elliot S. Pierce

U.S. Energy Research and Development Administration
Washington, D.C. 20545
Division of Energy Storage Systems
Attn: George Pezdirtz

U.S. Energy Research and Development Administration
Washington, D.C. 20545
Division of Conservation Research and Technology
Attn: John Belding
Karl Bastress
Bob Lawrence

U.S. Energy Research and Development Administration
Washington, D.C. 20545
Division of Fossil Energy Research
Attn: Alexander Mills

U.S. Energy Research and Development Administration
Washington, D.C. 20545
Division of Coal Conversion and Utilization
Attn: Fred Crim

T. A. Sandford, LASL
B. Banks, LASL
I. Lindstrom, LASL
E. H. Plassmann, LASL
L. Myer, SRL
J. E. Haywood, SRP
J. H. Owen, SRL
D. L. Hobrock, MD
D. Spangler, MD
H. L. Turner, MD
J. E. Dorr, DRF; Attn: J. D. Wagner
D. Ahmann, GE
F. P. Brown, GEND
D. Davis, ERDA/ALO; Attn: R. K. O'Neill
R. L. Wong, LLL, L-122
J. J. Ruminer, LLL, L-122
W. E. Nelson, LLL, L-125
R. S. Paige, LLL, L-125
R. W. Goluba, LLL, L-125
F. J. Ackerman, LLL, L-460
B. Hickman, LLL, L-460

G. A. Fowler, 1000
R. C. Maydew, 1330
A. Y. Pope, 1400
A. H. Mauney, 1530; Attn: H. W. Schmitt
T. B. Lane, 1540; Attn: H. Hardee
C. M. Tapp, 2150
J. C. Crawford, 2350
W. G. Perkins, 2353
J. C. King, 2500
D. H. Anderson, 2510; Attn: D. B. Hayes
E. A. Kjeldgaard, 2515
B. E. Bader, 4337
A. Narath, 5000
D. E. Amos, 5122
K. J. Touryan, 5260
R. L. Schwoebel, 5820
D. M. Mattox, 5834
E. K. Beauchamp, 5846
J. L. Chamberlin, 9531

T. B. Cook, Jr., 8000; Attn: C. H. DeSelm
W. C. Scrivner
L. Gutierrez, 8100; Attn: W. E. Alzheimer
R. D. Cozine
C. S. Selvage
A. N. Blackwell, 8110
A. F. Baker, 8111
D. R. Chenoweth, 8111 (10)
D. L. Hartley, 8115
C. W. Robinson, 8116
S. C. Johnston, 8116
D. E. Gregson, 8150
R. J. Page, 8157
A. S. Rivenes, 8158
W. G. Wilson, 8165
D. J. Bohrer, 8167
B. F. Murphey, 8300
R. Y. Lee, 8322
G. J. Miller, 8322
G. W. Anderson, 8330
J. E. Marion, 8332
G. C. Story, 8332
G. L. Scholer, 8333
A. J. Wiemken, 8333
W. Bauer, 8334
J. L. Wirth, 8340; Attn: A. R. Willis
S. C. Keeton, 8341
W. D. Wilson, 8341
E. H. Barsis, 8342

Technical Publication and Art Division, 8365, for TIC (2)
F. J. Cupps, 8265/Library Systems & Technical Processes Division, 3141
Library Systems & Technical Processes Division, 3141 (4)
Library and Security Classification Division, 8266-2 (5)